A Dynamic Pre-Clinical Testing Protocol for Intervertebral Disc Replacement Devices

Holsgrove, Tim

Award date:
2012

Awarding institution:
University of Bath

A DYNAMIC PRE-CLINICAL TESTING PROTOCOL FOR INTERVERTEBRAL DISC REPLACEMENT DEVICES

Timothy Patrick Holsgrove

A thesis submitted for the degree of Doctor of Philosophy

Centre for Orthopaedic Biomechanics
Department of Mechanical Engineering
University of Bath
February 2012

COPYRIGHT

ABSTRACT

Back pain is a common complaint and the origin of this frequently attributed to degenerative disc disease. In the most severe cases, the integrity of the disc and surrounding tissue is lost to such an extent that surgical intervention is necessary.

Fusion procedures are commonly used to treat severely degenerated discs. Yet this is known to alter the biomechanics of the operated level, and may create a progression of degenerative decline. Total disc replacement has emerged as a viable treatment but the complexity of the spine is reflected in the clinical results, which trail far behind the success of hip and knee arthroplasty. This may be due to a failure of total disc replacement procedures to restore the natural biomechanics of the spine.

The present study has led to the development of a dynamic pre-clinical testing protocol to quantitatively assess the efficacy of disc replacement devices. A six-axis spine simulator was designed and built, and the stiffness matrix testing of porcine lumbar specimens was completed, both with and without an axial preload. Intact specimens were tested, and the testing repeated after a total disc replacement procedure with a DePuy In Motion artificial disc. This is the first study to complete dynamic six-axis spinal testing of this kind.

The testing demonstrated the disc replacement device compared favourably with the intact porcine disc both in shear and axial stiffness. However, the low-friction, double ball and socket design of the In Motion device lacks stiffness in the three rotational axes, and it is unstable in lateral bending. Rotations are the primary movements in the spine, and it is crucial if the natural biomechanics are to be restored, that a disc replacement device should replicate the stiffnesses of these axes.

The next generation of disc replacement devices feature elastomeric materials that may more closely replicate the natural intervertebral disc. From patents registered with DePuy, this may also be true of the next generation of In Motion disc.

This research provides a means to complete standardised performance tests of new spinal devices and lays the foundations for future comparison studies. Additionally, the spine simulator and testing protocol would provide valuable data during the design stage of new total disc replacements, aiding the development of the next generation of artificial discs.

“Baby this town rips the bones from your back.”

Bruce Springsteen

ACKNOWLEDGEMENTS

I would like to thank all those who have provided support and guidance during the completion of this research. In particular I would like to thank my supervisors Sabina Gheduzzi and Tony Miles without whom this work would not have been possible, Richard Weston and Paul Griffiths for the time and effort taken to manufacture parts for the spine simulator, and Robin Long for his fundamental assistance throughout the project.

CONTENTS

LIST OF FIGURES

LIST OF TABLES

ANATOMICAL PLANES OF THE BODY

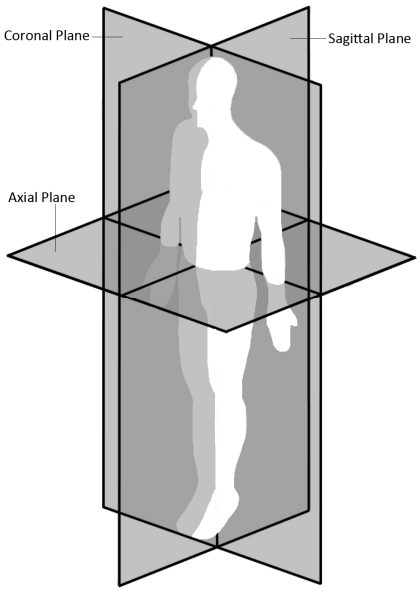

Figure 1: Anatomical planes of the body. Modified from Bridwell [1]

Table 1: Anatomical Terms

Term	Description
Coronal Plane	A vertical section passing through the standing body from one lateral side to the other.
Sagittal Plane	A vertical section passing through the standing body from anterior to posterior.
Axial Plane	A horizontal section passing through the standing body.
Anterior	Towards the front
Posterior	Towards the back
Ventral	Anterior
Dorsal	Posterior
Medial	Towards the midline of the body in the coronal plane
Lateral	Away from the midline of the body in the coronal plane
Proximal	Near to a point of attachment or origin
Distal	Away from a point of attachment or origin
Superior	Upper or above
Inferior	Lower or below
Cranial	Towards the head
Caudal	Towards the tail
Lordosis	Curvature in the vertebral column, convex anteriorly
Kyphosis	Curvature in the vertebral column, concave anteriorly
Prevertebral	Anterior to the vertebral column
Postvertebral	Posterior to the vertebral column
Intervertebral	Between two adjacent vertebral bodies

1 INTRODUCTION

The spine is a complex structure comprising vertebral bodies, intervertebral discs, facet joints, and numerous supporting ligaments and muscles [2-5]. Each joint level of the spine comprises an intervertebral disc and two facet joints [6]. These structures interact to provide motion in six degrees of freedom [5].

The degeneration or damage of any of the components of the spine may lead to pain or injury. Disc degeneration is known to lead to an alteration of the transfer of loads in the spine [4, 7, 8], and this may predispose a person to further injury. Back pain is increasingly common in the general population [9-11] and degeneration of the intervertebral disc is commonly a cause of this pain [7, 12-14]. Disc degeneration is characterised by a loss of fluid from the central nucleus pulposus, which can result in a loss of integrity of the outer annulus fibrosus [5]. This can inhibit the ability of the disc to transfer the high loads that are present in the spine without further damage occurring.

In severe cases of disc degeneration, in which debilitating pain is present, surgical intervention may be appropriate. At present, the gold standard treatment is fusion of the degenerated level [13, 15, 16]. This procedure aims to restore disc height, thereby correcting the load transfer through the spinal column and facets, and eliminate pain. However, in doing this, motion at the operated level is prevented. A fusion at one level may lead to the levels adjacent being subjected to higher strains during daily activities [9, 17, 18]; this may cause a degenerative cascade [19].

An alternative to fusion for the treatment of severe disc degeneration is total disc replacement. This procedure aims not only to eliminate pain and restore disc height, but also allow motion at the operated level, thus avoiding the problem of adjacent segment degeneration [9, 13, 20, 21]. This procedure has been carried out for over 50 years, initially in experimental cases but more recently using devices in clinical trials and approved by the FDA and implanted in thousands of cases of disc degeneration. However, although joint arthroplasty as a whole has seen great advances in clinical results in the past 50 years, particularly in the hip and knee, the complex nature of the spine has led to limited success [6, 22, 23], with results often comparable to the fusion procedure that disc replacement is intended to supersede [24].

The majority of disc replacement devices that have been used clinically are ball and socket designs, based on the technology, materials, and design of hip and knee prostheses. Such designs may fail to restore the biomechanics of the spine, which naturally has six degrees of freedom at each vertebral level. A great deal of work has been completed to understand more about the biomechanics of the natural spine, and how to treat degenerative disc degeneration but there remains little published work that assesses the effect of intervertebral disc replacement procedures in six degrees of freedom.

The aim of this research was to develop a quantitative testing protocol with which to assess the efficacy of total disc replacement devices. In order to achieve such an aim, the structure and loading of the spine was investigated, and the state of intervertebral disc prosthesis design, pre-clinical testing methods, and clinical results were assessed.

From the analysis of the motion and loading of the spine, and published pre-clinical testing protocols, a spine simulator testing machine was designed and manufactured. A dynamic testing protocol developed to assess intervertebral disc replacement device performance in six degrees of freedom.

The spine simulator and testing protocol were used to compare a currently available intervertebral disc replacement device with the intact disc under physiological loads and ranges of motion. The outcome of this research provides valuable data in terms of both assessing the predicted clinical performance of a disc replacement device, and in providing a method of improving artificial disc design.

2 SPINE ANATOMY AND BIOMECHANICS

2.1 Vertebrae and the Vertebral Column

The spinal column is made up of 32-33 vertebral bodies, most of which are separated by an intervertebral disc, allowing motion between adjacent vertebrae [2]. The motion between adjacent vertebral bodies is relatively small, however this results in a relatively large range of motion (ROM) in the whole spine [3].

The vertebral column is separated into 5 sections. Thus the vertebral bodies are identified by a section and a number associated with their position [2]. Numbering starts from the cranial end of each section. From the cranial to caudal ends the human spine comprises: 7 cervical (indicated C1-C7); 12 thoracic (indicated T1-T12); 5 to 6 lumbar (indicated L1-L5/L6); and 5 sacral (indicated S1-S5) vertebrae; finally the coccyx comprises 3 vertebrae (no abbreviation) (Figure 2). The vertebral bodies in the sacrum and coccyx are fused [2, 5].

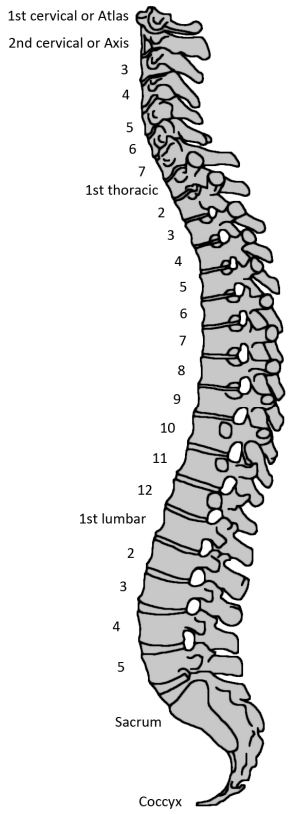

Figure 2: Vertebrae designation and curves of the vertebral column. Modified from Gray [2]

The vertebral column forms four curves when viewed in the lateral plane [2, 4]. The curvature of the cervical and lumbar spine is lordotic, while that of the thoracic and sacral coccyx spine is kyphotic (Figure 2). The curves provide some elasticity to the vertebral column [3-5].

The shape of the vertebral bodies is not constant throughout the vertebral column, though similar features can be identified. The vertebrae comprise a main body that is approximately elliptical when viewed in the axial plane. The vertebral body bears most of the compressive loading [3, 8]. Posterior to the main vertebral body is a passage, the spinal canal, which extends to the whole length of the spine and houses the spinal cord [2, 4]. The posterior structures of the vertebrae constitute an archway, the neural arch, characterised by various protrusions or processes, which serve as attachment points for muscles [3, 5]. Additionally, the posterior archways comprise two superior and two inferior articular processes that interlock with each other to form the facet joints, or zygapophyseal joints [2, 3, 5]. The facet joints bear some of the compressive loading, provide stability and serve to guide and limit the ROM between adjacent vertebral bodies [3].

The ROM in different spinal segments varies according to the characteristic geometry of the bony protrusions and facets of the vertebrae [3, 4].

The C1 vertebra, or Atlas, differs in appearance to other vertebrae (Figure 3). This does not have an elliptical body but comprises an anterior arch connected to a posterior arch, with two lateral protrusions called transverse processes [2, 3]. The C1 vertebra connects the base of the occipital bone of the skull to the vertebral column [2-4]. The C2 vertebral body has a blunt tooth-like protrusion, the dens, which extends superiorly from the body [2, 3]. The dens is characterised by an anterior facet providing a pivot and collar arrangement with the posterior archway of the C1 vertebra, allowing a large amount of axial rotation in the C1-C2 level [3, 4]. The C3-C7 vertebrae progressively increase in size, the C7 vertebra being characterised by a prominent spinous process [2, 3] (Figure 4).

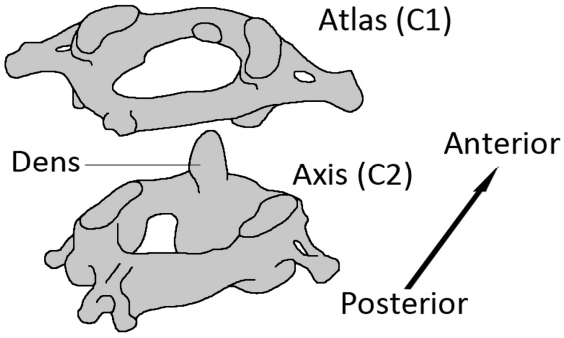

Figure 3: The C1-C2 vertebrae. Modified from Bridwell [25]

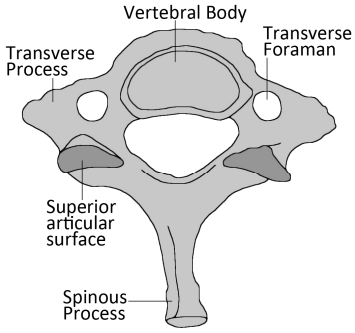

Figure 4: An axial view of the C7 vertebra. Modified from Gray [2]

The thoracic vertebral bodies gradually increase in size from the cervical spine to the lumbar spine, i.e. from superior to inferior [2, 4]. In addition to the facet joints comprising the superior and inferior articular processes, all of the thoracic vertebrae apart from T11 and T12 feature facets on the lateral sides of the vertebral bodies, which articulate with the heads of the ribs [2, 4] (Figure 5). The rib cage and sternum provide stability to the spinal column by significantly increasing the stiffness in flexion, extension, lateral bending and axial rotation [4].

The lumbar vertebrae increase in size from the thorax to the sacrum, reflecting the increase in compressive load transmitted by the spine [3]. In this segment the spinous processes are larger and extend more horizontally than those charactering the thoracic and cervical vertebrae, which extend posteriorly and caudally [2]. The lumbar vertebrae carry large loads [3] and as such the posterior archway comprises larger pedicles and there is no foramen in the transverse process [2] (Figure 6).

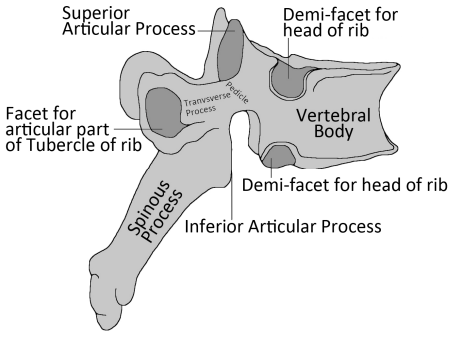

Figure 5: A lateral view of a typical thoracic vertebra. Modified from Gray [2]

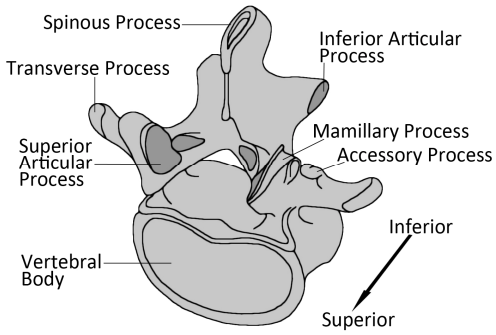

Figure 6: A typical lumbar vertebra. Modified from Gray [2]

Independently of its position in the spine, each vertebral body is characterised by a cortical bone outer surface and a trabecular bone interior [4, 5]. The superior and inferior surfaces of the vertebral bodies, the vertebral endplates, are the link between the vertebral bodies and the intervertebral disc [5]. The endplates are composed of hyaline cartilage [3, 5]. This allows the flow of fluid and nutrients in and out of the intervertebral discs [5].

The gradual increase in the size of the vertebral bodies from C1 to S1 reflects the increase in load that is transferred through the spine from the cranial to caudal ends of the vertebral column [4].

2.2 Intervertebral Disc

Adjacent vertebral bodies are separated by an intervertebral disc, with the exception of C1-C2 which articulate directly on each other, and the sacrum and coccyx, which are fused. The intervertebral discs allow limited motion in 6 degrees of freedom between adjacent vertebrae; the majority of motion occurs in three planes, in the form of flexion/extension, lateral bending, and axial rotation of the spine [6].

The intervertebral disc comprises an inner nucleus pulposus surrounded by an annulus fibrosus (Figure 7) and vertebral endplates of cartilage that bond the disc to the vertebral bodies [5]. The nucleus pulposus is a gel-like incompressible fluid, while the annulus fibrosus consists of several layers of collagen. Fibres in each layer of the annulus are orientated parallel at approximately $\pm 30°$ to the horizontal [3, 4]. Adjacent layers are characterised by fibres being orientated in opposite directions (Figure 7). The outer most layers of the annulus fibrosus are subject to the highest loads and as a result are attached directly to the vertebral bodies rather than the vertebral endplates [5].

The orientation of the fibres is such that in any direction of motion, at least half of the collagen fibres will be in tension. Tension in the fibres causes a resistive force, therefore providing elastic resistance to motion in the spine [5]. The angle at which the fibres are orientated is such that the disc can resist motion in all six degrees of freedom [5].

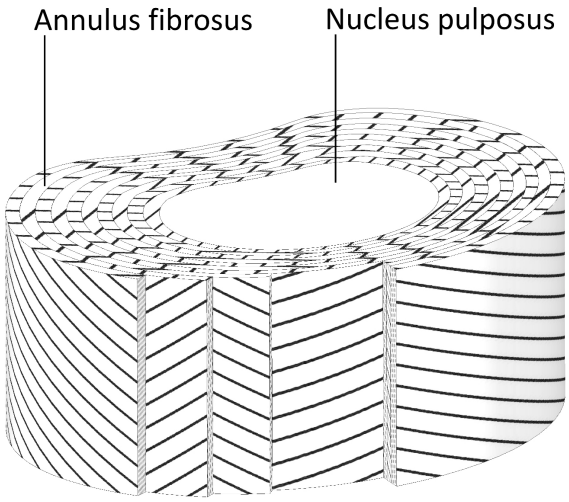

Figure 7: The collagen fibres of the annulus fibrosus are orientated at approximately $\pm 30°$ to the horizontal, with adjacent layers characterised by opposite orientation of fibres

Under axial compression the fluid-like substance that comprises the nucleus pulposus is forced against the interior wall of the annulus creating tension in the fibres (Figure 8), this can result in some barrelling of the annulus fibrosus. The force of the nucleus pulposus on the annulus fibrosus prevents the latter structure from buckling, allowing a proportion of the axial load to be transferred by the annulus fibrosus [5]. In axial tension, the superior and inferior surfaces of the disc are pulled apart causing the fibres to be in tension [4, 5] (Figure 8).

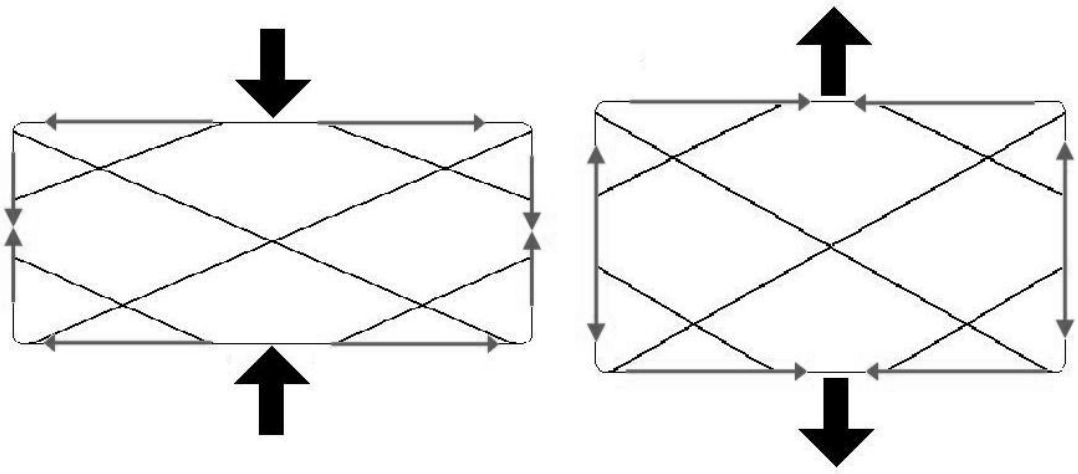

Figure 8: The behaviour of the annulus fibrosus under axial compression (left) and axial tension (right)

Under shear loading the fibres in one orientation are in tension and those in the other orientation are relaxed. This is the case for both lateral shear and anterior/posterior shear [5] (Figure 9).

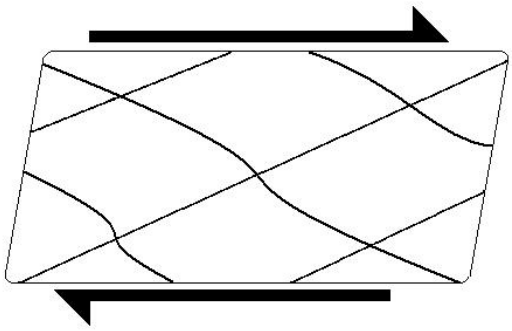

Figure 9: The behaviour of the annulus fibrosus under shear loading

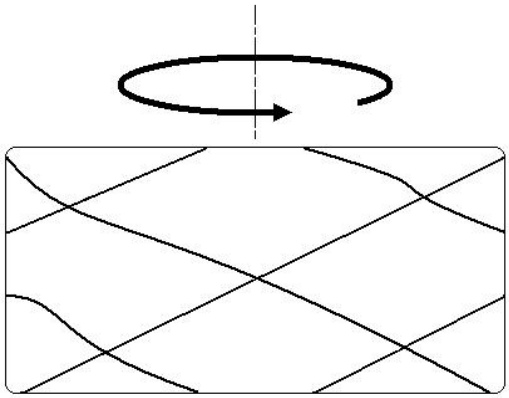

Figure 10: The behaviour of the annulus fibrosus in axial rotation

Under moments, either flexion/extension or lateral bending, one half of the disc will be in axial compression, the other half in axial tension [4]. This will result in the fibres of the annulus fibrosus being subjected to tensile forces; on one half of the disc due to axial compression and on the other half of the disc due to axial tension.

In axial rotation the fibres in one orientation are in tension, whilst those in the other orientation are relaxed [5] (Figure 10).

2.3 Ligaments

There are various ligaments that guide and limit motion of the vertebral column; some extend between adjacent vertebrae and others extend over several vertebral bodies [2, 5] (Figure 11).

The anterior longitudinal ligament, posterior longitudinal ligament and ligamentum flavum extend from the C2 vertebra down the length of the vertebral column to the sacrum [2, 4]. The anterior longitudinal ligament is attached to the anterior side of the vertebral column [2, 4, 5]. The posterior longitudinal ligament is attached to the posterior side of the vertebral bodies and is located inside the neural canal [2, 4, 5]. The ligamentum flavum is attached to

the laminae of the facets around the neural arch [2, 4, 5]. The supraspinous ligament is attached to the spinous processes of the vertebrae from C7 to the sacrum [2, 4].

The anterior and posterior longitudinal ligaments not only provide resistance to extension and flexion respectively [2, 3], but also provide some reinforcement to the anterior and posterior walls of the annulus fibrosus [26]. The ligamentum flavum and the supraspinous ligament limit flexion [2, 26]. Additionally, there are interspinous ligaments that attach between adjacent spinous processes and also limit flexion [2, 26]. The intertransverse ligaments, which are attached to the transverse processes are subject to tensile force during lateral bending [26]. However, in the lumbar region these ligaments comprise a thin membrane [2, 5] and as such are not capable of providing a large amount of resistance to lateral bending [5].

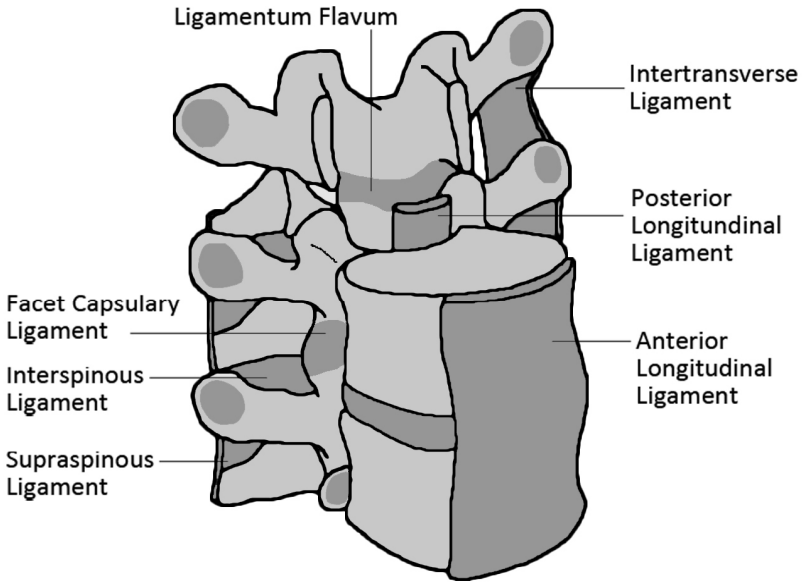

Figure 11: The major ligaments of the vertebral column. Modified from Bridwell [26]

The ligaments between the occiput, the posterior part of the skull, and the C2 vertebra are different and more numerous compared to the rest of the vertebral column [3]. The C1-C2 joint has a large ROM, particularly in axial rotation, and as there is no intervertebral disc ligaments provide most of the stability to this joint [4].

2.4 Musculature

The musculature of the spine not only provides a means to carry out movements, but contributes a large amount of stability to the structure. The vertebrae, intervertebral discs and ligaments alone do not fully stabilise the spinal column. If this structure was fixed at the sacrum, without the action of the muscles it would only be capable of carrying an axial load at T1 of approximately 20 N before buckling [4].

The muscles can be generally separated into two groups, prevertebral and postvertebral, these are located anteriorly and posteriorly with respect to the vertebral column respectively. In terms of movement, the prevertebral muscles are responsible for flexion and the postvertebral muscles are responsible for extension. Additionally, there are muscles that are positioned laterally to the vertebrae; with the role of providing lateral bending and increasing stability. Asymmetric use of the pre and postvertebral muscles can also create lateral bending and axial rotation. The postvertebral muscles can be separated further into deep, intermediate and superficial levels [4] (Table 2).

Table 2: Major muscles of the vertebral column [2, 4, 5, 27]

MUSCLE	DESCRIPTION	FUNCTION
POSTVERTEBRAL		
Deep	Short, connect adjacent vertebrae	
- Interspinales	Connects adjacent spinous processes	Extension
- Intertransversarii	Connects adjacent transverse processes	Extension
- Rotatores	Transverse process below to lamina above	Extension
- Levatores costarum	Transverse process to ribs	Extension
Intermediate	Transversospinalis attaches the tranverse process to spinous process above	
- Multifidus	Lumbosacral region	Extension
- Semispinales thoracis	Thoracic region	Extension
- Semispinales cervicis	Cervical region	Extension
- Serratus posterior-inferior	Posterior to the spinalis	Extension
Superficial	Collectively called the erector spinae and positioned posteriorly to the tranverse processes, either side of the spinous process	
- Ilicostales	Most laterally positioned	Extension
- Longissimus	Intermediate and largest	Extension
- Spinales	Most medially positioned	Extension
- Latissimus dorsi	Wraps around each posterior side from spinous processes to the lateral side	Extension, lateral bending

Table 2 continued…

PREVERTEBRAL		
- External oblique	Wraps around the abdominal region	Flexion
- Internal oblique	Wraps around the abdominal region	Flexion
- Transverse abdominis	Wraps around the abdominal region, interior to the internal oblique	Flexion
- Rectus abdominis	Along the midline, anterior to abdomen	Flexion
LATERAL		
- Quadratus lumbrum	Positioned laterally of tranverse process in the lumbar region	Lateral bending
- Psoas	Positioned against the lateral side of the vertebral body and anteriorly of the tranverse process in the lumbar region	Lateral bending

The cervical region has a greater ROM than other regions of the spine and this is reflected in there being a larger number of muscles than elsewhere in the spine. In addition to the muscles spanning one or two vertebrae and attaching at the spinous process and transverse processes, neck muscles also attach from points such as the clavicle and sternum and at various positions on the skull [2] (Figure 12).

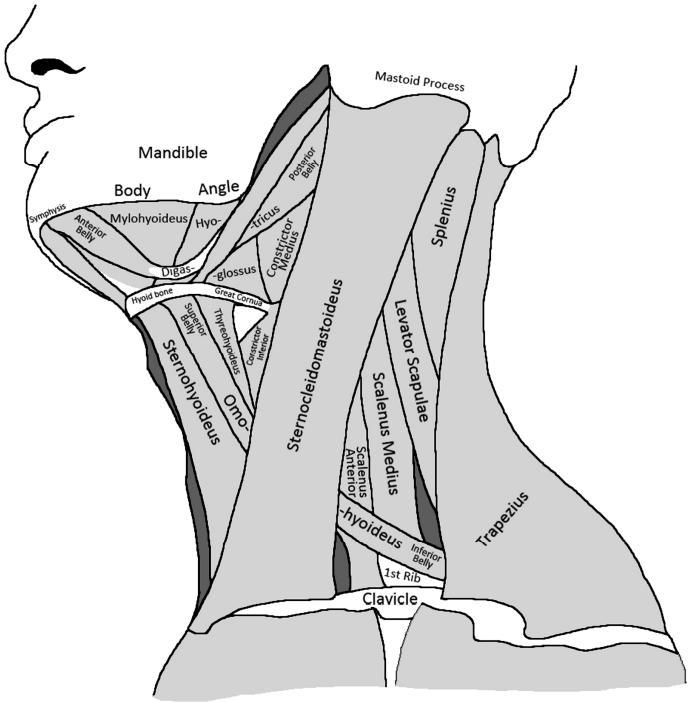

Figure 12: Muscle structure of the cervical spine. Modified from Gray [2]

2.5 Spinal loading and motion

The complexity of the spine makes it difficult to measure both ROM [28] and loading [29]. Nachemson [30] carried out accurate measurements of the compressive loading of the spine using a pressure sensitive needle inserted in the intervertebral disc of living volunteers. The invasive nature of this procedure means that it is not suitable for measuring vigorous activities, when spinal loading will be greatest [29, 31].

Skin surface techniques such as inclinometers, optoelectronic markers and electromagnetic devices, can measure overall ROM, but have limited use in determining movement between adjacent vertebrae [3], which vary greatly in different regions of the spine [4, 28, 32]. Radiographic measurements using low-dose fluoroscopy can be used to determine motion between adjacent vertebrae. White and Panjabi [4] published representative ranges of motion in flexion/extension, lateral bending and axial rotation from C0-S1 (Table 3).

Table 3: The approximate ROM of vertebral levels. Modified from White and Panjabi [4]

Level	Flexion/Extension (Combined)	Lateral Bending (One-Way)	Axial Rotation (One-way)
C0-C1	25°	5°	5°
C1-C2	20°	5°	40°
C2-C3	10°	10°	3°
C3-C4	15°	11°	7°
C4-C5	20°	11°	7°
C5-C6	20°	8°	7°
C6-C7	17°	7°	6°
C7-T1	9°	4°	2°
T1-T2	4°	5°	9°
T2-T3	4°	6°	8°
T3-T4	4°	5°	8°
T4-T5	4°	6°	8°
T5-T6	4°	6°	8°
T6-T7	5°	6°	7°
T7-T8	6°	6°	7°
T8-T9	6°	6°	6°
T9-T10	6°	6°	4°
T10-T11	9°	7°	2°
T11-T12	12°	9°	2°
T12-L1	12°	8°	2°
L1-L2	12°	6°	2°
L2-L3	14°	6°	2°
L3-L4	15°	8°	2°
L4-L5	16°	6°	2°
L5-S1	17°	3°	1°

Similar results to those in Table 3 were published by Adams et al. [5]. Serhan et al. [33], by comparing 10 studies that had determined lumbar ROM radiographically, reported similar values. In the cervical spine, ranges of motion similar to those in Table 3 were published in a review of the normal kinematics of the cervical spine by Bogduk et al. [34].

The ROM in the lumbar and cervical spine varies greatly between individuals [3, 35, 36] and with age [3, 5, 36]. Thus, measurements of the overall ROM of the spine may be of limited use [32].

In-vitro testing of the spine has shown that the limiting factor in axial compression is the strength of the vertebral body [3, 28]. The compressive strength of vertebral bodies rises from approximately 1300N at C3 to approximately 8000N at L4 [4, 28]. These loads may appear very high, however, it should be noted that the only common posture for which the compressive load in the spine is less than a person's body weight, is when in the prone position [28].

The reason why such high loads are experienced is predominantly due to the small lever arm of the postvertebral muscles that are engaged to stabilise and move the head and torso [28, 29]. If objects are carried in front of the body, even higher compressive loads will result. The overall loading of the spine depends greatly on three factors: posture; magnitude of external loads; and activity level, such as the speed at which a movement is carried out.

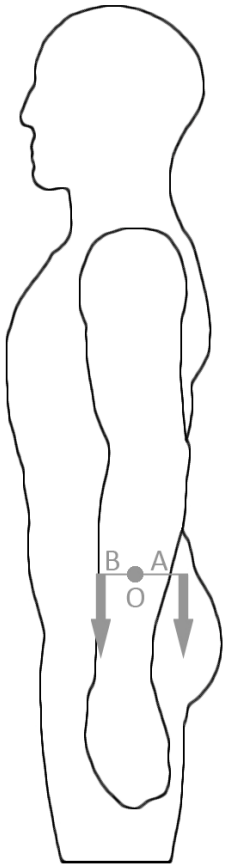

Figure 13: The lever arms due to postvertebral muscles (A) and body weight (B) from the centre of rotation (O).

With reference to Figure 13, let the static equilibrium of an average person of 70 kg standing upright be considered. It is assumed that the lever arm 'B', due to the weight of the torso and head, with respect to the centre of rotation, labelled O in Figure 13, is approximately 20 mm [3], the mass of the torso and head is approximately 60-65% of the total weight of a person [3, 37], and the lever arm 'A', due to the postvertebral muscles is 50 mm [3, 28]. To maintain equilibrium the required force from the muscles will be approximately 180 N. This results in an overall compressive load on the L4-L5 level of 625 N.

If the above example is used with the addition of a 10 kg object carried in front of the torso, with a lever arm of 200 mm with respect to the centre of rotation (Figure 14), the force required from the postvertebral muscles to maintain equilibrium will increase from 180 N to 570 N, thus increasing the overall compressive load on the L4-L5 level to 1110 N.

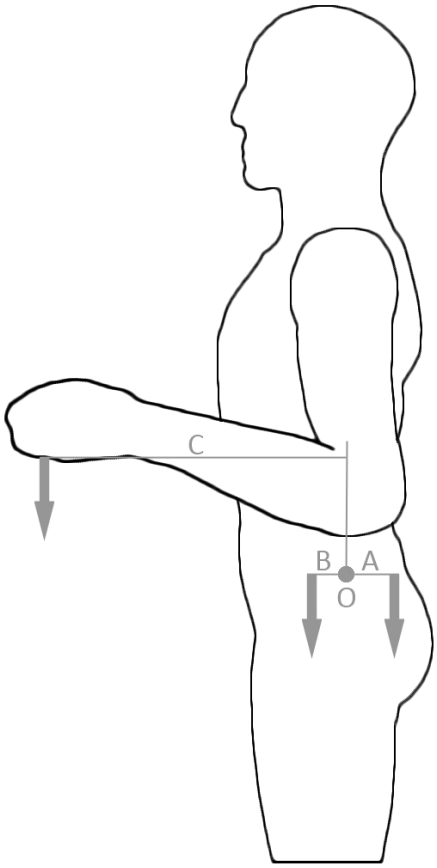

Figure 14: The lever arms due to postvertebral muscles (A), body weight (B), and an object carried in front of the torso (C) from the centre of rotation (O).

Posture affects the length of the lever arms through which loads are applied to the spine [3]; thus affecting the resulting loading on the spine. Forward bending is a posture often adopted when lifting objects from the floor, this strategy results in an increase of the lever arm of the weight component of the torso and head, and an increase of the lever arm of the force exerted by the object being carried. If the above example is modified to a forward leaning posture (Figure 15), the lever arm of the weight of the upper torso and head may increase from 20 mm to 80 mm, and the lever arm of the object being carried may increase to 300 mm, then the postvertebral muscle force will increase to 1300 N. In this case the L4-L5 level is no longer perpendicular to the loads and thus the loading due to the bodyweight and object will result in a compressive load and a shear load.

Evidently the bigger the load lifted the greater the effect on the spine. This can be easily seen by replacing the 10 kg mass in the above example with a 20 kg mass. In this case the postvertebral muscle force will increase from 1300 N to 1900 N.

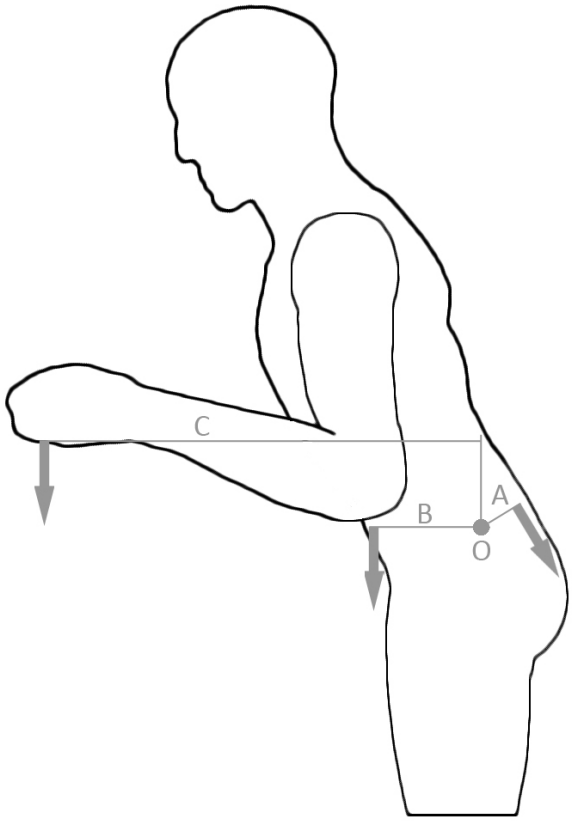

Figure 15: Leaning forward whilst lifting increases the lever arms of the torso weight (B) and of the object being lifted (C) from the centre of rotation (O).

It is through such movements and postures, that create large lever arms of the torso and head compared to the postvertebral muscles, that compressive forces of several thousand Newtons can easily be reached in the lumbar spine.

Nachemson [30] demonstrated that different postures greatly affected the intradiscal pressures, with forward flexion and rotation increasing the pressure by 400% compared to upright standing. Wilke et al. [38] quantified the changes in the intradiscal pressures in human subjects as they assumed various postures and completed a number of different tasks such as climbing stairs and lifting weights (Figure 16). Ledet et al. [39] measured the compressive loading of lumbar spine using sensor-embedded disc implants being placed into the intervertebral disc space of baboons; a load of more than 4 times in BW was measured in a flexed sitting position. Additionally to posture affecting intradiscal pressures [3, 5, 30, 38, 40, 41], Adams et al. [5] showed that posture can affect stress distribution within the zygapophyseal joints.

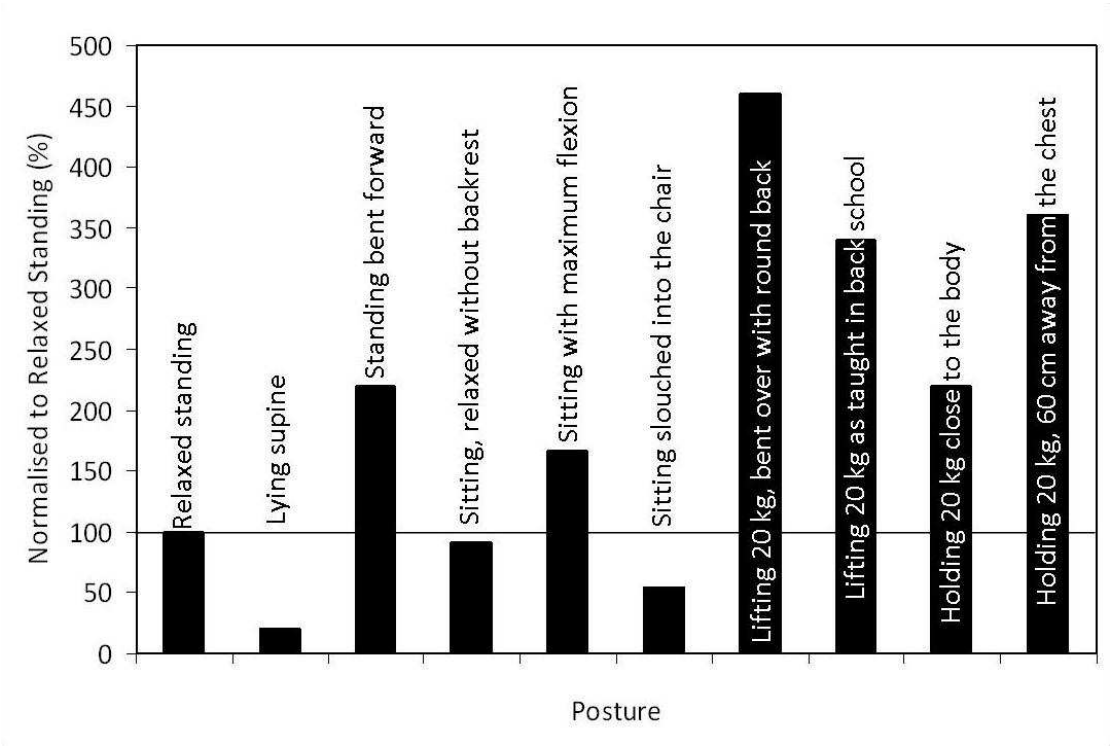

Figure 16: Intradiscal pressure in different postures, normalised to upright standing [38]

Activity level alters the muscle forces so if the spine is suddenly and unexpectedly loaded, muscles often overcompensate and create a higher force than required, ultimately resulting in higher spinal loads [31]. In walking or running peak loads occur twice during the gait cycle, due to the foot strike of each leg [28]. Axial compression during walking at L4-L5 is approximately 1.2-2 times BW [42], though forces much higher, up to 5-6 times BW, can occur in higher activity situations [28], such as jumping and landing. Manual handling often creates large loads in the spine. This can be due to a combination of the magnitude of loads that may be lifted, and the postures assumed when doing so [42-44], but also due to situations in which loads may be lifted quickly, or when sudden and unexpected loads are experienced [29, 31].

Though the largest forces in the spine are often experienced in the direction of axial compression, it is rare that a vertebral level will be perpendicular to all applied loads. This can create shear forces, often in the sagittal plane, that can be in the region of 140 N in normal walking [42, 43], but be as high as 1000 N in extreme events [43, 44]. In the example above of carrying a 20 kg mass whilst leaning forward (Figure 15), if the L4-L5 disc was angled at approximately 20° from the horizontal, the resulting axial compression would be nearly 2500 N and the shear in the sagittal plane would be approximately 220 N.

3 BACKPAIN

3.1 The Economic Impact of Back Pain

Back pain is a common complaint [9-11], and the impact of back pain on society is enormous. In the US back pain is the one of the most common reasons for sick leave [45] and represents the leading cause of lost wages [46]. In the UK in 2006 the Health & Safety Executive reported that one in every six working days lost is due to back pain, equating to 4.5 million working days and £335 million in losses to employers [47]. It is estimated that 80% of the British population will suffer from back pain at some point in their lives [47, 48]. The total health care costs in the UK are in the region of £1.6 billion per year [48]. Such figures are estimated to be similar in other western populations, and suggest that back pain is more of an economic burden than many other common illnesses [11].

With back pain being such a major problem throughout the general population, and the detrimental effects that this has on the economy, it is no surprise that the spinal implant market forms a large sector of the total orthopaedic market [49]. In recent years the spinal implant sector has demonstrated greater growth than any other orthopaedic market [50], with approximately 15.3% growth in 2008 to $6.8 billion [49]. The future value of the global spinal implant market is estimated at over $12 billion in 2017 [51], with a U.S. share of $8-9 billion by 2016-2017 [51, 52].

3.2 Introduction to Back Pain

Injury of the spine may result from normal physiological loads being applied to weak tissues, or from excessively high loads being applied to healthy tissues [32]. In the lumbar region, a sudden event such as stumbling whilst carrying a heavy object can result in excessively high forces. Damage is often a result of excessive muscle forces produced because of the alarming nature of the event [5, 31]. In the cervical region, serious injury from excessive loading most commonly occurs as a result of a head impact [53]. Furthermore, if the spine is loaded less due to back pain, it is possible that the tissues will weaken, predisposing the person to injury under otherwise normal loading conditions [32, 54].

Injury may also result from mechanical fatigue, which might manifest itself as fatigue fractures in the vertebral body or as damage to the disc [32]. Fracture of the vertebral body

is a particular problem in the elderly, who are more likely to be affected by osteoporosis [3, 32]. Damage to the vertebral body may indirectly result in pathology in the adjacent intervertebral discs if the integrity of the vertebral endplates is disrupted [5, 55].

The intervertebral discs are often implicated as a source of back pain [7, 17, 32], and this has been shown to be the case in damaged discs [4]. Pathologies include disc prolapse, annulus fibrosus ruptures, annular tears, endplate damage, and degenerative disc disease [5].

Loading the spine, through exercise, to improve tissue strength has been shown to improve non-specific chronic low back pain [56, 57]. It has been shown that a 4 week exercise program after microdiscectomy improves pain, hip and lumbar mobility, and reduces back muscle fatigability and disability compared to a non-exercising control group [54].

In many cases the cause of back pain is not attributable to the vertebrae or damaged discs and remains unclear [10, 12, 17]. This may be due to the difficulty in diagnostically locating the source of the pain in any given patient [5, 10]. There are many structures within the spine, all of which may become damaged, and which may result in pain. This includes possible damage to ligaments or muscles, damage to the facets or vertebral bodies, in addition to pathology in the intervertebral discs.

Psychological and psychosocial circumstances play a noteworthy role in back pain behaviour, though this does not tend to influence the cause of back pain, but rather the patient's response to its treatment [5, 10, 32].

3.3 Disc Degeneration

Spinal degenerative disease is thought to affect approximately 70-80% of the general population [58] and degenerative disc disease is an extremely common form of such degeneration [7, 12-14]. Genetic inheritance and loading history are both thought to be the main causes of intervertebral disc degeneration [32]. Ageing is also a key factor in degeneration of the discs [5, 7, 32, 55].

Over time a degenerating disc may lose fluid from the nucleus pulposus, which can alter the way loads are transferred to and from adjacent vertebrae [4, 7]. Adams et al. [59] in a study of the load bearing ability of degenerated cadaveric discs reported a reduction in pressure of

30% in the nucleus pulposus and a compressive peak stress increase of 160% in the annulus fibrosus compared to healthy discs. The annulus fibrosus may lose integrity, often collapsing into the nucleus [5]. This is likely to arise from the loss of fluid and the loss in pressure in the nucleus (Figure 17). The loss of fluid can lead to a loss of disc height and can eventually result in the vertebral endplates contacting each other. Additionally, a loss in disc height may alter the biomechanics of how the vertebral level behaves as a whole, as increased load may be carried by the facets. Pollintine et al. [8] demonstrated that in a healthy disc the facets transfer 8% of compressive loading, but with a severely degenerated disc this can increase fivefold to 40%.

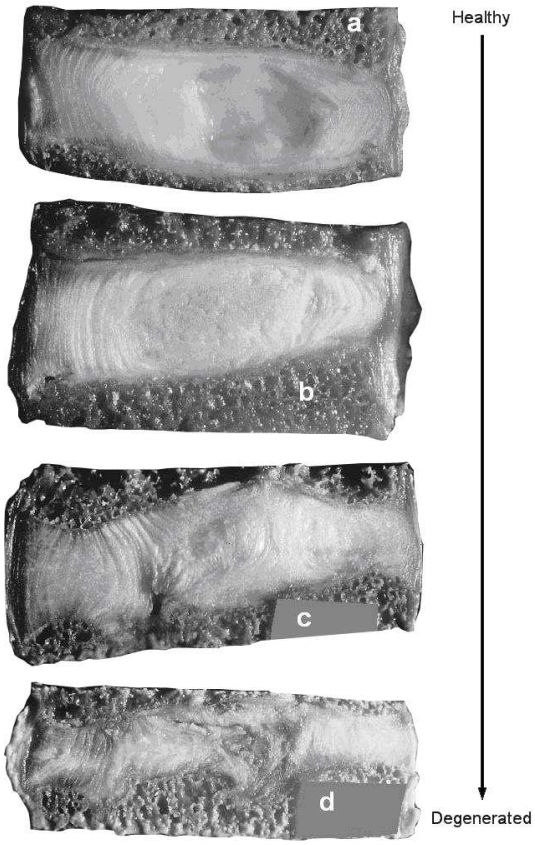

Figure 17: The degeneration of intervertebral discs. Modified from Adams et al. [59]. (a) A healthy disc. (b) Slight degeneration, the nucleus is fibrous and there is less of a boundary between the nucleus pulposus and the annulus fibrosus. (c) Mild degeneration with fluid loss in the nucleus pulposus and part of the annulus collapsed internally. (d) Severe degeneration, little fluid remains, there is a large loss in height, and there is damage to the vertebral endplates

3.4 Current Treatments for Back Pain

As with many degenerative conditions non-operative interventions are generally pursued before surgery. Exercise regimes have been shown to improve back pain, though specifically for degenerative disc disorder (DDD), non-operative intervention may also include anti-inflammatory medication, adjusting activities to try to reduce pain, and pain management [6, 60].

If these methods fail to provide patient satisfaction surgery might be considered. A surgical procedure may achieve pain relief and allow daily activities to be completed relatively freely on the part of the patient.

3.4.1 Microdiscectomy

Microdiscectomy can be performed to treat moderate DDD [13]; this aims to reduce pain by removing disc material that may be impinging nerves [6]. Microdiscectomy may be followed by a full discectomy and then by fusion if pain persists [6, 13].

3.4.2 Fusion

The first spinal fusion (or arthrodesis) was carried out by Albee and Hibbs in 1911 [4]. This is now the gold standard for the treatment of severe degenerative disc disease [13, 15, 16]. Arthrodesis surgery aims to completely eliminate motion at the operative disc level. It is postulated that the stabilisation of the level and prevention of articulation between the adjacent vertebrae will reduce pain [6].

Fusion procedures are often reported to result in accelerated degeneration of adjacent levels [17, 50, 61, 62]. This is referred to as adjacent segment degeneration, which may not necessitate any further intervention [63, 64]. By contrast, symptoms resulting from adjacent segment degeneration may be referred to as adjacent segment disease, and require further treatment [63, 64]. The causes of adjacent segment degeneration are not fully understood, and biomechanical studies have reported varied results [65], though it is generally accepted that the altered biomechanics of the vertebral column due to the fusion may accelerate degeneration at adjacent levels. Biomechanical studies have shown that post-arthrodesis,

patients often have a similar overall ROM compared to healthy subjects, this is accomplished by producing a greater ROM in the levels adjacent to the fusion level [61, 64]. It is the increased ROM that can lead to increased stress and strain at the levels adjacent to the fusion, which, in turn, might increase the rate of their degeneration [9, 17, 18].

It is often difficult in clinical situations to determine to what extent the degeneration that occurs in levels adjacent to a fused level is directly attributable to the fusion or to the natural progression of the underlying degenerative disc disease [63, 64].

Fusion results are often marginally more successful than non-operative treatments, in terms of the visual analogue scale for pain (VAS) and the Owestry disability index (ODI) outcome measures [10]. As a result, surgeons and patients alike are becoming less satisfied with the mixed long term results of spinal fusion [6, 44]. In a 10 year follow-up of the lumbar I/F Cage Brantigan et al. [66] reported that clinical success was achieved in 29 of 33 patients (87.8%). However, adjacent segment degeneration had developed in 61% and was clinically significant in 20% of the patients; with 5 patients (16 %) requiring fusion procedures at adjacent levels.

The Bagby and Kuslich cage (BAK; Zimmer Spine Inc., Warsaw, IN, USA) is a threaded interbody fusion cage, which is screwed into the intervertebral disc space. The device is used in conjunction with iliac crest bone graft to aid fusion through bone ingrowth. The BAK cage was approved by the FDA in 1996 [67], and was the first anterior cage to receive such approval [68]. As a result, the BAK cage was used as the control device in the first FDA clinical trial a total disc replacement device. The device was originally produced by Spine-Tech (Spine-Tech, Minneapolis, MN, USA) which was acquired by Sulzer for $595 million in 1998 [69, 70]. Sulzer Medica spun off from Sulzer in 2001, was renamed Centerpulse AG in 2002, and was acquired by Zimmer in 2003 for $3.2 billion [70-72].

Good fusion combined with low complication and revision rates with the BAK device haven been reported in the two-year follow-up results submitted to the FDA [73] and in published literature [74, 75]. However, Button et al. [76] reported that many of the positive results published were by designers of the device, used varied operative techniques or had follow-up rates as low as 25 %. The same paper by Button et al. reported the results for a cohort of 46 patients that underwent fusion surgery for one or two levels using the BAK cage. All procedures were completed by the same surgeon over a period of two years. Of the thirty

three patients that were followed-up there was a 30 % rate of non-union, a 22 % revision rate, and a 22 % complication rate. The study called into question the use of BAK cages without further instrumentation. Indeed, the BAK cage is no longer in general use [5, 77].

Bono et al. [78] reported that between 1979 and 2000, while trends in fusion procedures and devices significantly changed, the overall fusion rate and clinical outcomes remained unchanged. This has led to an increase in the popularity of motion preserving techniques, though developments in this field must be carried out with caution due to limited long-term follow-up available.

3.4.3 Disc Arthroplasty

The complicated nature of the spinal joints has resulted in spine arthroplasty lagging behind the development of other joint replacements such as the hip and knee, which have steadily improved in clinical outcome [6, 22, 23], with 10 year survivorship often exceeding 90% [79, 80].

Disc arthroplasty aims to restore the natural biomechanics of the spine, providing motion at the degenerated level, and in doing so, avoid the long-term complications associated with fusion procedures, in particular adjacent segment degeneration [9, 13, 20, 21]. By restoring natural biomechanics of the vertebral column it is hoped that that recuperation will be faster than with fusion [13, 24], and complications associated with fusion will be avoided [20]. There are currently two main methods of restoring motion to a severely degenerated disc: nucleus replacement and total disc replacement.

3.4.4 Nucleus replacement

Nucleus replacement procedures were first developed by Nachemson in the 1960s, consisting of the injection of a curing polymer into the nucleus through the annulus fibrosus [6]. The earliest patent for a nucleus replacement is that of Frowning, filed in 1975 and comprising a flexible bladder that is inserted into the nucleus pulposus and filled with a fluid [81]. There have since been a large number of patents, though few have been developed to the stage of commercial products. The major factor in the development of nucleus replacements is the ability to design and manufacture materials that reproduce the

mechanical properties of the natural nucleus [82]. Further to restoring the mechanical properties of the nucleus, material developments have led to the concept of restoring the physiological properties of the nucleus [6]. Since the development of hydrogel, many patents have been filed that are designed to expand in-situ, allowing for a smaller incision in the annulus [83, 84]. Memory-shape designs have also been developed to allow elongated devices to be inserted into a small annulus incision, before coiling up in the nucleus [82, 85, 86].

To date, no nucleus replacements have been approved by the FDA, though there are a small number that are approved in Europe or under investigational use in the US. Examples of such devices are the PDN (Raymedica, Inc., Bloomington, MN, USA), the Hydraflex (Raymedica, Inc., Bloomington, MN, USA), the Dascor (Disc Dynamics, Inc., Eden Prairie, MN, USA), and the Neudisc (Replication Medical, Inc., Cranbury, NJ, USA).

4 TOTAL DISC ARTHROPLASTY

4.1 History and development of disc arthroplasty

The first lumbar disc replacement was carried out in 1956 by Fernström, comprising a simple steel ball inserted between vertebral bodies [12, 50, 60, 87, 88] (Figure 18). Fernström completed this procedure in over one hundred patients [12, 89]. Initial outcomes published by McKenzie in 1972 were promising [90] and early outcomes appeared to be similar to fusion [12, 60, 89]. However, complications included a tendency for the steel ball to subside into the vertebral endplates and bodies [12, 60, 87]. The incidence of this was reported as being as high as 88% in a 4-7 year follow-up [50]. This major complication has been held responsible for the termination of the procedure [12]; though it is possible that the underlying reasons ultimately resulting in this termination may have been due to the poor outcomes compared to the vast improvement in success rates of total hip and knee replacements at that time.

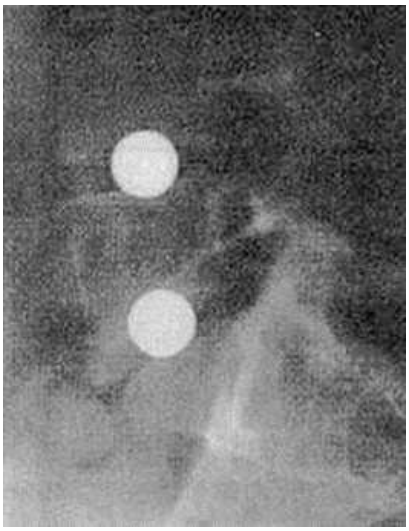

Figure 18: Fernström's steel ball bearings inserted in the intervertebral disc space. Subsidence in to the vertebral endplates can be seen [87]

Although initially used for the treatment of lumbar back disorders, 75 Fernström devices were also implanted in the cervical spine [88]. Again, initial results were promising [88, 89, 91] but the procedure was troubled by the same subsidence complications associated with the lumbar implants [88].

Since Fernström's early procedures there have been hundreds of patents for intervertebral disc prostheses. Of these wide ranging designs, only a very small number have been clinically used [12]. Many patents do not specify whether the design is for the lumbar or cervical spine. Different implant designs are generally used for the different areas of the spine, though devices may only be modified for this alternative application.

Fassio developed and patented an elastic design in 1976 [92] comprising a central silastic sphere and a synthetic resin incompressible plateau [12, 87] (Figure 19). This device was implanted in three patients but was affected by similar subsidence problems affecting the Fernström spheres [12, 87]. It was also found that, over time, the ROM provided by the implant was limited [12].

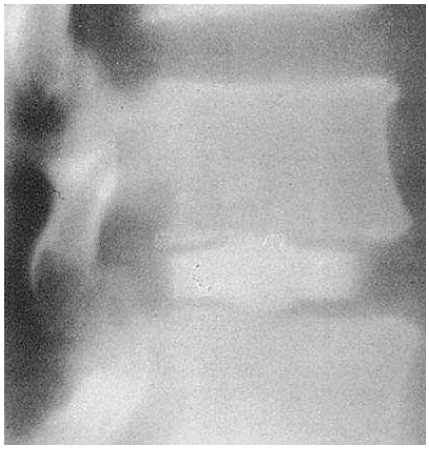

Figure 19: An x-ray of a Fassio device [12]

Intervertebral disc replacements became more frequent in the late 1980s, though the number of disc designs was still limited. It was in the 1990s that a great deal more patents of intervertebral discs were filed; and only in the 21st Century that more than a handful of designs have been used clinically.

4.1.1 Charité

Figure 20: The In Motion artificial disc, the latest version of the Charité design

The Charité lumbar disc was first developed by Buttner-Janz and Schellnack in 1982 and first used clinically in 1984 in the lumbar spine [12, 93]. The endplates were modified and the Charité II disc was patented in 1984 [93, 94]. The Charité III was patented by Keller in 1988 through Link Waldemar GMBH [95], which later produced the device via the subsidiary company, Link Spine Group. This design has remained relatively unchanged since, and is now produced by DePuy Spine (DePuy Spine, Inc., Raynham, MA, USA), after DePuy AcroMed acquired the Link Spine Group in 2003 at a cost of $375 million [96]. The latest version of the Charité disc is called the In Motion disc (Figure 20), which differs from the Charité III only in the endplate design, to aid implantation using improved instrumentation.

The principal design characteristic of the Charité disc consists of a biconvex core articulating on concave inner surfaces of the endplates to form a double ball and socket joint with a variable centre of rotation. The Charité was designed with the low-friction articulating surfaces of hip and knee prostheses in mind, and specifically the mobile sliding core design of knee replacement devices [93]. Attachment to the vertebral endplates is achieved with spikes and via bone ingrowth into a porous coating called TiCaP™ (Huys Industries Limited, Toronto, Ontario, Canada) [97].The disc is now one of the most well established artificial lumbar discs and was the first artificial lumbar intervertebral disc to be approved by the FDA [98].

O'Leary et al. [99] reported a significant increase in flexion/extension and lordosis with the Charité disc compared to an intact disc during in-vitro testing, both without axial preload and with an axial preload of 400 N.

Zeegers et al. [100] reported satisfactory clinical results in 70% of patients receiving a Charité total disc replacement at 2 year follow-up, though it was also reported that 18% of the devices were placed asymmetrically. A similar level of suboptimal or poor placement (17%) was reported by McAfee et al. [101], with such positioning significantly affecting the ROM.

Several papers have been published based on the FDA IDE clinical trial of the Charité disc [101-104]. The trial was designed to demonstrate the non-inferiority of the Charité disc compared to the BAK stand-alone cage fusion.

Blumenthal et al. [103] reported shorter hospitalisation and lower rates of reoperation, combined with significantly higher patient satisfaction at 24 months with the Charité lumbar disc replacement compared to anterior lumbar interbody fusion. However, these satisfaction questionnaires might well be deemed invalid because, although the study was randomised, it was not blinded. Patients wishing to take part in the study would generally be of the opinion that the Charité disc would be at least as good as the fusion alternative, else they would not agree participate in the study. Therefore it cannot be excluded that those patients receiving a Charité disc as part of the study would be more satisfied with their procedure than those randomised into the control group [68]. Blumenthal et al. [102] also reported that, at the 24 month follow-up, there was no significant difference in either the Oswestry Disability Index (ODI) or Visual Analogue Scale (VAS) clinical outcome scores.

The VAS is a scale that patients mark in response to a question, and is commonly used as a means of rapidly acquiring a measure of pain [105]. The ODI was designed to measure how lower back pain affects a person's ability to cope with daily living [106]. The questionnaire is multiple-choice and comprises ten questions, each with six responses. The scoring ranges from 0-5 for each response and a percentage of disability is calculated based on the answers, with 0 % being the lowest level of disability and 100 % the highest. Since the publication of the questionnaire in 1980, it has become one of the most commonly used outcome measures for spinal surgery [107]. Short Form 36 (SF-36) is also commonly used to assess patients. The form comprises 36 questions, the responses to which provide a health profile and a measure of quality of life in relation to health [108].

The FDA IDE trial was designed in such a way that it could not demonstrate superiority of the Charité, it could only demonstrate whether or not the Charité was inferior to the fusion control group [109]. It is also the case BAK stand-alone cage fusion procedures have rarely been carried out in recent years due to poor clinical results [110]. This means that the clinical trial of the Charité could only demonstrate that the device was not inferior to what is now regarded as a poor method of fusion. It has also been widely reported that by using a comparison with such a device, and through the methods used in the trial, bias toward the Charité group was introduced [109-111].

Among the outcome measures of the trial was flexion/extension ROM, however this parameter did not constitute part of the FDA approval criteria for the device [112]. The FDA regards clinical success in fusion if the operated level has less than 5° of motion. In the clinical study of the Charité device, 70 of 178 patients (39 %) that received a Charité device had a fusion according to the FDA limit [77]. Whilst this definition of fusion is widely accepted, it is worth noting that, adjacent levels characterised by close to 5° of motion, biomechanically cannot be considered as adequately fused.

This limitation was implicitly recognised for the ProDisc FDA clinical trial, which was the first total disc replacement trial to have ROM as a measure of success. In this trial a lower limit to ROM was imposed at 3°, with procedures failing to achieve this threshold being classified as failures [113, 114].

The full report of the Charité trial to the FDA indicates that there were 40 patients of 178 measured (22 %) with 3° or less motion in flexion/extension [115]. The same report declared that during the two-year follow-up there were 15 (7.3 %) device-related adverse events in the Charité group, and 4 (4.0 %) in the BAK control group [110, 115]. Concern has been raised as to why this data was omitted from the initial publication of the results of the FDA trial [110].

Following the approval meeting of the Charité device and concerns about the long-term outcomes [109], DePuy proposed a post-approval study that would follow-up all randomized patients involved in the study for a total of five years to establish longer-term results for the Charité device compared to the BAK fusion procedure [112]. Guyer et al. [113] reported the results of this post-approval study. There were no significant differences in clinical outcomes between single-level Charité total disc replacement and anterior interbody fusion at five

years follow-up. However, the original dataset is yet to be made publically available on the FDA post-approval studies database.

The length of follow-up represents another limitation of the initial trial, which was only designed to be two years long, resulting in only 133 patients (90 with Charité discs, 43 with BAK fusions) of the original 304 (43.8 %) in the trial being followed-up for the full five years. Of those followed-up, in the Charité group, there were 17 cases (18.9 %) with less than 5° ROM, and 14 cases (15.5 %) with less than 3° ROM. It has also been reported that the way in which the study was followed-up, and the patients that did and did not continue in the study, led to further bias toward the Charité group, and the "bogus inflation of device failure [in the BAK control group], which was artificially produced by selected dropout" [110]. Such mid-term follow-up studies do not bode well for the establishment of good long-term data on total disc arthroplasty and the potential it has to improve the clinical outcome of patients undergoing surgery for severe disc degeneration disease.

Lemaire was one of the named inventors in many of the Charité patents filed by Link Waldmar GMBH [116]. Lemaire et al. [117] published the clinical results of 100 patients implanted with 147 Charité total disc replacements between 1989 and 1993, with a minimum follow-up of 10 years (mean 11.3 years). The original cohort comprised 107 patients. It was reported that 62 % had an excellent outcome, 28 % a good outcome, and 10 % a poor outcome. At the latest follow-up 5 patients had retired and 91.6 % of the remaining 95 patients had returned to work, with 80 % returning to the same level of employment as prior to the total disc arthroplasty. The mean ROM was 10.3° in flexion/extension and 5.4° in lateral bending, there were 9 patients with less than 2° flexion/extension. The complication rate of 9 % was good compared to other published data, though it should be noted that the FDA trial published much more data regarding the follow-up. The clinical outcome measures used a modified Stauffer Coventry scoring system, rather than the VAS, ODI, and SF-36 that are generally used in such studies, making comparisons problematic.

Putzier et al. [118] reported the clinical results of 84 Charité I-III total disc replacements in 71 patients with 53 patients available for an average follow-up of 17 years. In this study, 60 % of the operative levels resulted in spontaneous ankylosis, and 23 % required fusion procedures at the operative level due to implant failure or pain. For the 17% that were functioning after 17 years, adjacent segment degeneration was not observed, though patient satisfaction was lower than those patients with spontaneous ankylosis.

4.1.2 Acroflex

Figure 21: The Acroflex artificial disc [12]

The Acroflex lumbar disc (DePuy Acromed, Raynham, MA, USA) (Figure 21) was developed by Steffee; the first patent was filed in 1989 [119]. The design comprised two rigid endplates separated by a rubber core. The device was implanted in 6 patients with varied results. Carcinogenic properties of a chemical used in the production of the core led to the discontinuation of the device [12]. The design was redeveloped in 1997, using a silicone core and modified endplates [120]. Clinical results failed to correspond suitably to pre-clinical testing and the device was subsequently withdrawn after a small number of implantations [12].

4.1.3 ProDisc

Figure 22: The ProDisc-L disc. Courtesy Synthes Ltd. (Synthes Ltd., Herts, UK)

The Prodisc-L lumbar disc (Figure 22) was developed by Marnay and Beyersdorff in the 1980s, though the first patent resembling the ProDisc-L was not filed until 1999 [121]. The IP rights to the ProDisc-L have been owned by a number of orthopaedic companies including Aesculap and then Spinal Solutions; the latter of which was acquired by Synthes Spine in

2003 [122], who now manufacture the ProDisc-L (Synthes Spine, Inc., West Chester, PA, USA). The ProDisc-L was approved by the FDA in 2006 [123].

Marnay and an associate first implanted the devices into 64 patients between 1990 and 1993 and then waited to assess the in-vivo performance before performing more procedures with the device [124, 125]. In 1998 there had been no device-related failures and 93% of the 58 patients available for follow-up were satisfied with their implants [125]. Huang et al. [21] reported the ROM and adjacent level degeneration of 42 of the 64 patients enrolled in the original study, after a mean follow-up of 8.7 years. Only 31 % of patients had greater than 5° of motion, though none of these patients were found to have adjacent level degeneration. Of the 69 % of patients with less than 5° of motion, 34 % had adjacent level degeneration. Huang et al. [126] also published data about the same 42 patients with the same mean follow-up of 8.7 years, reporting that 34 % had no motion at the operated level. No motion was regarded as anything less than 2°, due to possible error in the measurements. However, no patients had required further surgery. The mean ROM was 3.8° (SD 2.0°), which is barely above the minimum motion required for success in the FDA trial of the ProDisc. Huang et al. [127] also reported significant correlations between range of motion and clinical outcome in 38 patients with 51 ProDisc lumbar disc replacements after a mean follow-up of 8.6 years. Patients with a ROM of 5° or less in flexion/extension suffered significantly worse clinical outcomes than patients with greater than 5° of motion at the operated level.

Chung et al. [128] reported a prospective study of 47 ProDisc-L devices being implanted into 36 patients with a minimum of 2 years follow-up. All outcome measures were significantly improved post-operatively, with 16 patients having an ODI improvement of greater than 75%. Disc height and ROM were also significantly increased, with a mean ROM in flexion/extension of 12.7° at the 2 year follow-up. There were two approach related complications but no device related complications.

Zigler [125] reported a prospective randomized study comparing the ProDisc-L with 360° fusion, though the follow-up was only 12 months. Six month follow-up results were available for 55 patients with ProDisc-L devices, and 23 patients with fusion procedures. Blood loss and hospitalisation were significantly lower and ROM at 6 months was significantly higher for the ProDisc-L group. Clinical outcome measures and patient satisfaction both improved significantly post-operatively in both groups, and there was no difference between them. The flexion/extension ROM was not reported in degrees, which makes comparisons with

other studies difficult. Similar results of a six-month follow-up were reported by Delamarter et al. [129], with improvements in clinical outcomes post-operatively but no significant difference between the ProDisc group and the fusion control group.

The FDA trial for the ProDisc was the first total disc replacement trial that used ROM as a measure of success, in addition to clinical outcome measures. The full report of the FDA trial shows that 32 of the 116 patients (28 %) had a flexion/extension ROM of 3° or less at the 24 month follow-up [114]. However, the FDA granted approval for the disc, having viewed the data as successfully demonstrating non-inferiority to the circumferential fusion control group. The study has become noteworthy following the approval due to the potential conflicts of interest that many of the consulting surgeons had, yet did not disclose to the FDA [130]. This has resulted in three of the surgeons being fined for professional misconduct [131]. Such circumstances lead to a lack of confidence in the published material, and in the device itself.

Figure 23: The ProDisc-C disc. Courtesy Synthes Ltd.

Synthes Spine now also produce a ProDisc-C artificial cervical disc (Figure 23) developed by Marnay and Beyersdorff et al. in 2002 [132]. This has a similar ball socket, metal and polyethylene articulation as the ProDisc-L. The ProDisc-C received an approval letter from the FDA in October 2007 [133]. Bertagnoli et al. [88] reported the 12 month follow-up of 20 ProDisc-C devices implanted in 16 patients. Both pain and functional outcome scores improved post-operatively, no patients reported being unsatisfied during the follow-up period, and there were no cases of spontaneous ankylosis. A study by Nabhan et al. [134], which compared the ProDisc-C to anterior cervical discectomy and fusion with a one year follow-up, reported that the ROM decreased over time for both groups, though the loss of ROM of the fusion group was significantly greater than the ProDisc-C group. A reduction in pain was reported with no differences in clinical outcomes between the two groups.

4.1.4 Prestige

Figure 24: The Prestige disc [135]

The Prestige cervical disc (Figure 24) was developed by Gill et al. in 1998 [136]. Its design originates from an earlier metal on metal, more constrained ball and socket artificial disc, conceived in the early 1990s and used in a small number of patients [137]. The Prestige comprises stainless steel endplates with flanges that are screwed into the anterior sides of the vertebral bodies. The superior endplate has a convex protrusion that articulates on a concave and flat articulation surface on the lower endplate. The articulation surfaces are designed so as to create an unconstrained ball and socket joint, and thus limited translation and rotation in the coronal and sagittal planes is permitted, in addition to unlimited axial rotation.

Following initial clinical experience several design modifications were made to the original Prestige design. This lead to the successful clinical trial of the Prestige ST disc (Medtronic Sofamor Danek, Inc., Memphis, TN, USA), which, in 2007, became the first artificial cervical disc to be approved by the FDA [138]. The latest version of the Prestige disc is the Prestige STLP [139], which differs from the Prestige ST in the attachment of the endplates to the vertebral bodies; rails on the device endplates provide initial fixation to the vertebral endplates and the anterior flanges of the Prestige ST have been reduced in size to allow multi-level implantation.

Clinical results of the Prestige device have shown similar outcomes to fusion procedures. Sawin et al. [140] reported 24 month results of 118 patients that were part of a multi-centre randomised controlled trial that compared the Prestige ST device with allograft and anterior cervical plating. This study found no significant differences between the two groups in terms of blood loss or hospitalisation. Clinical measures improved post-operatively in both groups.

Radiographic measures showed that the Prestige disc maintained or restored motion at the operated level. Similar results were found in studies by Burkus [141] and by Ceola and Mace [142].

4.1.5 Bryan

Figure 25: The Bryan disc [143]

The Bryan cervical disc (Figure 25) was initially developed by Bryan et al. in 1993 [144] and patented in 2000 [145]. The Bryan disc is now produced by Medtronic Sofamor Danek and received FDA approval in 2009 [146]. The device comprises two titanium endplates with concave inner surfaces that articulate on a resilient biconvex polyurethane core. An elastic polyurethane membrane surrounds the core and seals a lubricant inside. The endplates are attached to the vertebral bodies via bone ingrowth into a porous surface and with screws via flanges. The disc is designed to allow limited motion in all six degrees of freedom [12, 145].

Sasso et al. [147] reported significantly improved clinical outcomes with the Bryan cervical disc replacement compared to fusion at two year follow-up. The Bryan disc group of 35 patients was characterised by a higher ROM at the operated level compared to the fusion group of 36 patients. There were five re-operations, four were in the control group and one in the Bryan group.

The four year follow-up of 63 patients with Bryan cervical disc replacements was reported by Goffin et al. [148]. Fifty-five patients had single-level replacements and 8 had bi-level replacements. Four single-level and one disc of a bi-level patient lost mobility. The results also suggest that the Bryan device does not lead to adjacent segment disease, which may be seen with fusion procedures.

4.1.6 Maverick

Figure 26: The Maverick disc [149]

The Maverick lumbar disc (Medtronic Sofamor Danek) (Figure 26) was first used clinically in 2002 [150, 151]. The disc is a two-piece, metal on metal, constrained ball and socket joint, with the centre of rotation toward the posterior of the disc space. Attachment to the vertebral endplates is achieved through keels and via bone ingrowth into a porous surface. A US clinical trial of the Maverick disc began in 2003 and was completed in 2010 [152], though it has not yet received FDA approval.

Gornet et al. [153] reported the initial results of a prospective, randomised, controlled, multi-centre study comparing the Maverick lumbar disc replacement with the LT CAGE with INFUSE Bone Graft control procedure. Patients were randomised in a 2:1 ratio to the Maverick disc. Fifty of 160 the patients enrolled into the study had reached the two year follow-up. Clinical outcomes were significantly improved at post-operative follow-up compared to pre-operative scores. Results are reported as being comparable to clinical outcomes of LT-CAGE with INFUSE procedure, though oddly, no direct comparison is made between the Maverick group and control group in the published material.

4.1.7 Mobidisc

The Mobidisc lumbar disc (Figure 27) was patented in 2001 by LDR Medical (LDR Medical, Troyes, France) [154], and has undergone clinical trials in Europe. It was due to begin FDA trials in the USA in 2007 [155], though no reports of the commencement of this trial were found. The Mobidisc is a ball and socket joint with a mobile polyethylene core. The upper endplate has a concave articulation surface corresponding to the superior articulation surface of the core. The lower endplate has a planar surface corresponding to the inferior

surface of the core. The lower endplate also features lugs to limit the translational motion of the core, which provides a variable centre of rotation. Attachment of the endplates is achieved via keels and a porous surface [156].

Figure 27: The Mobidisc [157]

Figure 28: The Mobi-C disc [158]

In 2002 LDR medical patented the Mobi-C [159] (Figure 28), a cervical version of the Mobidisc. Like the Mobidisc, this has undergone clinical trials in Europe; an FDA clinical trial began in December 2007 [160]. The Mobi-C uses a similar mobile core design to the Mobidisc but with a different configuration of lugs to limit translational motion in the sagittal and coronal planes.

4.1.8 Flexicore and Cervicore

In 2002 Errico et al. [161] patented a lumbar disc with Spinecore Inc. Stryker acquired Spinecore in 2004 and now market the design as the Flexicore disc (Stryker Spine, Allendale, NJ, USA) [162]. The Flexicore device (Figure 29) is a captured metal on metal, ball and socket joint, attached to the vertebral endplates via spikes and bone ingrowth.

Figure 29: The Flexicore disc [149]

Figure 30: The Cervicore disc [163]

Stryker also produce the Cervicore disc (Figure 30), originally developed by Spinecore in 2005 [164]. This is a metal on metal saddle joint, attached to the vertebral endplates via spikes, bone ingrowth and screws [164, 165]. Both the Flexicore and Cervicore are currently undergoing clinical trials.

4.1.9 Porous Coated Motion

Figure 31: The Porous Coated Motion disc. Courtesy of NuVasive Inc. (San Diego, CA, USA)

The Porous Coated Motion (PCM) cervical disc (Figure 31) was invented by McAfee, though further development was completed by Keller and Link, both of whom were also involved in the development of the Charité disc [97]. The disc was patented by Link Waldemar GMBH in 2002 [166], though further patents have been filed since by both Link Waldemar GMBH [167] and Cervitech [168] who produced the PCM disc until being acquired by NuVasive (NuVasive Inc., SanDiego, CA, USA) [169]. The disc is a constrained metal on polyethylene, ball and socket joint with a large radius of curvature. A polyethylene core fits into the lower endplate, the upper surface of the core is convex and the upper endplate has a corresponding concave articulation surface. The endplates are attached to the vertebral endplates with teeth and via bone ingrowth into a TiCaP™ porous coating [97]. Over 6000 such devices have now been implanted worldwide [169].

Pimenta et al. [97] reported significantly improved clinical outcomes at one year follow-up compared to preoperative scores. Eighty-one porous coated motion devices were implanted into 53 patients, 28 single-level, 22 bi-level, and 3 tri-level. Complications were limited to one case of ankylosis, and the displacement of one device anteriorly by 4mm, which did not result in any clinical symptoms.

4.1.10 Discocerv (Cervidisc Evolution)

Figure 32: The Discocerv disc (left); and a view of the ceramic core parts (right) [170]

In 2000 Scient'x filed a patent for a cervical disc prosthesis comprising titanium endplates with ceramic core parts that create a constrained ceramic on ceramic, ball and socket joint [171]. Later patents illustrate a developed design [172], which is marketed as the Discocerv (Scient'x-Alphatec Spine, Bretonneux, France) (Figure 32). One thousand devices have been implanted worldwide as of 2007 [173].

Ramadan et al. [170] reported the clinical results of the Discocerv, which only had a 3 month follow-up. In this study, 17 patients underwent a one or two level disc replacement. Results were good and patients satisfied, though it was not reported if clinical outcome measures were significantly better than preoperatively. Radiographic analysis showed restoration of motion at the operated levels, with a mean flexion/extension of 4.9° ± 5.6° and mean lateral bending of 8.4° ± 4.1°. However, the range of data in flexion/extension was 0 to 19°; meaning that even at three-month follow-up, at least one patient had no motion in flexion/extension.

4.1.11 Kineflex

Spinal motion (Spinal Motion, Inc., Mountain View, CA, USA) patented an intervertebral disc in 2002 [174], which comprises metal endplates with a toroidal polymer core. The endplates are concave, corresponding to the surfaces of the core and have a central peg to contain and limit motion of the core. Spinal Motion subsequently developed a more simple metal on metal, double ball and socket, mobile core device marketed as the Kineflex (Figure 33) and Kineflex-C (Figure 34).

Figure 33: The Kineflex disc [175]

Figure 34: The Kineflex-C disc [175]

Two metal endplates with concave inner surfaces articulate on a biconvex metal core. Attachment to the vertebrae is achieved through keels and via bone ingrowth into a porous surface [176]. The Kineflex has been used clinically since 2002, the Kineflex-C has been used clinically since 2003. Hahnle et al. [177] reported the two year results of Kineflex lumbar disc replacement procedures. Seventy five patients received 100 devices, though only 72 patients were available at the two-year follow-up. There was a significant improvement in clinical outcome scores compared to preoperatively with results for 61 of the 72 patients reported as being excellent or good.

4.1.12 Spinal Kinetics

Spinal Kinetics (Spinal Kinetics, Inc., Sunnyvale, CA, USA) was founded in 2003 and patented the M6 artificial cervical disc [178] (Figure 35). The disc incorporates a viscoelastic polymer nucleus surrounded by an annulus structure of polyethylene fibres and an outer sheath. The design aim is to replicate the mechanical properties of the natural intervertebral disc as closely as possible with limited motion in 6 degrees of freedom [179].

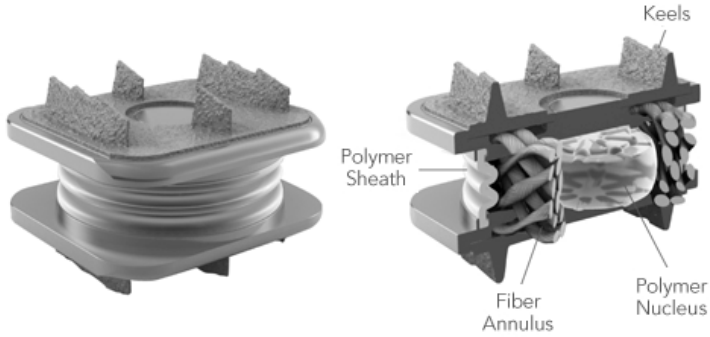

Figure 35: Spinal Kinetics M6 disc (left), and cross sectional view (right) [179]

Cadaveric testing demonstrated that the Spinal Kinetics design had promise [180, 181] and the M6C for the cervical spine was first implanted in 2007. The 10,000th M6C was implanted in March 2011 [182]. The M6L for the lumbar spine was first implanted in 2009 [183]. As yet, no clinical results are available in the literature for either version of the disc.

4.1.13 Secure-C

Figure 36: The Secure-C disc [163]

The secure-C cervical disc replacement (Figure 36) is produced by Globus Medical (Globus Medical, Inc., Audubon, PA, USA) and comprises two metal endplates attached to the vertebrae with protrusions and via bone ingrowth into a porous coating. The endplates are separated by a semi-constrained polymer core that allows a variable centre of rotation, and limited translational motion. An FDA clinical trial began in 2005 [184] though no clinical results were available in the literature.

4.1.14 Discover

Figure 37: The Discover disc [185]

DePuy has developed the Discover cervical disc replacement (Figure 37) using the same metal on polymer, double ball and socket mobile core design of the Charité disc. An international clinical trial of the Discover cervical disc began in 2006 [186]. Preliminary results of a small number of patients (n=25) implanted with the Discover device were promising but larger studies are necessary with long-term follow-up in order to suitably assess the performance of the device [185].

4.1.15 Neodisc

Figure 38: The Neodisc. Courtesy of NuVasive, modified with permission

In 2004 McLeod and Reah patented the Neodisc elastomeric cervical disc replacement [187] (Figure 38), which is now produced by Nuvasive. This comprises a silicone filling material surrounded by an embroidered polyester fabric. The fabric is designed to promote bone ingrowth, and also has extensions for screw attachment to the vertebral bodies. An FDA clinical trial of the Neodisc commenced in September 2006 and is ongoing [188, 189].

4.1.16 CADisc

The CADisc was developed by Ranier Technology (Ranier Technology Limited, Cambridge, UK) in 2002 and uses a novel method of injecting multiple stiffness polymers into a mould [190]. This manufacturing technique results in a one-piece disc with a graduated Young's modulus that is lowest at the centre, and highest at the circumference. The design aims to replicate the stiffness of the nucleus pulposus and annulus fibrosus of the natural disc.

Figure 39: The Ranier CADisc-L. Courtesy of Ranier Technology Ltd. (Cambridge, UK)

Figure 40: The Ranier CADisc-C. Courtesy of Ranier Technology Ltd.

The design was originally used in a lumbar disc, the CADisc-L (Figure 39), which has undergone a European clinical Trial [191]. A cervical disc, the CADisc-C (Figure 40), is now also in production and has been used as part of a European clinical trial [192].

4.1.17 Physio-L

The Physio-L disc (Nexgen Spine, Inc., Whippany, NJ, USA) is a lumbar disc consisting of two titanium endplates separated by an elastomeric core comprised of polycarbonate polyurethane. The first patent relating to this device was published in 2006 [193], with a separate patent relating to the fixation of the elastomeric core to the titanium endplates being published at the same time [194]. Later patents demonstrate the development of the design into the device now currently available and in clinical use [195]. The core is mechanically fixed to the endplates by injection moulding it through perforated plates. There is a central keel on the endplates for initial stability in addition to a titanium bead coating for long-term fixation via bone ingrowth. Pimenta et al. [196] have reported the 12 month follow-up of 12 patients (8 single-level, 4 bi-level). Clinical outcomes improved significantly compared to pre-operative scores, and the mean range of motion at the operated level was 13.3° ±5.5°.

4.1.18 Freedom

The Freedom lumbar disc replacement was patented in 2003 by AxioMed Spine (AxioMed Spine Corporation, Ohio, USA) [197]. The device comprises two endplates separated by an elastomeric core. Additionally, there are retaining parts that connect the core to the

endplates. There are spikes and a porous coating on the outer surface of the endplates and retaining parts to provide primary fixation to the vertebral endplates through mechanical means, and secondary fixation through bone ingrowth. A clinical trial of the device began in 2008 [198].

4.1.19 XL TDR

The XL TDR (Nuvasive) is a constrained metal on metal, ball and socket lumbar disc replacement designed to be implanted using a posterolateral approach. To facilitate this, the endplates are much larger when viewed in the coronal plane than in the sagittal plane. The endplates have spikes for initial fixation and a porous surface for long-term stability via bone ingrowth. A clinical trial of the device began in 2009 [199].

4.1.20 Triumph

The Triumph lumbar disc replacement (Globus Medical) is designed to be implanted using a posterolateral approach and to allow physiological ranges of motion irrespective of the insertion angle. The endplates are much longer in the coronal plane than in the sagittal plane, to facilitate the surgical approach. It is a two-piece, metal on metal, constrained ball and socket design. The endplates have keels for initial fixation and a porous coating for long-term stability via bone ingrowth. A clinical trial of the device began in 2010 [200].

4.2 Review of Clinical Devices

The clinical outcomes reported above suggest that the current generation of disc arthroplasty devices does not greatly improve on discectomy and interbody fusion procedures in treating severely degenerated discs [21, 24, 66, 118, 126, 127, 201]. Long-term follow-up data remains limited for such procedures and there still remains a void of knowledge on the long term effect of the altered biomechanics of the spine, due to either arthrodesis or arthroplasty [5, 17, 24]. The latest generation of elastomeric disc replacement devices show potential to improve long-term clinical outcomes, though this data will not emerge for many years.

The range of motion at the operated level varies hugely between studies of the same device, suggesting that these implants may not offer a consistent restoration of the biomechanics of the spine, or adequate prevention of tissue growth into the device.

4.2.1 Disc Design

Ball and socket based designs are the most commonly used, whether consisting of a simple ball and socket, or including a mobile core. Ball and socket joints may be constrained, as with the ProDisc-C (Figure 41), or unconstrained, as with the Prestige (Figure 42). The level of constraint is related to the congruity of the articulating surfaces. The long-term effects of constraint in intervertebral disc design remain unclear; constrained devices may reduce shear forces in the posterior elements of the spine, though unconstrained devices are more likely to allow the natural instantaneous axis of rotation [15]. The centre of rotation of a functional spinal unit is not fixed, but it is generally within or just inferior to the intervertebral disc [28]. This fact should be considered when designing an intervertebral disc replacement.

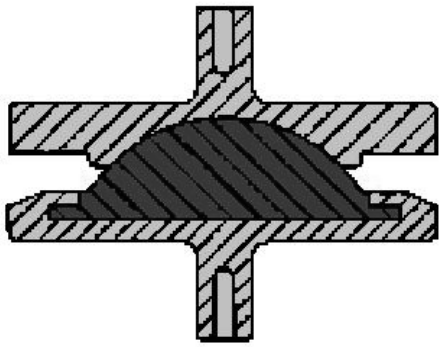

Figure 41: The ProDisc-C is a constrained ball and socket design. Modified from Marnay et al. [132]

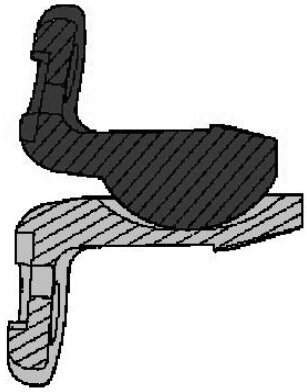

Figure 42: The Prestige is an unconstrained ball and socket design. Modified from Sofamor Danek Holdings Inc. [136]

All devices with mobile cores that are currently being used clinically are unconstrained because they are designed to allow some level of translation in the sagittal and coronal planes. However, devices with mobile cores may have a constrained design if translation is only possible in the axial plane. There are generally two types of mobile core, single and double ball and socket designs. The Charité is a double ball and socket design with both endplates forming a ball and socket joint with the lens-shaped core (Figure 43). The Mobidisc and Mobi-C have a mobile core but only one ball and socket joint, as one core-endplate interface is planar (Figure 44).

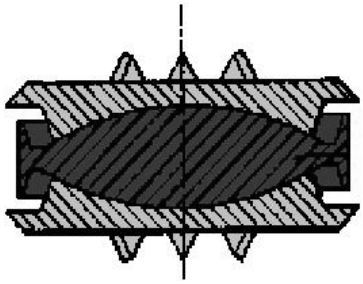

Figure 43: The double ball and socket design of the Charité disc. Modified from Link Waldmar Gmbh Co. [116]

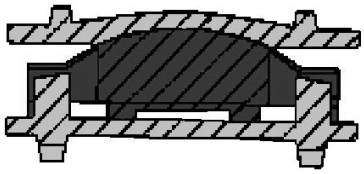

Figure 44: The ball and socket with mobile core design of the Mobi-C. Modified from LDR Medical [202]

4.3 Systematic Patent Review of Disc Replacement Devices

A systematic review of intervertebral disc implant designs was completed. This was carried out by searching through the database of the European Patent Office, esp@cenet [203]. Access to worldwide patents is available through this website. The objective of this search was to investigate the trends in disc design with a view to predict future designs that may provide greater clinical success than the current generation of disc replacements.

Each hit on esp@cenet was checked and if relevant added to a custom developed database. Total disc replacements and nucleus replacements were included. Fusion devices, vertebra replacement, facet joint replacements, etc. were not included unless they also described and made claim to a novel total disc or nucleus replacement.

An additional search of known patents, primarily from the review paper by Szpalski et al. [12], was carried out and transferred to the database. Following the multiple searches, duplicates were purged. Patents up to 31/12/2006 were filed.

Each patent was then assigned an identification number. The resulting database consisted of 619 patents to analyse and classify from 1956 until the end of 2006. The designs covered by the patents were classified according to design philosophy and material characteristics (Table 4).

The materials and manufacturing thereof were often not specified in the claims of a patent, though preferred materials were often suggested in the description. Preferred materials were recorded in the materials classification, and variations recorded in the description. If no preference was evident, the materials classification was left blank.

Likewise the method of attachment to the vertebrae was often not covered, or many possible variations given within the patent. The preferred embodiment was used for the classification, and variations described were recorded in the description.

If images resembled a known device, for example the Charité, a note was made. If images were recognised from a previous analysis, the ID number of the previous patent was recorded to allow similar or related patents to be identified.

The ROM was estimated as far as was reasonably possible from the claims, description and images in the patent. If different embodiments resulted in different ranges of motion this was recorded in the description and the preferred embodiment used in the ROM classification. If some or all ranges of motion could not be identified, no classification was defined.

Table 4: Data assigned to each patent

Classification	Description
ID	Database identification number for patent.
Title	Patent Title, as published.
Publication Date	Publication date of the patent application.
Patent Number	The number assigned to the patent when the patent application is published.
Inventor	The recorded inventor(s) of the patent.
Applicant	The recorded owner(s) of the patent.
European Classification	The classification groups that the patent belongs to, according to the European classification system.
International Classification	The classification groups that the patent belongs to, according to the international classification system.
Earliest Published Date	The earliest publication date of a patent and its equivalent patents.
Earliest Equivalent Patent Number	The publication number of the earliest equivalent patent.
Implant	Total disc or nucleus replacement.
Area	Cervical, lumbar, or both.
Design Type	Ball/socket, elastomeric, etc.
Parts	Approximate number of parts of the device.
Key Materials	Key design materials, such as elastomer, or articulation materials such as metal/polymer.
Attachment	Method of attachment to the vertebrae.
Equivalent Design	If the design is similar to a known design used clinically, e.g. Charité, Bryan, etc.
Comparable ID	The ID of a previous patent of similar design, which may or may not be an equivalent or otherwise linked patent.
Flexion/Extension	Range of motion: No; Yes; or Yes but limited through design.
Lateral Bending	Range of motion: No; Yes; or Yes but limited through design.
Axial Rotation	Range of motion: No; Yes; or Yes but limited through design.
Sagittal Translation	Range of motion: No; Yes; or Yes but limited through design.
Coronal Translation	Range of motion: No; Yes; or Yes but limited through design.
Axial Translation	Range of motion: No; Yes; or Yes but limited through design.
Comments	Any required comments, such as lack of English for description/claims, etc.
Brief Description	Brief description of embodiment(s) of the patent.

4.3.1 Results

Once classification was completed, it was possible to analyse the custom database for trends in disc design. The number of patents published per year, total numbers of designs and the distribution of design types for each year was found (Figure 45). Inventors and applicants that applied for high numbers of patents and known designs were identified so as to establish the design history of the most active patent applicants (Figures 46 and 47). Both nucleus and total disc replacements are presented in the results, as the claims of many patents overlapped, with different embodiments of the same design relating to nucleus and total disc replacements.

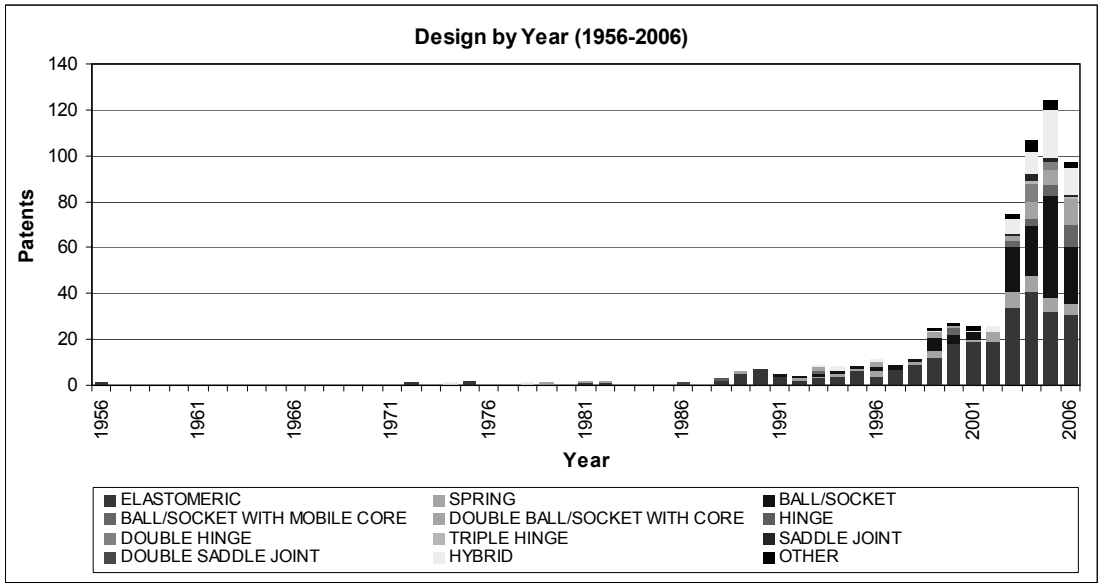

Figure 45: Total number of patents by design type per year (1956-2006)

The characterisation by design type allows possible trends to be identified. Changes in design philosophies may be due to market trends, or to technological advances. The data shows that the number of patents for hybrid designs has increased in recent years. This may be due to the lack of long-term success in simpler one-mechanism systems such as ball and socket or elastomeric designs. However, it may also be due to the shear number of patents already published in these areas over the last 50+ years. This proliferation might have led to novelty being found in the generally more complex hybrid designs.

It is from the most active patent inventors and applicants that it might be expected that future products will emerge. The further a design is along the development stage, the more likely it is to have a number of patents attributed to it regarding different novel aspects of

the device. Alternatively, a holding company that owns the rights to a large number of patents may see the potential in a design and purchase the rights to it.

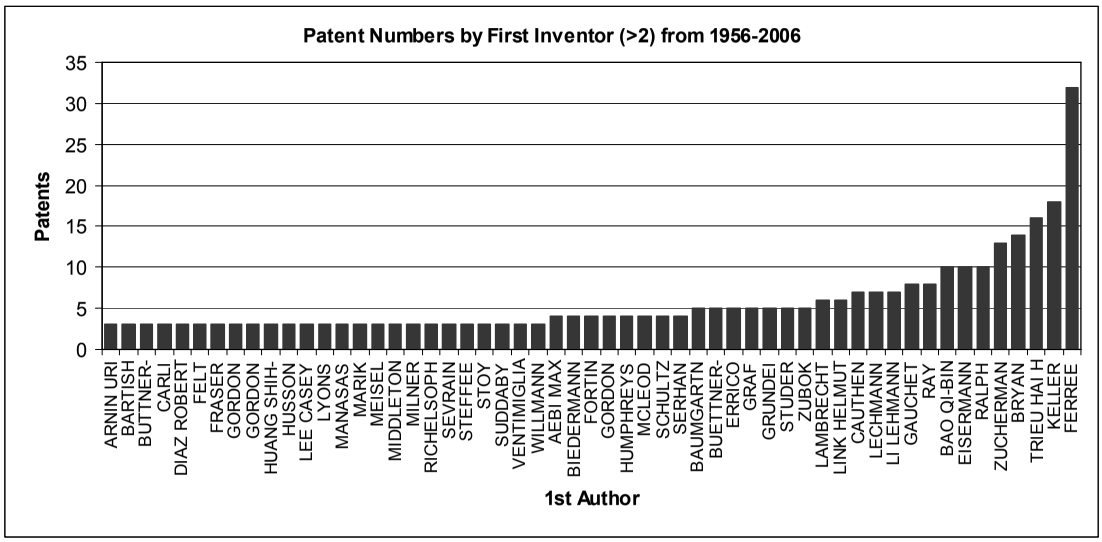

Figure 46: First inventors with greater than 2 patents from 1956-2006

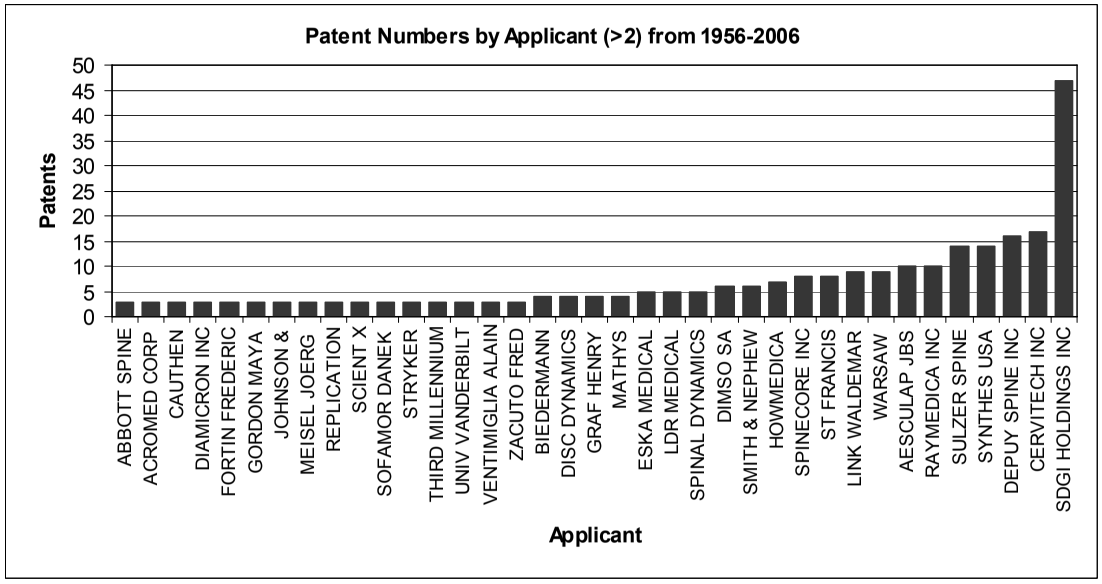

Figure 47: Applicants with greater than 2 patents from 1956-2006

Whilst the compilation of the data into these rough trends may be useful as a starting point, it is only through searching more deeply into the data and using multiple comparisons that one may be able to predict the likely designs of future generations of disc replacement devices.

4.3.2 Trends and Predictions

The results show that there has been an increase in hybrid design types in recent years (Figure 45). A hybrid design involves a combination of design elements; this may involve the integration of a more common design, such as a ball and socket assembly, with a more unusual feature, such as spring elements, for example. This may work to stiffen and limit rotational motion (Figure 48), or it may be to allow limited translations as well as rotations (Figures 49 and 50). The Bryan disc is currently the only hybrid design that has been used clinically.

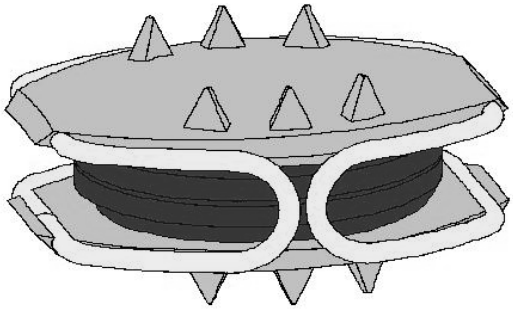

Figure 48: This may be a future generation of the DePuy Charité disc. Modified from DePuy Spine Inc. [204]

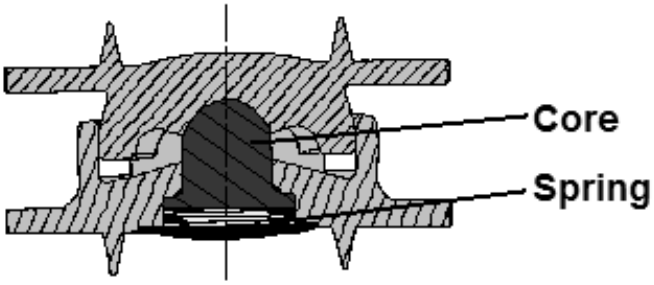

Figure 49: A spring under the core allows limited axial translation with a constrained ball and socket design. Modified from Diaz and Doubler [205]

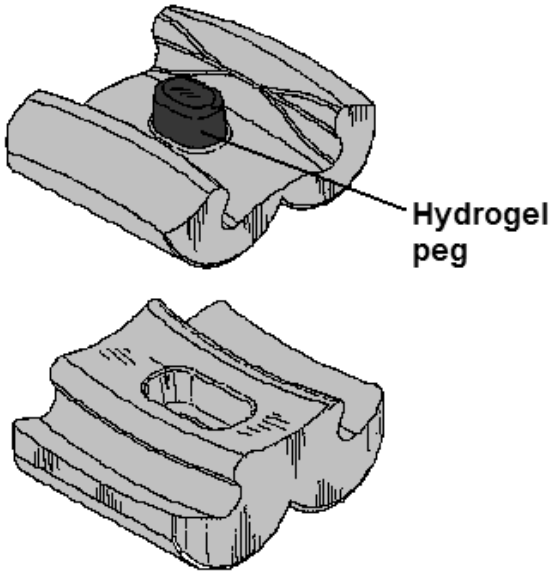

Figure 50: An embodiment of this patent incorporates a hydrogel peg. Modified from Kinetic Spine Technologies Inc. [206]

Results show that elastomeric designs form a large percentage of the total number of patents, and have done throughout the history of intervertebral disc arthroplasty. However, elastomeric designs are less commonly used clinically, other than in nucleus replacement procedures. Of the elastomeric devices classified in the patent review 131 were classified as total disc replacements and 121 nucleus replacements; yet there are presently very few elastomeric total disc replacements that are used clinically. It is possible that the poor early outcomes of this implant type, embodied by the Acroflex disc, provoked a move away from purely elastomer devices for total disc replacement procedures. The lack of improvement in ball and socket devices may, in turn, have led the spinal market to re-evaluate elastomeric devices in recent years.

The natural disc behaves in an elastomeric fashion but its structure also provides limitations in movement. It is likely that the discrepancy between the large number of elastomeric designs that have been patented compared to the number in clinical use may be to do with the demands on such devices to stand up to high loading over a long period of time and the added complexity required to limit the motion. It is possible that the majority of elastomeric designs fail to develop into commercial products because of these difficult design requirements. The spinal kinetics M6 disc demonstrates this principle well, in providing a limited ROM in 6 degrees of freedom, but requiring a relatively complicated structure of a polymer nucleus, woven fibre annulus and outer sheath fixed between two metal endplates in order to do so.

The same is true of the Physio-L disc. Whilst the end result is simple, with two metal endplates separated by an elastomeric core, the manufacturing process to mechanically attach the elastomeric core to the endplates is quite complex and costly. Such a manufacturing method may prevent complications of device failure due to separation of the core form the endplates, as happened with the Acroflex device due to debonding.

Likewise, the CaDisc is a relatively simple one-piece device but requires a novel manufacturing process of simultaneously injecting different layers of polyethylene into a mould to create a disc with varying stiffness from the centre to the exterior [190].

Other simple designs that have been patented and may provide suitably limited ROM include a patent filed in 1992 by Baumgartner of Sulzer Medizinal Technik AG [207] (Figure 51). The design comprises two rigid endplates that are attached to the neighbouring vertebrae and separated by a cylindrical elastomeric core. Geometrical features on the endplates have been engineered to limit motion in five degrees of freedom. Axial rotation could be limited if the endplates were elliptical when viewed in the axial plane, causing the features on the endplates to interfere with each other after a given amount of rotation.

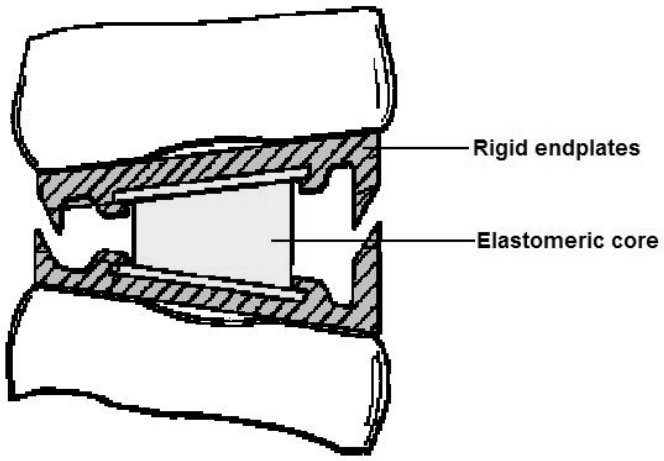

Figure 51: An elastomer core separates two rigid endplates. Modified from Sulzer Medizinaltechnik AG. [207]

An example of a design that may provide limited motion in all six degrees of freedom was filed in 2003 by Aaron [208]. One embodiment of this patent (Figure 52) comprises two rigid endplates with a core comprising a piston and cylinder arrangement. The gap between the piston and cylinder is filled by an elastomeric material to allow limited motion of the

endplates relative to each other. Surrounding the core is a further ring of elastomer that is stiffer than that of the core. The piston and cylinder arrangement is shown to be oval in cross-section and this serves to limit axial rotation. This design provides limited rotations and translations in all planes of motion.

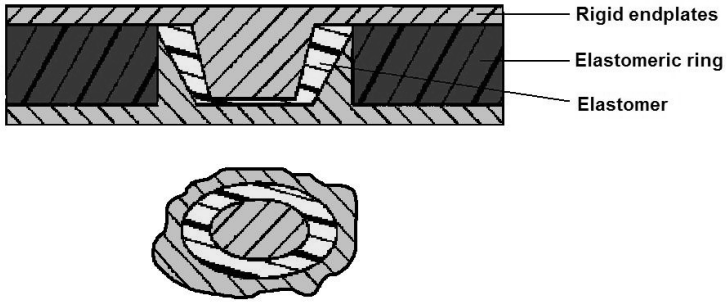

Figure 52: Two different stiffnesses of elastomer are used to limit motion between the endplates. Modified from Fournitures Hospitalieres Ind. [208]

In 2005 Rivin patented a device characterised by two rigid endplates separated by an elastomeric core, that provides limited motion in all degrees of freedom, with axial rotation limited only by the stiffness of the elastomer [209] (Figure 53). The core is attached to the endplates to allow movement by the shearing of the elastomer. The geometry of the endplates limits motion in flexion, extension and lateral bending, while translations are limited by the thickness and stiffness of the elastomer. The success of this device would rely on the secure fixation of the elastomer to the endplates.

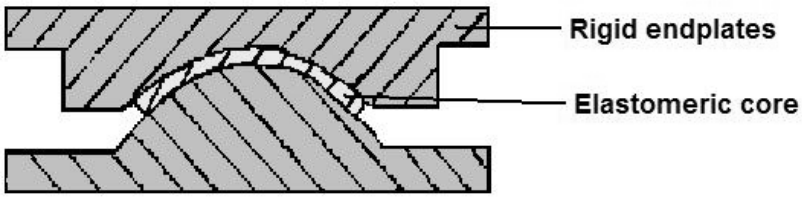

Figure 53: A layer of elastomer between endplates provides motion through shear. Modified from Rivin [209]

Ferree is the first named inventor of 32 patents, making him the most prolific intervertebral disc inventor found during the patent review. Ferree and Tompkins filed a patent in 2006 [210] comprising two rigid endplates separated by a cushioning ring, resembling a tyre, which is attached to the endplates. The tyre assembly may be filled with a material such as a

fluid, foam, hydrogel, or similar. In one embodiment of this concept there is a piston and cylinder assembly that prevents translations in the sagittal and coronal planes (Figure 54). However, if the piston fits into the cylinder with clearance, limited translations would also be possible in the anterior, posterior, and lateral directions. Some embodiments of the design feature alternate piston arrangements, while in others the piston and cylinder assembly has been removed entirely (Figure 55).

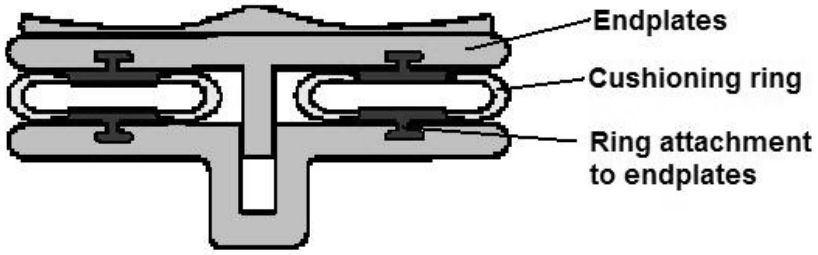

Figure 54: An embodiment of Ferree and Tompkins 2006 patent with a piston and cylinder assembly. Modified from Ferree and Tompkins [210]

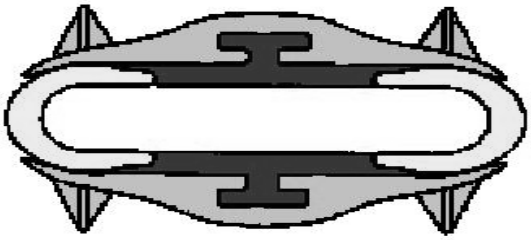

Figure 55: A further embodiment of the 2006 patent of Ferree and Tompkins, without a piston and cylinder assembly. Modified from Ferree and Tompkins [210]

5 PRE-CLINICAL TESTING OF DISC REPLACEMENT DEVICES

5.1 Introduction to Testing Methods and Standards

Pre-clinical testing is crucial in determining the safety and suitability of any spinal device prior to clinical use [211]. Testing should assess wear and fatigue performance based on the projected life cycle of the implant and should be carried out under simulated working conditions in terms of loading and environment. Fatigue and wear tests require long testing periods, and as such it is impractical to complete them using cadaveric specimens. However, biomechanical tests to assess the efficacy of a new device can be performed on biological specimens, and ideally this assessment should be performed in comparison with an equivalent device with proven clinical outcomes [212]. The pre-clinical testing protocols should aim to improve the overall quality of devices that are to be used clinically, and allow benchmarking with the performance of the healthy spine.

With an increasing number of devices becoming available, it is important that testing protocols are standardised [211, 212]. Presently, wear and fatigue testing are the only requirements a device must meet prior to clinical trials, these are briefly summarised in the next section. For a fair assessment of the functional characteristics of all types of disc replacements, including those without moving parts, these requirements should be extended to include studies in regard to the efficacy of each device in providing ranges of motion, under simulated working conditions, comparable to those of the healthy spine.

5.2 Review of Total Disc Replacement Pre-Clinical Testing Standards

Three standards are concerned with the pre-clinical testing of intervertebral disc replacement devices. Two are written by ASTM International, and one by the International Standards Organisation (ISO).

ASTM F2423-05 [213] specifies the loading for the wear testing of intervertebral disc prostheses. For this type of testing, position control is recommended by the standard, although load control may also be justifiable. The completion of 10 million cycles at a frequency of 2 Hz or less, without failure, is set as the minimum endurance limit. Loading in flexion/extension, lateral bending and axial rotation are required. The required 10 million

cycles must be completed on the same device in all three rotational axes, whether this is carried out through a series of tests in one ROM at a time on the same device, or through combined loading. The cervical and lumbar test profiles are summarised in Table 5.

Table 5: ASTM pre-clinical testing recommendations

	Axial preload (N)	ROM (degrees)	Moment (Nm)
Cervical intervertebral disc prostheses test profile			
Flexion/extension	100	± 7.5	± 2.0
Lateral bending	100	± 6.0	± 2.0
Axial rotation	100	± 6.0	± 4.0
Lumbar intervertebral disc prostheses test profile			
Flexion/extension	1200	± 7.5	± 10.0
Lateral bending	1200	± 6.0	± 12.0
Axial rotation	1200	± 3.0	± 10

The standard ASTM F2346-05 [214] is concerned with the in-vitro static testing conditions for intervertebral disc prostheses in compression, combined compression and shear, and torsion. It also specifies the requirements for dynamic fatigue tests in the abovementioned modes of loading.

The standard specifies the apparatus and testing conditions, such as applied load and displacement, for the devices. Position control is recommended for static tests to failure where the rate of the test should not exceed 25 mm/min or 60 deg/min. The use of a compressive preload of 100, 300, and 500 N for cervical, thoracic, and lumbar devices respectively, is suggested for axial rotation tests.

The standard also suggests some appropriate geometric features of the devices, such as height, which should be in the region of 4, 6 and 10 mm for the cervical, thoracic and lumbar spine respectively, so as to match the disc height in the human spine.

Fatigue testing is recommended to be carried out at a frequency of 2 Hz or less in a 0.9 % saline solution at 37°C, though other solutions may be suitable. The suggested maximum loads are 25, 50 and 75 % of the maximum load applied in the static testing. The fatigue test should end at the point of functional failure, or the attainment of 10 million cycles without functional failure.

Finally, ISO 18192-1:2011 [215] outlines the testing procedures for the wear testing of intervertebral disc replacements. The recommendations are similar to those specified in the

ASTM guidelines for testing in position control (Table 6). Shear loading cycles are required in addition to angular displacements (Table 7).

Table 6: ISO pre-clinical testing recommendations

	Axial preload (N)	ROM (degrees)
Cervical intervertebral disc prostheses test profile		
Flexion/extension	100	± 7.5
Lateral bending	100	± 6.0
Axial rotation	100	± 4.0
Lumbar intervertebral disc prostheses test profile		
Flexion/extension	1200	-3.0 to +6.0
Lateral bending	1200	± 2.0
Axial rotation	1200	± 2.0

Table 7: ISO pre-clinical testing shear loading recommendations

Cervical shear force loading profile	Shear Force (N)
Minimum	50
Maximum	150
Lumbar shear force loading profile	
Minimum	600
Maximum	2000

Bovine serum at a temperature of 37°C is the recommended fluid test medium. The testing frequency should be 1 Hz, though a frequency of 2 Hz may be used with justification. The test shall end after the failure of the implant, or the completion of 10 million cycles without failure.

5.3 Review of In-Vitro Spinal Testing Methods

International standards for the testing of disc replacement devices have only been available in the past few years and the focuses of the standards is on wear and fatigue testing. A device that is successfully subjected to the recommended loading conditions will not necessarily replicate the biomechanics of a natural disc in-vivo, as stated in the scope of each standard [213-215]. It is also worth noting that the ASTM standards suggest using displacement control, though Panjabi has described several limitations of this method [65]; if displacement control is used, rather than load control, there is a difficulty in having to choose the various axes of rotation. In load control, pure moments can be applied to an

unconstrained specimen, resulting in motion about the natural axes of rotation of the tissue or device being tested [65].

Altered biomechanics may result in problems at the operated level, and may also result in adjacent disc degeneration [64, 65], which is one of the primary arguments for carrying out total disc replacement over fusion [21]. The testing standards move some way to providing a standardised framework of pre-clinical testing to assess the efficacy of a total disc replacement device. However, these standards do not cover all the tests that are required to kinematically assess a new spinal device against the natural spine. Therefore further standards are necessary to allow such an assessment, and only by being standardised will the comparison with other total disc replacement devices be possible.

Wilke et al. [212] reported on a series of workshops with professionals from all aspects of spinal device development and clinical application in an attempt to reach a consensus on the various aspects of in-vitro testing. Goel et al. [211] proposed a process for the development and testing of spinal devices prior to clinical use, stating that it is important that testing is continually developed and improved, though the importance of the standardisation of testing protocols throughout the medical community is also emphasised.

With this in mind, a review of the literature was completed to assess in-vitro test protocols that assessed the behaviour of natural discs and/or intervertebral disc replacements (Table 8). Preparation methods, test set-up, loading regime, and outcome measurements were investigated to compare the different test methods employed by research groups. The tests varied in the aims and measured outcomes, thus some aspects were not comparable between tests. For example, comparing the number of cycles for a wear test and a flexibility test would be meaningless; though a comparison of the magnitude and application of loads may provide information about the standardisation of testing protocols.

Table 8: Papers assessed during review of in-vitro test protocols

Ref	Author(s)	Disc	Test	Description
[143]	Anderson	Bryan	Wear	Measure wear of disc in combined flexion/extension and axial rotation
[143]	Anderson	Bryan	Wear to failure	Measure wear of disc in combined flexion/extension and axial rotation
[46]	Bertagnoli	Neudisc	Radial deformity	Compare disc prototype with raw material
[46]	Bertagnoli	Neudisc	Confined compression	Determine equilibrium hydration and lifting force
[46]	Bertagnoli	Neudisc	Fatigue	Fatigue testing using fixed strain control
[46]	Bertagnoli	Neudisc	Ramp to failure	Failure test in either axial compression, lateral bending, or flexion
[216]	Chung	Cadaveric	Flexural stiffness	Constrained loading in flexion
[216]	Chung	Cadaveric	Flexural stiffness	Unconstrained loading in flexion
[217]	Cunningham	Cadaveric/Charité/BAK/BAK+ISOLA	Multi-directional flexibility	Pure unconstrained moments applied in turn
[218]	Dickey	Cadaveric/Porcine	Flexion biomechanics	Comparison of human and porcine disc in flexural loading
[219]	Dickey	Porcine	Flexion biomechanics	Comparison of long spine specimen with single FSU
[220]	Gardner-Morse	Porcine	Axial preload	6 degrees of freedom test with varying axial preload
[221]	Gardner-Morse	Cadaveric	Axial preload	6 degrees of freedom test with varying axial preload
[222]	Kotani	Cadaveric/Anterior3DF/Anterior BAK/Pedicle screw + BAK/Posterior 3DF/Pedicle screw + posterior cage	Multi-directional flexibility	Load/displacement test using 6 unconstrained moments
[33]	Serhan	Charité	ASTM wear test	Wear test of Charité prosthesis under ASTM wear test guidelines
[223]	Wilke	Cadaveric	Muscle force influence	Preliminary test of universal spine simulator

The literature review covers a range of studies with a variety of aims originating from different research groups. This will allow an understanding of how standardised testing might be achieved, and will allow better comparisons to be made between the studies completed by different research groups.

Most procedures involving biological specimens dissected all musculature leaving ligaments intact [46, 217-219, 223] and also left the facet capsule intact [46, 217, 222]. Gardner-Morse and Stokes carried out stiffness testing of porcine motions segments first with the ligaments and facet capsule left undisturbed by the dissection procedure, and then repeated the same tests with the ligaments and the entire facets removed [220]. Gardner-Morse et al. [221] also completed stiffness testing of cadaver motion segments with the ligaments and facet intact and then repeated testing with both dissected. Both of these studies showed a reduction in stiffness in the absence of the ligaments and facets.

In addition to the dissection of specimens, storage and potting is important in providing consistent and reliable results. Cadaveric or porcine specimens are generally stored at approximately -20°C and thawed at room temperature [216, 218, 219, 222]. Specimens can be potted using a variety of materials and methods, including PMMA, dental cement, screws, and pins; a combination of methods may also be employed [46, 216], though low-melting allow may also be used [212]. Generally specimens are potted such that the intervertebral disc under investigation is parallel to the base of the test rig [46, 216, 218, 219].

Once potted various solutions can be used to prevent specimens from drying out during testing or to simulate the fluid environment in-vivo, these include: saline solution [216, 217, 220, 221, 223]; bovine serum [33, 143]; or Hank's buffered salt solution (HBSS) [46]. The methods of applying the solution may include: wrapping the specimen in soaked cotton wool [216] or plastic film [218, 219, 223]; or submerging the specimen in a bath [220, 221]. ASTM F2423 guidelines suggest the use of bovine serum at 37°C for the wear testing of total disc prostheses [213]; a period of hydration may also be employed prior to wear testing [46, 143]. However, tissue specimens are often tested at room temperature or below to prevent accelerating the degradation of the specimens, which would result in significantly altered mechanical properties [212].

Testing regimes can vary considerably in the mode of control, the magnitude of applied load and displacement, and the frequency. Quasistatic loading is often used for flexibility testing. For example, in two studies by Gardner-Morse one cycle took 87 seconds to provide a maximum movement of 3° or 1 mm [220, 221]. Such testing may result in very different outcomes to dynamic tests [212]. Frequencies between 0.5 and 5 Hz are suggested in the ASTM guidelines for dynamic testing [214]. In load control, moments in the region of $\pm$ 8 Nm are used for lumbar testing in flexion and extension, lateral bending, and axial rotation [217, 222, 223], though the extension moment may be reduced and the flexural moment increased [218, 219]. Cervical testing moments used may be in the region of $\pm$ 4 Nm [143].

Spinal testing generally requires the measurement of forces and motion in six degrees of freedom. A six-axis load cell is often used for the measurement of loads [218-220, 223]. Depending upon the spinal testing apparatus, motion may be measured directly through the drive system, an independent method may be employed, or a combination of systems may be utilised. For example, it is possible to determine position directly from the encoder signals of a motor. Alternatively, a contactless displacement transducer could be used to measure the translational position of an axis [223], or a marker-based contactless measurement system may be used to identify the relative position of vertebrae in a multi-segment specimen [217, 222].

In addition to the test protocols above, there is also a great deal of information in the literature concerning the development of spinal testing machines to assist in the development of in-vitro test methods that aim to closely replicate the in-vivo biomechanical environment [65, 216, 223, 224].

It is crucial that the loading in-vitro reflects the in-vivo situation but it is also important that any testing machine provides good repeatability. The more complex a test set-up, the more likely it is that errors will be introduced. This is true in the alignment and position tracking of multi-segment specimens, the application of forces to simulate muscles, or the analysis of complex loading patterns. Likewise, dynamic tests are vital to assess the suitability of a device and should be performed at an appropriate rate; too slow and creep effects may come into play, too fast and the mechanical system inertia will cause inaccuracies [212].

In recent years there has been a move toward the testing of multi-segment cadaveric specimens to more accurately reflect the in-vivo biomechanical environment, and also to assess adjacent segment affects. Dickey and Kerr [219] demonstrated that the neutral zone and ROM of a single L3-L4 functional spinal unit is significantly larger when assessed in isolation than as part of a L2-L5 multi-segment specimen. This may be due to the severing of ligaments than span more than one level. Lysack et al. [224] have shown that applying pure moments can minimise off-axis loading. The gain in popularity of the application of pure moments to the spine allowed a further advance to be made by Panjabi [65] in the development of the hybrid method. This method aims to investigate adjacent segment effects due to both fusion and arthroplasty devices using physiological loads and ranges of motion. The method consists of the application of a defined unconstrained pure moment to an intact multisegment specimen to establish the overall range of motion. Then an unconstrained moment is applied to the specimen after implantation of a spinal device until the same overall ROM is reached. It is then possible to compare the different level effects due to the device under investigation, and additionally compare the adjacent level effects of different devices [211].

5.4 Finite Element Modelling of the Spine

With the limitations of in-vitro testing outlined above, and the power of modern computers, numerical methods, such as those based on the finite element approach (FEA), are increasingly popular as a way of investigating the behaviour of human tissues. A number of FEA models of the spine have been developed to investigate a wide range of topics including muscle forces and loading [225-228], posture [229], anatomical geometry [230], and the role of the ligaments, facets, and nucleus pulposus in spinal motion [231].

The advantages of FEA models are that they can be used relatively quickly and cheaply compared to in-vitro studies [211]. In-vitro studies of the spine often do not take into account muscle forces, which can be included in FEA models more easily. The speed and cost of FEA models make it ideal in reducing the number of design iterations that are physically tested in the development of devices. With adaptation algorithms it is also possible to converge to a more efficient design for given loading and boundary conditions. Such algorithms can also be used to model the device over time to investigate bone ingrowth and remodelling [211].

However, with such models validation is imperative in linking to the final in-vivo situation [231]. For this reason, the material properties, interactions and boundary conditions applied to the model are of vital importance. Additionally, the more complex the model, the more important a good validation process is completed. Schmidt et al. [232] reported a calibration method that used a stepwise process of validating the FEA model with in-vitro results after a new tissue was added until all tissues to be included were in place. This model was compared to an identical model that simply had material properties taken from the literature. The models provided good comparison to in-vitro data in the intact state but when defects were added the calibrated model provided much better results.

Whilst FEA modelling is clearly a powerful tool in the investigation and development of disc replacements, it is important that it is combined with other methods to achieve reliable results.

6 EXISTING SPINAL TESTING MACHINES

There are only a small number of research groups completing multi-axis testing of spinal constructs. This is likely due to the complex apparatus that is required to apply appropriate physiological loading to spinal specimens.

Almost all spinal testing machines in the literature adhere to one four design concepts: a gimbal head mounted on an XY platform, which is in turn mounted on a Z actuator; a hexapod; a robotic arm; or a system of cables and pulleys arranged to provide pure rotation that may have translational guides or be entirely unconstrained. A review of the testing devices developed by different research groups is presented in the following sections.

6.1 Gimbal Head and Translation Platform Apparatus

Wilke et al. [223] have developed a spine testing device that has six active axes (Figure 56). It comprises an XY platform, allowing independent translations in the X and Y axes mounted on a frame that allows translation in the Z axis. A gimbal head is mounted on the XY platform that can provide independent rotations about the X, Y and Z axes. All axes can be individually constrained or released and this can be carried out in any combination. It is therefore possible using this apparatus to apply pure moments in all three planes simultaneously, and translational loading may also be applied. Both load and position control are possible in all six axes.

Rotations are driven by a stepper motor through a harmonic drive gear (Harmonic Drive, Limburg/Lahn, Germany) and clutch system. The clutches allow the decoupling of each of the axes, if required. The motors have a torque of 55 Ncm, which is increased through the harmonic drive gear ratio of 160:1. Rotations can be applied up to a speed of 2°/sec. The torque capacity in each axis is 50 Nm. The rotational position is measured using rotary variable differential transformers (RVDT, Nototechnik, Ostfilden, Germany) mounted on the gimbal. Counterweights are used on the non-drive side of the gimbal to balance the weight of the stepper motor, gear, and clutch assembly.

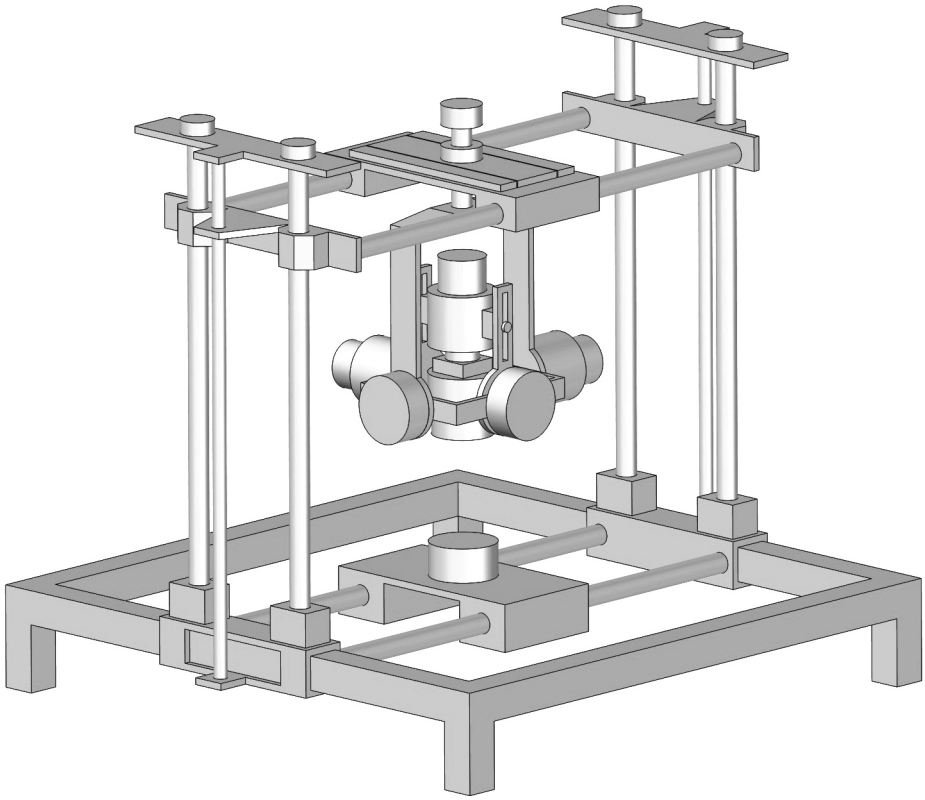

Figure 56: An image based on the six-axis testing machine of Wilke et al.

Translations in the X and Y axes are provided by stepper motors connected to the sliding platform via cables and pulleys. The position is measured in each axis using contactless displacement transducers (Balluff, Neuhausen/Filden, Germany). Shear force in the X and Y axis is measured using load cells (Burster, Germbah, Germany) fixed between the cables.

A spindle adjusts the vertical height of the sliding platform and further active translation is possible. The axial position is measured using a contactless displacement transducer (Balluff, Neuhausen/Filden, Germany). Loading in the Z axis is applied via two parallel pneumatic cylinders, which can apply a total axial preload of 1000 N.

A six-axis load cell (Schunk, Lauffen/Necker, Germany) is mounted between the gimbal and the cranial end of the specimen. The torque capacity is 40 Nm in all three planes, 500 N in anterior/posterior shear and medial/lateral shear, and 1500 N in axial compression/extension. It is also possible to mount the load cell between the mounting platform and the caudal end of the specimen.

Additionally, this test machine has 5 pairs of muscle groups, the load of which is achieved through a pneumatic system via cables attached to the specimen with screws. The pneumatic system allows the muscle forces to be varied and dynamic muscle forces to be applied to the specimen. The five muscles pairs are: multifidus to caudal; iliocostalis and longissimus; psoas major at corpus vertebrae; pasoa major at processus transversus; and multifidus to cranial.

Initial work focused on the load-displacement characteristics of one multi-level cadaveric specimen in flexion/extension using a constant force of 80 N per muscle pair for five muscle groups [223]. The intradiscal pressure was also measured at the L4-L5 level using a pressure transducer. The specimen was tested without muscle forces, with each pair of muscle forces applied individually, and with all five muscle pairs applied simultaneously. It was found that almost all configurations that included muscle forces increased the stiffness of the spinal segment. The load-displacement plot, from which the stiffness is obtained, was S-shaped without muscle forces but with all muscle forces it was almost linear, with a much reduced neutral zone. The intradiscal pressure was higher in the neutral position with all muscle forces, compared to the experiments where no muscle forces were applied.

In subsequent work the same group applied pure moments in all three planes to multi-level cadaveric specimens and measured the intradiscal pressure of the L4-L5 disc with and without muscle forces [233]. Each pair of muscle forces was applied individually, and with all five muscle pairs applied simultaneously, using forces of 80 N per muscle pair. It was found that the intradiscal pressure in the neutral position was significantly higher when muscle forces where present compared to loading cases without. It was also found that the application of muscle forces substantially altered the load-pressure characteristics of the specimens.

Using the same testing machine Rohlmann et al. [234] investigated the ROM and intradiscal pressure of multi-level cadaveric specimens using pure moments applied in all three planes with and without a 280 N follower-load. The follower-load aims to reproduce the effect of muscle forces and was applied using dead weights connected by cables passed through eyelets fixed laterally in both sides of the vertebral bodies of the specimens. The follower-load significantly increased the intradiscal pressure, significantly reduced the ROM in axial rotation (31 %), reduced the ROM by a small but significant amount in lateral bending and

flexion/extension, and significantly increased the neutral zone in lateral bending and flexion/extension.

A further study aimed to determine the erector spinae muscle forces in multi-level cadaveric specimens in flexion/extension [235]. In this study, each specimen was subjected to 124 loading cases. This comprised various combinations of applying a vertical preload to represent the force due to the mass of the torso and head, a follower load to represent local muscle forces of the spine, a force due to the rectus abdominis, and a supporting force due to the abdomen. Each of the loading combinations was completed with a hip-flexion of 0°, 10°, 20°, and 30°, and between 15° of extension and 20° of flexion in 5° steps. For each load case, the force due to the erector spinae was adjusted until the resultant moment measured was zero. The intradiscal pressure of the L4-L5 disc was measured during all testing cases.

The study aimed to assess whether the intradiscal pressure measured with the application of the muscle forces was similar to that measured in-vivo, and whether the erector spinae muscle force necessary to bring the system into equilibrium was similar to in-vivo measurements. It was found that the intradiscal pressure more closely matched in-vivo measurements than the muscle forces but the results would still provide useful inputs for computational models due to the difficulty in measuring the forces of individual muscle groups in-vivo.

Cunningham et al. [217], Kontani et al. [222], and Lebwohl et al. [236] have carried out multidirectional flexibility tests on a more simplified machine to that developed by Wilke et al. and described above. It comprises a gimbal head that allows independent rotations in all three axes. Each rotation is driven by a stepper motor through a gear and clutch system. This allows the decoupling of one or more axis if desired. This is mounted on an XY platform comprising two linear guide rails, which in turn is mounted on an MTS material testing machine (Z axis). Pure unconstrained moments are possible using this set-up (Figure 57). The XY platform is passive, so shear loads cannot be applied to specimens.

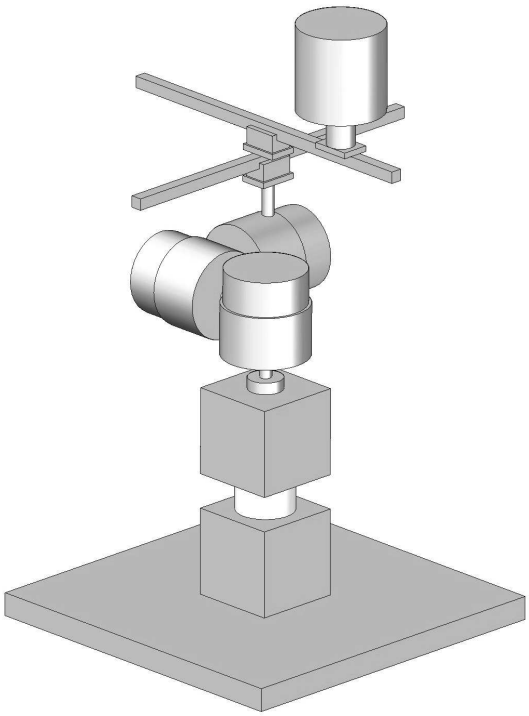

Figure 57: An image based on the test machine described by Cuningham et al.

The machine has been used to apply pure unconstrained moments in all three axes on multi-level specimens without axial preload. For each load case moments of ±8 Nm were applied at a rate of 3°/s. Three cycles were performed for each load case, with data only being taken on the third cycle. Light emitting diode markers were fixed to the anterior aspect of the vertebral bodies and an Optotrak 3020 motion analysis system (Nothern Digital Inc.) was used to determine the movement of the specimen during testing. The peak range of motion and neutral zone were determined for each test.

In the study by Cunningham et al. [217], L2-S1 cadaveric specimens were tested in the intact state, followed by testing after reconstruction at the L4-L5 level. The reconstructions carried out were firstly a Link SB Charité Artificial Disc Prosthesis (Link Spine Group, Bandford, CT), this was then replaced with a BAK device (Centerpulse Spinetech, Mineapolis, MN), and finally the BAK device was combined with ISOLA posterior pedicle screw and rod instrumentation (DePuy-AcroMed, Raynham, MA). The data was normalised with respect to the results for the intact specimen. The Charitè disc replacement resulted in significantly higher axial rotation (44 %) but no significant difference in flexion/extension or lateral bending were identified. The BAK cage significantly reduced flexibility in flexion/extension and lateral bending but produced no difference in axial rotation compared to the intact disc.

When posterior instrumentation was implanted in addition to the BAK cage the flexibility was significantly reduced further in flexion/extension, and reduced to a level that was significantly different from the intact specimen in axial rotation.

Similarly, in a later study by Kotani et al. [222], cadaveric specimens were tested in the intact state, followed by testing after various reconstructions. Testing was first completed on intact L1-S1 specimens, then with a 3DF posterior disc replacement (two implants) at the L2-L3 level, followed by posterior interbody fusion cages (Brantigan cage) and VSP pedicle screw fixation (Depuy-AcroMed Inc.) at the same level. Then the cranial fixation to the spine testing machine was altered from the L1 vertebra to the L3 vertebra and tested in the intact state, followed by reconstructions at the L4-L5 level. Firstly a total 3DF disc replacement (single implant) was implanted, then anterior BAK devices (two anterior cages) (Centerpulse SpineTech, Inc.), and finally anterior BAK cages plus posterior VSP pedicle screw fixation. At the L2-L3 level it was found that the 3DF disc replacement resulted in no significant difference in flexibility in flexion/extension, lateral bending, or axial rotation. The fusion at the L2-L3 level resulted in significantly lower flexibility in all three rotations compared to both the intact disc and the 3DF replacement. At the L4-L5 level neither the 3DF device nor the BAK cages significantly altered the flexibility in any rotational axis compared to the intact disc. The combination of the BAK cages and posterior screw and rod fixation resulted in significantly lowered flexibility in all three rotational axes compared to the intact disc.

Gedet et al. [237] have developed a spine test-rig to apply pure moments about all three axes. Rotations are applied via brushless DC motors (EC40 BL D 120 W KL 2WE, Maxon Motors, Switzerland) driven through a 230:1 reduction gearbox (GP42C 15NM 4ST KL) mounted on a cardinal frame. Each motor has a digital position encoder (ENC HEDL 5540 500IMP 3K, Maxon Motors, Switzerland). The flexion/extension and lateral bending axes have a counterbalance to prevent a moment due to the weight of the motor/gearbox assembly. There are three axes to allow free translations. The horizontal axes are connected to the machine frame and the vertical axis is counterbalanced.

The specimen is fixed at the cranial-end to the cardinal frame and at the caudal-end to the translation axes. A six-axis load cell is used to measure moments and forces (MC3A 1000, Advanced Mechanical Technology Inc., Watertown, MA, USA). Markers are placed on each

segment of the specimen and intersegmental displacement is measured using an optoelectric motion analysis system (Optotrak 3020, Northern Digital Inc.).

Testing completed using the above testing machine has been aimed at investigating the errors that can occur in such multi-axes machines. Two different linear guides were compared; a caged-bearing design (SHS 15C C1, THK Co., Ltd., Tokyo, Japan) and a precision roller (FDA 15, Franke GmbH, Aalen, Germany). Three different marker configurations were also compared, as this is another potential source of error in kinematic testing. For all tests a polymer tube was used as an equivalent to a multi-level spinal specimen. The bending stiffness of the tube was approximately equivalent to a cadaveric spinal specimen but allowed for greater reproducibility over multiple tests than biological specimens. Position control was used and a rotation of ±10° was applied in each plane using a step-based waveform. Results showed that the precision pulley created less friction than the caged-bearing design.

Gay et al. [238] and Ilharreborde et al. [239] have used a custom multi-level spinal test-rig with six-degrees of freedom, comprising two passive translational axes and four active axes. The passive axes equate to translations in the coronal and sagittal planes of the spinal specimen. Axial translation is applied using pneumatic jacks. Three motorised step-less drive mechanisms apply rotations in flexion/extension, lateral bending and axial rotation. Each rotational axis has a load capability of 20 Nm. A six-component JR3 load cell (JR3 Inc., Woodland, CA, USA) at the base of the machine is used to measure the loads in all six axes.

Control of the machine is achieved using a custom Labview program (National Instruments Corporation, Austin, TX, USA). This program allows the application of flexion/extension, lateral bending, or axial rotation. Each of these rotations can be applied individually or simultaneously. The program allows the input of rotation speed and number of cycles. The caudal end of the specimen is fixed to the base via the load cell. The cranial end of the specimen is fixed to the machine via the sliding platform, thus providing a means of applying pure moments.

Active markers are placed on each of the vertebral levels of interest and measurements are taken using an Optotrak optoelectric system (Northern Digital Inc.) and three cameras (The

MotionMonitor, Innovative Sports Training, Inc., Chicago, IL, USA). The load and displacement data is acquired continuously during testing.

Gay et al. [238] assessed the effect of flexion/extension loading rate and disc degeneration on the neutral region of cadaveric functional spinal units. Specimens were tested between ±5 Nm at 0.5, 3.0, and 6.0°/sec with an axial preload of 300 N. It was found that loading rate had a significant effect on all parameters, with the neutral zone decreasing in range of motion and increasing in stiffness as the loading rate increased. Increased degeneration (degenerative grade 1-4) was found to result a reduced neutral zone ROM. The neutral zone stiffness was lower in degenerated discs with a degenerative grade 1-3, though there was with a small increase in stiffness from grade 3-4.

The machine has been used to assess the measurement accuracy and reproducibility of the optoelectric displacement measuring system in dynamic tests, which was compared to static tests [239]. In dynamic testing, five cycles were completed in each rotational axis (flexion/extension, lateral bending, and axial rotation), load control was used, with a maximum applied moment of 7.5 Nm. The measurement with the markers was compared to that of an inclination sensor (CXTLA02, Crossbow Technology, Inc., Milpitas, CA, USA), which was attached to the structure to which the specimen was fixed. It was found that the method using the optoelectric system allowed for both accurate and reproducible dynamic testing.

6.2 Hexapod Apparatus

A range of stiffness matrix studies with various axial preloads have been completed in the Department of Orthopaedics and Rehabilitation at the University of Vermont using a ‘Stewart platform’ or ‘Hexapod’ robot [220, 221, 240, 241]. This comprises two platforms, one static and one moving, connected by six linearly independent actuators. The moving platform is positioned by adjusting the length of the actuators. Each actuator comprises a stepper motor (Oriental Motor USA Corp., Torrance, CA, USA) driving a precision lead screw (Ball Screws and Actuators Co., Inc., San Jose, CA, USA). The length of the actuator is measured using a linear encoder (Model LDK, Dynamics Research Corp., Willmington, MA, USA) and a six-axis closed-loop controller (DMC-1860, Galil Motion Control, Inc., Rocklin, CA, USA) calculates the required length of each actuator for any desired position of the moving

platform within the overall range of motion of the machine. The moving platform is fitted with a six-axis loadcell (MC3A-6-500, Advanced Mechanical Technology Inc., Waltham, MA, USA) and onto this the cranial end of the specimen is fixed using a fixation plate. The caudal end of the specimen is fixed to the static base. There is a plexiglass vessel between the moving and fixed platform to allow a specimen to be submerged in a temperature controlled fluid during testing. A custom interface (Labview version 5.1, National Instruments, Austin, TX, USA) is used for testing and to acquire all position and load data.

With this set-up, investigations of the stiffness matrix of a functional spinal unit and the stiffening and stabilising effect of an axial preload, which is present in-vivo due to muscle action, were carried out. An initial study subjected a single porcine lumbar spinal unit to quasistatic displacements and rotations about each axis, with and without a 500 N axial preload, whilst in a saline bath cooled to 4°C [240]. This initial study formed the basis of the testing protocol that Gardner-Morse and Stokes et al. would use in later stiffness matrix testing (Table 9). All the studies outlined below used sawtooth waveforms. The cycle time of the initial study was 174s [240], this was reduced to 87s in later studies [220, 221]. This is likely to be due to the reduced magnitude of applied displacements and rotations, rather than a change in the testing speed. A total of 4-5 cycles were recorded in all the studies for the testing in each of the six axes.

Table 9: Protocols adopted by Gardner-Morse, Stokes et al.

				Rotations (deg)			Translations (mm)		
REF.	Sample		Axial Preload (N)	Flex/ Ext	Lat. Bend	Axial Rot.	A-P Shear	Lat. Shear	Comp /Ext.
[240]	Porcine	1	0, 500	±4.0	±4.0	±4.0	±3.0	±1.5	±0.4
[241]	Human	4	0, 250, 500	±1.0	±1.5	±1.0	±0.5	±0.5	±0.35
[220]	Porcine	6	0, 200, 400	±0.8	±1.0	±0.8	±0.3	±0.3	±0.2
[221]	Human	8	0, 250, 500	±1.0	±1.5	±0.8	±1.0	±0.5	±0.35

The studies have demonstrated that the application of an axial preload increases the stiffness of a functional spinal unit, and increases linearity, and hysteresis of the neutral zone of a functional spinal unit. The studies have also demonstrated the importance of the facets and posterior elements in addition to the intervertebral disc in providing stiffness to the spinal structure in the majority of movements.

6.3 Robotic Arm Apparatus

Gilbertson et al. [242] has used a 6-joint serial-articulated robotic manipulator (Unimate, PUMA model 762, Staubli AG, Pfäffikon, Switzerland) and control system (Unimate, Mark II, Staubli, Inc.) for six-axes spinal testing. The assembly can be used in either position or load control. The caudal end of the test specimen is fixed and the cranial end mounted to the robotic arm via a six-axis load cell (UFS Model 4015A100-U760, JR^3 Inc, Woodland, CA). The loadcell has a capability to measure ±445 N in the X and Y axes, ±890 N in the Z axis, and ±50 Nm about all three axes.

The set-up was used in a new combined load and displacement testing modality, termed the hybrid method. It should be noted that this is not the same as the hybrid testing method developed by Panjabi et al. [65]. The method described by Panjabi et al. involves applying pure moment loads on an intact specimen and measuring the range of motion; then the previously determined range of motion is applied as a pure moment to a specimen with spinal construct and the load measured. This allows the comparison of different spinal reconstructions with an intact specimen over physiological loads and ranges of motion. The hybrid method developed by Gilbertson et al. uses an algorithm that aims to make use of load and position control at different parts of a cycle. This is based on control systems working more effectively in position control in the neutral region of a spinal specimen and load control when in the elastic zone.

6.4 Cable and Pulley Apparatus

Cripton et al. [243] have developed a testing machine that can apply pure moments in all three planes and assessed different methods of applying axial preloads on cadaveric lumbar functional spinal units. Bearing-mounted pneumatic cylinders and steel cables were used to apply loads to the rims of pulleys mounted on the cranial end of the specimen. The cranial and caudal ends of the specimen were mounted in PMMA blocks. The caudal end was then rigidly mounted to a six-axis load cell (MC3A-6-1000, Advanced Mechanical Technology Inc.). IRED markers were attached to the block each vertebra was mounted in and the position was measured using an optoelectronic system (Optotrak 3020, Nothern Digital Inc.). From this the relative motion of the upper vertebra relative to the lower vertebra were calculated.

Testing carried out using the apparatus described above assessed the effect of four different methods of applying axial preloads on the flexibility of human lumbar functional spinal units in flexion/extension, lateral bending, and axial rotation [243]. Specimens were subject to preloads of 0, 200, and 400 N. Loading under each preload condition was applied in steps up to a maximum of ±5 Nm. The position at the end of each load-step was measured. Two cycles were completed for each load case, with data only being taken from the second cycle. When the preload was unconstrained, as in the form of a pendulum attached to the cranial end of the specimen, a high artefact moment was produced but a low artefact shear force. Constrained preloads, such as a follower load applied through guides on the lateral sides of the vertebral bodies, resulted in the opposite.

A similar test machine was used by Miura et al. [244] in an investigation into cervical spine kinematics using axial preloads in-vitro. This study used multi-segment human cervical spine specimens with the aim of determining the moments required to obtain kinematics comparable to those measured in-vivo in all three rotational planes. A compressive preload of 100 N was applied to the specimens. Each load case comprised three cycles, which consisted of the load being applied in three equal steps. Data was only taken from the third cycle. The first protocol comprised applying pure moments of 1 Nm in each of the three rotational planes. The second protocol comprised pure moments of 2 Nm in flexion/extension, 4 Nm in axial rotation, and 2 Nm in lateral bending. It was concluded that the second protocol more accurately reflected the physiological range of motion.

Freudiger et al. [245] developed an apparatus to apply loads to multi-level specimens with four computer-controlled actuators via two anterior and two posterior ropes. A compressive load of up to 6000 N can be applied and the shear loading in both the X and Y axis can also be varied. Specimens are completely unconstrained, with the caudal end being fixed and the load applied via the ropes to the cranial end. Motion is measured using a contactless, magnetic-field based FASTRAK system (Polhemus, Colchester, Vermont, USA). Receivers are fixed to Kirschner wires that are attached to the spinal processes of the two vertebrae of interest.

Flexion/extension testing has been carried out on cadaveric lumbar spines using the test apparatus above [245]. The study evaluated the behaviour of multi-level specimens in the intact state, and then after the implantation of the DYNESYS (Sulzar Medica AG, Winterthur,

Switzerland). The DYNESYS is a dynamic neutralisation system comprising pedicle screws that are connected with a polyester tensioning cord and separated with a polyurethane spacer. This system is an alternative to fusion surgery and is designed to provide posterior stabilisation to a damaged spinal level, yet still afford some range of motion to the patient. It was found that in flexion the DYNESYS significantly reduced flexion angle and anterior displacement, and significantly increased the downward displacement of the posterior edge of the vertebral body. This suggests that the centre of rotation moved posteriorly with the implantation of the DYNESYS. In extension the DYNESYS significantly reduced the posterior displacement but had no significant effect on other displacement measures.

Lysack et al. [224] developed a test machine that can apply pure moments in one axis to a spinal specimen. The caudal end of the specimen is fixed to a base plate that is mounted on a six-axis loadcell (MC3-6-250, Advanced Mechanical Technology Inc.). The cranial end of the specimen is loaded by a micro-stepper driver-indexer (Panther LE2-DE, Intelligent Motor Systems Inc., Marlborough, CT) powering a linear actuator (B8.5-T2-23S1, Dynact Inc., San Jose, CA) that raises or lowers a floating crosshead. The floating crosshead is connected to a series of cables and pulleys that link to a main pair of pulleys mounted on the cranial end of the specimen. The main pair of pulleys is supported by a pair of cables on a constant tension spring. The cables linking the crosshead and main pulleys are tensioned using dead weights. The actuator is controlled by specialized software (Quickstep 2, Psi Software Inc., Marlborough, CT). A maximum moment of 28 Nm could be applied at a maximum frequency of 0.5 Hz. Displacement of the L3 and L4 vertebral bodies was measured using an infrared light emitting diode (IRED) optoelectronic stereophotogrammetry system (Optotrak 3020 Position Sensor, Nothern Digital Inc.). Three IREDs were positioned on each vertebral body of interest. The testing apparatus can be used for flexion/extension and lateral bending tests, though the pulleys and specimen would require remounting to change the axis of load application.

Multi-level (L2-L5) porcine specimens were tested in flexion/extension and lateral bending using the apparatus described above [224]. Moments of 5 Nm were applied at a frequency of 0.1 Hz for five cycles. Only the fifth cycle was used for data analysis. No axial preload was applied. Loading was applied in flexion/extension and in left and right lateral bending. The effect of the load on the relative displacement of the L3 vertebra with respect to the L4

vertebra was calculated. It was found that the apparatus provided a simple means to determine the dynamic characteristics of the neutral and elastic regions of spinal specimens.

The testing machine was subsequently modified for later studies [218, 219]. The same method of a floating table, cable, and pulley arrangement is used, with the addition of a linear guide that the main pair of pulleys is suspended from using cables. Such a set-up allows the main pulleys to translate more easily than when previously mounted via cables to a fixed point, thus off-axis loading is reduced.

Dickey and Kerr [219] investigated the effect of specimen length in flexion/extension. Porcine multi-level specimens were tested first in the intact state, then without supraspinous and interspinous ligaments at the L2-L3 and L4-L5 levels, and finally the specimen was transected at the L2-L3 and L4-L5 levels and the L3-L4 functional spinal unit was tested. Loads of approximately 3 Nm in extension to 13 Nm in flexion were applied in 5 cycles at a rate of 0.5°/sec. Data was taken from the fifth cycle only. No axial preload was applied. The relative motion of the L3 and L4 vertebrae was acquired in all tests. There were no differences in stiffness, range of motion, or neutral zone between the multi-level specimens with intact or cut supraspinous and interspinous ligaments. The FSU specimens had a significantly larger neutral zone and overall range of motion than the multi-level specimens but there was no significant difference in stiffness.

Dickey et al. [218] compared multi-level porcine and human specimens under pure flexion/extension moments. For the human specimens, the T11/T12 levels and L3/L4 were fixed for testing of the T12-L3 levels, with the central L2/L3 level being the level of interest. Three human specimens were studied at the L2/L3 level and three at the L1/L2 level, the L5/L6 level was studied in the porcine specimens. Five quasistatic cycles of between approximately 10 Nm in flexion and 2 Nm in extension were applied to the specimens without an axial preload. Only the fifth cycle was used for data analysis. Moment/angle plots were created from the load/displacement data acquired. The neutral zone stiffness of the porcine specimens was significantly lower than the cadaveric specimens. The overall range of motion of the porcine specimens was significantly larger than the cadaveric specimens but there was no significant difference in the elastic zone stiffness.

6.5 Discussion

The gimbal head design may comprise six active axes that can be used in either load or position control as in the case of Wilke et al. [223]. Alternatively, a simpler design with active rotational axes, a passive XY platform and an active Z-axis vertical actuator can be used as in the case of Cunningham et al. [217]. The former implementation provides more flexibility when designing testing protocols but requires a more complex control system and more space. The latter is compact and will fit on to a large number of single-axis vertical testing machines common in biomechanics laboratories. Whilst moments may be applied, the XY platform is passive so that movement is permitted to ensure moments are pure, but translational loading, to apply shear forces to spinal constructs, is not possible.

The hexapod design provides active control in all six axes but has a disadvantage of requiring a relatively complex controller. Hexapods are expensive compared to simpler designs that may be custom built in-house. Commercially available hexapods tend to be designed with high accuracy and repeatability in mind at the expense of speed, range of motion, and load capability. This means that very large systems would be required to meet the demands of simulating in-vivo loading and range of motion using multi-segment specimens. Garner-Morse and Stokes et al. [220, 221, 240, 241] have used a hexapod for the quasistatic stiffness matrix testing of single functional spinal units. This system was able to cope with the loading and range of motion for such testing but the actuators of the hexapod have a maximum unloaded linear velocity of 1.27 mm/sec [240], and therefore may not be able to produce the speed required for dynamic testing, and the size of the system may not be accommodate the range of motion necessary for multi-level testing.

Reviewing the literature suggests that pulley-based designs tend to be custom-built for specific pure moment testing. Such systems can be built relatively cheaply but if full control is required in all six axes, size and complexity are increased significantly. Such designs only tend to be used for active control in rotational axes and allow passive movement in the translational axes. This is often achieved through attaching pulleys directly to the unconstrained cranial end of a specimen. Pulley-based apparatus may limit testing protocols as it is often necessary to remount specimens in order to test a different axis, which may introduce alignment discrepancies.

7 SPINE SIMULATOR DESIGN

In order that physiological motion of the spine could be replicated in-vitro, a six-axis testing apparatus was required. This would be used to complete the stiffness matrix testing of functional spinal units in six degrees of freedom, achieved through a rotation and a translation in each of the three planes (Figure 58). The application of a movement or load in more than one axis simultaneously was also required for future studies that may adopt more complex loading regimes.

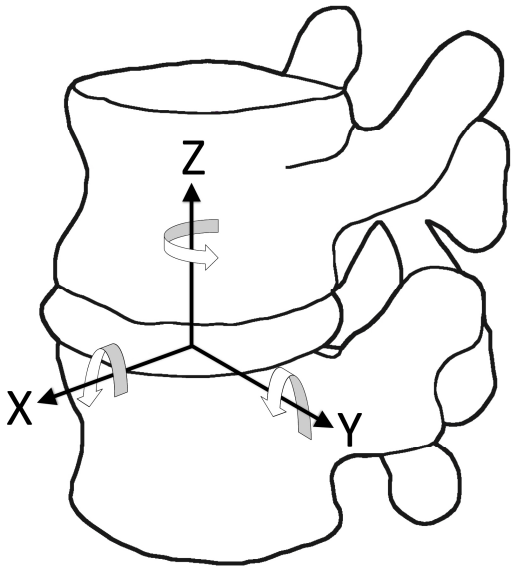

Figure 58: Orientation of the 6 axes required

The spine simulator developed as part of the present study combined elements of the testing methods of Wilke et al. [223], and Stokes et al [240]. This consists of a testing machine that is able to apply dynamic loads and movements in six degrees of freedom, similar to that developed by Wilke et al., combined with the stiffness matrix testing method of Stokes et al.. This will allow the repeatable and quantitative characterisation of specimens six degrees of freedom.

The testing protocols possible with such a simulator will provide the specific stiffness characteristics of the natural spine and allow direct quantitative comparison with artificial disc replacement devices. From this it will be possible to advance the design process of

intervertebral disc arthroplasty devices, leading to improved patient outcomes and satisfaction, particularly with regard to long-term follow-up.

The spine simulator was developed so that once the stiffness matrix studies are complete a method of adding muscle forces will be developed to further improve the understanding of the spine, and spinal implants.

7.1 Design Requirements

Two axes were available from an existing Zwick testing machine (Zwick Testing Machines Ltd., England), which was capable of applying compression/extension and axial rotation of 25 KN and 200 Nm respectively. These were designated as the translational and rotational movements in the Z axis, denoted TZ and RZ respectively.

The additional four axes were designed as an add-on structure to the Zwick testing machine. This allowed reasonable design flexibility but geometrical constraint. The add-on was required to fit within the 560 x 490 mm area of the Zwick base platform. The height of the add-on was less of a concern, due to the large amount of vertical translation available in the Zwick crosshead.

7.1.1 Loading Requirements for Spinal Testing

The loading requirements for the spine simulator were based on the capability of similar apparatus described in the literature. For example, the testing machine developed by Wilke et al. [223] has a maximum load capability of 40 Nm in bending, 500 N in shear, and 1000 N in axial compression. In stiffness matrix testing of porcine lumbar spines by Stokes et al. [240], the maximum measured loads were in the region of 35 Nm in rotation and 350 N in shear. Similar loading capabilities were desired from the spine simulator (Table 10).

Table 10: Required load capacity of the spine simulator

	Translations	Load (N)	Rotations	Moment (Nm)
X	A/P shear	500	Flex/ext	40
Y	M/L shear	500	Lat bending	40
Z	Axial compression	1000+	Axial torsion	40

7.1.2 Range of Motion Required for Spinal Testing

The ranges of motion of the natural human spine at each level are reasonably documented and this data was used to determine a suitable range of motion for the spine simulator. Though the testing for this study was to concern the lumbar spine, efforts were made so as to allow the testing of any region of the spine in future studies.

The initial testing using the spine simulator would use functional spinal units (two vertebral bodies separated by an intervertebral disc). However, it was taken into account that carrying out multi-level testing would be desirable in future projects. The spine simulator would be constructed so to be capable of testing single levels to the extremes of motion, and multi-level specimens to a realistic physiological range of motion. Therefore, the range of motion was maximised within the geometrical constraints of fitting the add-on apparatus within the Zwick test machine base platform.

Approximate normal ranges of motion in the spine are reported for the lumbar and cervical spine in Tables 11 and 12, respectively. Translations in both shear and axial compression are small compared to the rotational ranges of motion. Gardner-Morse and Stokes used shear displacements of ±0.5 mm and axial compression/extension of ±0.35 mm for the stiffness matrix testing of human functional spinal units in the linear region. These values are considerably less than the physiological range of motion [221]. Stokes et al. [240] used translations of ±0.4 mm for axial compression/extension, ±1.5 mm for lateral shear, and ±3.0 mm for anterior/posterior shear in similar stiffness matrix testing of porcine functional spinal units. Neither of these studies however, tested the specimens in the extremes of motion. Miller et al. [246] applied loads of 980 N in anterior and posterior shear, and 490 N in left lateral shear to cadaveric lumbar functional spinal units. Each load produced in the region of 10 mm translation of the superior vertebral body relative to the inferior vertebral body.

Table 11: Approximate range of motion of the lumbar spine. Modified from White and Panjabi [4]

Level	Flexion/Extension (Combined)	Lateral Bending (One-Way)	Axial Rotation (One-Way)
T12-L1	12°	8°	2°
L1-L2	12°	6°	2°
L2-L3	14°	6°	2°
L3-L4	15°	8°	2°
L4-L5	16°	6°	2°
L5-S1	17°	3°	1°

Table 12: Approximate range of motion of the cervical spine. Modified from White and Panjabi [4]

Level	Flexion/Extension (Combined)	Lateral Bending (One-Way)	Axial Rotation (One-Way)
C0-C1	25°	5°	5°
C1-C2	20°	5°	40°
C2-C3	10°	10°	3°
C3-C4	15°	11°	7°
C4-C5	20°	11°	7°
C5-C6	20°	8°	7°
C6-C7	17°	7°	6°

7.1.3 The Simulation of Muscle Forces In-Vitro

The importance of muscles in providing stability to the spine is well documented [220, 221, 240, 247-249]. White and Panjabi stated that if the spinal column including intervertebral discs and ligaments but without muscles were fixed at the sacrum, it would only be capable of carrying an axial load at the T1 level of 20 N before buckling [4]. This would not even support the weight of the upper body. Muscles provide the required stability in addition to providing a means of carrying out movements.

The action of spinal muscles is complex and there remains a great deal of uncertainty in how the muscles work to stabilise and move the spinal column. This creates great difficulty in appropriately simulating muscle forces in-vitro. Of particular interest in spinal testing is the axial preload, which has been shown to increase spinal stiffness [220, 221, 240, 241, 249]. However, achieving a universally accepted method of applying such a force in-vitro, if indeed a preload is used at all remains to be established [4, 243]. This is of particular importance in multi-segment testing, when potential inaccuracies and limitations in the test set-up may be amplified due to the increased length and range of motion of the specimen.

Artefact forces and moments resulting from an axial preload should be avoided. A vertical preload may be applied directly onto the cranial end of the specimen [220, 221, 240]. This may be appropriate in certain circumstances, such as the testing of functional spinal units, though for multi-segment specimens it may be more suitable to apply a load on either side of the vertebral specimen at the approximate centre of rotation of the vertebral levels [234, 235, 244, 249]. In the latter method the load is often referred to as a follower load as it approximately follows the tangent of the curvature of the lumbar spine [250]. The follower load concept was adopted by Cripton et al. [243] for flexion/extension and lateral bending testing in their study into various methods of preload application. The main limitation associated with this approach is that it will always be difficult to entirely dispose of artefact forces arising from the use of the follower load given that the centre of rotation in the natural disc is not constant [5], while the follower load method depends upon knowing the centre of rotation of the disc.

In tests completed using the custom spine tester developed by Wilke et al. [223], no specific axial preload due to the weight of the torso and head was applied but the force from 5 muscle groups was simulated using cables. It was found that by applying different muscle forces, the load-deformation characteristics and intradiscal pressure of the spine was significantly altered.

Further testing by Wilke et al. [235] has since being carried out to determine trunk muscle forces in flexion and extension. For this investigation symmetrical pairs of muscles, including the erector spinae and the rectus abdominis, a follower load representing local muscles, a vertical preload replicating the bodyweight and a supporting force of the abdomen were simulated. A total of 124 load cases were studied, which comprised altering the application

and magnitude of the different loads, the angle of flexion/extension, and hip flexion without bending of the lumbar spine. Following the positioning of the spine with stepper motors, the loads were applied and then the resultant moment was reduced to zero by adjusting the erector spinae muscle force.

This study is the only one found in the literature in which the preload due to the bodyweight has been applied ventrally to the vertebral bodies. The preload was applied vertically downwards at a distance of 30 mm from the centre of the T12-L1 disc. Such a preload can only reasonably be applied if, as in the above case, muscle forces are simulated to balance the moment created by the preload.

In addition to testing in the rotational axes, investigating the shear characteristics of the natural disc and a disc replacement device may provide insight into how the device may perform in-vivo. Stiffness matrix testing was completed by the Department of Orthopaedics and Rehabilitation at the University of Vermont. This included testing on both porcine [220, 240] and human lumbar motion segments [221, 241]. Testing was completed using axial preloads of various magnitudes, applied to the cranial end of a functional spinal unit, to determine the effect of such loading on the spinal stiffness. This testing has given an excellent insight into the natural mechanical properties in a spinal motion segment, which is crucial to the development of disc replacement devices that replicate the natural biomechanics as closely as possible.

7.1.4 Control System Requirements

The stiffness matrix tests will require position control only but the test machine should allow both load and position control to permit alternative testing protocols in future studies. A combination of the two control methods should be possible for different axes during the same test procedure, i.e. independent control of all axes should be achieved.

Stiffness matrix testing involves moving one axis by a given distance or angle, and allowing no movement in all other axis. In contrast, pure load testing requires a position or load demand in one axis whilst maintaining a zero load in all other axes. Any combination of applied positions and loads was desired to maximise the potential for complex loading situations in future studies.

7.2 Design and Development

7.2.1 Design Concepts

Initial research into existing testing machines suggested that a robotic arm or hexapod would be able to provide the required loading and range of motion. However, the cost of these machines is prohibitive. Therefore a custom machine was designed and built based around the concept of an XY platform and gimbal head; the XY platform would provide shear translations (TX and TY) and onto this a gimbal head would be mounted that could apply rotations about the X and Y axes (RX and RY). This assembly would be mounted onto the existing Zwick testing machine, which was capable of providing the Z axis translation (TZ) and rotation (RZ) (Figure 59).

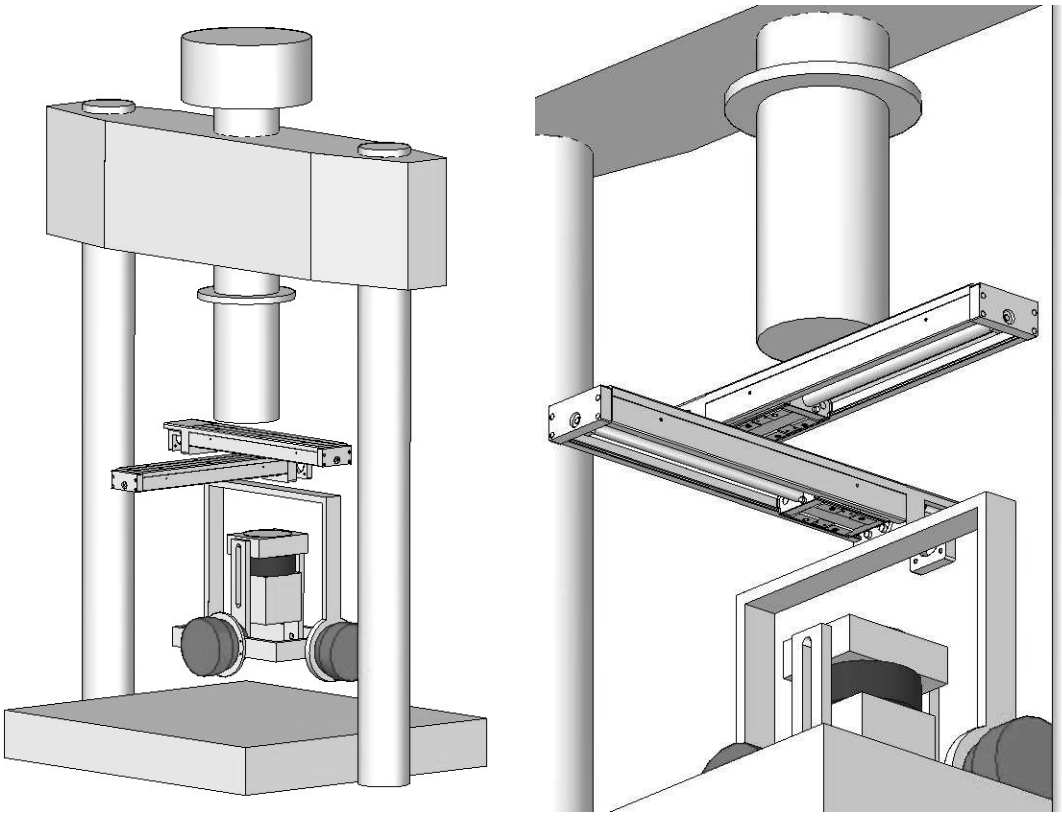

Figure 59: XY platform and gimbal head concept

The translations in the XY platform would be produced using ball screw driven linear actuators mounted perpendicular to each other. It was important to keep the axial length of the motor and gear assembly of each axis of the gimbal head to a minimum; it was anticipated that harmonic drive gears and flat brushless motors would be suitable for this

purpose. Harmonic drive gears were used in the test-rig developed by Wilke et al. [223] and would be suitable for this apparatus due to the low axial length, high gear ratio, and zero backlash that they provide.

A harmonic drive gear comprises three main components: a circular spline, a flexspline, and a wave generator. The circular spline is a rigid steel ring with internal teeth. The flexspline is a thin-walled ring with external teeth and a mounting flange. The wave generator is an elliptical shaped plug that is connected to the input shaft. The harmonic drive is generally used with the flange on the flexspline as the output drive, and using this configuration, the circular spline is fixed to the assembly housing. The flexspline is smaller in diameter to the circular spline, and therefore has fewer teeth. The wave generator elastically deforms the flexspline, causing teeth to engage with the circular spline. As the wave generator rotates the area of tooth engagement moves, causing the flexspline to rotate in the opposite direction to the wave generator.

Each rotation of the wave generator causes the flexspline to rotate two teeth in the opposite direction. This allows large gear reductions in a small axial length, and because more than one tooth is engaged at any time the assemblies have a high torque capacity and zero backlash.

The predominant challenge was in fitting the XY platform within the 560 x 490 mm area of the Zwick test base, whilst still offering a reasonable range of motion in each axis. The crucial dimension was the width of 560 mm, as the pillars that the Zwick crosshead is mounted on are positioned either side of the test base (Figure 60). In axial torsion the entire XY platform and gimbal head below it would be rotated. Therefore the maximum length possible in the XY platform or gimbal as measured from the centre of rotation in the z-axis to the farthest point from it was required to be less than 280 mm.

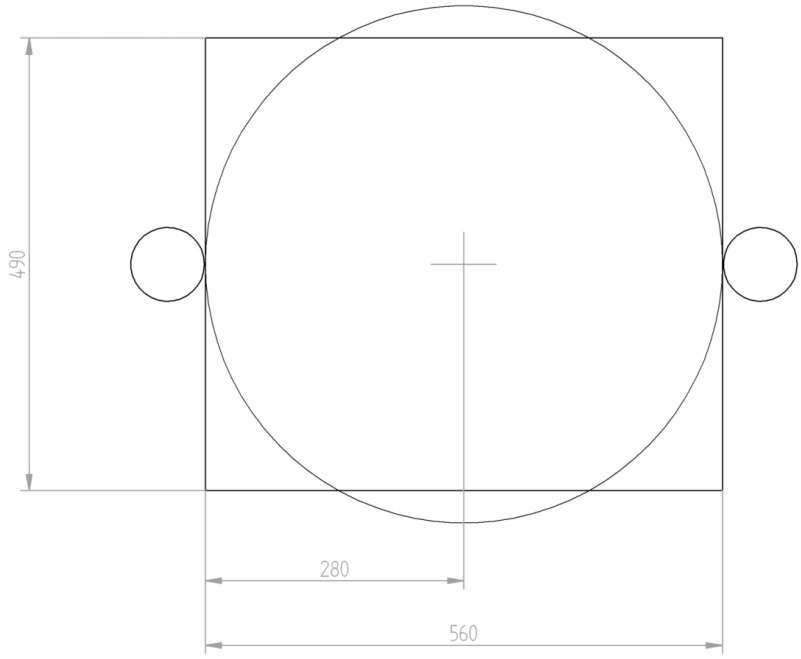

Figure 60: Zwick baseplate and area for spine simulator

If pure moments are to be applied to a specimen in future studies, the XY platform will have to translate freely to ensure that there is no shear loading on the specimen [224]. The amount of translation required is related to the angle of rotation and the length of the specimen (Table 13). In order to estimate the translation required for multi-level tests it was assumed that each level would flex equally, i.e. for a rotation of 50° in a specimen of 6 vertebral bodies and 5 intervertebral discs, each level would have 10° of rotation (Figure 61).

Table 13: Required translation for multi-axis specimens based on Figure 61

Level	Angle (Degrees)	Translation (mm)
L1-L2	10	97.0
L2-L3	10	66.3
L3-L4	10	40.6
L4-L5	10	20.6
L5-S1	10	6.9

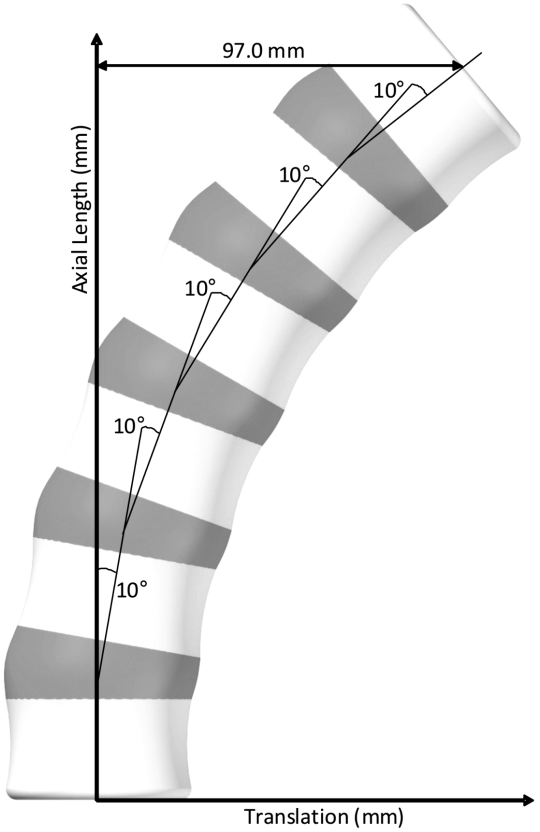

Figure 61: Estimating the translation of multi-level specimens

The spine simulator would therefore be designed to have ±100 mm of translational motion in the X and Y axes.

7.2.2 XY Platform Design

In order to measure the load in the X and Y axis, each linear actuator would have two platforms. One would be fixed and driven by the ball screw actuator and one would be free. A loadcell would be fixed to the driven platform and connected to the free platform, upon which the next level of the simulator would be fixed. This would allows the X and Y loads to be driven through the load cells and prevent any off-axis loading of the loadcell. The disadvantage of having two carriages is that the range of motion in the X and Y axes is reduced.

In addition to the motor and actuator assembly of the XY platform, and the motor and gear assembly of the gimbal head, load cells were required for all four axes. The Zwick testing

machine that was providing the final two axes already has all position and load sensors. The load cells were arranged in such a way as to minimise the effect on the overall dimensions of the simulator to avoid reducing the range of motion achievable. In the case of the torque in the X and Y axis, this meant acquiring transducers of minimal axial length.

The initial design allowed estimates of the off-axis loading on the XY platform to be made (Figure 62), based on the load capability in the requirement specification. THK (THK UK, West Midlands, UK) and Bosch Rexroth (Bosch Rexroth Ltd., St. Neots, UK) products were assessed for suitability. Both companies were able to provide components meeting the specified requirements but it was found that Bosch were more costly and were suited to providing an entire product system with control software. THK were able to offer a more tailored product that would better integrate with other products and software, and the existing Zwick testing machine.

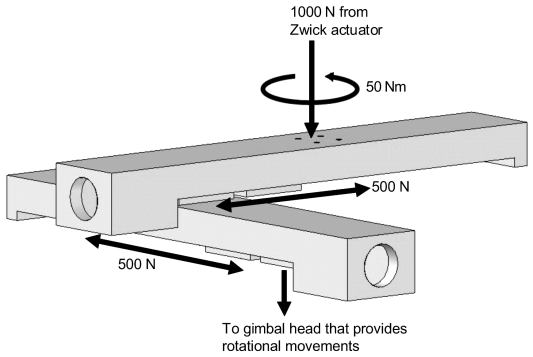

Figure 62: XY Platform concept and load calculation

THK recommended the KR33 linear guide actuator. The 300 mm model would be the longest that would fit within the required area. A travel of 185.4 mm is possible when using two short carriages. It was clear from the technical data that the moments produced through the carriage due to off-centre loading would be the limiting factor in part selection. It was estimated from this that the maximum lever arm in the X and Y axis would be no larger than 150mm. Using this lever arm to estimate the maximum moments resulted in axial moments of 50 Nm, and lateral and longitudinal moments on the carriages of 150 Nm.

The KR33 with short carriages only have a load capacity of 44 Nm for longitudinal and axial moments. The capacity of the long carriages is 166 Nm but this did not offer a suitable safety factor. In order to meet the load requirements two long carriages on the larger KR45 model

would be required. However, the longest actuator that would fit within the required space was 440 mm and provides a stroke of 105 mm. The actual stroke length would be reduced once the loadcell and coupling were assembled. This was not sufficient to provide the required translations for multi-segment specimens.

Therefore a new design was developed using a parallel arrangement of two linear guide rails and one linear ball screw for each translational axis (Figure 63). Each linear guide rail features two small carriages to increase the rigidity of the assembly. A loadcell connects the ball screw to a platform mounted on the linear guides, thus ensuring that the loadcell is not subjected to off-axis loading and that the XY platform is suitably rigid (Figure 64).

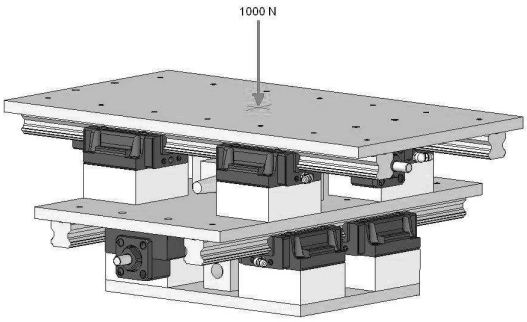

Figure 63: Linear guides and ballscrew

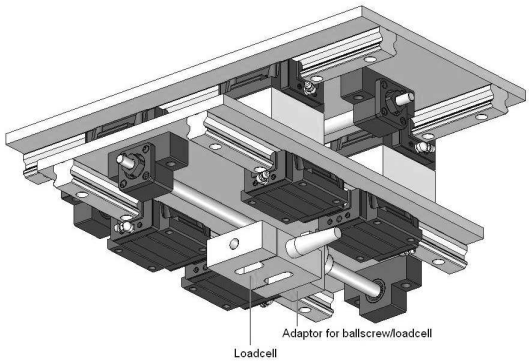

Figure 64: Linear guides and ballscrew

This design uses HSR25 linear guides (THK), which meet the required load capacity, including a safety factor of two (Table 14). However, the load capacities listed are for only one rail, therefore two parallel rails would result in increased load capacity. A BNK1202 ball screw (THK) was chosen, which has a dynamic and static load capacity of 1.7 kN and 3.6 kN respectively. The ball screw is fixed at one end to allow coupling to a motor, and is supported at the other end (Figure 65).

Table 14: HSR25 linear guide rail load ratings

Load Description		Load Type	Load Rating
Radial (kN)	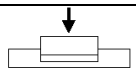	Dynamic	19.9
		Static	34.4
Reverse Radial (kN)	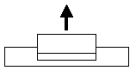	Dynamic	19.9
		Static	34.4
Side (kN)	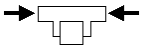	Dynamic	19.9
		Static	34.4
MA two blocks (Nm)		Static	2740
MB two blocks (Nm)	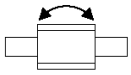	Static	2740
MC one block (Nm)		Static	344

Whilst this parallel rail arrangement improves the rigidity of the XY platform, it also increases the maximum diagonal dimension of the assembly, which in turn lowers the maximum possible range of motion available in translation. The width of 560 mm can not be increased but it is permissible that the depth of the assembly be more than the 490 mm of the Zwick base platform, provided that it does not come into contact with the pillars of the Zwick test machine when rotated in the Z axis.

The ball screw and loadcell require a space of 150 mm between the linear guide rails. It was estimated that the requirement of ±100 mm translation could be achieved, though more certainty would be gained as all parts were either designed or selected. A 400 mm rail is used in the X axis and a 350 mm rail in the Y axis. The linear guide carriages are spread further apart in the X axis for mounting the Y axis onto it, giving both axes approximately the same travel.

Two 615 load cells (Procter & Chester (Measurement) Ltd., UK) are used in the XY platform, each with a load capacity of ±500 N. Each load cell is fixed to the ball screw at one end and to the plate that is mounted on the linear guides at the other end (Figure 65).

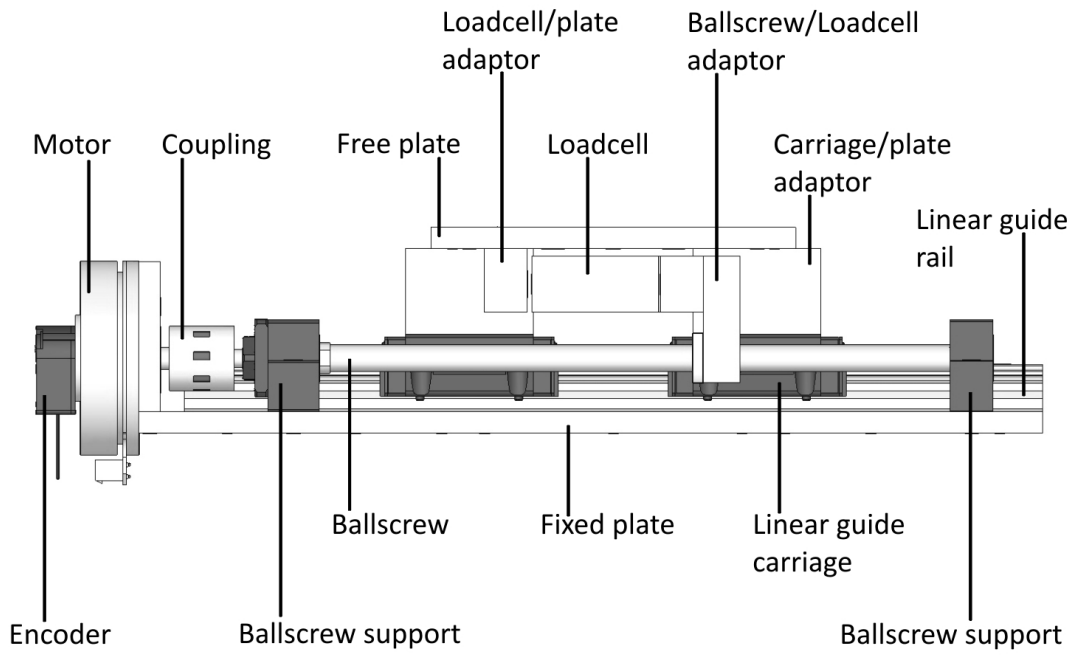

Figure 65: Side view of translation axis, one linear guide assembly is removed for clarity

Flat brushless motors are used to drive the ball screw in order to keep the length of the assembly to a minimum. Maxon motors (Maxon Motor UK Ltd., Finchampstead, UK) were consulted and the Maxon EC90 motor was recommended. The 24 V model of this motor has a continuous load capacity of 387 mNm, so it is easily able to provide the estimated 176 mNm to drive the ballscrew. The motors are both pre-fitted with a Maxon HEDL5540 encoder. The motor assembly and ball screw are coupled using a Lenze GESM jaw coupling (Lenze Ltd., Bedford, UK) due to the modular design that allows a variety of shaft sizes to be connected. The coupling is rated at 3.7 Nm, which easily meets the required torque.

The design led to the overall length of the X and Y axis to be 470 mm and 444 mm respectively. The axial rotation actuator of the Zwick has a range of motion of ±45°. The requirement of ±100 mm of travel in the X and Y axis was met. However, it is not possible to apply 100 mm of translation in the X axis at the same time as 45° of rotation in the Z axis (Figure 66). Such combined movements would cause the add-on apparatus to contact the pillars of the Zwick testing machine. This was not seen as a major problem due to it being unlikely that applying such extremes of motion in both axes simultaneously would be required. However, should testing be carried out in load control, the limitations should be noted and taken into account in the control software so that any contact between parts is avoided.

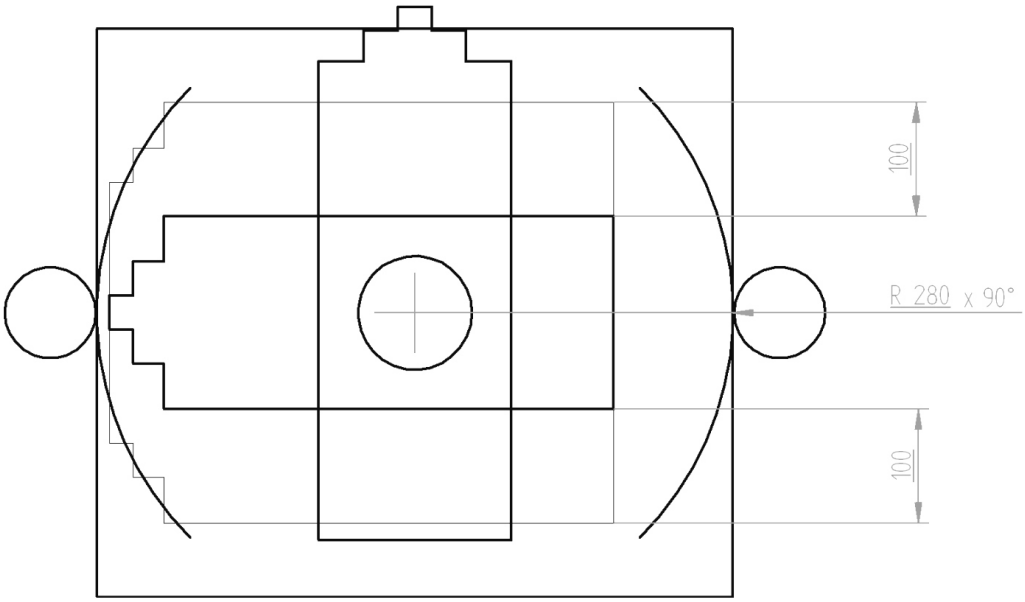

Figure 66: Spine simulator footprint. Black lines show the Zwick, XY platform, and 280 mm radius arc. Grey show the ±100 mm movement of the Y axis mounted on the X axis.

This design was suitable to fully develop, provided that the gimbal head assembly did not interfere with the Zwick test machine. Both the X and Y axes have a range of approximately ±100 mm and a load capacity of load 500 N.

7.2.3 Gimbal Head Design

The gimbal provides two rotational axes (RX and RY), with the Zwick testing machine providing the third (RZ). The gimbal comprises an outer frame, an inner frame, and a specimen pot for accommodating the cranial end of a specimen. The outer frame is mounted to the XY platform, the internal frame is mounted within the outer frame, and the pot is mounted within the internal frame. The outer and inner frames are linked via a motor/gear assembly and bearing unit, as is the inner frame and specimen pot (Figure 67). This arrangement allows independent rotations in the X and Y axis. Height adjustment of the specimen pot is integrated into the design to allow the centre of rotation of the disc of a functional spinal unit to be aligned with the centre of rotation of the rotational axes (RX, RY and RZ). The height adjustment also allows adjustment for multi-level specimens in future studies.

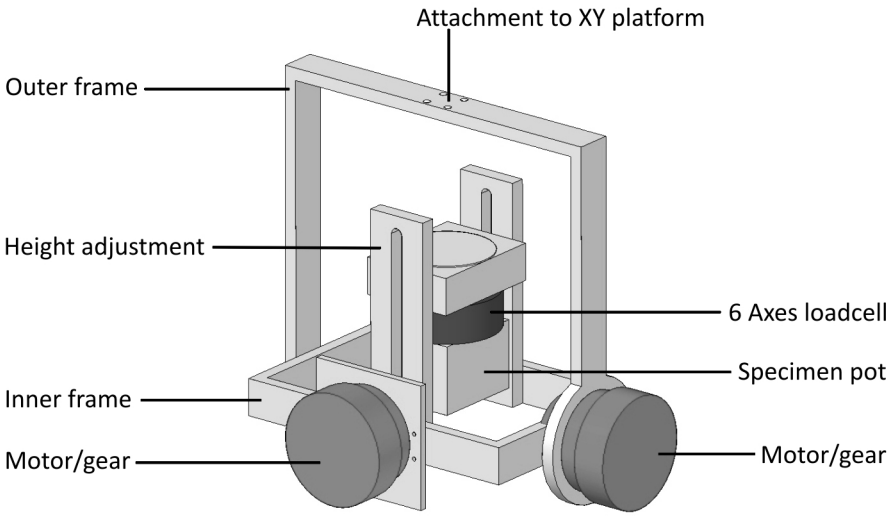

Figure 67: Initial gimbal frame design

Basic beam calculations were completed on the initial design. Due to the high loads that would be present the vertical sides of the outer gimbal head were modified to steel channel section (Figure 68).

It was important that the axial length of the motor and gear assembly were minimised. Harmonic drive gears are used on the test machine developed by Wilke et al. [223]. Such gear assemblies can provide high gear ratios and zero backlash within a compact unit. Harmonic Drive (Harmonic Drive UK Ltd., UK) suggested the HFUC gear assembly with a built in bearing unit, which is available pre-assembled with a Maxon EC90 motor and HEDL 5540 encoder. The 24 V EC90 motor (product no. 323772) has a maximum continuous torque of 387 mNm. A step-down ratio of 80:1 gives a maximum continuous torque of just under 31 Nm. However, the stall torque of the motor is 4670 mNm, which allows higher torques to be briefly applied. The harmonic driver gear has a repeated and momentary peak torque of 43 Nm and 87 Nm respectively. The bearing unit of the harmonic drive gear has a dynamic and static load capacity of 5.78 kN and 9.0 kN respectively, and a maximum permissible dynamic and static tilting moment with a safety factor of two of 64 Nm and 80 Nm respectively. The maximum permissible axial and radial loads on the bearing unit are 3.21 kN and 2.15 kN respectively.

An additional bearing unit is used on the non-drive side of the RX and RY axes (Figure 69). The bearing is predominantly loaded radially, though some axial loading is present when shear loading is applied. The SKF 6200 (AB SKF, Gothenburg, Sweden) single-row, deep-groove, sealed bearing has a dynamic and static radial load capacity of 5.4 kN and 2.36 kN respectively, and an axial load capacity of 0.59 kN. This suitably withstands the loads expected in the spine simulator. Counterweights were placed on the non-drive side of the RX and RY axes. These counteract the moment due to the weight of the motor and gear assembly. They are also used to locate the non-drive side bearing housing.

TRS torque transducers (Procter & Chester (Measurement) Ltd, UK) were selected for the RX and RY axes. They have a compact size and low axial length compared to other products available. The capacity of ±50 Nm matches the torque requirement.

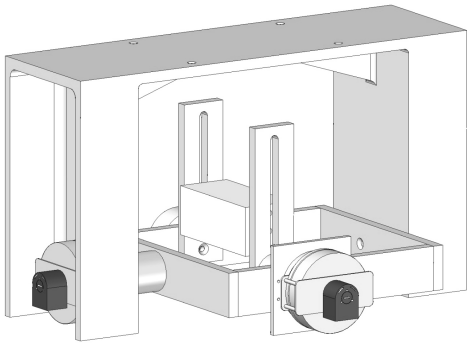

Figure 68: Modified gimbal design

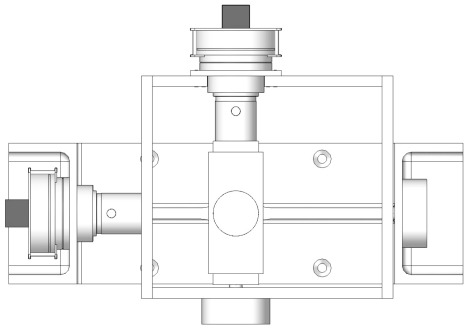

Figure 69: Gimbal X and Y axes of rotation

The length of the inner frame, upon which the RY axis is mounted, was sized so as to provide a range of motion of approximately ±45°. The width was designed to be able to accommodate porcine and human specimens. Anatomical measurements of the human thoracic vertebrae indicate that the T1 is the widest of the thoracic region, being 75.3 mm from edge to edge of the transverse processes [4]. Busscher et al. [251], comparing the anatomy of the human and porcine spines, found that the total width of the transverse processes in the lumbar region to be approximately 75 mm and 90 mm in porcine and human specimens respectively. This study used 6 porcine spines from 4 month-old pigs with a mean mass of 40 kg, and 6 human spines from males with a mean age and height of 72 years and 182 cm respectively. The width of the transverse processes of the T1 vertebra was the widest of the thoracic region, approximately 80 mm, which reasonably matched with the value published by White and Panjabi [4]. Dath et al. [252] found that the transverse

processes of the L3 and L4 vertebrae were the widest of the lumbar region in porcine specimens, 125.9 and 125.8 mm from edge to edge respectively. The wider dimension found by Dath et al. is likely due to the spines being from pigs with an age range of 18 to 24 months and a mass of 60 to 80 kg, rather than 4 months and 40 kg as in the study Busscher et al. [251].

Though the above data is limited, it suggests that the transverse processes of porcine spines in mature pigs are larger than those in mature humans. The width of the internal frame was therefore designed with a specimen clearance of 134 mm.

During the development of the gimbal design, it was found that the six-axis loadcell would be more easily accommodated underneath the caudal specimen pot. This increases the height of the specimen from the base plate, thus providing a larger range of motion in the RX axis without the internal gimbal frame interfering with the base plate. Additionally, it removes the mass of the loadcell from the simulator, preventing an unnecessary increase to the simulator inertia. A large inertia may cause the simulator to overshoot the desired position or cause unwanted vibration during dynamic testing. An existing AMTI MC3-A-1000 (Advanced Mechanical Technology Inc., MA, USA) six-axis loadcell was available. The load capacity is 2200 N in the X and Y axes, and 4400 N in the Z axis. The torque capacity is 110 Nm in the X and Y axes, and 56 Nm in the Z axis.

7.2.4 Simulating Muscle Forces In-Vitro

The present study focused on stiffness matrix testing without muscle forces. However, the simulator was designed so to allow the introduction of muscle forces at a later stage. The addition of muscle forces to the spine simulator would enhance the ability to replicate physiological loading in-vitro. Recent work has greatly increased the understanding of the complex structure of the spine but there remains a great deal still to learn about the role of muscles within this complex structure [211, 212, 234, 235, 253]. Further knowledge in this area would provide invaluable information for the development of spinal instrumentation.

A study investigating the force and position of muscle forces was completed, with the view to modifying the spine simulator to include key muscle forces at a later date. A beta-testing

license for Skeleton and Muscles (SAM) software was provided by Marlbrook (Marlbrook (UK) Ltd., Worcestershire, UK) prior to the general release to the public.

SAM works through Simulink functions in Matlab (MathWorks, Inc. MA, USA), and models the muscle forces, joint forces, and movements of the human skeleton based on input conditions set by the user. The model comprises 666 muscle units in 196 muscles on a full human skeleton, which itself consists of 35 joints and 36 segments. The model does not feature finger or toe joints. Input conditions consist of gravity and boundary conditions, movements of the skeleton about a joint, and forces or pressures that may be present on a position or area of the body.

7.2.4.1 Validation of SAM Software

It was important to first validate the software against published muscle force data. The conditions of part of a study by Dolan et al. [37] to estimate erector spinae muscle activity during bending and lifting activities were input as closely as possible in SAM and the results compared with those obtained by Dolan et al. using EMG measurements in-vivo. The skeleton model was set to a male with a mass of 77 kg. To simplify the input parameters, a static loading situation was modelled. The SAM skeleton was positioned with the spine in 9.5° of curvature and the arms hanging vertically downwards. Reaction loads of half the bodyweight were placed underneath each foot acting vertically upwards to simulate gravity. A load of 98.1 N was applied to each hand, representing a total of 20 kg being held in both hands. The model was run for 10 seconds, with muscle loads being calculated by the software from 3-10 seconds. The delay in muscle force calculation allows the model to stabilize prior to estimating muscle forces and was a setting that was recommended by the manufacturer.

Setting the curvature of the spine to 9.5° allowed a comparison not only with the results from the 20 kg lift but with the male subject in the static reproducibility tests that were completed as part of the study by Dolan et al. For this, the subject was in a fixed spinal curvature and was asked to pull vertically up on a loadcell for 3.3 seconds. The load that the subject exerted on the load cell was not published, so the load may not have equated to the 20 kg used in the SAM model but the body position was replicated, which would allow some comparison to be made.

The reproducibility testing of the male subject with a lumbar curvature of 9.5° carried out by Dolan et al. resulted in an estimated extensor moment of 316 Nm (S.D. 19). The lifting of a 20 kg mass by 10 subjects resulted in a peak extensor moment in the region of 300 Nm. A similar extensor moment would be expected in the SAM model (Figure 70).

Another study by Dolan et al. [254] used the same measurement system to estimate erector moments when carrying weights using a squat lift and stoop lift technique. These findings could be used to assess the numerical predictions of the SAM model. The 21 male subjects in this study had a mean mass of 77.0 kg, matching that of the SAM model. The peak erector moment estimated when lifting a 20 kg mass was 329 Nm using the squat lift and 280 Nm using the stoop lift. This compares well with the previously mentioned study by Dolan et al. From this published data, an erector moment of approximately 300 Nm was expected using the SAM model.

Figure 70: Muscle force simulation using SAM software

It was found that over the 7 seconds period in which the muscle forces were calculated, the magnitude fluctuated slightly (Figure 71), whereas one would expect constant forces due to the static nature of the test. This may be a result of the optimisation strategy implemented within the software to allow the calculation of a solution to this statically undetermined problem. Therefore the mean force over the 7 second period was taken and the individual muscle forces were added together to obtain a total for each muscle group. The muscle groups of the spine that produced the largest forces were the erector spinae, multifidis lumbar, and the psoas major.

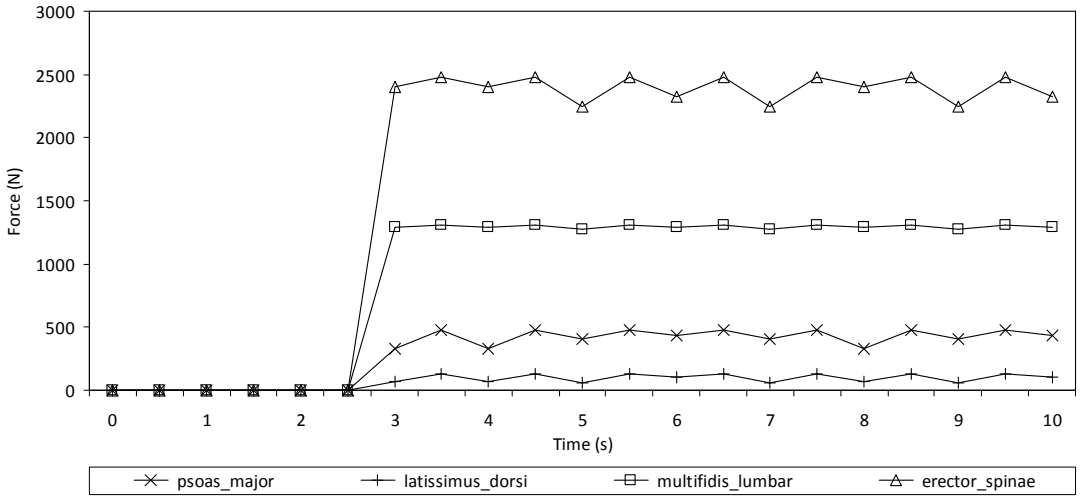

Figure 71: Muscle forces for a subject holding a 20 kg mass with 9.5° of lumbar curvature

The total extensor moment was estimated using a lever-arm of 0.05m [3, 28]. The total muscle force due to the erector spinae muscles was 2397 N giving an extensor moment of only 120 Nm. This is far less than the 300 Nm estimated by Dolan et al. [37, 254]. However, Dolan et al. [37] found that the passive tension from the back muscles and fascia might be as high as 100-150 Nm. In the case of the static reproducibility tests, the mean value was 54.3 Nm at 9.5° of lumbar curvature. This would mean that the extensor moment would be higher than that estimated in SAM, though this would still only make it approximately 200 Nm, 100 Nm less than expected based on the in-vivo measurements by Dolan et al.

It is likely that this is because other muscle groups need to be included in the erector moment and the activity of other muscles may have been included in the EMG activity used in the study by Dolan et al. Indeed, such unknowns are discussed in the paper [37].

Including the multifidis lumbar muscle forces of 1297 N would give a total muscle force of 3694 N and an extensor moment of 185 Nm. If the 428 N of the psoas major is also included, the extensor moment increases to 206 Nm. With the addition of a passive tension of 54.3 Nm, this gives a reasonable comparison to the EMG data obtained by Dolan et al. of approximately 300 Nm. The lower value may be due to the SAM software using optimisation algorithms, whereas the body may tend to overcompensate to ensure stability. This may result in some muscles actually working against extension, therefore requiring higher extensor muscle forces. Such antagonistic muscle activity is discussed by Dolan et al. in the study used for validation of the SAM software [37], and in a study investigating dynamic forces during manual handling [29]. Rohlman et al. [227] found using a finite element model, that replicated the loading conditions of the experimental work by Wilke et al. [235], that an increase from 20 N to 50 N in the rectus abdominus increases the force of the erectus spinae muscles by 100-150 N.

From the comparison outlined above, it was decided that muscle forces using data obtained using SAM software would be a worthwhile addition to the spine simulator. Therefore, further simulations were completed using the SAM software with input parameters of the stiffness matrix testing completed by Stokes et al. on a porcine disc [240]. Only the rotations of ±4° in each plane could be used, as the software has simplified the spinal levels to only allow rotational movement.

7.2.4.2 Materials and Methods

Separate investigations were completed for flexion, extension, left lateral bending, right lateral bending, left axial rotation, and right axial rotation. The model began each test in an upright neutral position, and the L4-L5 joint was rotated with the rest of the body remaining static. As with the previous tests, the skeleton model was set to be male with a mass of 77 kg and reaction loads of half the bodyweight were placed underneath each foot acting vertically upwards to simulate gravity. The movement of the L4-L5 joint was completed at a rate of 0.5°/sec until 4° of rotation was reached. The model was run for 10 seconds with the muscle forces being calculated from 3-10 seconds.

7.2.4.3 Results

The same muscles as in the validation tests were investigated (erector spinae, multifidis lumbar, psoas major), plus the rectus abdominis as this group had increased muscle activity in extension, and the latissimus dorsi, which had increased activity in lateral bending. These muscle groups, with the exception of the latissimus dorsi, were the same used by Wilke et al. [223, 235] in flexion/extension studies using simulated muscle forces.

Most of the predicted muscle activity was reasonably constant (Figures 72-75), with more of varied muscle force in the erector spinae during flexion/extension, and in the rectus abdominis in extension. The slight drop in almost all muscle group forces between 9.5 and 10 seconds may be due to the rotation reaching 4° at 9.5 seconds and the model being in a static position between this point and the end of the test at 10 seconds.

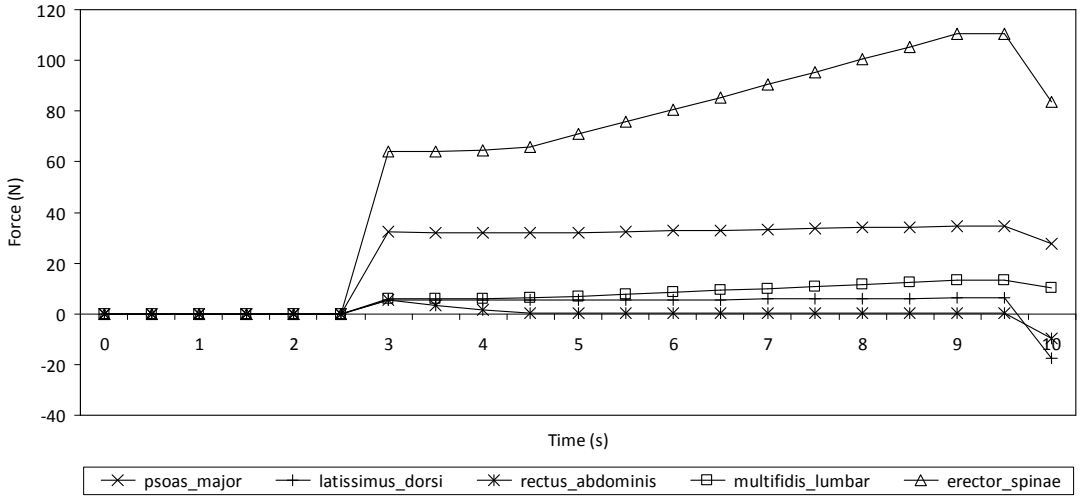

Figure 72: Muscle forces for a ramp from 0-4° of flexion

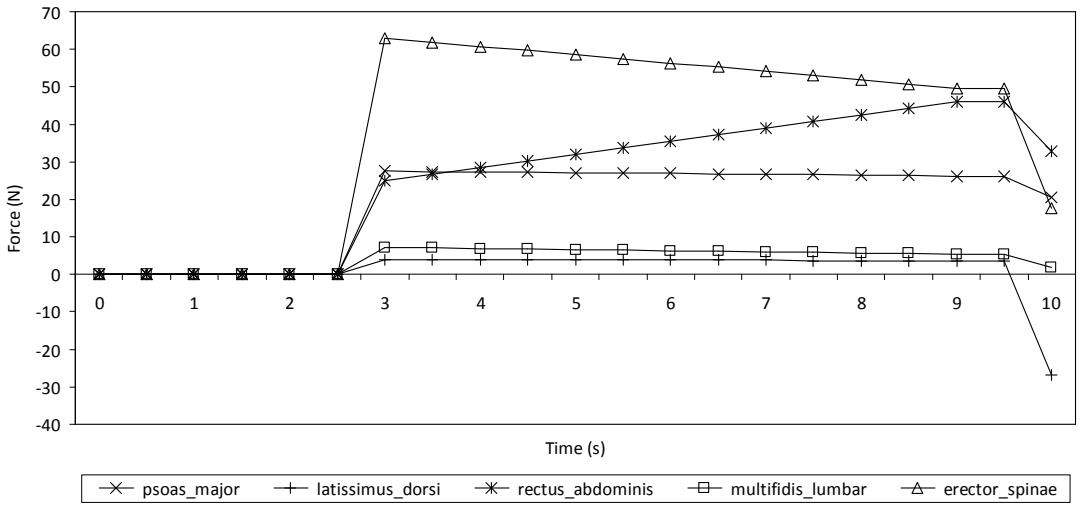

Figure 73: Muscle forces for a ramp from 0-4° of extension

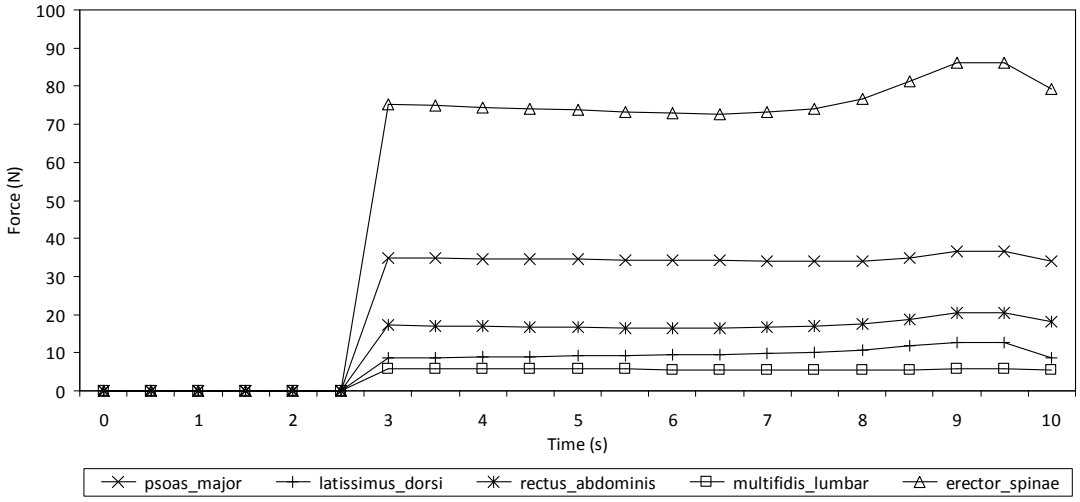

Figure 74: Muscle forces for a ramp from 0-4° of left lateral bending

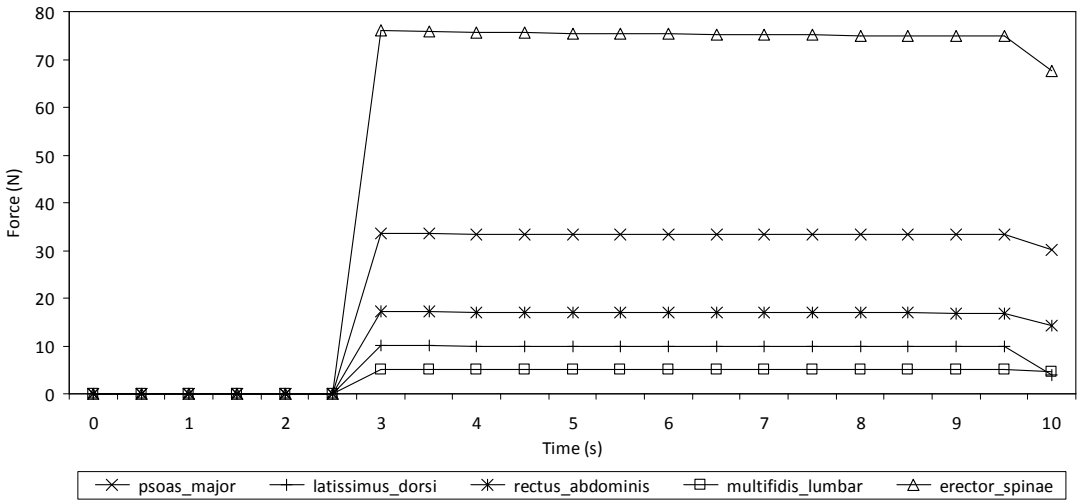

Figure 75: Muscle forces for a ramp from 0-4° of left axial rotation

Due to the relatively constant muscle forces predicted between 3 and 9.5 seconds, it was decided worthwhile to use the mean muscle force during this period (Table 15). This would mean that dead-weights or tensioned cables could be used to apply the forces, rather than a system similar to that used by Wilke et al. of computer controlled pneumatic actuators connected to cables.

The forces in left and right lateral bending were not equal, and nor were they in left and right axial rotation. Symmetry in the coronal plane should have resulted in equal forces in each direction and it is unknown why this is not the case from the results obtained from the SAM model. The mean force of each direction was taken to obtain overall muscle forces for lateral bending and axial rotation.

Table 15: Mean muscle forces (N) due to rotational motion

	Flexion	Extension	Lateral Bending	Axial Rotation
Erector Spinae	85	56	67	71
Multifidis Lumbar	9	6	6	5
Psoas Major	33	27	33	32
Latissimus Dorsi	6	4	9	8
Rectus Abdominis	1	36	15	16

The magnitude of the muscle forces for each rotational direction investigated was reasonably consistent. Therefore, the forces were simplified to one muscle force for all movements by taking the mean for each muscle group from all tests completed using the SAM software (Table 16). This would be more practical for in-vitro testing in the ±4° range that was investigated.

Table 16: Mean muscle forces (N) for major muscle groups

Erector Spinae	Multifidus Lumbar	Psoas Major	Latissimus Dorsi	Rectus Abdominis
69	6	32	7	16

7.2.4.4 Analysis of Muscle Force Predictions

In order to simulate the predicted muscle forces in-vitro, the directions of the forces are required. The muscle attachment points used in SAM software are not accessible; therefore previously published data was investigated. The work of Shirazi and El-Rich et al. [229, 255] has used muscle loading in finite element models of the spine. Shirazi was contacted regarding the attachment points of the muscles and it was found that the spine and muscle positions used in his work had been completed as part of a PhD by Babak Bazrgari, which Shirazi made available [256]. This provided the coordinates used for the spinal column and muscle attachments (Figure 76).

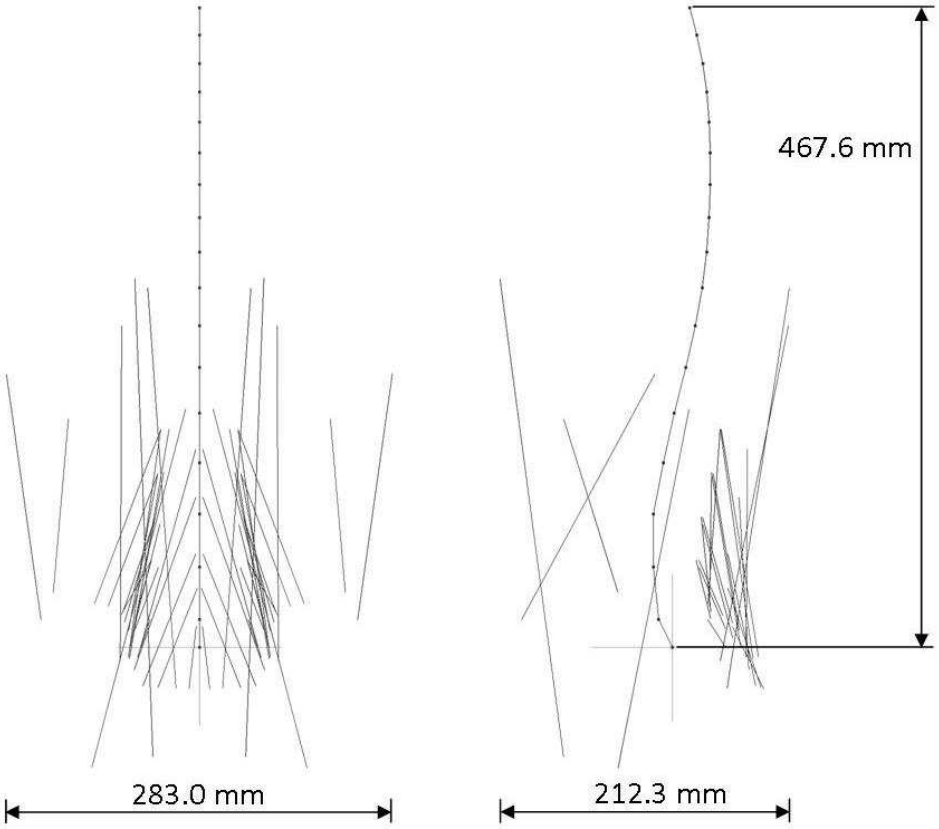

Figure 76: Spinal column and muscle attachment points used by Shirazi and El-Rich et al. [229, 255]. The dots represent the centre of mass of the vertebral bodies, joined to form the spinal column. Additional lines represent the iliocostalis, iliopsoas, longissimus, multifidus, quadratus lumborum, internal oblique, external oblique, and rectus abdominus muscles

The muscles of interest were simplified to be represented by one muscle pair (Figure 77), so as to be more practically applied in-vitro. This is similar to the method used by Wilke et al., and a comparison was made to the vectors used in their work.

In the simplified model, all muscle forces would be applied in a downward direction, likewise the force due to the bodyweight. The abdominal pressure would be in a vertically upward direction. The position of the latissimus dorsi, bodyweight, and abdominal pressure were not included in the model by Bazrgari, therefore the bodyweight and abdominal pressure positions were taken from the published work by Wilke et al. [235]. The work by Wilke et al. tested specimens in flexion/extension only, whereas the abdominal pressure would create an upward force across the front of the torso that would alter the equilibrium when movements are applied in the coronal plane. Therefore, the abdominal pressure was split

into two forces 50 mm from the midline of the spine to more accurately represent the effect of the force in movements such as lateral bending, lateral shear, and axial rotation. The coordinates of the latissimus dorsi were estimated from the general anatomy of the muscle [257], as no data in the literature could be found.

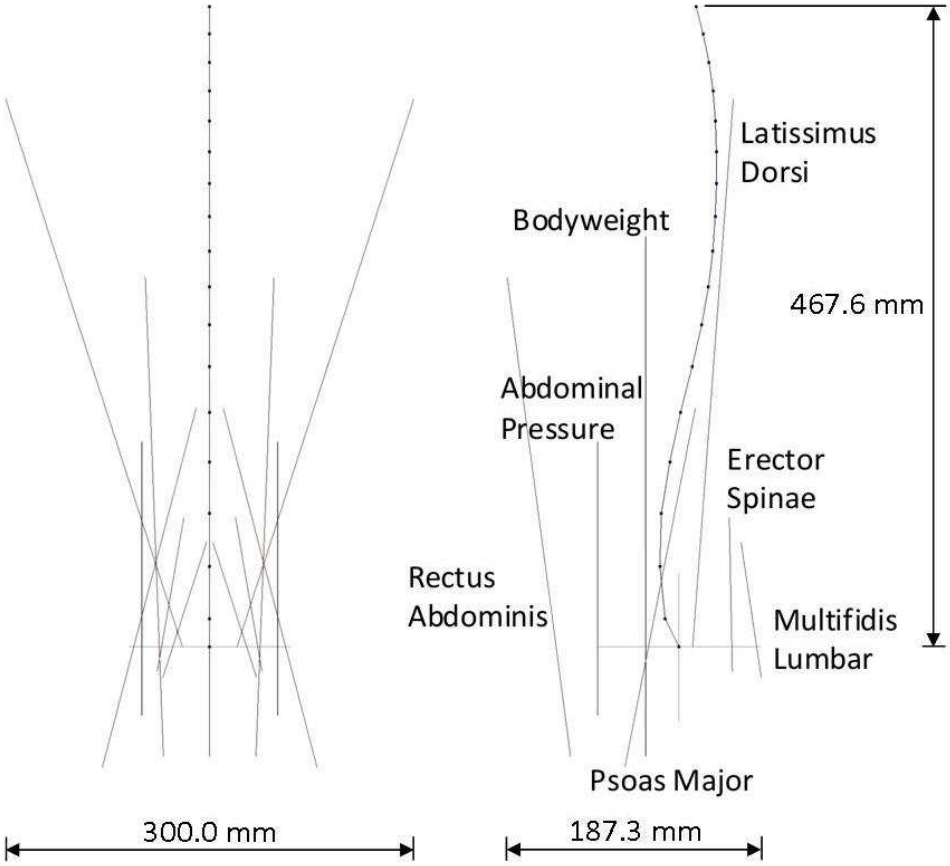

Figure 77: Spinal column and simplified muscle group attachment points. The dots represent the centre of mass of the vertebral bodies, which are joined to form the spinal column. Additional lines represent the muscles, as labelled. All muscle forces act downwards with the exception of the abdominal pressure

For appropriate muscle forces, bodyweight, and abdominal pressure to be used in-vitro, it is important that the forces produce zero resultant force or moment on the spine. The resultant load in the axial plane is not zero, due to the spine being under constant compression. As all forces are symmetrical in the coronal plane, it was only necessary to determine the resultant forces and moments in the sagittal plane.

Moments were taken about the centre of the L4-L5 disc. For ease of application in the laboratory, muscle forces were rounded to the nearest 10 N. The force due to the bodyweight acting on the lumbar spine was taken as 60% of the total bodyweight [37], rounded to the nearest 10 N; the total body mass was 77 kg. The resultant horizontal force was 1.05 N posteriorly, and it was judged that this was within an acceptable range. Following this, the abdominal pressure was adjusted until the resultant moment about the L4-L5 disc was zero. This returned a value of 56.16 N vertically upwards, which was rounded to 56 N, so as to be more practically applied in-vitro, with a resultant moment of 0.01 Nm. The sagittal shear was unaffected by the abdominal pressure, as the force is applied vertically.

The forces were then resolved vertically to determine the level of compression that the spine was subjected to. The total compression was 570 N, which equated to 75% of the bodyweight. This is in the 500-800 N range that would be expected for a person standing in an upright and relaxed position [5]. However, it is at the lower end of the range, this is likely due to the previously discussed tendency of antagonistic muscles forces and overcompensation, which is not taken into account in the SAM software. The muscle forces would need to be increased by 120% in order to result in a compressive force of 790 N. With the muscle forces adjusted in this manner the resultant shear load was 2.32 N and the resulting moment about the L3-L4 disc was -0.06 Nm without any adjustment using the abdominal pressure force.

It may be appropriate for in-vitro tests to use lower and higher muscle force tests. This may allow data to be acquired that better reflect the range that is expected in-vivo. The lower forces would be those estimated from the SAM model, the higher forces would be 120% greater, equating to the maximum likely muscle forces to occur in-vivo (Table 17).

The highest muscle force predicted using the SAM software, that of the erector spinae, was 70 N, which is similar to that applied to muscle groups in most of the work by Wilke et al. [223, 235]. Most of the other predicted muscle forces were lower to those applied by Wilke et al., even using the upper range defined above. A comparison was made to the previously described study by Wilke et al. [223] that used five pairs of symmetrical muscle forces, each characterised by a magnitude of 80 N per pair. It was calculated that the resultant sagittal shear would be -0.28 N and the compressive force on the spine would be 224 N. This is lower than would be expected in-vivo and is certainly due to the fact that whilst large muscle

forces were incorporated into the test procedure there was no force due to the bodyweight. The resultant moment due to the muscle forces in the test procedure used by Wilke et al. could not be calculated as the position of the muscle vectors in relation to the L4-L5 disc centre was not available. However, the diagram published by Wilke et al. of the vectors in relation to the spine suggests that it would be non-zero [223].

Table 17: Muscle forces and the resultant loading of the L4-L5 level

	Lower Muscle Forces	Higher Muscle Forces
Multifidus Lumbar (N)	10	22
Erector Spinae (N)	70	154
Psoas Major (N)	30	66
Rectus Abdominus (N)	20	44
Latissimus Dorsi (N)	10	22
Bodyweight (N)	490	490
Abdominal Pressure (N)	-56	0
Resultant Sagittal Moment (Nm)	-0.01	-0.06
Resultant Sagittal Shear (N)	1.05	2.32
Resultant Compressive Load (N)	573	796
Resultant Compression (% of BW)	76%	105%

7.2.4.5 Conclusions

This investigation has combined estimates from SAM software, with previous in-vivo and in-vitro results to provide a range of muscle forces for future biomechanical tests. The estimated forces result in very low moment and shear force in the sagittal plane, and produce compressive forces comparable to those measured in-vivo. Coordinates for the five simplified muscle groups, bodyweight, and abdominal pressure have been estimated in relation to the vertebral column.

Given that, for the activities of interest studied with SAM software, muscle forces are approximately constant, it would be possible in future studies to use cables and dead weights to apply muscle forces to simulate the lower and upper range of muscle forces in-vivo.

The validation of SAM software as a conservative estimate of muscle forces provides a basis to use this software to predict muscle forces for studies using different activities to those described in the present one. A higher estimate of muscle forces could be added, as described above, based on in-vivo studies, in order to create a lower and upper range of muscle forces that represent the physiological range and could be applied during in-vitro tests.

7.2.5 Control System Design

7.2.5.1 Introduction

An existing dSPACE (dSPACE Inc. Wixom, MI, USA) controller was available to use for the spine simulator. This system works through Matlab (MathWorks, Inc. MA, USA), using the Simulink function to create the control system model. The control model is then built via dSPACE add-ons in Matlab. The dSPACE system can use the built model in real-time and communicates through analogue inputs and outputs to and from the various motors and load cells of the simulator. The existing Zwick actuators are controlled separately by the Zwick 9600 controller due to the difficulty and permanence of synchronising both controllers. However, analogue outputs from the Zwick controller are fed into dSPACE, allowing a single data acquisition system to be used.

Both position and load control are required in all six axes, and the control of each axis is to be entirely independent. However, the timing board in the dSPACE system is unable to recognise encoder pulses as a trigger signals. It is the trigger signals that can be used by the dSPACE system to count the pulses from the encoders and determine the position of each motor. The dSPACE unit in the simulator comprises a DS2001 input board, a DS2103 output board, and a DS4001 timing board. The EC90 motors are connected to the dSPACE controller via individual Maxon EPOS2 24/5 controllers (Product no. 367676, Maxon Motor UK). Replacing the DS4001 board with a DS3002 incremental encoder interface board would allow the position of up to six motors to be determined.

Purchasing the DS3002 timing board was not possible due to budgetary constraints. Therefore, an open-loop based position controller was developed. Whilst this has

limitations, the individual Maxon controllers do use closed-loop control but the acquisition system is not suitable for the stiffness matrix testing. An output signal from the dSPACE system is fed into the analogue input of the Maxon controller. The analogue input has been configured as a position demand signal in the controller. This is the case for all four motors and encoders. Once the control model was built, it was tested to ensure that the open-loop system was adequate for stiffness matrix testing.

7.2.5.2 Simulink Control Model

A simulink model template from a previous research project was used to create a control model in Matlab with 14 input channels: 6 from the 6 axes load cell; 4 from the Zwick hydraulic test machine corresponding to the load, stroke, torque and angle in the Z axis; and 4 from the custom add-on to the Zwick comprising load data from either a loadcell or a torque transducer of the X and Y axes. There are also 4 output channels, one to each of the 4 motors responsible for creating translations and rotations in the X and Y axes (Figure 78).

The rotational and translational axes (RX, RY, TX, TY) are configured so as to be independently controllable but can be simultaneously started (Figure 79). Additionally, limits have been set using an electric stop to prevent the applied load exceeding 50 Nm in the RX and RY axes, and 500 N in the TX and TY axes. Saturation blocks are used to prevent the desired position exceeding a stated value, ±45° for RX and RY and ±50 mm for TX and TY. The range of motion possible in the TX and TY axes is ±92 mm but it was initially set to a maximum of ±50 mm so that the resolution of the position command voltage was almost doubled. The stiffness matrices of functional spinal units would require translations of less than ±10 mm, and therefore the increased resolution would provide more accurate position control.

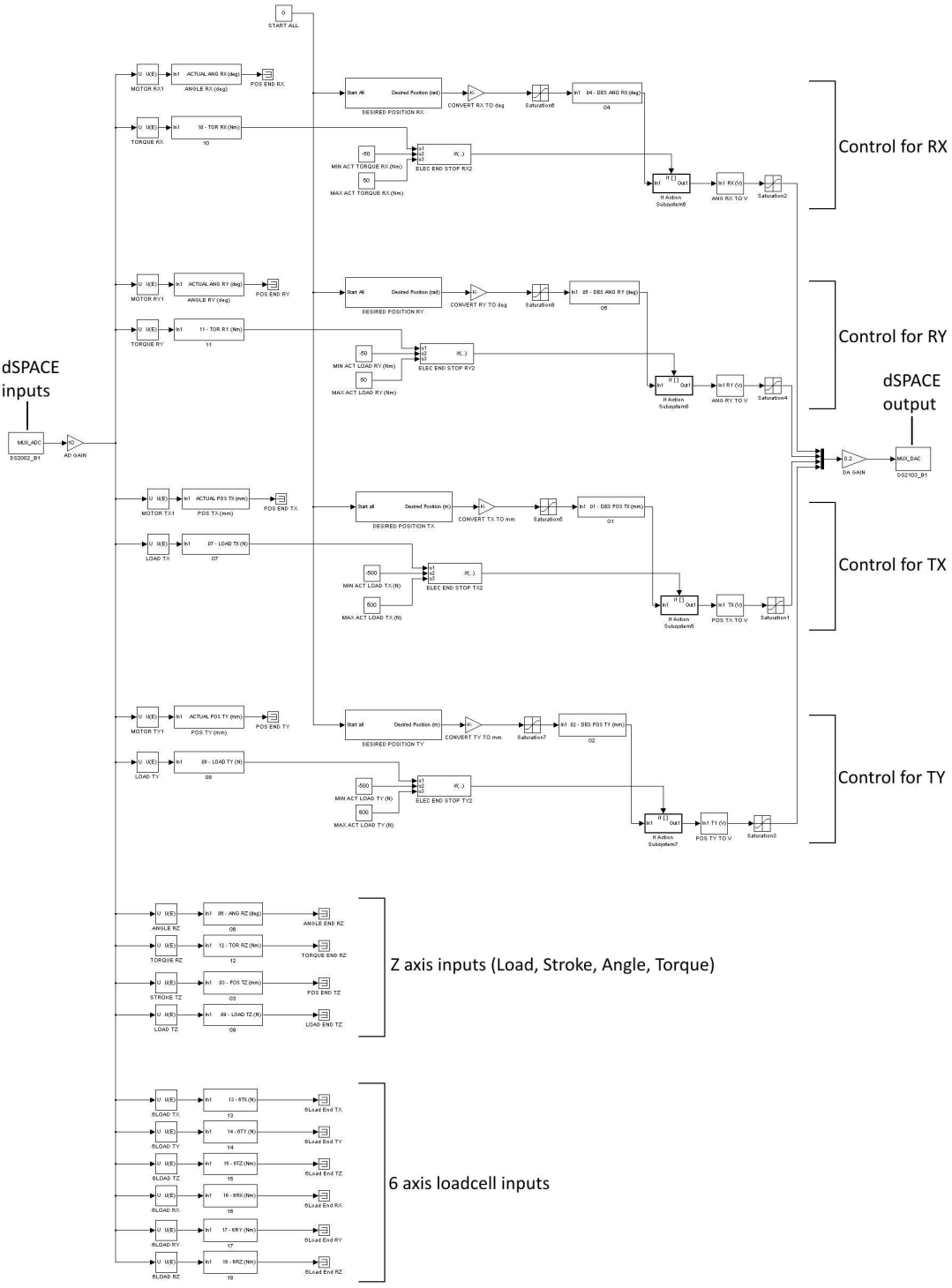

Figure 78: Overall control model. An enlarged section of the control for RX and RY can be seen in Figure 79

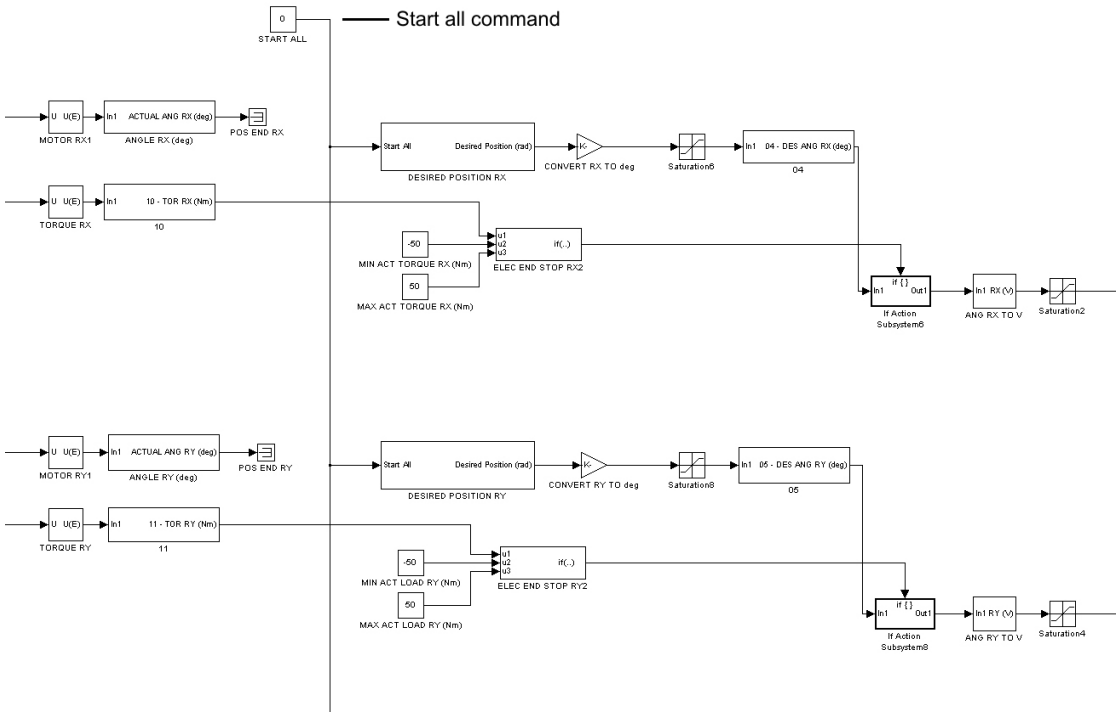

Figure 79: Control diagram for RX and RY axes

The desired position of the TX, TY, RX, and RY axes are created using the same format of signal generator (Figure 80). This is initially completed in radians and metres, and then converted to degrees and millimetres to allow for graph generation in the dSPACE software with appropriate units, before being finally converted to volts for the dSPACE outputs and feeding into the Maxon controller in the range of 0-5 V.

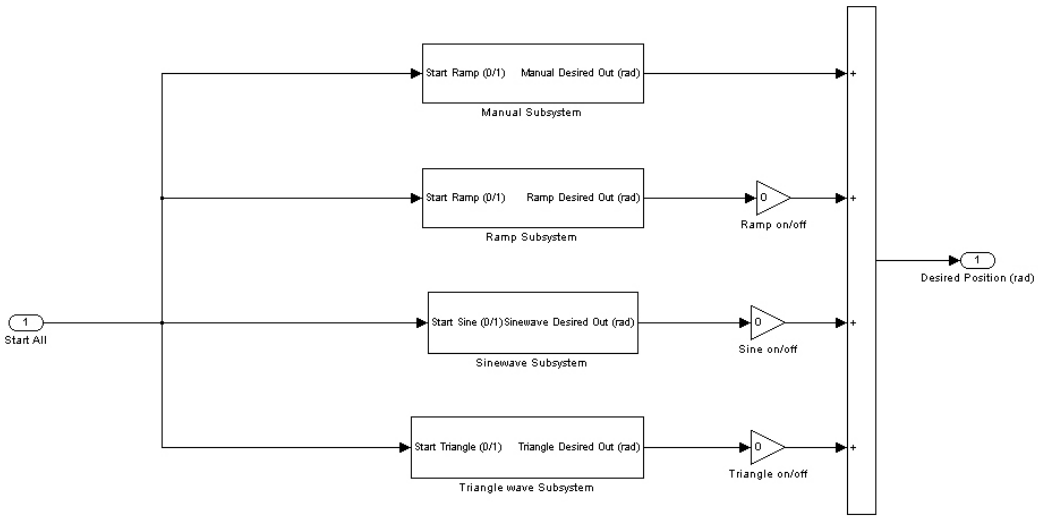

Figure 80: Desired position signal generator

The signal generator was developed using separate function blocks to build a sine wave, triangle wave, ramp, and manual control. The sum of these functions provides the final output signal. This configuration allows individual waveforms to be switched on and off, so that a signal waveform or ramp can be applied, or more complex signals can be created by using more than one signal generator at a time.

Each signal generator requires input criteria. Sine and triangle waves require amplitude, frequency and number of cycles (Figure 81). The ramp signal requires the finish position and the rate of movement. The manual signal is a ramp function requiring position only. To generate a signal, the signal criteria are set, the desired signals are turned on, and then once all signals for all desired axes are input, the “START ALL” switch is used to commence the generation of all signals simultaneously.

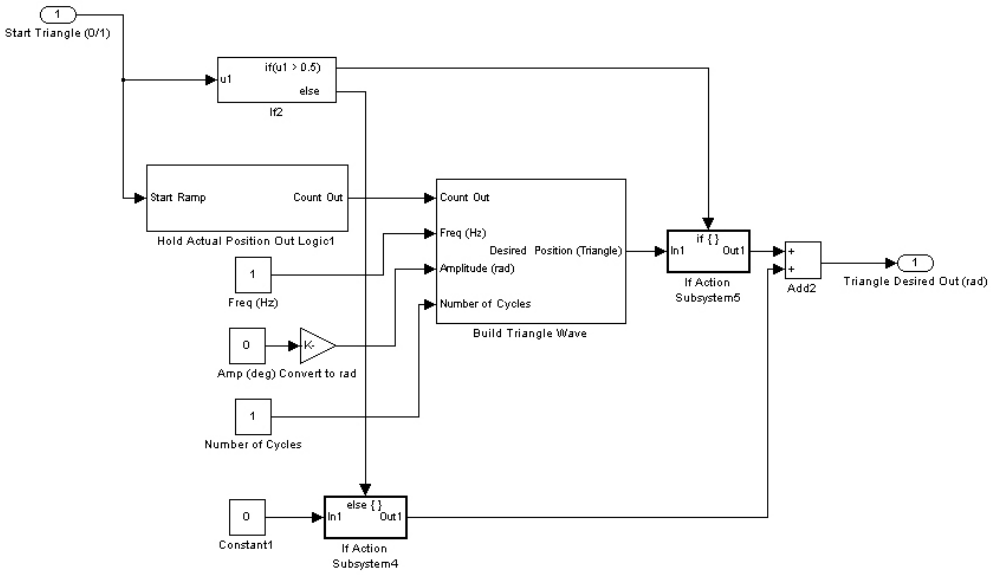

Figure 81: Triangle wave signal generator and input criteria

The step size is used in all the signal generators to determine the desired position at a given time. The step size is multiplied by the step count in the timing board to provide the time, which can then be used in the ramp, sine, or triangle functions along with the amplitude and frequency to calculate the position (Figure 82).

The sine and triangle wave generators use exactly the same function blocks with the exception that the sine function block in the sine wave is replaced by a Laplace expansion function block in the triangle wave.

The ramp function uses the step size to calculate the time. From the time and the rate that has been input, the position at a given time can be calculated until the stop position is reached (Figure 83). The manual function works in an identical fashion but with the rate preset so that only the desired position is required as an input.

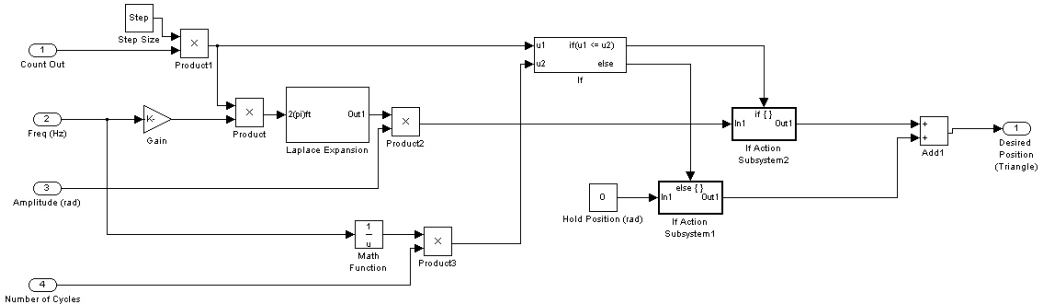

Figure 82: Building the triangle wave signal

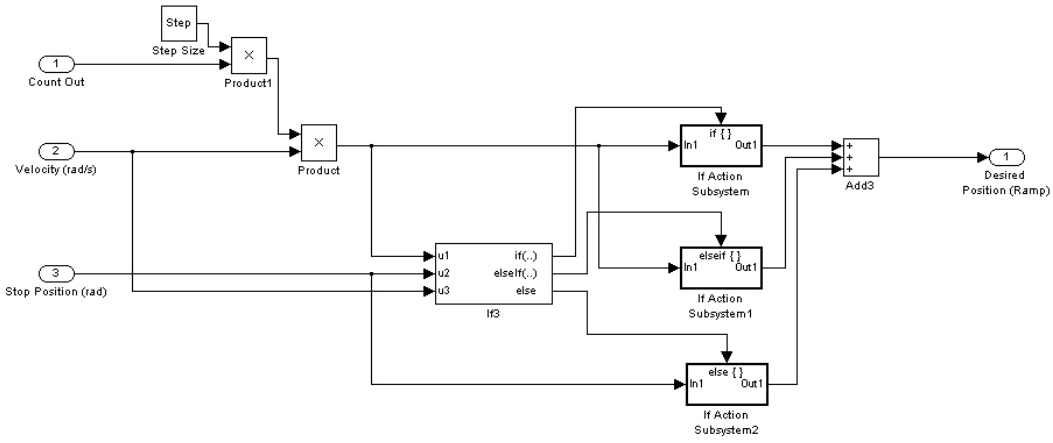

Figure 83: Building the ramp signal

7.2.5.3 Spine Simulator User Interface

Once a simulink model has been built using the dSPACE add-ons in Matlab, the dSPACE controller can use the built model using dSPACE Control Desk software (version 3.5). This allows a user interface to be custom developed. A layout was created that allows independent control of the four axes of the spine simulator (Figure 84). Control of the remaining two axes is via the existing Zwick control system.

Sine, triangle, or ramp waveforms, plus a manual position control can be applied in position control for any number of cycles and in any combination. Data from all load cells is acquired and the layout also allows for the setting of offsets for the six-axis loadcell. Data acquisition for the entire spine simulator (six axes) is completed using the same Control Desk user interface.

The step size of the dSPACE model was set to 0.01 seconds. This means that the sample time is also 0.01 seconds, allowing a data acquisition speed of 100 Hz, though it can be reduced in the acquisition settings. The frequency of 100 Hz is faster than published data for spinal testing, though most previous studies have used quasistatic tests and would therefore require a much slower sampling rate. The dynamic multi-axis flexibility testing by Spenciner et al. [258] was completed at a rate of 0.1 Hz over 5 cycles from 0±8 Nm, with the data from the last cycle being recorded at 50 Hz.

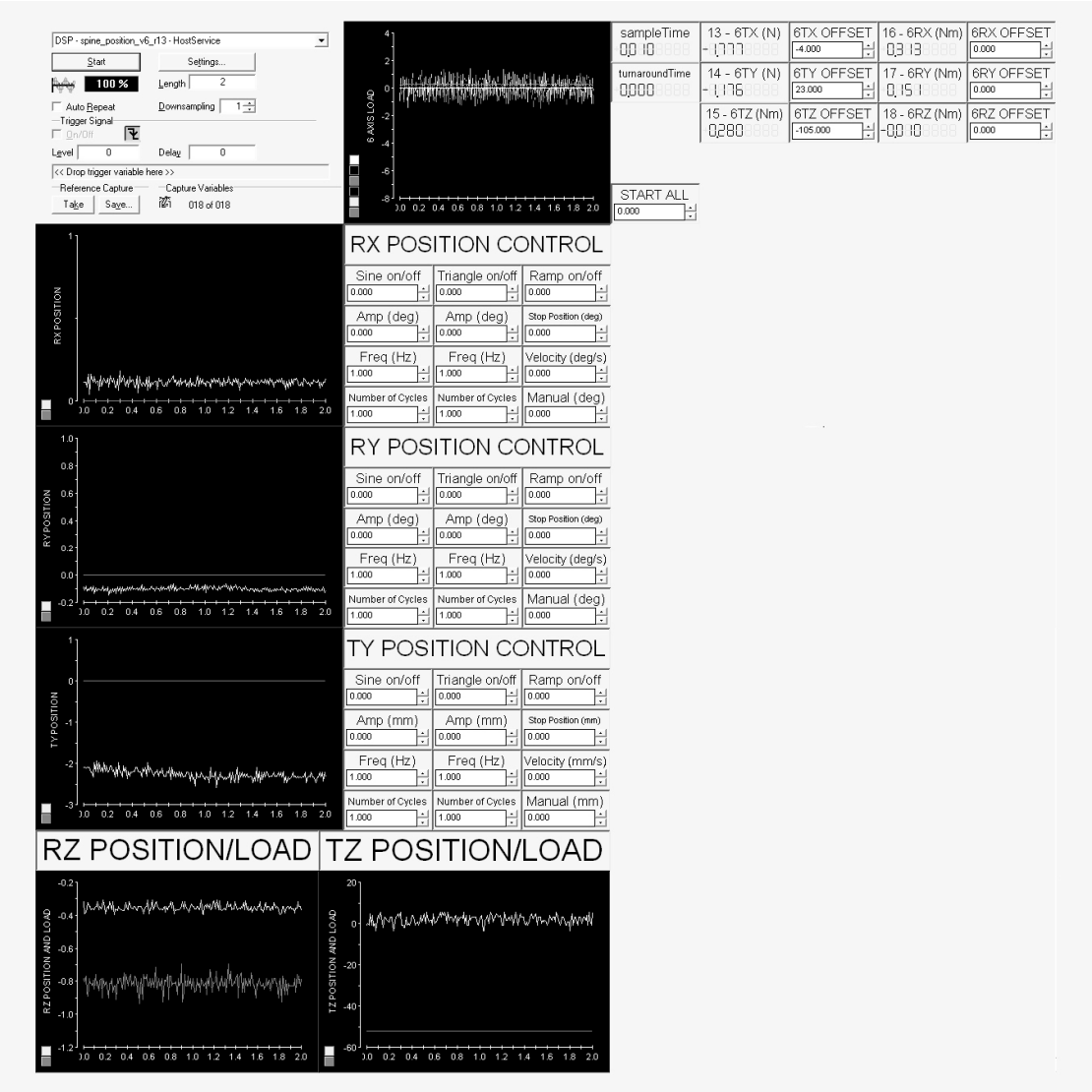

Figure 84: Custom dSPACE Control Desk user interface

7.2.6 Control System Validation

7.2.6.1 Introduction

The dSPACE controller works using an open-loop system, with no feedback control based on the difference between the desired position and the actual position. However, the Maxon motors all have a separate Maxon controller that uses closed-loop control. The analogue signal from dSPACE is input into the Maxon controller, which moves the motor to the desired position, and uses feedback to ensure that the actual position matches the desired position as closely as possible. The actual position can only be determined using the Maxon

data acquisition software, which is not suitable for the stiffness matrix tests because the duration of the tests exceeds the maximum acquisition time of the software.

Therefore it was necessary to complete tests to ensure that the desired position signal from dSPACE that feeds into the Maxon controllers was closely matched by the actual position. Provided that this was the case, it was thought reasonable to use the desired position for the matrix testing data. This is a limitation of the spine simulator but, once the Maxon controllers are appropriately tuned, the actual position should closely match the desired position.

Initial confirmation of the control system was carried out by moving each of the TX, TY, RX, and RY axes to set positions using the control user interface and measuring the position independently. This was in the form of vernier callipers in the TX and TY axes, and a digital spirit level in the RX and RY axes. This ensured that the desired position reasonably matched that acquired via the controller.

7.2.6.2 Materials and Methods

Various testing frequencies were used to compare the desired position from dSPACE with the actual position in the Maxon controller software. A synthetic model of a functional spinal unit (FSU) was used during the tests, which would provide a similar loading environment to the stiffness matrix tests.

The model was used to represent an isolated disc, comprising vertebral bodies machined from cylinders of nylon and bonded to a Nitrile rubber disc with contact adhesive (Evo-Stik 528, Bostik Limited, UK). The diameter of the vertebral bodies and intervertebral disc was 50 mm. The height of the intervertebral disc was 10 mm while that of the vertebral bodies was 25 mm. Two holes were drilled in each the cranial and caudal end of the specimen. These holes were tapped and bolts inserted to provide stability when potted using low melting alloy (MCP75, Mining & Chemical Products Ltd., Northamptonshire, UK). Care was taken to ensure that the disc was orientated horizontally, so as to be aligned with the transverse plane. The height of the spine simulator was adjusted so that the centre of rotation for the X, Y, and Z axes coincided with the centre of the disc.

Once the FSU was potted and secured in the spine simulator, each Maxon Motor was tuned using Maxon software. This automatically sets the PID gains by cycling the motor and optimising the values based on the load encountered. Once this preliminary step was completed a custom tuning process was undertaken. This allows the amplitude, maximum acceleration and other parameters to be customised prior to the gain optimisation being performed as before. The maximum acceleration was reduced from the default to 5000 rpm/s, and the amplitude over which the gains were set was set to 1000 qc (equating to 2.25° or 1 mm).

Comparison tests were carried out for all four axes that used a Maxon motor: TX, TY, RX, and RY. The amplitudes tested were the same as those that were used by Stokes et al. [240] and were planned to be used in the stiffness matrix tests of the present study. These amplitudes were: 4° in RX and RY, 3 mm in TX and 1.5 mm in TY. Both sine and triangle waves were tested at frequencies of 0.05 Hz, 0.1 Hz, 0.2 Hz, 0.5 Hz, and 1.0 Hz. Additionally a complex waveform comprising a combination of sine wave at 0.35 Hz and a triangle wave at 0.22 Hz was used. The amplitude of the sine and triangle wave in the complex waveform was 2° each in rotations, 1.5 mm in TX and 0.75 mm in TY.

The frequencies were chosen to cover a wide range of physiological speeds. A frequency of 0.05 Hz is equivalent to 0.8°/sec in rotation. Slower movements would have been difficult to assess, as the maximum length of data acquisition using the Maxon software is 12 seconds. Frequencies of less than 0.05 Hz would have meant that a peak to peak comparison was not possible. The highest frequency of 1 Hz equated to 16°/second.

7.2.6.3 Results

The error between the desired and actual position tends to increase as the frequency increases (Tables 18 and 19). This was expected and is likely to be caused by the inertia of the portion of the simulator in motion. Peak to peak and maximum error are generally higher using a triangle wave than a sine wave but the mean error is similar for any given frequency. The error increases dramatically from 0.5 Hz to 1 Hz; it is likely that 1 Hz is too high a frequency to accurately use for testing using this control system.

Plots of the desired position and actual position emphasize the breakdown at 1.0 Hz, particularly in the case of the triangle wave (Figures 85-88). The waveform becomes rounded in profile and at the point of desired direction change the actual position overshoots and lags behind the desired signal.

Table 18: Positional Error of the spine simulator in the RX and RY axes

Axis	Wave	Amp	Freq	Peak to Peak error			Max Error		Mean Error	
		(deg)	(Hz)	(qc)	(deg)	(%)	(qc)	(deg)	(qc)	(deg)
RX	Sine	4	0.05	5	0.011	0.14	15	0.034	5	0.012
RX	Sine	4	0.10	2	0.005	0.06	23	0.052	4	0.010
RX	Sine	4	0.20	1	0.002	0.03	26	0.059	4	0.009
RX	Sine	4	0.50	2	0.005	0.06	35	0.079	9	0.021
RX	Sine	4	1.00	107	0.241	3.00	64	0.144	27	0.062
RX	Triangle	4	0.05	1	0.002	0.03	33	0.074	5	0.012
RX	Triangle	4	0.10	18	0.041	0.51	27	0.061	4	0.009
RX	Triangle	4	0.20	23	0.052	0.65	40	0.090	4	0.009
RX	Triangle	4	0.50	41	0.092	1.16	73	0.164	9	0.021
RX	Triangle	4	1.00	120	0.241	3.40	112	0.252	23	0.053
RX	Complex	2+2	0.35+0.22	18	0.041	0.60	30	0.068	6	0.014
RY	Sine	4	0.05	5	0.011	0.14	15	0.034	4	0.009
RY	Sine	4	0.10	4	0.009	0.11	24	0.054	3	0.008
RY	Sine	4	0.20	0	0.000	0.00	32	0.072	4	0.009
RY	Sine	4	0.50	9	0.020	0.25	34	0.077	8	0.018
RY	Sine	4	1.00	95	0.214	2.66	54	0.122	23	0.052
RY	Triangle	4	0.05	6	0.014	0.17	23	0.052	5	0.011
RY	Triangle	4	0.10	14	0.032	0.40	30	0.068	4	0.009
RY	Triangle	4	0.20	27	0.061	0.77	36	0.081	4	0.009
RY	Triangle	4	0.50	91	0.205	2.59	69	0.155	8	0.018
RY	Triangle	4	1.00	110	0.214	3.12	96	0.216	20	0.045
RY	Complex	2+2	0.35+0.22	2	0.005	0.07	37	0.083	6	0.014

The desired signal also deviates marginally from a true sine or triangle wave at frequencies of 1.0 Hz. The analogue output from the dSPACE controller remains a true sine or triangle wave at 1 Hz, so the error may be due to the sampling rate of the Maxon controller in processing the analogue input signal. A frequency of 1.0 Hz would be too fast for spinal testing of such amplitude. This doesn't present an issue as 0.5 Hz equates to 8°/second, which is faster than the upper range recommended for spinal testing by Wilke et al. [212].

Table 19: Positional Error of the spine simulator in the TX and TY axes

Axis	Wave	Amp	Freq	Peak to Peak error			Max Error		Mean Error	
		(mm)	(Hz)	(qc)	(mm)	(%)	(qc)	(mm)	(qc)	(mm)
TX	Sine	3	0.05	8	0.008	0.13	17	0.017	5	0.005
TX	Sine	3	0.10	0	0.000	0.00	21	0.021	4	0.004
TX	Sine	3	0.20	4	0.004	0.07	26	0.026	4	0.004
TX	Sine	3	0.50	8	0.008	0.13	25	0.025	7	0.007
TX	Sine	3	1.00	68	0.068	1.12	55	0.055	18	0.018
TX	Triangle	3	0.05	7	0.007	0.12	26	0.026	5	0.005
TX	Triangle	3	0.10	23	0.023	0.38	26	0.026	5	0.005
TX	Triangle	3	0.20	8	0.008	0.13	36	0.036	4	0.004
TX	Triangle	3	0.50	62	0.062	1.03	64	0.064	7	0.007
TX	Triangle	3	1.00	75	0.075	1.25	59	0.059	20	0.020
TX	Complex	1.5+1.5	0.35+0.22	3	0.003	0.06	31	0.031	5	0.005
TY	Sine	1.5	0.05	2	0.002	0.07	17	0.017	4	0.004
TY	Sine	1.5	0.10	3	0.003	0.10	19	0.019	4	0.004
TY	Sine	1.5	0.20	5	0.005	0.17	18	0.018	4	0.004
TY	Sine	1.5	0.50	12	0.012	0.40	32	0.032	6	0.006
TY	Sine	1.5	1.00	38	0.038	1.27	39	0.039	13	0.013
TY	Triangle	1.5	0.05	12	0.012	0.40	16	0.016	4	0.004
TY	Triangle	1.5	0.10	10	0.010	0.34	24	0.024	5	0.005
TY	Triangle	1.5	0.20	6	0.006	0.20	24	0.024	5	0.005
TY	Triangle	1.5	0.50	31	0.031	1.04	50	0.050	6	0.006
TY	Triangle	1.5	1.00	64	0.064	2.15	61	0.061	12	0.012
TY	Complex	0.75+0.75	0.35+0.22	18	0.018	0.71	23	0.023	6	0.006

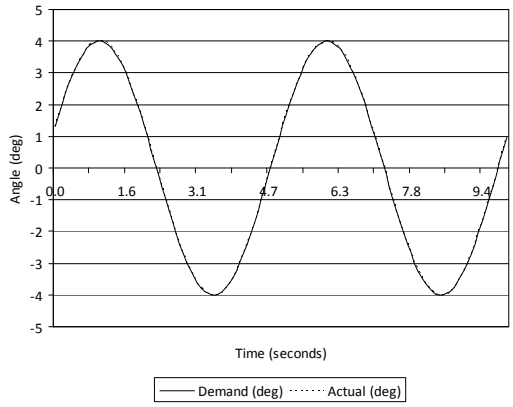

Figure 85: RX sine waveform at 0.2 Hz

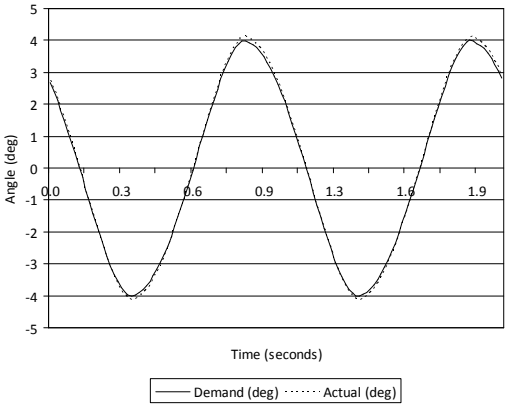

Figure 86: RX sine waveform at 1.0 Hz

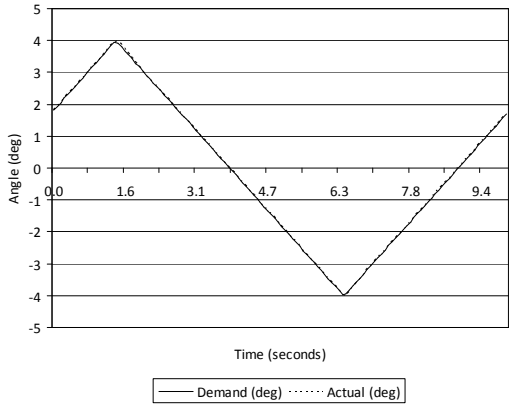

Figure 87: RX triangle waveform at 0.1 Hz

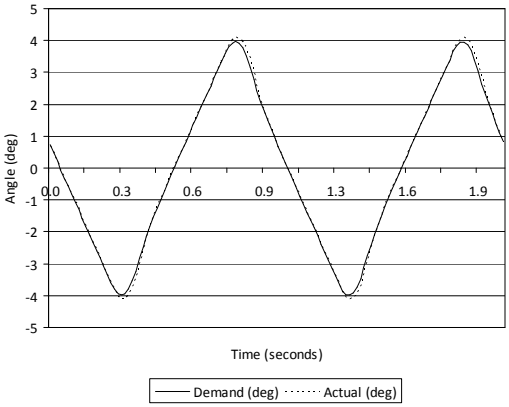

Figure 88: RX triangle waveform at 1.0 Hz

7.2.6.4 Discussion and Conclusions

If the results from the frequencies of 1.0 Hz are discounted the maximum errors are when using the triangle waveform at 0.5 Hz. The maximum mean errors are 0.021°, 0.018°, 0.007 mm, and 0.006 mm in the RX, RY, TX, and TY axes respectively. The maximum peak to peak errors are 1.16 %, 2.59 %, 1.03 %, and 1.04 % in the RX, RY, TX, and TY axes respectively (Figure 89).

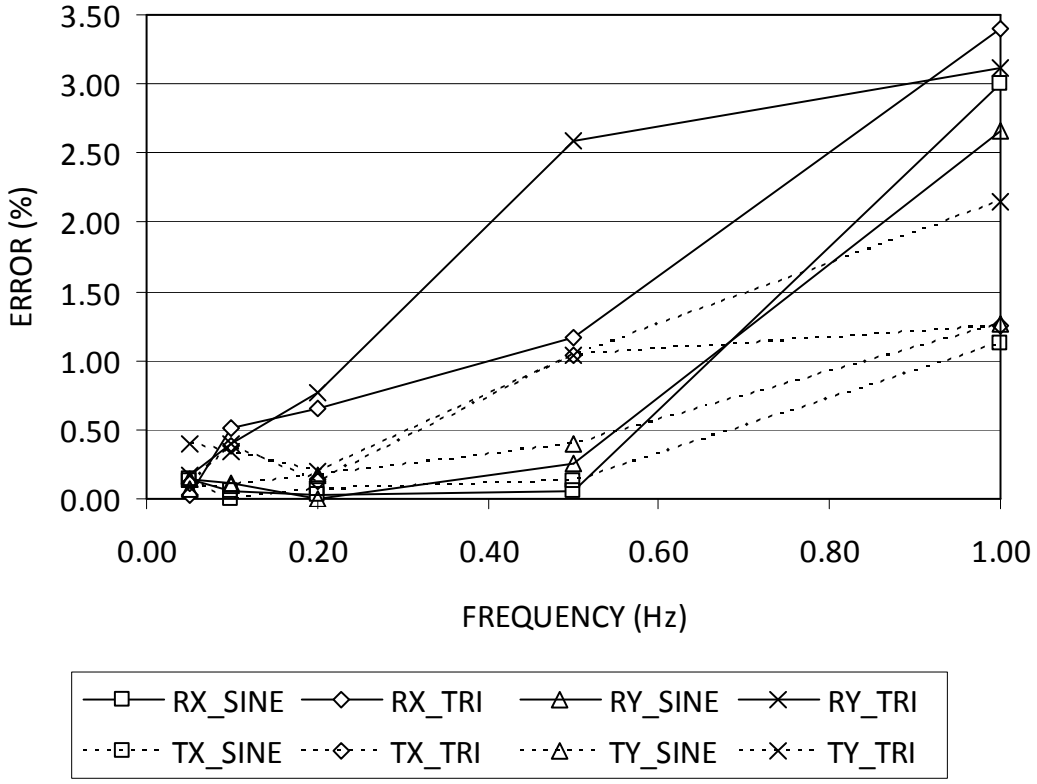

Figure 89: Peak to peak error of the TX, TY, RX, and RY axes

The maximum peak to peak error of 2.59 % in the RY axis represents a difference of 0.205° from the desired peak to peak amplitude of 8°. The method of using the desired position data would be reasonable up to the frequency of 0.5 Hz for the amplitudes tested.

This outcome provides a good basis for completing spinal tests at physiological speeds. A series of workshops with various medical professionals published by Wilke et al. [212] stated that spinal specimens could be loaded at a rate of between 0.5°/sec and 5°/sec without affecting the results substantially. Slower speeds might introduce the effects of creep and faster results might introduce the inertial effects of the test machine.

7.3 Spine Simulator Solution

7.3.1 Final Design

A spine simulator has been developed that is capable of providing independent motion in six degrees of freedom (Figure 90). Each axis can be used in position control and all position and load data are acquired at 100 Hz.

A Zwick testing machine provides translations and rotations in the transverse plane (TZ and RZ respectively). An XY platform is mounted on the dual axis actuator of the Zwick machine, providing translations in the X and Y axes (TX and TY respectively). A gimbal head is mounted underneath the XY platform, which provides rotations in the X and Y axes (RX and RY respectively). The cranial specimen holder is fixed to the gimbal head, and the caudal specimen holder is fixed to the base plate via a six-axis load cell. The weight of the motor and gear assemblies of the RX and RY axes are balanced on the gimbal head by counterweights. The height of the cranial specimen holder can be adjusted to fix a specimen with the centre of rotation appropriately placed. The height of the Zwick crosshead can also be adjusted to accommodate a large range of specimen lengths within the spine simulator.

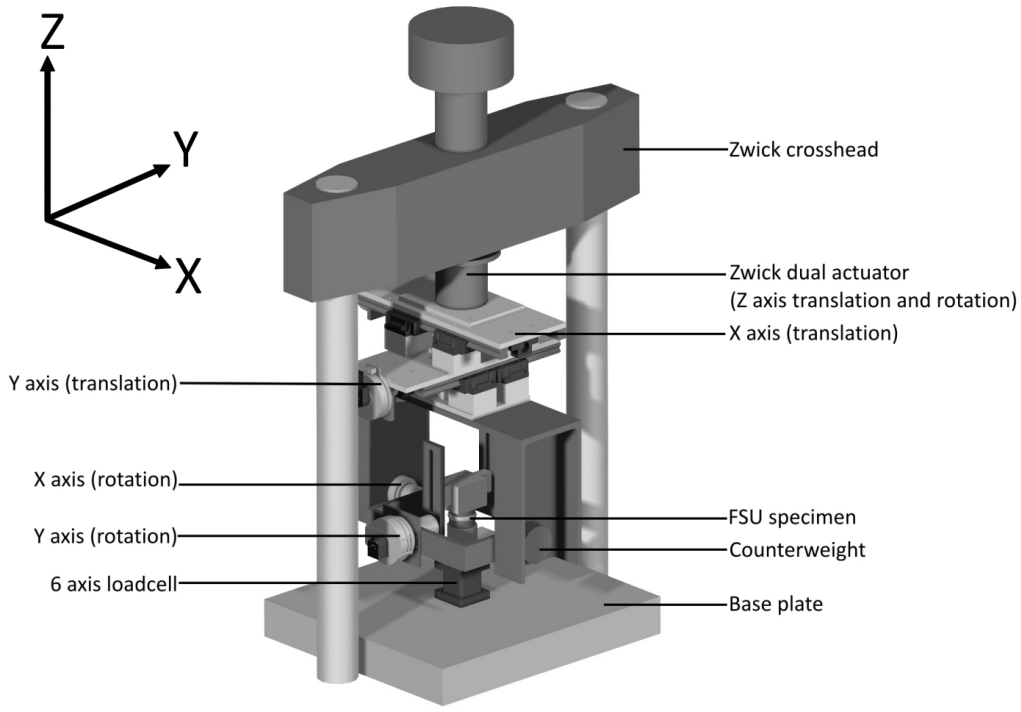

Figure 90: Final spine simulator design

The motors used throughout the XY platform and gimbal head are the Maxon EC90 flat brushless motor, with Maxon encoders. These motors emit 500 pulses per rotation, and with the quadrature encoder give a resolution of 2000 counts/rotation.

The X and Y rotational axes use harmonic drive gear and bearing units. They have a step-down ratio of 80:1, giving a maximum continuous torque of just under 31 Nm, though higher torques can be briefly applied. Torque transducers with a maximum capacity of ±50 Nm are mounted between the harmonic drive unit and the specimen in each rotational axis. The gear reduction provides a theoretical resolution of 0.00225° in the X and Y axis. The transmission accuracy of the harmonic drive gear is ±0.025° or less, and the repeatability is ±0.0017° or less.

Each translational platform comprises two linear guide rails mounted in parallel with a ball screw assembly. The ball screw is powered by a Maxon EC90 motor via a Lenze coupling. The continuous torque of 387 mNm allows for maximum translational loads of just over 1000 N. A load cell with a capacity of ±500 N is mounted between the ballscrew and platform allowing measurement of the translational load free of any off-axis loading. The ball screw lead of 2 mm/rotation gives a theoretical resolution of 0.001 mm in the X and Y axis. However, the representative travel distance error of the ballscrew is ±0.018 mm.

Separate power supplies are used for the Zwick controller, the six-axis loadcell, the load cells and torque transducers of the X and Y axes, and the Maxon controllers. Two separate computers are used for the control of the Zwick machine, and for the dSPACE system, respectively.

Control of the Z axis is achieved using Zwick Workshop 94, the remaining four axes are controlled using a dSPACE controller combined with four Maxon EPOS2 25/5 controllers, one corresponding to each of the four Maxon EC90 motors in the X and Y axes. dSPACE Control Desk software is used for the user interface for the X and Y axes, and for the data acquisition system for all axes. Sine, triangle, and ramp waveforms can be set independently for each axis at any frequency and for any number of cycles. Data acquisition is carried out at 100 Hz by default but may be lowered if required. The desired position is output as an analogue signal to the appropriate Maxon controller, which uses the signal to control the position of

the motor. Analogue signals from the load cells and torque transducers in the X and Y axis, from the Zwick controller in the Z axis, and from the 6 axis load cell feed into the dSPACE controller.

7.3.2 Solution Specification

The spine simulator was built using a modular design (Table 20). The XY platform was mounted onto the Zwick testing machine (Figure 91). The gimbal head was then mounted below the XY platform (Figure 92). The simulator can move independently in all six axes, with a range of motion suitable for simulating physiological ranges for both functional spinal units and multi-level specimens. The speed range of each axis can accommodate all but the fastest movements likely to occur as part of normal motion.

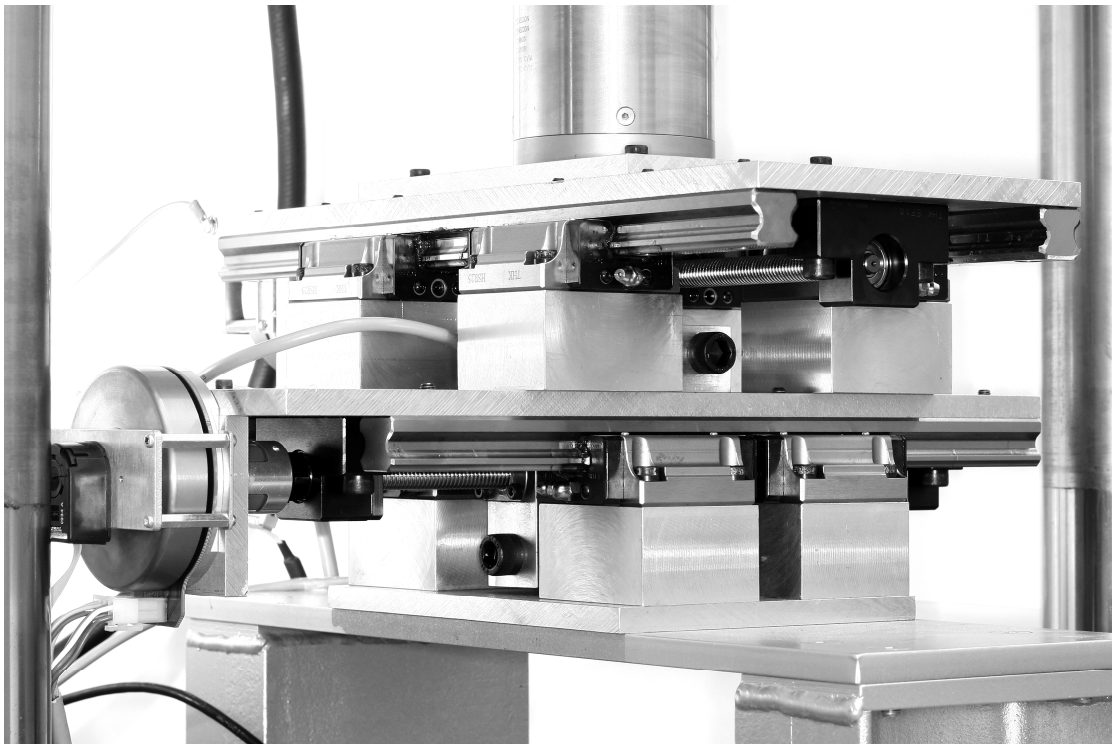

Figure 91: The XY platform of the spine simulator

Table 20: Spine simulator component details

Part	No.	Manufacturer	Product Code	Description
X & Y Axis	4	Maxon UK	323772	EC90 flat brushless motors
X & Y Axis	4	Maxon UK	110518	HEDL5540 encoders
X & Y Axis	4	Maxon UK	367676	EPOS2 24/5 controller
X & Y Axis	4	Maxon UK	278584	Motor cable
X & Y Axis	4	Maxon UK	276248	Connector set
X & Y Axis	4	Maxon UK	275934	Encoder extension cable
XY Platform	2	THK	BNK1202-3RRG0 + 354LC5Y	Ballscrew assembly
XY Platform	2	THK	EK10	Fixed ballscrew support
XY Platform	2	THK	EF10	Free ballscrew support
XY Platform	2	THK	HSR25B2SS + 400L	Linear guide
XY Platform	2	THK	HSR25B2SS + 350L	Linear guide
XY Platform	2	PCM	615	±500 N loadcell
XY Platform	2	Lenze	13003535	GESM coupling 8 mm
XY Platform	2	Lenze	13003534	GESM coupling 10 mm
XY Platform	2	Lenze	13008702	GESM hard element
Gimbal	2	Harmonic Drive UK	HFUC-17-2UH-SP	Harmonic Drive Gear and bearing unit
Gimbal	2	PCM	TRS	±50 Nm torque transducer
Gimbal	2	SKF	442-0060	6200 ZRSH sealed bearing
Z Axis	1	Zwick	25-200	25 kN/200 Nm hydraulic testing machine/controller
Z Axis	1			Computer with Zwick Workshop control interface
XYZ Axes	1	AMTI	AMTI MC3-A-1000	Six-axis loadcell
XYZ Axes	1	dSPACE	DS2001	32ch analogue input board
XYZ Axes	1	dSPACE	DS2103	32ch analogue output board
XYZ Axes	1	dSPACE	DS4001	Realtime interface board
XYZ Axes	1			Computer with dSPACE Control Desk 3.5 interface

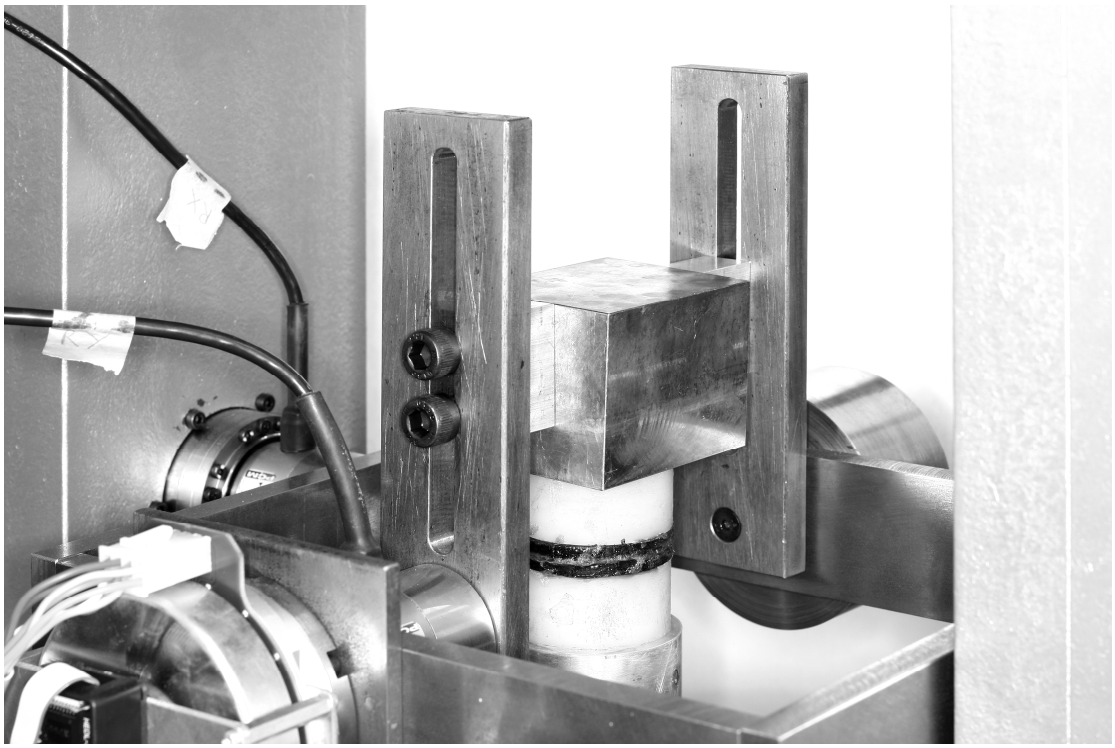

Figure 92: The gimbal head of the spine simulator with a synthetic FSU mounted

The XY platform can apply translations in the X and Y axes; the gimbal head can apply rotations in the X and Y axes; and the Zwick testing machine can apply translation and rotation in the Z axis (Figure 93). The range of motion meets that set out in the requirement specification excluding translation in the X and Y axes. This has been reduced from ±100 mm to ±92 mm in both axes. The load capacity meets or exceeds that in the requirement specification (Table 21).

Table 21: Spine Simulator Range of motion and load capacity

Axis	ROM	Repeatability	Load Capacity
X Translation	±92 mm	±0.018 mm	±500 N
Y Translation	±92 mm	±0.018 mm	±500 N
Z Translation	±50 mm	±0.02 mm	±4400 N
X Rotation	±45°	±0.025°	±50 Nm
Y Rotation	±45°	±0.025°	±50 Nm
Z Rotation	±45°	±0.02°	±56 Nm

Figure 93: The spine simulator including the Zwick testing machine

7.3.3 Conclusions

The spine simulator meets almost all of the design requirements, and all those required for the stiffness matrix testing of a single-level specimen. The range of motion and load capacity of the spine simulator is suitable for both single- and multi-level specimens, and it is able to accommodate both porcine and cadaveric specimens of the cervical, thoracic, and lumbar regions. Testing can be completed statically, quasistatically, and dynamically. The axes are independently controlled, and any number of the six axes can be used simultaneously using individual waveforms.

The control validation testing has shown that the four axes (TX, TY, RX, and RY) built onto the existing Zwick testing machine (TZ and RZ) can be accurately positioned under dynamic loading conditions. The maximum peak to peak error at a rotation speed of 8°/sec was 2.59 % using a triangle waveform. This error is due to the actual position lagging behind the rapid change in direction of the desired position due to the inertia of the part of the spinal simulator in motion. At slower speeds that are more likely to be used in dynamic testing of spinal specimens the error was far less. At 0.1 Hz, representing a rotational speed of 1.6°/sec, the maximum peak to peak error was 0.51 %, equating to 0.041° over the ±4° cycle, the mean error was 0.009°. In the translational axes at 0.1 Hz, the maximum peak to peak error was 0.38 %, or 0.023 mm, and the mean error was 0.005 mm.

The inertia of the simulator was a source of worry in terms of axial rotation, as the XY platform and gimbal head must be rotated. This was investigated further in the stiffness matrix validation testing using the same synthetic functional spinal unit as the control tests described above.

7.3.4 Future Developments to the Spine Simulator

There exists the possibility to amend the control model to use a closed loop control system if the dSPACE timing board is replaced with the DS3002 board. This would allow independent controlling of each axis in either load or position control. Additionally, a further modification may be to remove the XY platform and gimbal head from the Zwick test machine and build a framework with ballscrew and linear guide actuators upon which they can be mounted. Rotations in the Z axis could be added to the inside of the gimbal head, which would greatly

reduce the inertia of the simulator in axial rotation. This would provide a standalone six-axis spine simulator that used Maxon motors throughout and was entirely controlled using the dSPACE system. This would make the spine simulator far more user friendly and would free-up the Zwick testing machine for other research projects.

Load control is not possible in the current spine simulator, thus preventing the possibility of applying pure, unconstrained moments to spinal specimens. This could be integrated into the simulator at a later date with the DS3002 timing board and the amendment of the control system to provide closed loop control based on feedback from the six-axis load cell or on-axis load cells and torque transducers.

The muscle force predictions provide an excellent basis for future spinal testing that would more accurately replicate in-vivo conditions in the spine. Such a test set-up would not only be useful in understanding more about the natural spine but would be a valuable resource for aiding the design and development of spinal devices, and in particular disc arthroplasty devices. These devices are clinically underperforming compared to hip and knee arthroplasties, and using a multi-axis test-rig with the addition of major muscle group forces would allow a better means of understanding why this is so, and what actions might improve long-term outcomes.

8 STIFFNESS MATRIX VALIDATION TESTING

Two sets of preliminary validation tests were completed prior to the stiffness matrix testing of single-level porcine specimens: synthetic specimen testing; and a porcine pilot study. Both sets of validation tests were used to assess the performance of the spine simulator, and refine the testing protocol prior to the commencement of the full tests. This would reduce any learning effects occurring during the full porcine tests.

8.1 Synthetic Stiffness Matrix Validation Testing

The synthetic spinal unit had previously been used to validate the open loop control system that was used for the TX, TY, RX, and RY axes. It was then used as a specimen to validate the completion of stiffness matrix tests at various frequencies. This allowed the development and refinement of the testing protocol prior to testing porcine specimens.

8.1.1 Materials and Methods

A first set of experiments was carried out on the synthetic isolated disc specimen already described in Chapter 7.2.6.2 (page 138). It was estimated, based on the control validation tests, that the stiffness of this specimen would be marginally higher than that of a porcine disc. However, the specimen was deemed suitable for the initial simulator validation, as it would allow the performance of the spine simulator to be assessed under loading conditions similar to those encountered during the testing of porcine specimens.

The specimen was potted using low melting alloy (MCP75), with bolts in the cranial and caudal ends of the specimen to increase stability. The disc was orientated horizontally, so as to be aligned with the transverse plane. The height of the spine simulator was adjusted so that the centre of rotation for the X, Y, and Z axes coincided with the centre of the disc. The orientation of the coordinate system was as previously described (Figure 58); the same as that used in the study of a porcine specimen by Stokes et al. [240], and of that suggested by Wilke et al. [212] (Table 22).

Table 22: Orientation of the coordinate system

	Positive	Negative
TX	Anterior Shear	Posterior Shear
TY	Left Lateral Shear	Right Lateral Shear
TZ	Axial Extension	Axial Compression
RX	Right Lateral Bending	Left Lateral Bending
RY	Flexion	Extension
RZ	Left Axial Rotation	Right Axial Rotation

A stiffness matrix is comprised of the results from six tests. For each test, one axis is cycled whilst the other five axes are held stationary. The load is measured in all six axes, allowing both the load corresponding to the movement applied, and the five off-axis loads to be measured. From the movement applied and the loads measured, the stiffnesses are calculated. This procedure is repeated for all six axes, resulting in a total of 36 stiffness terms arranged in a 6x6 matrix (Table 23) based on the six movements (TX, TY, TZ, RX, RY, and RZ, with T representing translations and R representing rotations) and the six loads (FX, FY, FZ, MX, MY, and MZ, with F representing forces and M representing moments). For example, for a test in the TX axis, all other axes are held stationary while the TX axis is cycled. The load in all six axes is measured. From this the stiffness in all six axes relating to a translation in the TX axis is calculated. This provides the six stiffness terms in the first column of Table 23. Following this a different axis is cycled and the stiffness values calculated until all 6 columns of the matrix are complete.

Table 23: The 6x6 stiffness matrix and units

	TX	TY	TZ	RX	RY	RZ
FX	N/mm	N/mm	N/mm	N/rad	N/rad	N/rad
FY	N/mm	N/mm	N/mm	N/rad	N/rad	N/rad
FZ	N/mm	N/mm	N/mm	N/rad	N/rad	N/rad
MX	Nmm/mm	Nmm/mm	Nmm/mm	Nmm/rad	Nmm/rad	Nmm/rad
MY	Nmm/mm	Nmm/mm	Nmm/mm	Nmm/rad	Nmm/rad	Nmm/rad
MZ	Nmm/mm	Nmm/mm	Nmm/mm	Nmm/rad	Nmm/rad	Nmm/rad

Stiffness matrix testing was completed using the synthetic specimen at frequencies of 0.1 Hz and 0.5 Hz, and with axial preloads of either 0 N or 500 N. This resulted in 4 matrices, as indicated in Table 24. For each test 5 triangle wave cycles were completed and data acquired at 100 Hz. The movement in each axis was constant for all matrices: ±3 mm, ±1.5 mm, and ±0.4 mm in the TX, TY, and TZ axes respectively, and ±4° in the RX, RY, and RZ axes. These movements and axial preloads were the same as the study by Stokes et al. [240] using a porcine functional spinal unit. Such values were chosen because they are approximate general ranges of motion present in the natural human disc during daily activities.

Table 24: Stiffness matrix tests completed using the synthetic functional spinal unit

	Matrix S01	Matrix S02	Matrix S03	Matrix S04
Frequency	0.1 Hz	0.1 Hz	0.5 Hz	0.5 Hz
Preload	0 N	500 N	0 N	500 N

While using biological specimens it is common practice to apply an axial preload for a period of time prior to the start of testing to allow the specimen to equilibrate to the preload [220, 221, 238, 240, 241, 249]. The set of experiments reported here with a preload of 500 N did not include a period of equilibration due to the synthetic nature the materials making up the specimen. Creep in the natural disc is a predominantly fluid-mediated phenomenon, which would not be replicated in the synthetic specimen. Therefore the synthetic specimen would not suffer creep to the same extent or modality as a biological specimen. It was thought that commencing the tests shortly after setting the 500 N preload would provide suitable data for the validation tests.

8.1.2 Data Analysis

The first two cycles of the tests were considered preconditioning cycles and were not used for subsequent analysis. The stiffness matrices were compiled using data from the last three cycles. The stiffness was calculated for the centre of the superior vertebral body. This required the moments in the RX and RY axis to be adjusted using a rigid body transformation. The transformation was carried out based on geometric measurements of the specimen and the spine simulator. A translation in the Y axis would lead to a force FY and an associated moment in the X axis. The magnitude of this moment would be different at the

six-axis loadcell compared to the centre of the superior vertebral body. The transformation was based on the spine simulator and vertebral bodies being rigid. The measured moment (MX_{6axis}) was added to the moment due to the measured force FY and the distance between the datum of the 6-axis loadcell and the centre of the superior vertebral body (a), thus allowing the magnitude of the moment at the centre of the superior vertebral, MX, to be calculated body (Figure 94).

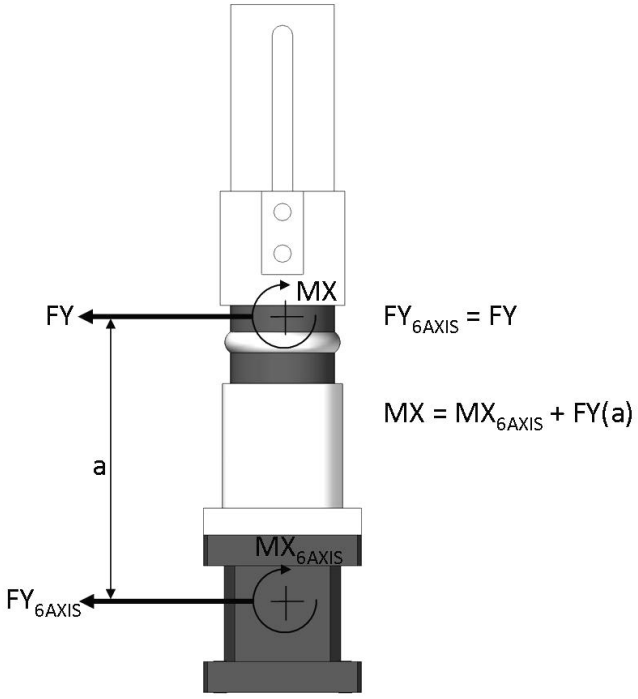

Figure 94: Moment MX transformation

In the Z axis, the centre of the disc was in axial alignment with the six-axis loadcell datum, thus no transformation was necessary. Once the loads were corrected, based on the geometric considerations above, the stiffness was calculated from the load-displacement data using the linear least squares method. This is the same method used by Stokes et al. and Gardner-Morse and Stokes [221, 240] in previous stiffness matrix studies. Although the stiffness can form an S-curve, characterised by a neutral zone and elastic zone (Figure 95), this is not always the case and linearity increases with the application of an axial preload [220, 223].

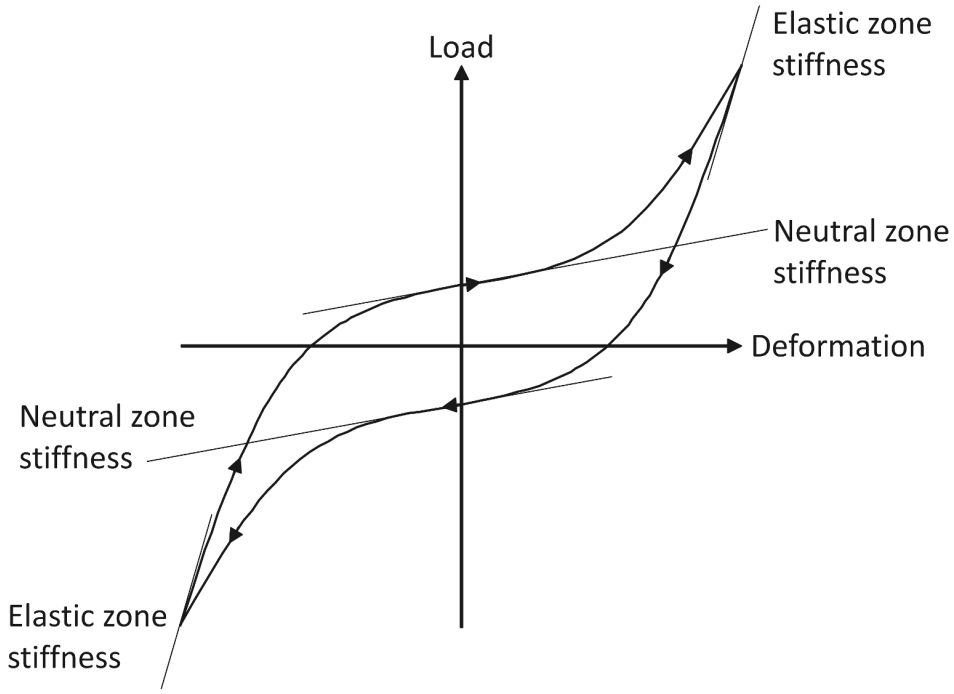

Figure 95: S-Curve of a non-linear stiffness material

The stiffness matrix is composed of 36 stiffness terms, with the six principal stiffnesses forming the diagonal. The stiffnesses are named according to the position in the matrix, with the first number corresponding to the active axis from TX, TY, TZ, RX, RY, and RZ numbered 1-6 respectively, and the second number corresponding to the measured load from FX, FY, FZ, MX, MY, and MZ numbered 1-6 respectively. So, if a stiffness is based on a rotation in the X axis (RX), and the load in the Y axis (FY), the stiffness would be referred to as $K_{4,2}$.

Stokes et al. [240] have argued that the 36 term matrix should be symmetrical about the diagonal. This is based on the conservation of energy and the assumption that the material properties are linear. For example, if an anterior/posterior translation is applied (TX) and the stiffness measured in all six axes ($K_{1,1}$, $K_{1,2}$, $K_{1,3}$, $K_{1,4}$, $K_{1,5}$, $K_{1,6}$); there will be a stiffness associated with the moment created in the Y axes ($K_{1,5}$). It would follow that if a rotation is applied in the Y axes (RY), the stiffness $K_{5,1}$ due to anterior/posterior shear in the X axes would be the same as $K_{1,5}$. These off-diagonal terms can be calculated by taking the average of the two symmetrical stiffnesses [221], e.g. the average of $K_{1,6}$ and $K_{6,1}$, of $K_{2,3}$ and $K_{3,2}$, etc.

Furthermore, Gardner-Morse and Stokes [221] indicated that some of the stiffness terms would be expected to be zero due to symmetry in the sagittal plane. For example, if

flexion/extension is applied, it is expected that the associated shear force in the coronal plane would be zero. This leaves 12 stiffness elements, one of which, anterior/posterior shear under axial translation ($K_{3,1}$ in Table 25) Gardner-Morse and Stokes found to be negligible. Notable off-diagonal stiffnesses are those caused by the flexion/extension moment under anterior/posterior shear ($K_{5,1}$), and by the lateral bending moment under lateral shear ($K_{4,2}$).

Table 25: Stiffness matrix with principal stiffnesses white on black, off-diagonal stiffnesses black on white, symmetrical on light-grey, and possibly negligible stiffnesses on mid-grey

	TX	TY	TZ	RX	RY	RZ
FX	$K_{1,1}$	$K_{2,1}$	$K_{3,1}$	$K_{4,1}$	$K_{5,1}$	$K_{6,1}$
FY	$K_{1,2}$	$K_{2,2}$	$K_{3,2}$	$K_{4,2}$	$K_{5,2}$	$K_{6,2}$
FZ	$K_{1,3}$	$K_{2,3}$	$K_{3,3}$	$K_{4,3}$	$K_{5,3}$	$K_{6,3}$
MX	$K_{1,4}$	$K_{2,4}$	$K_{3,4}$	$K_{4,4}$	$K_{5,4}$	$K_{6,4}$
MY	$K_{1,5}$	$K_{2,5}$	$K_{3,5}$	$K_{4,5}$	$K_{5,5}$	$K_{6,5}$
MZ	$K_{1,6}$	$K_{2,6}$	$K_{3,6}$	$K_{4,6}$	$K_{5,6}$	$K_{6,6}$

However, O'Reilly et al. [253] found from tests on cadaveric functional spinal units with intact discs and after a disc replacement that the matrices were not symmetrical. It was claimed that the assumption of symmetry in the stiffness matrix is valid only for small rotations and it does not take into account the non-conservative nature of forces from the facets and ligaments that are present in the spinal joint. Therefore the results of the validation tests with the synthetic FSU and porcine FSU would assess whether or not it was appropriate to assume symmetry.

8.1.3 Results

Initial tests suggested that the axial preload and test frequency had the expected effect of increasing the stiffness of the specimen. The results for the four matrices were converted into N, mm, and rad (Tables 26-29). These results are for one synthetic specimen that was potted and positioned in the spine simulator prior to all four stiffness matrix tests being completed.

Table 26: Matrix S01, 0.1 Hz, 0 N preload

	TX	TY	TZ	RX	RY	RZ
FX	**27**	-5	0	-6	-20	59
FY	-4	**32**	-3	-84	-16	25
FZ	4	-8	**314**	168	165	27
MX	-239	718	-131	**140,833**	29,868	-739
MY	-889	-104	450	29,874	**73,671**	-1,988
MZ	106	-1	98	-1,404	435	**22,185**

Table 27: Matrix S02, 0.5 Hz, 0 N preload

	TX	TY	TZ	RX	RY	RZ
FX	**28**	-5	0	-11	-21	66
FY	-5	**33**	-3	-72	-20	16
FZ	5	-9	**302**	35	286	43
MX	-258	722	6	**138,134**	40,159	-1,369
MY	-949	-110	427	28,241	**89,158**	-2,401
MZ	114	8	119	-1,306	768	**24,104**

Table 28: Matrix S03, 0.1 Hz, 500 N preload

	TX	TY	TZ	RX	RY	RZ
FX	**32**	-2	-7	-67	-85	-16
FY	-5	**40**	2	120	-46	137
FZ	32	-2	**1,399**	489	372	10
MX	-315	446	-388	**256,330**	70,984	2,005
MY	-1,008	-295	711	73,453	**152,573**	-2,229
MZ	43	19	51	-2,956	327	**56,866**

Table 29: Matrix S04, 0.5 Hz, 500 N preload

	TX	TY	TZ	RX	RY	RZ
FX	**35**	-1	-7	-67	-93	-12
FY	-5	**40**	2	-129	-51	141
FZ	-4	7	**1,403**	454	394	-55
MX	-329	457	-265	**284,118**	79,475	2,028
MY	-1,127	-352	781	79,097	**167,023**	-3,317
MZ	43	28	-66	-3,369	653	**71,299**

The results demonstrated that the characteristics of the load-displacement curves differed between stiffness terms, with some exhibiting the S-curve of a neutral and elastic zone (Figure 96), and others appearing have a strongly linear relationship (Figures 97 and 98). Irrespective of the load-displacement characteristics, the results demonstrated that the three cycles over which the data was analysed was consistent for all stiffness terms.

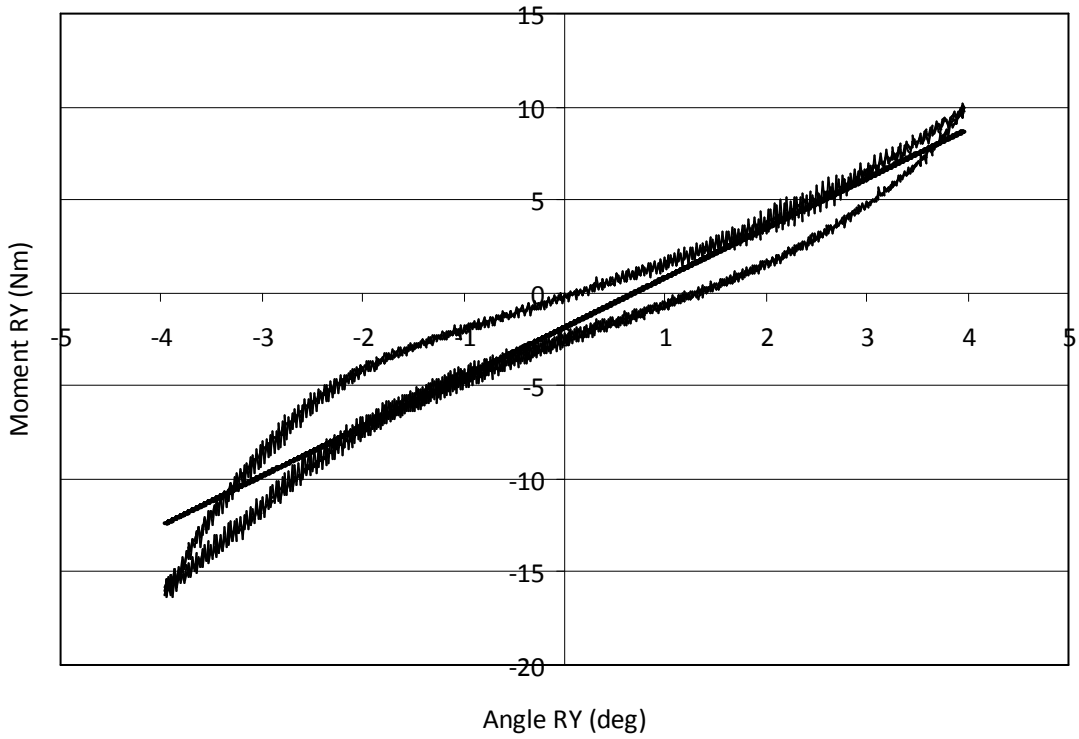

Figure 96: $K_{5,5}$ at 0.1 Hz and under a 500 N preload demonstrating a consistent S-curve for three cycles

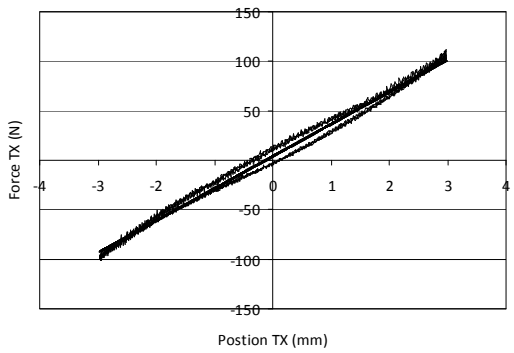

Figure 97: $K_{1,1}$ at 0.1 Hz and under a 500 N preload demonstrating linear behaviour

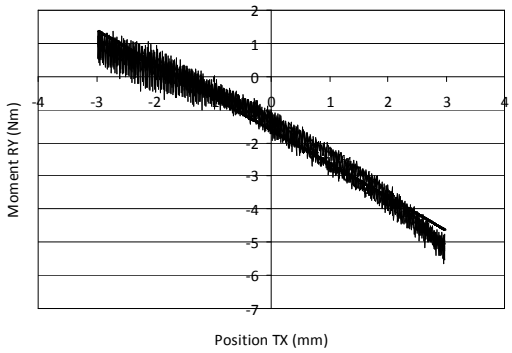

Figure 98: $K_{1,5}$ at 0.1 Hz and under a 500 N preload demonstrating linear behaviour

The only concern from the tests was that in angular rotation due to the large inertia of the XY platform and gimbal head. This led to a torque spike at the point of direction change, particularly at 0.5 Hz. However, it was observed that this only occurred in the axis loadcell and did not appear to be transferred down through to the 6-axis loadcell (Figures 99 and 100).

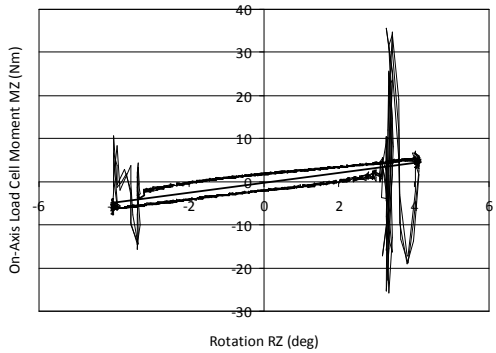

Figure 99: MZ against RZ measured by the individual axis loadcell with torque pulses

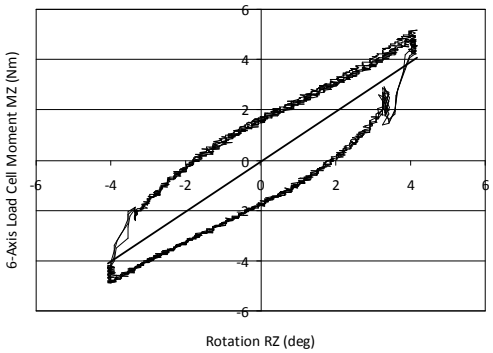

Figure 100: MZ against RZ measured by the 6-axis loadcell without torque pulses

The results showed that the synthetic specimen was less stiff in the principal translation axes ($K_{1,1}$, $K_{2,2}$, $K_{3,3}$), less stiff in axial rotation ($K_{6,6}$), and stiffer in lateral bending and flexion/extension ($K_{4,4}$, $K_{5,5}$ respectively) than the porcine lumbar FSU measured by Stokes et al. [240]. This was true with both 0 N and 500 N preloads. Principal stiffnesses were lower than those measured of a human lumbar FSU [221].

Converting the flexibility data of isolated human FSU specimens without axial preload and at a loading rate of 0.1 Hz obtained by Spenciner et al. [258] showed that the synthetic FSU tested, compared reasonably in flexion/extension and lateral bending. No values of the flexibility were reported, but from plots of the results, it was estimated that the stiffnesses in lateral bending, flexion/extension, and axial rotation were approximately 121,000 Nmm/rad, 95,000 Nmm/rad, and 113,000 Nmm/rad respectively.

8.1.4 Discussion

The spine simulator performed with no observable vibration and minimal noise was recorded in the data acquisition. The final three cycles of all tests were consistent and demonstrated that completing five cycles, discarding the first two and analysing the remaining three would be a suitable method for later tests (Figures 96-98). It has been recommended for spinal testing that the first two cycles be used for preconditioning and should be discarded prior to analysis of the data, further cycles should be consistent and can be used for data analysis [212].

The concerns of torque pulses being transferred to the specimen in axial rotation were attributed to the positioning of the RZ axis load cell. This load cell is mounted between the rotational actuator and the XY platform. A large impulse is necessary to create the sudden change in direction required to perform a triangle wave due to the relatively large inertia of the XY platform and gimbal head. This impulse would be transferred from the actuator to the XY platform through the RZ axis load cell, thus creating a torque spike in the load cell. However, a plot of the position of the RZ axis over time shows that there is little deviation from the desired triangle wave, and the torque spike was not measured in the six-axis load cell positioned underneath the specimen. Thus it is unlikely that the impulse would cause detrimentally high torques to the specimen.

The initial tests suggest that the linear least squares method is a suitable means to obtain stiffness values. Although rotational axes under testing may have exhibited S-curves (Figure 96), as described above, the shear-force and off-axis loads/moments were linear (Figures 97 and 98). The linear least squares method was used by Stokes and Gardner-Morse et al. [220, 221, 240, 241], though in some cases the testing was limited in amplitude to approximately

cover the neutral zone only. However, using the same method might allow some comparison to be made with the previously published data.

The linear least squares method has limitations in that it does not take into account the possibility of a neutral zone; however, not all axes demonstrated a neutral zone. Using several methods to calculate the stiffness terms in a matrix may be suitable but only provided that the stiffness characteristics are consistent for different specimens, so that the same method is used to calculate the same stiffness term between specimens. This is true of different specimen types, or if the stiffness is calculated for the intact disc and a disc replacement device. This would ensure that a like-for-like comparison is made.

Comparisons made with previously published data showed that the synthetic specimen was less stiff in most of the principle stiffness terms than cadaveric lumbar FSUs, and was less stiff in all principal stiffnesses except flexion/extension and lateral bending compared to a porcine FSU. The synthetic specimen is similar to an isolated disc, without the facets; this would explain why many of the stiffnesses measured are lower than those obtained for a functional spinal unit. Additionally, Spenciner et al. [258] used pure, unconstrained moments, whereas stiffness matrix testing uses positional control and applies movement in one axis with all other axes constrained. This may affect how reliably the flexibility data can be converted and compared to principal stiffness terms of a stiffness matrix.

The matrices from these initial tests were not symmetrical. However, the synthetic specimen does not feature facets or ligamentous structures that would lead to the non conservative loads described by O'Reilly et al. [253]. The difference in symmetric stiffness terms may be due to mis-alignment of the specimen, or may be within the error measurement of the spine simulator. Further testing with biological specimens will allow the matrix symmetry to be more thoroughly assessed.

8.1.5 Conclusions

The tests demonstrated that the spine simulator is capable of performing dynamic stiffness matrix tests on spinal specimens. Triangle waves can be achieved with good accuracy, the load can be measured in with relatively low levels of noise and interference, and the data can be captured from tests at 100 Hz. The limitations in comparing the results of the

synthetic specimen with previously published data of cadaveric and porcine spinal specimens aimed to be addressed in the porcine pilot study, which used a porcine lumbar FSU to complete further preliminary stiffness matrix tests.

8.2 Porcine Pilot Study

Tests were completed using a porcine functional spinal unit to compare the results of the spine simulator with results obtained by Stokes et al. [240] using a hexapod testing machine.

Various frequencies were used, though the sample size of only one would not allow any definitive conclusions about the effect of the rate of movement on the associated loads or moments. The study by Stokes and Gardner-Morse was likewise a pilot study, with a sample size of one, investigating the test method that the authors had developed. Comparisons between the two results were therefore limited but gave an insight into the testing method for the full porcine tests that would follow.

This testing was also used to ascertain the characteristics of a porcine specimen in the spine simulator and allow any final adjustments to the test apparatus and testing protocol prior to the full tests. The aim of this pilot study was to assess the suitability of the testing protocol for stiffness matrix testing.

8.2.1 Materials and Methods

An L3-L4 porcine functional spinal unit was harvested from an organically farmed pig aged between eight and twelve months at the time of slaughter and having a mass of approximately 60 kg (Bartlett & Sons Ltd., Bath, UK). The specimen was dissected from a longer section of spine on the day of being acquired. The musculature was removed, whilst the ligaments and the facet joint capsules were left intact. The specimen was then double-sealed in plastic bags and frozen at a temperature of -24°C until the day of testing. Such a procedure of sealing specimens prior to freezing has been recommended as a storage method that does not significantly affect the mechanical properties of the specimens once thawed for testing [212, 259]. Pflaster et al. [260] found no significant difference in moisture

content of cadaveric discs due to multiple freezing cycles compared with the post-mortem levels.

On the morning of testing the specimen was left to thaw in a sealed bag for approximately 3 hours at room temperature. During the last hour of thawing, the specimen was removed from the plastic bags and three self-tapping screws were driven into the vertebral bodies at the cranial and caudal ends of the specimen prior to being potted in aluminium specimen holders using low melting alloy (MCP75). Care was taken to ensure the alignment of the intervertebral disc with respect to the horizontal plane. Once the specimen was potted, it was wrapped in plastic food wrapping to minimise moisture loss. The specimen was left to continue thawing until three hours had elapsed from the time the specimen had been removed from storage.

The specimen was mounted in the spine simulator with the centre of the intervertebral disc aligned with the centre of rotation for the X, Y and Z axes. Prior to fixing the base of the specimen via the six-axis loadcell to the base plate, the load cells and torque transducers on each axis were used to make final adjustments to the specimen position to ensure the load was as close to zero as possible on each axis. Once fully mounted in the spine simulator the position was set to zero and a 2 second reading taken at 100 Hz. From this data, the offsets of the six-axis loadcell were taken and input into the control software.

All testing was completed at room temperature. A total of 60 tests were completed, comprising one test for each of the six axes at 5 frequencies with an axial preload of 0 N and 500 N. This resulted in a total of 10 stiffness matrices (Table 30). The motion applied in each axis was as with previous tests using the synthetic specimen. The tests were completed first with 0 N preload; the order of these tests was chosen for the various axes and frequencies based on the ease of application using the control software. This resulted in the testing of one axis at a time over all frequencies before testing another axis until the tests were completed.

The axial translation axis was then set to load control and 500 N of compression applied. This was maintained for 3 hours to equilibrate the specimen prior to the 30 tests with an axial preload of 500 N. The length of this equilibration period is the same at that used by Stokes et al. [240] when completing similar stiffness matrix testing of a porcine lumbar spinal unit.

Again, the order of the tests with the 500 N preload was chosen based on the ease of application using the control software.

Prior to the tests with an axial preload being completed, the TZ axis was changed back from load control to position control. If left in load control with a preload of 500 N, the position would not be restrained, which result in the stiffness due to the axial compressive load (FZ) any movement in the other five axes being zero because the force would be constant. This would not reflect the associated compressive forces due to movements in other axes. Therefore all axes other than that under investigation in each test were held stationary, including TZ. The axial translation was adjusted before the start of each test, if it had drifted from 500 N as a result of the previous test.

The choice of testing frequencies was based on the need to allow comparisons with other studies and the necessity to evaluate the full frequency range of the spine simulator. Stokes et al. [240] used quasistatic testing, with a frequency of 0.00575 Hz. This frequency was therefore used to allow comparisons with their work. The frequency of 0.05 Hz was used as this represents the lower end of dynamic testing speeds recommended by Wilke et al. [212]. The frequency of 0.1 Hz matched that applied by Spenciner et al. [258]. A maximum frequency of 0.5 Hz was used as this represented the maximum velocity upon which, according to the control validation tests, the spine simulator could maintain accurate positioning, and was also estimated to be at the upper end of physiological motion, representing 8°/sec in rotations. A fifth frequency of 0.3 Hz was chosen for completeness, representing an intermediate value between 0.1 Hz and 0.5 Hz.

Table 30: Matrix tests completed using the porcine functional spinal unit

	Matrix P01	Matrix P02	Matrix P03	Matrix P04	Matrix P05
Frequency	0.00575 Hz	0.05 Hz	0.1 Hz	0.3 Hz	0.5 Hz
Preload	0 N	0 N	0 N	0 N	0 N
	Matrix P06	Matrix P07	Matrix P08	Matrix P09	Matrix P10
Frequency	0.00575 Hz	0.05 Hz	0.1 Hz	0.3 Hz	0.5 Hz
Preload	500 N	500 N	500 N	500 N	500 N

8.2.2 Results

The stiffness matrices (Tables 31-40) were obtained from the last three cycles of the load and displacement data using the previously described linear least squares method.

Table 31: Matrix P01, 0.00575 Hz, 0 N preload

	TX	TY	TZ	RX	RY	RZ
FX	**27**	2	2	-14	242	-55
FY	-1	**36**	-2	-159	-11	233
FZ	3	-7	**135**	-128	-2,862	-56
MX	-145	915	6	**6,154**	435	837
MY	-634	-226	-1,469	4,314	**59,192**	-11,551
MZ	-97	-52	-332	-3,558	1,180	**68,113**

Table 32: Matrix P02, 0.05 Hz, 0 N preload

	TX	TY	TZ	RX	RY	RZ
FX	**28**	2	3	-15	243	-60
FY	-1	**34**	-3	-167	-5	296
FZ	1	-5	**146**	35	-2,044	-172
MX	-118	835	57	**6,595**	1,054	1,180
MY	-649	-208	-1,525	1,954	**46,553**	-17
MZ	-60	-61	-498	-3,804	-390	**78,810**

Table 33: Matrix P03, 0.1 Hz, 0 N preload

	TX	TY	TZ	RX	RY	RZ
FX	**28**	2	3	-11	245	-55
FY	-1	**35**	-4	-168	-4	304
FZ	2	-6	**146**	6	-2,785	-118
MX	-117	838	18	**6,755**	1,341	1,581
MY	-663	-207	-1,485	338	**59,725**	-1,570
MZ	-67	-70	-558	-3,724	-103	**77,120**

Table 34: Matrix P04, 0.3 Hz, 0 N preload

	TX	TY	TZ	RX	RY	RZ
FX	**29**	-2	4	-15	258	-53
FY	-1	**35**	-4	-177	-4	315
FZ	1	-6	**166**	-321	-3,278	-254
MX	-114	840	58	**9,425**	1,524	1,518
MY	-678	-217	-1,774	2,636	**68,400**	-1,524
MZ	-56	-66	-628	-4,372	-57	**80,672**

Table 35: Matrix P05, 0.5 Hz, 0 N preload

	TX	TY	TZ	RX	RY	RZ
FX	**30**	2	4	-16	261	-40
FY	-1	**35**	-3	-179	-6	322
FZ	2	-6	**133**	10	-3,484	-210
MX	-121	842	150	**10,772**	99	1,891
MY	-718	-219	-1,377	2,361	**72,433**	-2,458
MZ	-55	-71	-626	-4,607	-34	**79,721**

Table 36: Matrix P06, 0.00575 Hz, 500 N preload

	TX	TY	TZ	RX	RY	RZ
FX	**33**	2	-28	-6	311	-32
FY	-2	**38**	7	-176	-51	174
FZ	18	-8	**1,163**	-1,515	-8,771	-287
MX	-172	749	-86	**150,699**	-762	1,495
MY	-1,100	-99	-14,138	17,790	**175,703**	-2,361
MZ	-106	122	-501	1,765	-2,246	**67,609**

Table 37: Matrix P07, 0.05 Hz, 500 N preload

	TX	TY	TZ	RX	RY	RZ
FX	**36**	2	-27	-28	244	-26
FY	-2	**40**	8	-162	-52	225
FZ	-1	-3	**1,295**	-363	-7,718	-380
MX	-129	820	-82	**228,530**	-2,951	3,661
MY	-1,025	-180	-15,962	-1,753	**190,428**	-4,538
MZ	-126	122	-519	-831	-3,994	**74,868**

Table 38: Matrix P08, 0.1 Hz, 500 N preload

	TX	TY	TZ	RX	RY	RZ
FX	**36**	2	-25	-14	269	-25
FY	-2	**40**	9	-177	-65	239
FZ	26	2	**1,350**	-1,275	-9,050	-445
MX	-101	823	-13	**202,884**	-3,684	3,661
MY	-1,373	-257	-16,589	14,135	**210,631**	-4,137
MZ	-145	121	-522	40	-3,604	**76,788**

Table 39: Matrix P09, 0.3 Hz, 500 N preload

	TX	TY	TZ	RX	RY	RZ
FX	**36**	2	-26	-20	274	-25
FY	-2	**41**	10	-179	-66	249
FZ	27	3	**1,390**	-1,248	-9,604	-548
MX	-119	868	57	**219,873**	-4,051	4,011
MY	-1,369	-304	-17,054	14,484	**218,698**	-3,071
MZ	-132	137	-547	-527	-3,203	**80,094**

Table 40: Matrix P10, 0.5 Hz, 500 N preload

	TX	TY	TZ	RX	RY	RZ
FX	**36**	2	-26	-24	261	-20
FY	-2	**40**	9	-188	-66	250
FZ	10	3	**1,357**	-1,241	-9,769	-669
MX	-172	848	71	**232,724**	-5,718	4,200
MY	-1,174	-361	-16,632	15,304	**226,834**	-1,639
MZ	-82	249	-552	-1,581	-2,773	**81,074**

Most stiffnesses increased as the testing frequency increased. This would be expected given the viscoelastic nature of the tissue of which the porcine specimen is comprised.

The test frequency caused the principal stiffnesses to increase in all cases excluding shear (Tables 41 and 42); this effect was similar without preload and with the application of the 500 N preload. The shear stiffness increased initially but remained approximately constant thereafter (Tables 41 and 42).

Table 41: Principal stiffnesses with 0 N preload at various frequencies

	TX	TY	TZ	RX	RY	RZ
0.00575 Hz	27	36	135	6,154	59,192	68,113
0.05 Hz	28	34	146	6,595	46,553	78,810
0.1 Hz	28	35	146	6,755	59,725	77,120
0.3 Hz	29	35	166	9,425	68,400	80,672
0.5 Hz	30	35	133	10,772	72,433	79,721

Table 42: Principal stiffnesses with 500 N preload at various frequencies

	TX	TY	TZ	RX	RY	RZ
0.00575 Hz	33	38	1,163	150,699	175,703	67,609
0.05 Hz	36	40	1,295	228,530	190,428	74,868
0.1 Hz	36	40	1,350	202,884	210,631	76,788
0.3 Hz	36	41	1,390	219,873	218,698	80,094
0.5 Hz	36	40	1,357	232,724	226,834	81,074

The non-principal stiffnesses were more variable under different loading rates and axial preloads. The majority increased in magnitude with test frequency but not all; some terms remained constant and others decreased slightly (Table 43 A&B). The same is true of the application of the 500 N preload, which caused most stiffness terms to increase in magnitude but not all (Table 43 C). The stiffness in lateral bending $k_{4,4}$ was very low without an axial preload but increased under the 500 N preload to be similar to that of flexion/extension, and comparable to previously published data.

Table 43: The effect of increasing test frequency on stiffness magnitude with 0 N preload (A), 500 N preload (B), and the effect of applying a preload on the stiffness magnitude (C).

↑ denotes an increase, ↓ a decrease, ↔ constant, and ↕ denotes no obvious pattern

A - 0 N Preload						
	TX	TY	TZ	RX	RY	RZ
FX	↑	↔	↔	↔	↑	↓
FY	↔	↔	↔	↑	↔	↑
FZ	↔	↔	↕	↕	↑	↑
MX	↔	↔	↑	↑	↑	↑
MY	↑	↔	↔	↕	↑	↕
MZ	↓	↑	↑	↑	↕	↑

B - 500 N Preload						
	TX	TY	TZ	RX	RY	RX
FX	↔	↔	↔	↔	↔	↓
FY	↔	↔	↔	↑	↑	↑
FZ	↕	↔	↑	↕	↑	↑
MX	↔	↑	↕	↑	↑	↑
MY	↔	↑	↑	↕	↑	↕
MZ	↕	↑	↑	↕	↕	↑

C - Effect of Preload						
	TX	TY	TZ	RX	RY	RZ
FX	↑	↔	↑	↔	↔	↓
FY	↔	↑	↑	↔	↑	↓
FZ	↑	↔	↑	↑	↑	↑
MX	↔	↔	↕	↑	↓	↑
MY	↑	↕	↑	↕	↑	↕
MZ	↑	↑	↔	↓	↑	↔

8.2.3 Discussion

The stiffness terms that Gardner-Morse and Stokes had regarded as negligible due to symmetry sagittal plane [221] were assessed as to whether this was the case in the porcine validation tests. However, conclusions regarding stiffnesses due to asymmetry in the sagittal plane were limited. It would be expected that certain stiffness terms would cancel out over the course of tests with multiple specimens, a sample size of one would not provide such cancelling out.

The stiffness matrices do not appear to be symmetrical, though some terms suggest symmetry might occur in certain circumstances. The full tests will therefore analyse data in terms of a non-symmetrical, 36 term matrix.

It is possible that the period of testing, combined with the large number of tests completed would have had an effect on the mechanical properties of the specimen. The cycling of the specimen may cause excessive fluid loss in the intervertebral disc. The total number of cycles was 300 (5 for 60 tests), the testing time was approximately 8.5 hours, and the total time from removal from freezing until the end of testing was 11.5 hours.

Wilke et al. [261] found that the range of motion of porcine specimens increased with increased exposure to room temperature, though the increase was less than 10 % during the first 10-20 hours of exposure. They also found that the range of motion of ovine specimens increased with accumulated cycles. The increase was less than 10 % in specimens wrapped in saline soaked gauze that was periodically replenished with saline spray. Specimens that were air-exposed exhibited an increased in range of motion of approximately 30 % over 500 cycles.

It is possible that the testing completed did result in some alterations in the mechanical properties over the testing period. It is likely that if this was the case, it would be due to the accumulated cycles, rather than the exposure to room temperature. Therefore, the full porcine tests will be completed at one frequency only, thus reducing both the number of accumulated cycles and the total exposure time.

The testing protocol will be modified to limit the number of test cycles and the testing time for each specimen. This will be achieved by testing specimens over one frequency only, and by reducing the equilibration time after the application of an axial preload. The moisture level maintenance of specimens will also be enhanced by spraying specimens with 0.9 % saline solution, before wrapping them in food packaging plastic. This has been shown to maintain moisture levels well compared with air exposed specimens or drip irrigated specimens [260, 261].

The maximum stiffness zero error was calculated from the six-axis loadcell hysteresis (0.2 %) and linearity error (0.2 %), and the testing range of motion and peak to peak error (Figure 101). The peak to peak error is the difference in amplitude from the maximum and minimum actual position values compared to the desired peak to peak amplitude. This error may be caused by the actual position overshooting or undershooting the desired position. Due to the inertia of the spine simulator components, and the triangle waveform used in the

stiffness matrix tests, it is more likely that the actual position would overshoot the desired position. However both outcomes were considered in the zero error calculation. The maximum load error is based on the capacity of the load cell in each axis, which results in a maximum error of 440 Nmm in the rotational Y axis, for example. As Figure 101 shows, the maximum stiffness error is based on a load error of the maximum amount, combined with the position undershooting by the maximum peak to peak error. The zero error was calculated value for each stiffness term in the matrix (Table 44).

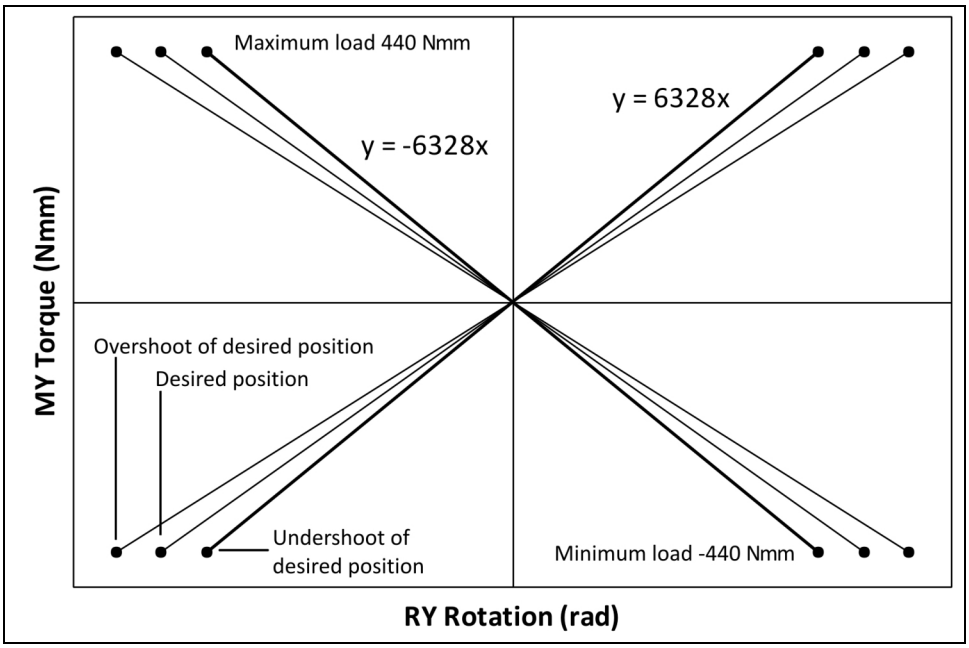

Figure 101: Zero error calculation of stiffness $k_{4,4}$ using maximum positional and load errors

The peak to peak error changes with the testing frequency, though this only marginally changes the stiffness zero error. The error for the appropriate frequency was used to compare with the stiffness results above. The test frequency of 0.1 Hz was the middle test frequency for the validation porcine tests and the likely test frequency for the full tests (Table 44).

Table 44: Zero error for stiffness terms at a test frequency of 0.1 Hz

	TX	TY	TZ	RX	RY	RZ
FX	**±3**	±6	±23	±127	±127	±126
FY	±3	**±6**	±23	±127	±127	±126
FZ	±6	±12	**±45**	±253	±253	±252
MX	±147	±294	±1128	**±6335**	±6328	±6303
MY	±147	±294	±1128	±6335	**±6328**	±6303
MZ	±75	±150	±574	±3225	±3221	**±3209**

Stiffnesses were only considered to be negligible if the magnitude across all testing frequencies, with either 0 N or 500 N preload, was less than the calculated zero error. This showed that some terms regarded as negligible by Gardner-Morse and Stokes were not found to be within the zero error of the spine simulator (Table 45). Some of the non-zero stiffnesses would be expected to be negligible due to sagittal plane symmetry. The full tests with multiple samples may lead to the mean stiffnesses being reduced to a negligible magnitude.

Table 45: Stiffness terms below the zero-error on white

	TX	TY	TZ	RX	RY	RZ
FX	$K_{1,1}$	$K_{2,1}$	$K_{3,1}$	$K_{4,1}$	$K_{5,1}$	$K_{6,1}$
FY	$K_{1.2}$	$K_{2,2}$	$K_{3,2}$	$K_{4,2}$	$K_{5,2}$	$K_{6,2}$
FZ	$K_{1,3}$	$K_{2,3}$	$K_{3,3}$	$K_{4,3}$	$K_{5,3}$	$K_{6,3}$
MX	$K_{1,4}$	$K_{2,4}$	$K_{3,4}$	$K_{4,4}$	$K_{5,4}$	$K_{6,4}$
MY	$K_{1,5}$	$K_{2,5}$	$K_{3,5}$	$K_{4,5}$	$K_{5,5}$	$K_{6,5}$
MZ	$K_{1,6}$	$K_{2,6}$	$K_{3,6}$	$K_{4,6}$	$K_{5,6}$	$K_{6,6}$

The zero error calculation is higher than the actual error may be. This is because the calculation is based on hysteresis and linearity errors of the six-axis load cell and these are minimised through the test and analysis methods. Hysteresis error is minimised as the resulting force or moment due to a movement is made linear using the least squares method to calculate the stiffness. Discounting the hysteresis error would halve the zero errors of Table 44. The error due to linearity is minimised if the loads are near full capacity [262], which will vary between individual tests. This means that the zero error calculation is useful

in determining if a stiffness term is definitely not zero, but is limited as a measure of defining stiffnesses as negligible. The zero error calculations will therefore be used as a guide only.

It is understood that Stokes et al. [240] used personal judgement to determine negligible stiffnesses. For this reason, all stiffness values will be assumed non-zero until the final analysis of the full porcine tests. This will allow statistical analysis to determine whether or not any variables introduced to the specimens create a significant difference, even if the stiffness values are low in magnitude.

Stokes et al. [240] carried out tests on a porcine specimen at a frequency of 0.00575 Hz with a preload of 0 N and 500 N. Comparing the principal stiffnesses obtained at this test frequency in the porcine pilot study with those previously published showed that the shear stiffness was lower in both the sagittal and coronal planes ($K_{1,1}$ and $K_{2,2}$ respectively) with 0 N and 500 N preload. The stiffness in lateral bending ($K_{4,4}$) with 0 N preload was lower than previously published data, but higher with a 500 N preload. The stiffness in flexion/extension ($K_{5,5}$) with a preload of 0 N and 500 N was higher than the previously published data. The principal stiffnesses in axial compression ($K_{3,3}$) and axial rotation ($K_{6,6}$) were higher in the present study with a 0 N preload but lower with the 500 N preload. There was no obvious correlation between the current study and previously published data as regard to the non-principal stiffnesses.

Only qualitative conclusions can be drawn from this study due to sample size but the majority of the results are the same order of magnitude at those published by Stokes et al. [240] and demonstrate that the spine simulator has the potential to work effectively in measuring spinal stiffness matrices. Aside from the general specimen variation that would occur between two porcine lumbar FSUs, the age and lumbar level of the specimen tested by Stokes et al. was unknown, which if different from the present study, would be likely to affect the stiffness properties.

Previously published data by Stokes and Gardner-Morse et al. of porcine and cadaveric functional spinal units (FSU) and isolated discs (ISD) with various axial preloads shows a large variability in stiffness in the principal stiffness terms (Table 46). All the data was obtained using the same test apparatus. All specimens were submerged in a 4°C saline bath and tested quasistatically.

Table 46: Quasistatic stiffness data ($K_{1,1}$, $K_{2,2}$, $K_{3,3}$ in N/mm, $K_{4,4}$, $K_{5,5}$, $K_{6,6}$ in Nmm/rad)

Ref	Specimen	Preload (N)	$K_{1,1}$	$K_{2,2}$	$K_{3,3}$	$K_{4,4}$	$K_{5,5}$	$K_{6,6}$
[240]	Porcine FSU	0	35	49	67	11,500	13,300	35,400
[220]	Porcine FSU	0	400	400	500	93,000	168,000	374,000
[220]	Porcine FSU	200	600	600	2,500	243,000	355,000	486,000
[220]	Porcine FSU	400	700	800	3,500	355,000	486,000	542,000
[240]	Porcine FSU	500	108	190	2,080	98,800	105,000	11,500
[220]	Porcine ISD	0	37	50	520	30,000	15,000	7,000
[220]	Porcine ISD	200	90	170	2,500	179,000	105,000	30,000
[220]	Porcine ISD	400	170	260	3,400	262,000	164,000	45,000
[221]	Cadaver FSU	0	251	332	438	174,000	241,000	564,000
[221]	Cadaver FSU	250	368	447	1,700	256,000	366,500	706,000
[221]	Cadaver FSU	500	426	523	2,420	306,500	431,000	783,000

The large variability demonstrates the difficulty in comparing the results of different studies, even within the same research group. The results within each study show what would be expected in terms of a stiffness increase due to axial preload, and a reduction in shear and bending principal stiffnesses when the facets are removed. However, the stiffness terms of an individual porcine FSU [240] are approximately an order of magnitude lower than those obtained in a later study, which tested specimens over a smaller range of motion about the neutral zone [220]. Two studies showed an increase in axial rotation stiffness ($K_{6,6}$) as the axial preload increased, with both porcine functional spinal units and isolated discs [220], and with cadaveric functional spinal units [221]. This is contrary to the individual porcine FSU tests in which $K_{6,6}$ was reduced by a factor of approximately 3 with the application of a 500 N preload [240].

The porcine pilot study completed found that the stiffness $K_{6,6}$ increased from approximately 68,000-81,000 Nmm/rad as the testing rate increased from 0.00575-0.5 Hz with both a preload of 0 N and 500 N.

8.2.4 Conclusions

The spine simulator performed well with the porcine specimen. The validation testing has been used to refine the methods for the full porcine tests.

The testing protocol will be amended to improve the maintenance of moisture levels and minimise the testing time, as this has been shown to have a large effect on the mechanical properties of biological specimens. It is evident form the variability of published data, that it is crucial to follow every detail of a rigorously set-out testing protocol.

9 PORCINE STIFFNESS MATRIX STUDY

The dynamic stiffness matrix testing of porcine specimens with intact discs and with a disc replacement device, with preloads of 0 and 500 N, was completed. To the knowledge of the author, this is the first dynamic six-axis testing of a disc replacement device.

The full porcine tests were split into two groups: functional spinal unit (FSU) specimens; and isolated disc (ISD) specimens, comprising a functional spinal unit with the facets and processes removed. In both groups, six specimens (two L1-L2, two L3-L4, and two L5-L6) were tested first with an intact disc, and after the intervertebral disc had been replaced by a DePuy In Motion device. Tests were completed at a single frequency (0.1 Hz), with preloads of 0 N and 500 N. This allowed multiple comparisons to be made, most importantly the comparison of the intact disc with a leading disc replacement device.

The In Motion device is a double ball and socket design, with two cobalt-chrome endplates and a lens shaped ultra-high molecular weight polyethylene (UHMWPE) core. The endplates feature spikes for primary stability, along with a textured titanium coating for secondary stability through bone in-growth. The In Motion device is an updated version of the well-established Charité disc replacement. The difference between the two devices is that the In Motion has a flat section on the outer faces of the endplates to aid implantation with the use of improved surgical instrumentation.

The double ball and socket design of the device results in a non-fixed centre of rotation and also allows translation in the anterior/posterior and medial/lateral directions (Figures 102-104). The device used in this study was medium in size and comprised one endplate with an angle of 0°, one endplate with an angle of 5°, and an 8.5 mm core.

The In Motion surgical instrumentation was not available for implantation. However, the operative technique was followed, and a spine surgeon assisted in completing a disc replacement procedure on a porcine lumbar FSU prior to commencing the full porcine tests for training purposes. This allowed the specimen preparation and device implantation to resemble the clinical situation.

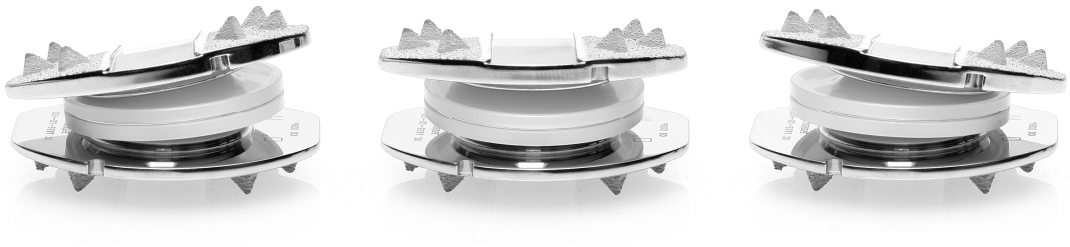

Figure 102: The In Motion device viewed from the anterior aspect in right lateral bending (left), neutral position (centre), and left lateral bending (right)

Figure 103: The In Motion device viewed from the right lateral aspect in extension (left), neutral position (centre), and flexion (right)

Figure 104: The In Motion device viewed from the right lateral aspect in a combination of extension and left axial rotation (left), flexion and left axial rotation (centre), and extension and right axial rotation (right)

9.1 Porcine Specimen Rationale

Tests to compare porcine FSU specimens with an intact intervertebral disc and with the disc replaced with a DePuy In Motion device were performed. The low-friction double ball and socket design of the arthroplasty device was expected to result in lower rotational stiffness compared to the intact disc.

This set of experiments will provide a good understanding of the biomechanical changes introduced in the behaviour of a FSU by a disc replacement device. However, the facets and the ligaments of the transverse and spinous processes have the potential to shield some of the differences between the intact disc and the disc replacement device. Therefore, specimens with the facets removed were also studied to provide a like-for-like comparison between natural intervertebral disc and the DePuy in Motion device.

These isolated disc (ISD) specimens aimed to focus the stiffness testing on the area that the In Motion device was designed to replace. In order to perform well, the disc replacement device should have similar mechanical properties to the natural disc; ISD testing would allow this to be determined.

The anterior longitudinal ligament (ALL) is resected and the posterior longitudinal ligament is released as part of the surgical procedure for the implantation of the In Motion device [263]. Therefore, in order to replicate the natural biomechanics of the spine, the arthroplasty device should behave similarly to the ALL along with the intervertebral disc itself. These ligaments were left intact for the testing of the isolated natural disc but both were resected during the implantation of the In Motion disc. The ALL was resected as part of the surgical procedure and the posterior longitudinal ligament (PLL) was resected due to the much smaller disc height of the porcine specimens, combined with the need to position the size medium implant within the smaller vertebral space of the porcine specimens.

Without the PLL being resected, the In Motion device would have been difficult to fit within the limited height of the porcine disc space. Forcing the endplates apart would have created a large extension moment, and would have required a large moment to position the specimen neutrally in the spine simulator. This would have affected the stiffness matrix results significantly, and would not have reflected the in-vivo situation with a human motion

segment, which has a greater disc height than the porcine specimens used in the present study. It has been shown that the disc height is a more important factor affecting ROM than whether or not the PLL has been resected [264].

9.2 Materials and Methods

Twelve porcine functional spinal units were harvested from organically farmed pigs aged between eight and twelve months at the time of slaughter, with masses of approximately 60 kg (Bartlett & Sons Ltd., Bath, UK). The specimens were dissected from longer sections of spine (generally T12-S1) on the day of procurement. Three spinal levels were prepared; four L1-L2, four L3-L4, and four L5-L6. Musculature was removed. The ligaments and the facet joint capsules were left intact on six specimens (two L1-L2, two L3-L4, and two L5-L6). The facets of the other six specimens were entirely removed, leaving the isolated intervertebral disc, anterior and posterior longitudinal ligaments. The specimens were labelled, triple bagged, and then frozen at a temperature of -24°C until the day of testing.

On the morning of testing each specimen was left to thaw for 3 hours at room temperature in a sealed plastic bag to minimise moisture loss due to evaporation. During the last hour of thawing, the specimen was removed from the plastic bag and three self-tapping screws were driven into the vertebral bodies at the cranial and caudal ends of the specimen prior to being potted in aluminium specimen holders using the low melting alloy (MCP75). The specimen was potted with the intervertebral disc aligned horizontally. The cranial end of the specimen was potted first, followed by the caudal end. The spine simulator was used to lower the specimen into the caudal pot, which allowed the alignment to be finely adjusted. In the case of each pot, as soon as the Wood's metal had solidified, the pot was submerged in water so as to prevent overheating of the specimen. Once the specimen was potted, it was sprayed with 0.9 % saline solution and wrapped in plastic food wrapping in order to maintain an adequate moisture level.

The specimen was then mounted in the spine simulator with the centre of the intervertebral disc aligned with the centre of rotation for the X, Y and Z axes. Prior to fixing the base of the specimen via the six-axis loadcell to the base plate, the load cells and torque transducers on each axis were used to make final adjustments to the specimen position to ensure the load was as close to zero on each axis as possible. Once fully mounted the position of the axes

was set to zero, and a 2 second reading taken at 100 Hz. From this data, the offsets of the six-axis loadcell were taken and input into the dSPACE control software.

The testing was completed in position control and to the same range of motion as in the previous testing; ±3 mm, ±1.5 mm, ±0.4 mm, ±4°, ±4°, and ±4° in the TX, TY, TZ, RX, RY, and RZ axes respectively. Testing was completed at 0.1 Hz in all axes; this resulted in a rate of rotation of 1.6°/sec, which is within the range suggested by Wilke et al. [212] for dynamic spinal testing. It was also the same frequency as used by Spenciner et al. [258] in a study which completed multi-axis flexibility testing of cadaveric lumbar spinal specimens. Data was acquired at a rate of 100 Hz. Five cycles were completed for each test, with the first two being used as preconditioning cycles, which were excluded from the data analysis.

Preloads of 0 N and 500 N were used, as in the validation testing. However, the equilibration time of 3 hours would result in prohibitively long testing times given that it would need to be applied twice; once with the intact disc and again after the disc replacement device was implanted. Such a testing time may be detrimental to the mechanical properties of the specimen.

Gay et al. [238] applied a preload with an equilibration time of 30 minutes prior to testing on human functional spinal units. It was therefore decided for the full tests to apply a preload for 30 minutes, complete a stiffness matrix test, continue to apply the preload and complete another stiffness matrix test 60 minutes after the initial preload application. Following testing on the intact disc, the In Motion device would be implanted and the same testing procedure undertaken (Figure 105). This protocol would allow the length of equilibration time on specimens sprayed with 0.9 % saline and wrapped in food packaging plastic at room temperature to be assessed.

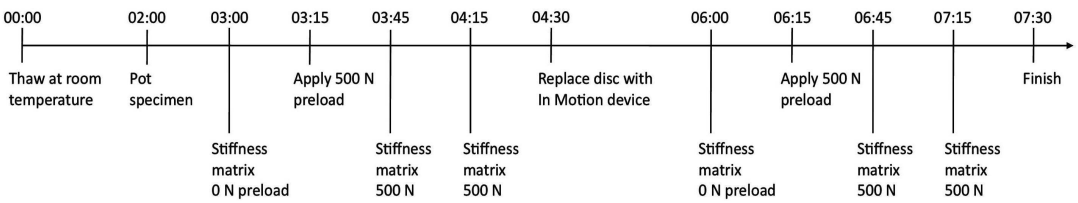

Figure 105: Estimated testing timeline

It was estimated that with this test protocol, the testing would be completed in approximately 7:30 hours, including thaw time. Testing over such a time would minimise the degradation of the specimens and the associated changes in mechanical properties.

The intact spine was first tested following the above procedure (Figure 106). The specimen was then removed from the test rig, but all fixtures left in place so that it could be returned to the same position. The intervertebral disc was replaced with a DePuy In Motion device following the manufacturer's operative technique (Figure 106). The specimen was then sprayed again with 0.9 % saline solution and wrapped in plastic food wrapping before being re-mounted in the spine simulator. The same procedure was completed for the isolated disc specimens (Figure 107).

Figure 106: Intact FSU specimen (left), intact FSU specimen sprayed and wrapped (centre), FSU specimen with In Motion device prior to being sprayed and wrapped (right)

Figure 107: Intact ISD specimen (left), intact ISD specimen sprayed and wrapped (centre), ISD specimen with In Motion device prior to being sprayed and wrapped (right)

When the specimen was re-mounted in the spine simulator following the implantation of the In Motion device, the offsets of the six-axis loadcell were taken again, input into the dSPACE controller and the stiffness matrix tests repeated. This resulted in a total of 6 stiffness matrices being measured for each specimen (Table 47). Within each stiffness matrix, the order of testing of the six axes was randomised so as to minimise any residual effects of the previous test(s) on the results of any axis. During testing the axial position was adjusted between each test in order to maintain the correct preload, if required.

Table 47: Matrix tests completed for each of the twelve specimens

	Matrix 01	Matrix 02	Matrix 03
Condition	Intact	Intact	Intact
Preload	0 N	500 N (30 minutes)	500 N (60 minutes)
	Matrix 04	Matrix 05	Matrix 06
Condition	Device	Device	Device
Preload	0 N	500 N (30 minutes)	500 N (60 minutes)

The test protocol (Table 48) was carefully repeated for each specimen, and the start and finish time of each stiffness matrix test noted so that consistency could be checked.

Table 48: Summary of testing protocol for pre-dissected porcine specimens

Step	Procedure
1	Take specimen out of freezer (-24°C) and allow to thaw at room temperature
2	During thawing, drive screws into cranial and caudal end of specimen
3	During thawing, pot cranial end of specimen in Wood's Metal
4	During thawing, pot caudal end of specimen in Wood's Metal
5	During thawing, spray the specimen with 0.9 % saline solution
6	During thawing, wrap the specimen in food packaging plastic film
7	During thawing, mount specimen on 6-axis loadcell and spine simulator
8	3 hours of thawing complete
9	Adjust position of specimen to zero loads on all axes
10	Fix base of specimen
11	Take 2 second reading
12	Use reading to calculate offsets for 6-axis loadcell
13	Adjust offsets of 6-axis loadcell in dSPACE software
14	Activate the motors for TX, TY, RX, and RY axes
15	Complete randomised stiffness matrix test with 0 N preload
16	Change TZ axis to load control
17	Note axial displacement (mm)
18	Apply a preload of 500 N
19	After 30 minutes change TZ axis to position control
20	Note axial displacement (mm)
21	Complete randomised stiffness matrix test with 500 N preload
22	Adjust TZ as required during testing to maintain 500 N preload
23	Note axial displacement at end of stiffness matrix test (mm)
24	Change TZ axis to load control
25	Apply a preload of 500 N
26	60 minutes after initial application of preload change TZ axis to position control
27	Note axial displacement
28	Complete randomised stiffness matrix test with 500 N preload
29	Adjust TZ as required during testing to maintain 500 N preload
30	Note axial displacement at end of stiffness matrix test (mm)
31	Adjust preload to zero

Table 48 continued…

32	Remove specimen from the spine simulator and 6-axis loadcell
33	Remove food packaging plastic film from around specimen
34	Replace the intact disc with the In Motion device
35	Spray the specimen with 0.9 % saline solution
36	Wrap the specimen in food packaging plastic film
37	Re-mount the specimen on the 6-axis loadcell and spine simulator
38	Take 2 second reading
39	Use reading to calculate offsets for 6-axis loadcell
40	Adjust offsets of 6-axis loadcell in dSPACE software
41	Repeat steps 15-33
42	Unpot specimen and dispose of biological waste

9.3 Porcine Stiffness Matrix Results

9.3.1 Specimen Stiffness Matrices

The stiffness was calculated from the last three of the five cycle test in each axis using the linear least squares method. All tests showed good repeatability in the final three cycles. The stiffness was calculated at the centre of the superior vertebral body. The resulting stiffness terms of the six specimens in each group were used to obtain a mean stiffness value. This resulted in 12 matrices, six corresponding to the testing of the functional spinal units (FSU01-FSU06) (Tables 49-54), and six corresponding to the testing of the isolated discs (ISD01-ISD06) (Tables 56-61). The results of the FSU specimens are comparable to the individual specimen tested for the porcine validation test. The tables below report the mean stiffnesses of the 36 terms of each matrix. More comprehensive matrices comprising the mean and standard deviation can be found in the appendix (page 253).

Table 49: Matrix FSU01, mean stiffness with 0 N preload and an intact disc

	TX	TY	TZ	RX	RY	RZ
FX	**32**	2	2	-16	-7	-41
FY	-1	**36**	1	-77	-8	369
FZ	15	-3	**326**	-168	-2,910	19
MX	-107	766	568	**41,245**	639	7,048
MY	-1,025	-228	-3,088	5,317	**67,118**	-3,552
MZ	-88	210	32	-4,200	-425	**108,056**

Table 50: Matrix FSU02, mean stiffness with 500 N (30 min) preload and an intact disc

	TX	TY	TZ	RX	RY	RZ
FX	**37**	2	-3	-8	-39	13
FY	-1	**40**	4	-91	-26	365
FZ	31	-4	**1,195**	-700	-6,918	-137
MX	239	708	1,612	**119,600**	-2,367	2,022
MY	-1,280	-260	-13,486	15,978	**131,253**	-3,191
MZ	-68	351	-354	-294	990	**124,931**

Table 51: Matrix FSU03, mean stiffness with 500 N (60 min) preload and an intact disc

	TX	TY	TZ	RX	RY	RZ
FX	**37**	2	-3	0	-18	9
FY	-1	**40**	4	-78	-37	341
FZ	33	-4	**1,278**	-375	-7,532	-139
MX	-102	669	2,101	**152,472**	-1,317	2,908
MY	-1,337	-280	-13,876	12,915	**145,169**	-3,700
MZ	-64	321	-301	2,347	1,431	**122,627**

Table 52: Matrix FSU04, mean stiffness with 0 N preload and an In Motion disc

	TX	TY	TZ	RX	RY	RZ
FX	**22**	1	-10	13	123	0
FY	-1	**28**	-2	-180	7	-74
FZ	-3	-8	**405**	-765	-2,416	-179
MX	-122	503	487	**20,993**	902	-1,818
MY	-524	-104	-3,569	9,939	**54,004**	1,718
MZ	-7	-97	-59	2,267	318	**23,429**

Table 53: Matrix FSU05, mean stiffness with 500 N (30 min) preload and an In Motion disc

	TX	TY	TZ	RX	RY	RZ
FX	**32**	2	-17	19	74	10
FY	-1	**40**	4	-176	-3	-16
FZ	-8	-1	**1,062**	-1,969	-7,165	-174
MX	-159	662	564	**19,573**	2,104	-5,907
MY	-318	-276	-12,700	23,729	**117,174**	573
MZ	-37	515	-68	3,433	152	**41,900**

Table 54: Matrix FSU06, mean stiffness with 500 N (60 min) preload and an In Motion disc

	TX	TY	TZ	RX	RY	RZ
FX	**32**	2	-17	26	95	2
FY	-1	**41**	5	-183	-11	-35
FZ	-6	0	**1,109**	-2,053	-7,907	-164
MX	-181	652	519	**17,638**	3,252	-6,608
MY	-708	-289	-13,083	25,803	**114,325**	667
MZ	-27	514	-5	4,403	59	**43,358**

Generally the spread of data was less in the principal stiffness terms compared to the non-principal terms. Most stiffness terms that were expected to be negligible due to sagittal plane symmetry were found to be within the calculated zero error. Some stiffness terms were marginally above the zero error in only some testing conditions, and others were consistently above the zero error (Table 55).

Table 55: Non-zero stiffness terms that were expected to be negligible in FSU specimens

Stiffness	Condition	Preload
$K_{1,4}$	Intact	500 N (30 min)
$K_{1,4}$	In Motion Device	500 N (30 min and 60 min)
$K_{1,6}$	Intact	0 N
$K_{3,4}$	Intact	500 N (30 min and 60 min)
$K_{4,3}$	Intact	500 N (30 min and 60 min)
	In Motion Device	0 N, 500 N (30 min and 60 min)
$K_{4,5}$	Intact	500 N (30 min and 60 min)
	In Motion Device	0 N, 500 N (30 min and 60 min)

As explained previously in Chapter 8.2.3 (page 170), the zero error is a useful guide in predicting that a stiffness term is definitely not zero but is more limited in determining if a term is zero. The actual error is likely to be less than the calculated zero error. The results did show that many of the stiffnesses that were expected to be negligible were indeed very low, with stiffnesses based on forces less than ±10 N/mm or ±50 N/rad (<1 N/deg), and stiffnesses based on moments less than ±100 Nmm/mm or ±5000 Nmm/rad (<0.1 Nm/deg).

Table 56: Matrix ISD01, mean stiffness with 0 N preload and an intact disc

	TX	TY	TZ	RX	RY	RZ
FX	**29**	1	3	1	-8	26
FY	-1	**28**	1	20	7	326
FZ	15	-5	**392**	-699	-58	-110
MX	-109	700	640	**20,704**	-39	6,306
MY	-634	-180	-364	1,246	**11,682**	-2,509
MZ	-46	291	-139	-1,048	812	**39,619**

Table 57: Matrix ISD02, mean stiffness with 500 N (30 min) preload and an intact disc

	TX	TY	TZ	RX	RY	RZ
FX	**33**	2	-6	23	2	44
FY	-1	**38**	9	15	4	374
FZ	17	6	**1,245**	-1,741	-882	-202
MX	-78	856	2,314	**65,000**	-969	8,651
MY	-989	-213	-1,304	1,584	**27,982**	-3,466
MZ	-46	396	-147	-3,298	644	**48,220**

Table 58: Matrix ISD03, mean stiffness with 500 N (60 min) preload and an intact disc

	TX	TY	TZ	RX	RY	RZ
FX	**32**	1	-6	26	-37	37
FY	-1	**37**	10	34	3	366
FZ	28	7	**1,323**	-1,532	-924	-211
MX	-65	825	2,497	**95,604**	429	9,103
MY	-971	-197	-1,423	2,369	**39,941**	-3,187
MZ	-52	395	395	-2,840	324	**46,438**

Table 59: Matrix ISD04, mean stiffness with 0 N preload and an In Motion disc

	TX	TY	TZ	RX	RY	RZ
FX	**8**	0	0	-6	-22	-2
FY	0	**4**	3	4	9	-3
FZ	6	3	**283**	-601	585	7
MX	-5	74	543	**-692**	1,344	-155
MY	-71	-28	307	-824	**1,419**	8
MZ	-14	-2	22	-14	36	**59**

Table 60: Matrix ISD05, mean stiffness with 500 N (30 min) preload and an In Motion disc

	TX	TY	TZ	RX	RY	RZ
FX	**25**	2	-5	14	-129	3
FY	-1	**40**	10	112	24	-1
FZ	18	7	**1,135**	-2,200	2,504	19
MX	-51	946	2,035	**-184**	5,373	265
MY	-619	-204	1,909	-5,846	**12,404**	-581
MZ	-53	-23	47	-302	302	**969**

Table 61: Matrix ISD06, mean stiffness with 500 N (60 min) preload and an In Motion disc

	TX	TY	TZ	RX	RY	RZ
FX	**25**	2	-5	17	-150	2
FY	-1	**38**	11	111	24	-7
FZ	27	8	**1,195**	-2,238	2,628	45
MX	-42	873	2,140	**-397**	5,508	150
MY	-636	-192	2,364	-4,756	**13,380**	-692
MZ	-54	-22	52	-329	308	**1,078**

The tests performed on the ISD specimens resulted in only two stiffness terms that were expected to be negligible due to sagittal plane symmetry being non-zero, $k_{3,4}$, and $k_{4,3}$. However, these were found to be non-zero in all test cases, with the exception of $k_{3,4}$ with an intact disc and 0 N preload.

A large number of stiffnesses were below the zero error with the In Motion device and an ISD specimen, even in those terms that would be expected to be non-zero. With a preload of 0 N, only 4 stiffness terms were greater than the zero error. These were the stiffnesses of anterior load due to anterior shear ($k_{1,1}$), and axial load due to axial translation ($k_{3,3}$), lateral bending ($k_{4,3}$), and flexion/extension ($k_{5,3}$). With a 500 N preload 12 terms were greater than the calculated zero error. Such an outcome was expected due to the low-friction double ball/socket design of the In Motion device. Using the intact disc, there were 13 terms greater than the zero error with a 0 N preload, and 17 terms greater than the zero error with a 500 N preload (30 minutes).

Stiffnesses that may be regarded as negligible were considered for both the FSU and ISD specimens (Tables 62 and 63 respectively). Mean stiffnesses that were consistently equal to or lower than ±10 N/mm, ±50 N/rad (<1 N/deg), ±100 Nmm/mm, and ±5000 Nmm/rad (<0.1 Nm/deg) with preloads of 0 N and 500 N (30 and 60 minutes) were considered negligible. In most cases these values represent stiffnesses inside the zero error margin, which may exceed the actually error, as previously described in Chapter 8.2.3 (page 170).

Table 62: Negligible stiffness terms for intact FSU specimens shown on white

	TX	TY	TZ	RX	RY	RZ
FX	$K_{1,1}$	$K_{2,1}$	$K_{3,1}$	$K_{4,1}$	$K_{5,1}$	$K_{6,1}$
FY	$K_{1.2}$	$K_{2,2}$	$K_{3,2}$	$K_{4,2}$	$K_{5,2}$	$K_{6,2}$
FZ	$K_{1,3}$	$K_{2,3}$	$K_{3,3}$	$K_{4,3}$	$K_{5,3}$	$K_{6,3}$
MX	$K_{1,4}$	$K_{2,4}$	$K_{3,4}$	$K_{4,4}$	$K_{5,4}$	$K_{6,4}$
MY	$K_{1,5}$	$K_{2,5}$	$K_{3,5}$	$K_{4,5}$	$K_{5,5}$	$K_{6,5}$
MZ	$K_{1,6}$	$K_{2,6}$	$K_{3,6}$	$K_{4,6}$	$K_{5,6}$	$K_{6,6}$

Table 63: Negligible stiffness terms for intact ISD specimens shown on white

	TX	TY	TZ	RX	RY	RZ
FX	$K_{1,1}$	$K_{2,1}$	$K_{3,1}$	$K_{4,1}$	$K_{5,1}$	$K_{6,1}$
FY	$K_{1.2}$	$K_{2,2}$	$K_{3,2}$	$K_{4,2}$	$K_{5,2}$	$K_{6,2}$
FZ	$K_{1,3}$	$K_{2,3}$	$K_{3,3}$	$K_{4,3}$	$K_{5,3}$	$K_{6,3}$
MX	$K_{1,4}$	$K_{2,4}$	$K_{3,4}$	$K_{4,4}$	$K_{5,4}$	$K_{6,4}$
MY	$K_{1,5}$	$K_{2,5}$	$K_{3,5}$	$K_{4,5}$	$K_{5,5}$	$K_{6,5}$
MZ	$K_{1,6}$	$K_{2,6}$	$K_{3,6}$	$K_{4,6}$	$K_{5,6}$	$K_{6,6}$

The data for each stiffness term was checked for normality using the Shapiro-Wilke test, and it was found that 27 out of the total of 432 stiffness terms were not normally distributed ($p<0.05$) (Table 64).

Table 64: Non-Normally distributed stiffness terms

Specimen	Condition	Preload	Stiffness	P value
FSU	Intact	0 N	$K_{1,4}$	0.002
FSU	Intact	0 N	$K_{2,2}$	0.011
FSU	Intact	0 N	$K_{2,4}$	0.020
FSU	Intact	0 N	$K_{6,3}$	0.046
FSU	Intact	500 N (30 min)	$K_{1,4}$	0.000
FSU	Intact	500 N (30 min)	$K_{2,5}$	0.017
FSU	Intact	500 N (30 min)	$K_{6,5}$	0.007
FSU	Intact	500 N (60 min)	$K_{6,5}$	0.012
FSU	In Motion Device	500 N (30 min)	$K_{4,4}$	0.011
FSU	In Motion Device	500 N (60 min)	$K_{4,4}$	0.004
ISD	Intact	0 N	$K_{1,5}$	0.008
ISD	Intact	0 N	$K_{2,6}$	0.022
ISD	Intact	0 N	$K_{5,6}$	0.006
ISD	Intact	500 N (30 min)	$K_{2,2}$	0.015
ISD	Intact	500 N (30 min)	$K_{2,4}$	0.008
ISD	Intact	500 N (30 min)	$K_{2,5}$	0.009
ISD	Intact	500 N (30 min)	$K_{3,4}$	0.012
ISD	Intact	500 N (30 min)	$K_{5,4}$	0.037
ISD	Intact	500 N (60 min)	$K_{2,4}$	0.004
ISD	Intact	500 N (60 min)	$K_{5,5}$	0.037
ISD	Intact	500 N (60 min)	$K_{6,4}$	0.047
ISD	In Motion Device	0 N	$K_{1,2}$	0.005
ISD	In Motion Device	0 N	$K_{2,2}$	0.024
ISD	In Motion Device	0 N	$K_{2,4}$	0.012
ISD	In Motion Device	0 N	$K_{6,3}$	0.017
ISD	In Motion Device	0 N	$K_{6,4}$	0.041
ISD	In Motion Device	500 N (60 min)	$K_{6,3}$	0.006

The majority of stiffnesses were normality distributed, and statistical comparisons were made using ANOVA or independent t-tests (Table 65). ANOVA was used for multi-group comparisons as this test is robust even when data is not normally distributed [265]. The Games-Howell post-hoc test was used as equal-variance between groups could not be assumed.

Independent t-tests were used for comparisons of two groups of data, which are suitable for normally distributed data, but have also been shown to be robust for non-normally distributed data [266]. The Levene statistic was used to check for equal-variance, which allowed the significance to be based on equal-variance assumed or not assumed for each comparison made.

The effect of isolating the disc of the specimens was assessed using independent t-tests of the FSU and the ISD specimens with intact intervertebral discs for preloads of 0 N, 500 N (30 minutes), and 500 N (60 minutes) (Table 66).

Table 65: Statistical comparisons of stiffness results

Comparison	Group 1	Group2	Group 3	Test
Specimen type – 0 N	FSU	ISD		T-test
Specimen type – 500 N (30)	FSU	ISD		T-test
Specimen type – 500 N (60)	FSU	ISD		T-test
Preload – FSU – intact discs	0 N	500 N (30)	500 N (60)	ANOVA
Preload – FSU – In Motion discs	0 N	500 N (30)	500 N (60)	ANOVA
Preload – ISD – intact discs	0 N	500 N (30)	500 N (60)	ANOVA
Preload – ISD – In Motion discs	0 N	500 N (30)	500 N (60)	ANOVA
Condition – FSU specimens	Intact	In Motion		T-test
Condition – ISD specimens	Intact	In Motion		T-test

Table 66: Comparison of the stiffness of FSU specimens and ISD specimens with an intact disc. Black denotes a significant difference ($p<0.05$)

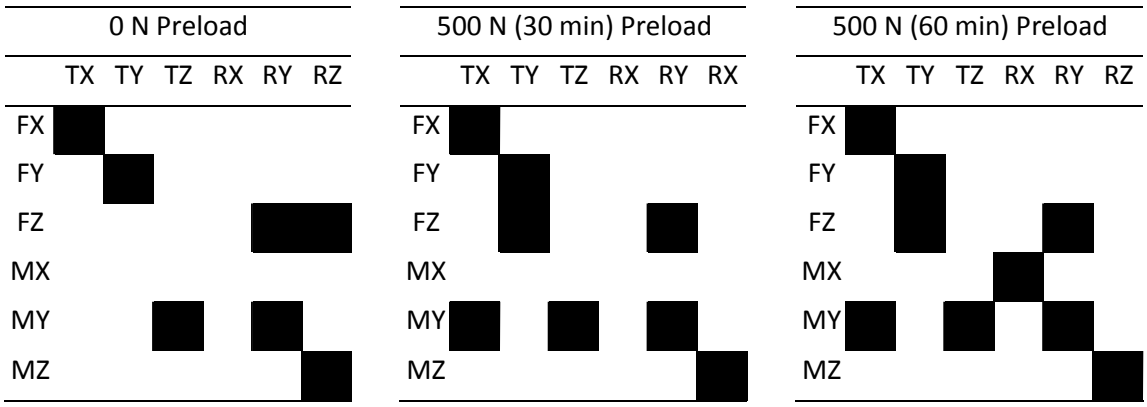

The facets and ligaments provide stability in all six degrees of freedom, as well as limiting the range of motion. Isolating the disc significantly reduced some stiffness terms, including all of the principal stiffnesses with the exception of the axial compression stiffness term $k_{3,3}$, and lateral bending stiffness, $k_{4,4}$, with a 0 N preload and 500 N (30 min) preload.

The effect of preload was investigated by carrying out ANOVA to compare a preload of 0 N, 500 N (30 minutes), and 500 N (60 minutes). This was completed for intact discs and specimens with In Motion disc replacements, in both the FSU and the ISD specimens (Tables 67-70).

Table 67: Comparison of stiffness due to preload for FSU specimens with intact discs. Black denotes a significant difference ($p<0.05$)

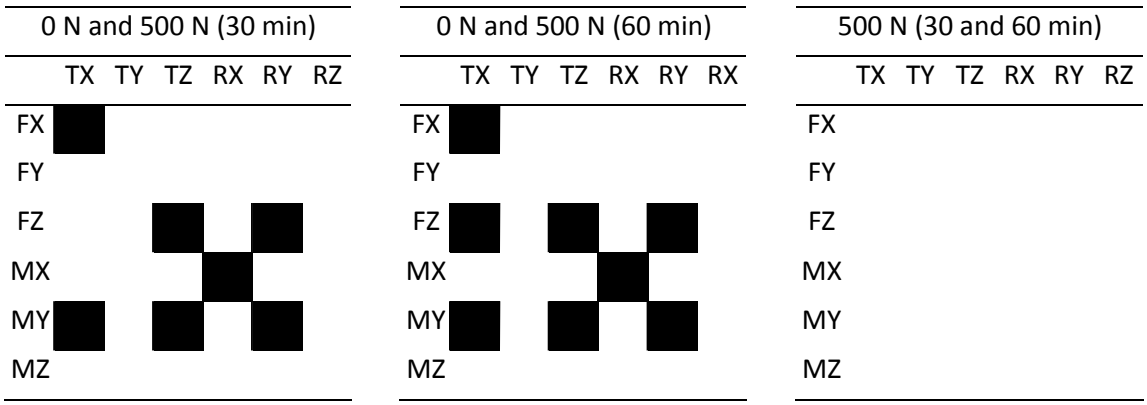

Table 68: Comparison of stiffness due to preload for FSU specimens with In Motion discs. Black denotes a significant difference ($p<0.05$)

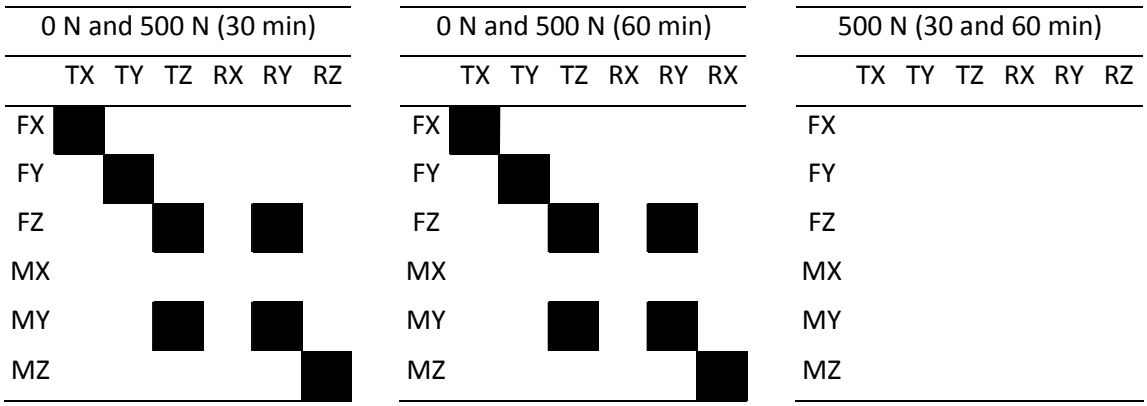

Table 69: Comparison of stiffness due to preload for ISD specimens with intact discs. Black denotes a significant difference ($p<0.05$)

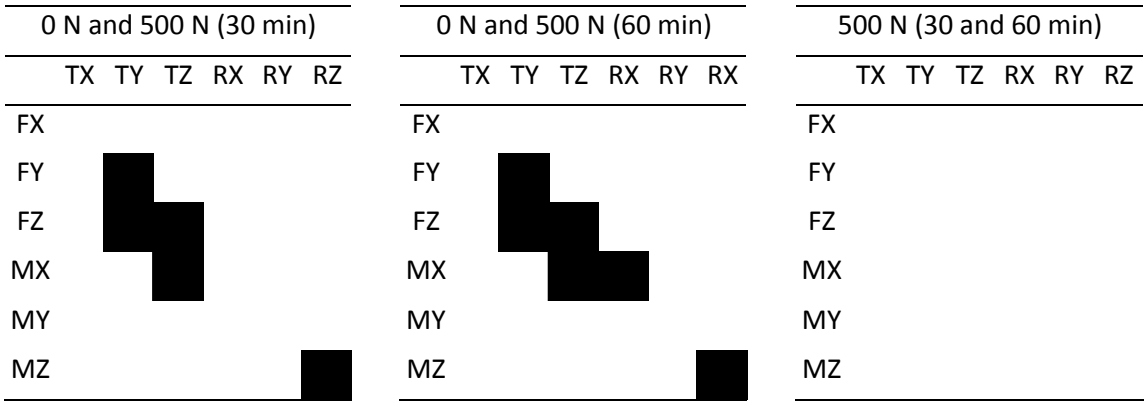

Table 70: Comparison of stiffness due to preload for ISD specimens with In Motion discs. Black denotes a significant difference ($p<0.05$)

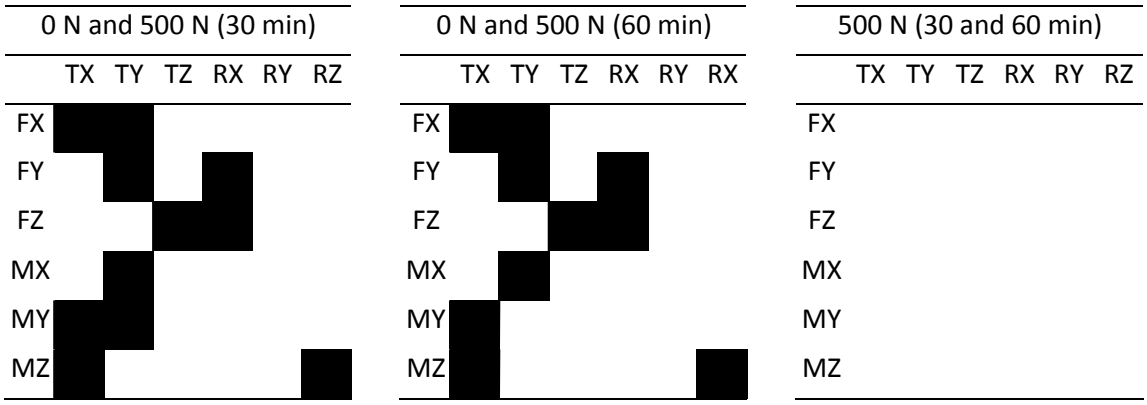

There was a significant difference in some stiffness terms when comparing a preload of 0 N and 500 N. Such stiffnesses were often the principal stiffnesses, though $k_{1,5}$ and $k_{3,5}$ were also significantly different with a 500 N preload when compared to a preload of 0 N in some

cases. The stiffness $k_{1,5}$ is the flexion/extension moment due to anterior/posterior shear, and $k_{3,5}$ is the flexion/extension moment due to axial compression/extension. Many non-principal stiffness terms were low in magnitude or demonstrated large variability between specimens, thus resulting in no significant difference between preloads.

There was no significant difference in any stiffness term between the preload of 500 N after 30 minutes and 60 minutes. This was the case for both functional spinal units and isolated discs, and for intact and In Motion discs.

When comparing preloads of 0 N and 500 N (30 minutes), the same stiffness terms were significantly different as with the comparison of 0 N and a 500 (60 minutes) in all but two cases. These instances occurred in stiffness $k_{4,4}$ in the ISD specimens with intact discs, and in stiffness $k_{2,5}$ in the ISD specimens with the In Motion device. This would emphasize there was little measureable difference in stiffness due to an increased stabilisation time of the 500 N preload from 30 to 60 minutes.

In addition to analysing the effect of preload on the stiffness of the various specimens, independent t-tests were used to compare the intact disc with the In Motion device. This was completed at all preloads, and with both the FSU and the ISD specimens (Tables 71 and 72).

Table 71: Comparison of stiffness with an intact disc and the In Motion disc for FSU specimens. Black denotes a significant difference ($p<0.05$)

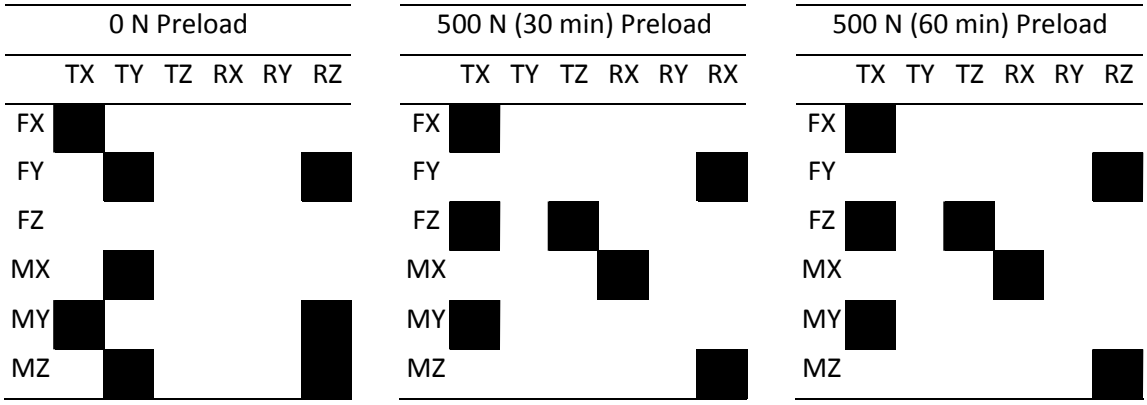

Table 72: Comparison of stiffness with an intact disc and the In Motion disc for ISD specimens. Black denotes a significant difference ($p<0.05$)

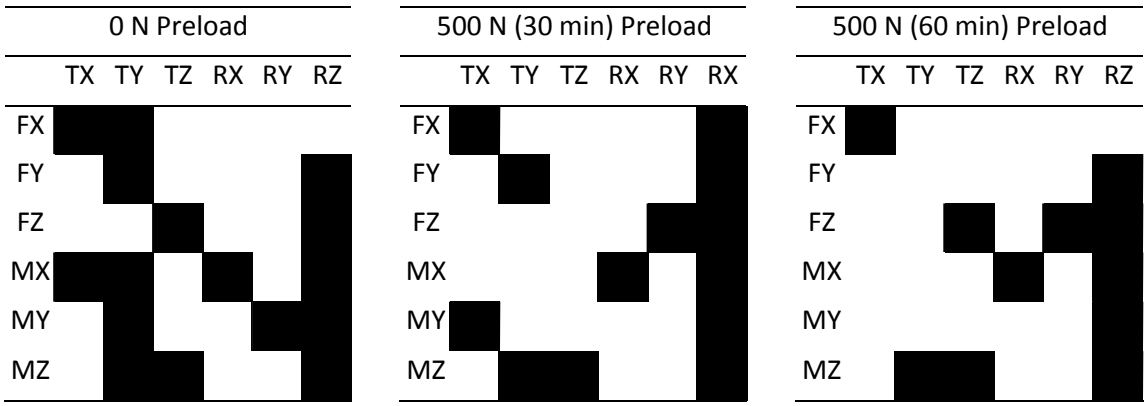

More stiffness terms were significantly different in the isolated disc specimens. This is likely due to a shielding effect of the facets and ligaments of the transverse and spinous processes in the functional spinal unit specimens. However, $k_{6,6}$, the axial rotation stiffness, was significantly lower in all comparisons, as was the anterior/posterior shear stiffness ($k_{1,1}$), and the lateral shear force due to axial rotation ($k_{6,2}$). The lateral bending stiffness ($k_{4,4}$) was found to be significantly lower with the In Motion device in all cases, with the exception of FSU specimens and a 0 N preload. All six principal stiffnesses were significantly lower with the In Motion device in ISD specimens and a preload of 0 N.

There was little effect due to the increased equilibration time. There was no change in significantly different stiffnesses in the FSU specimens, and only three in the ISD specimens. The flexion/extension stiffness was found to be significantly lower with the In Motion discs in the ISD specimens with a 0 N preload, yet was not significantly different with a 500 N preload. It was expected that the low-friction design of the In Motion device would lead to significant differences with the intact disc in both lateral bending and flexion/extension with and without axial preloads. It is thought that the reason for this is due to the transformation of moments, which created a large spread of data between specimens, particularly when preloads were applied. This is discussed further in Chapter 9.4.

9.3.2 Linearity of Stiffness Terms

The R^2 value of each stiffness term was calculated to assess the linearity. The results with intact discs were similar to those found in the previous tests, the principal shear stiffnesses ($k_{1,1}$ and $k_{2,2}$ respectively) and axial compression ($k_{3,3}$) with the intact disc in both the FSU and ISD specimens were highly linear (Figures 108-110), as was the stiffness in axial rotation ($k_{6,6}$) (Figure 113). The principal rotational stiffnesses in lateral bending and flexion/extension ($k_{4,4}$ and $k_{5,5}$ respectively) behaved less linearly but still offered a reasonable argument for the adoption of the linear least squares method (Figures 111 and 112).

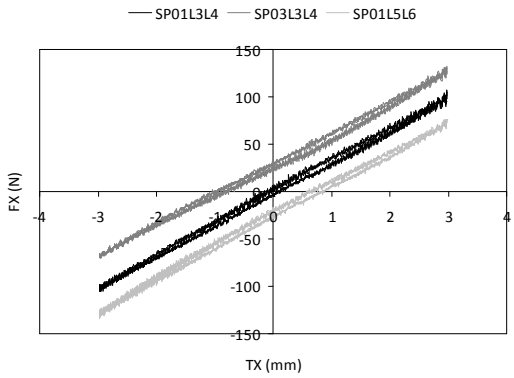

Figure 108: The linear behaviour of $k_{1,1}$ for three ISD specimens with intact discs, and a 500 N (30 minutes) preload

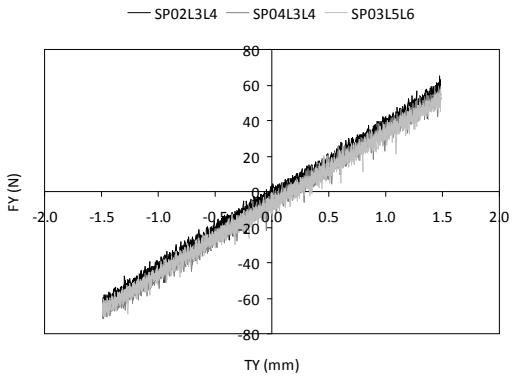

Figure 109: The linear behaviour of $k_{2,2}$ for three FSU specimens with intact discs, and a 500 N (30 minutes) preload

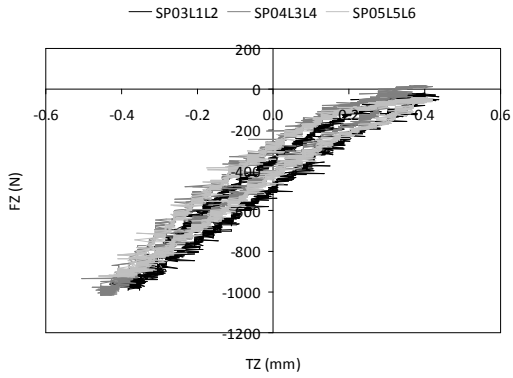

Figure 110: The linear behaviour of $k_{3,3}$ for three FSU specimens with intact discs, and a 500 N (30 minutes) preload

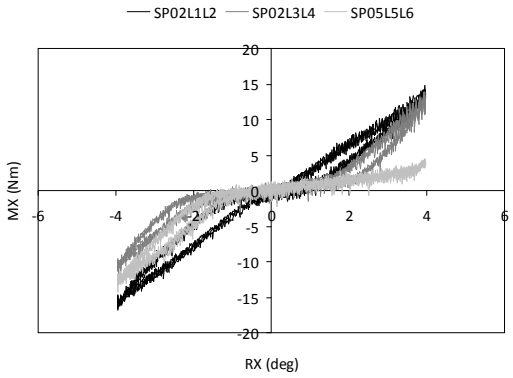

Figure 111: The non-linear behaviour of $k_{4,4}$ for three FSU specimens with intact discs, and a 500 N (30 minutes) preload

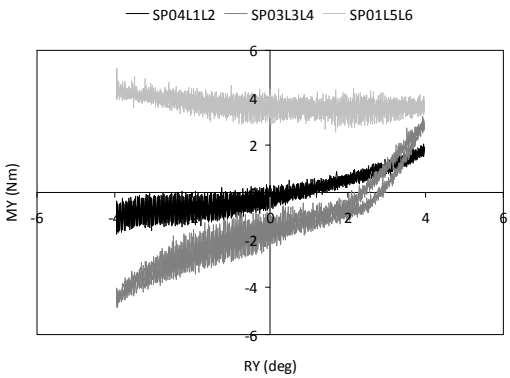

Figure 112: The variable behaviour of $k_{5,5}$ for three ISD specimens with intact discs, and a 500 N (30 minutes) preload

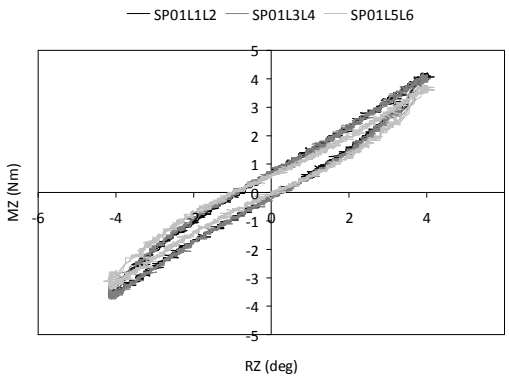

Figure 113: The fairly linear behaviour of $k_{6,6}$ for three ISD specimens with intact discs, and a 500 N (30 minutes) preload

The non-principal stiffnesses were often more varied in both the stiffness characteristics, and the inter-specimen behaviour. However, some non-principal terms exhibited repeatable characteristics and non-negligible stiffnesses (Figures 114 and 115). Some of the terms did appear linear but due to the low magnitude of forces or moments of some terms there was a relatively large amount of noise, which greatly reduced the R^2 value. Some of these terms were considered to have negligible stiffness and inspection suggested that the linear method was suitable in classifying these stiffness terms as such (Figures 116 and 117).

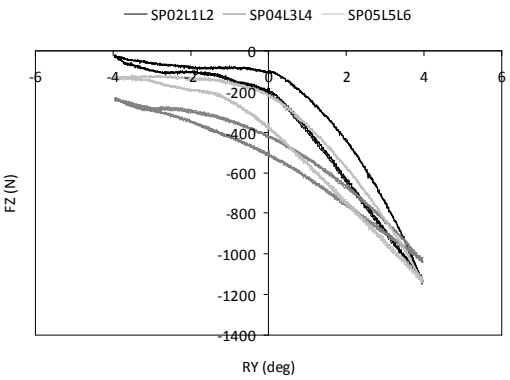

Figure 114: Non-Negligible and consistent characteristics of $K_{5,3}$ for three intact FSU specimens with a 500 N (30 minutes) preload

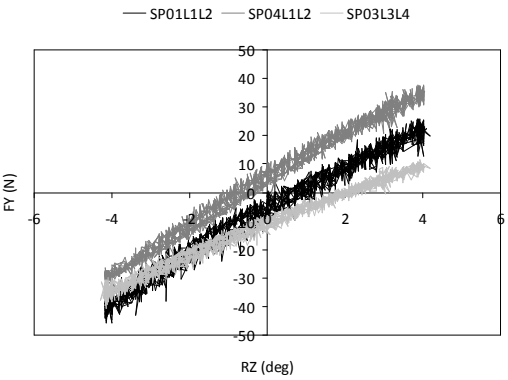

Figure 115: Non-Negligible and consistent characteristics of $K_{6,2}$ for three intact ISD specimens with a 500 N (30 minutes) preload

The relatively large amount of noise in Figure 116 is due to the forces being very low but observation shows that using the linear method would be suitable as a method of calculating the stiffness and using the result to consider the stiffness negligible. Figure 117 shows the

moments in the X axis due to rotation in the Y axes. These moments are due to asymmetry of the specimens and any misalignment of the specimens in the spine simulator. Though these terms are individually non-negligible, as was expected, the stiffnesses cancelled out over the six specimens tested resulting in the mean stiffness $K_{5,4}$ being within the zero error range. Using the linear method in this case also proved to be acceptable, given the large variety of stiffness characteristics observed.

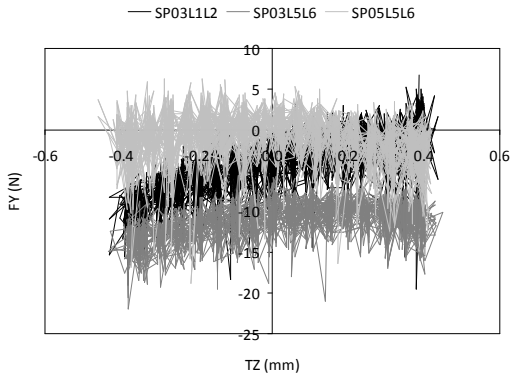

Figure 116: The large noise associated with negligible stiffness $K_{3,2}$ for three intact FSU specimens with a 500 N (30 minutes) preload

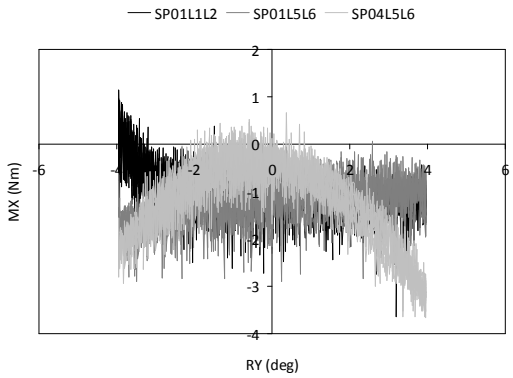

Figure 117: The variable characteristics of negligible stiffness $K_{5,4}$ for three intact ISD specimens with a 500 N (30 minutes) preload

The R^2 value of each of the 36 stiffness terms in each matrix was calculated. The R^2 values compared reasonably with data published on functional spinal unit and isolated disc porcine specimens by Gardner-Morse and Stokes [220]. The study by Gardner-Morse and Stokes found that the linearity increased with the application of an axial preload. However, their study only used small range of motion, focusing on the stiffness around the neutral posture. The present study suggests that the same is true over larger range of motion.

Some stiffness plots demonstrated reasonable linearity but with different stiffnesses in the positive and negative phase (Figure 114). It is possible that in some cases more accurate stiffness values could be obtained by measuring the stiffness separately in the positive and negative phases, for example flexion and extension. The current study has shown the linear least squares method over the entire range of motion of three cycles to be an appropriate method of stiffness calculation in the majority of the stiffness terms.

Statistical analysis was undertaken to assess the effect of preload on linearity. Shapiro-Wilke normality tests showed that there were 91 terms that were not normally distributed out of

the total of 432 terms ($p<0.05$). A multi-group comparison was made using ANOVA with a Games-Howell post-hoc test for FSU and ISD specimen types, with intact discs and In Motion discs. Comparisons were made between preloads of 0 N, 500 N (30 minutes), and 500 N (60 minutes) (Tables 73-76).

Table 73: Comparison of linearity due to preload for FSU specimens with intact discs. Black denotes a significant difference ($p<0.05$)

0 N and 500 N (30 min)						
	TX	TY	TZ	RX	RY	RZ
FX						
FY						
FZ			■			
MX				■		
MY			■			
MZ						

0 N and 500 N (60 min)						
	TX	TY	TZ	RX	RY	RX
FX	■					
FY						
FZ			■			
MX			■	■		
MY			■			
MZ						

500 N (30 and 60 min)						
	TX	TY	TZ	RX	RY	RZ
FX						
FY						
FZ						
MX						
MY						
MZ						

Table 74: Comparison of linearity due to preload for FSU specimens with In Motion discs. Black denotes a significant difference ($p<0.05$)

0 N and 500 N (30 min)						
	TX	TY	TZ	RX	RY	RZ
FX						
FY						
FZ			■		■	
MX				■	■	
MY			■		■	
MZ						

0 N and 500 N (60 min)						
	TX	TY	TZ	RX	RY	RX
FX						
FY		■				
FZ			■		■	
MX				■	■	
MY		■	■		■	
MZ						

500 N (30 and 60 min)						
	TX	TY	TZ	RX	RY	RZ
FX						
FY						
FZ						
MX						
MY						
MZ						

Table 75: Comparison of linearity due to preload for ISD specimens with intact discs. Black denotes a significant difference ($p<0.05$)

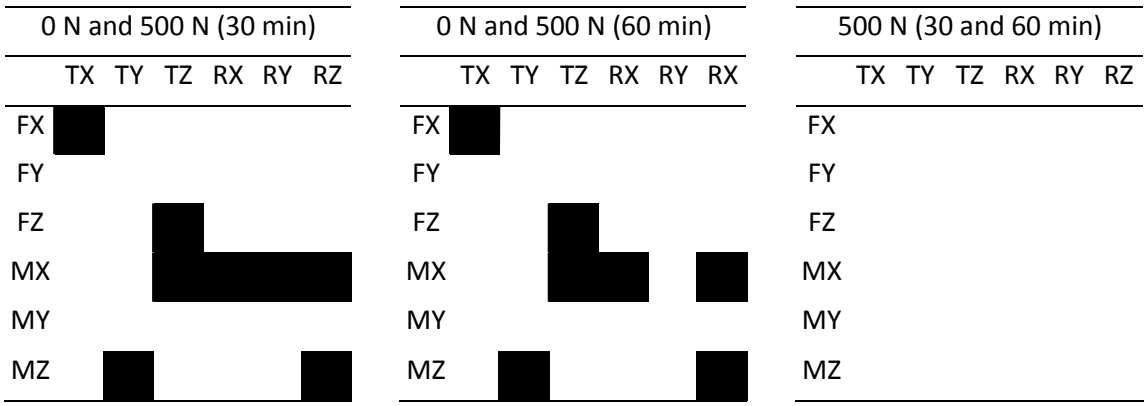

Table 76: Comparison of linearity due to preload for ISD specimens with In Motion discs. Black denotes a significant difference ($p<0.05$)

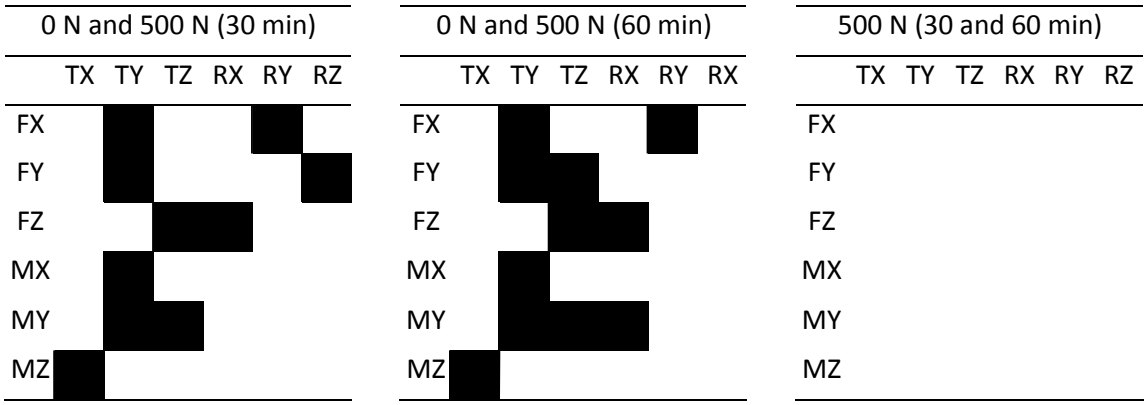

There is no significant difference in the R^2 values of the stiffness data of the tests that were completed with a preload of 500 N after 30 minutes compared to those completed with the same preload after 60 minutes. This is true of all stiffness terms for both FSU and ISD specimens with both intact discs and In Motion discs.

Significant differences in the R^2 values due to preload were due to an increase in the R^2 value when a preload was applied in all but one case. The R^2 values of lateral bending stiffness in FSU specimens with the In Motion disc were significantly lower with an axial preload of 500 N compared to 0 N preload. This may have been due to a lower measured moment in the six-axis load cell with the In Motion device compared to the intact disc but a similar shear force measurement. This would result in an increase in noise in the transformed moment measurement, and a reduction in the R^2 value.

The results show approximately the same differences due to preload than those published by Gardner-Morse and Stokes [221]. The previously published tests were conducted in the region of the neutral zone only. Some of the differences measured as significant by Gardner-Morse and Stokes that were not found to be significant in the present study was due to the measured linearity with a preload of 0 N being higher than that previously published, and the linearity with a preload of 500 N being similar to that previously published by Gardner-Morse and Stokes who applied a preload of 400 N. Therefore, even though the linearity was similar to the previously published data, the difference in this study was not found to be significant. This was the case for $K_{2,2}$ for which the R^2 value in ISD specimens increased from 0.961 with a preload of 0 N to a value of 0.996 with preloads of 500 N (30 minutes and 60 minutes). This was not found to be significant, whereas in the study by Gardner Morse and Stokes [220] the increase from 0.82 to 0.96 with the introduction of a 400 N preload was significantly different.

Comparing the linearity of the non-principal stiffnesses is problematic due to Gardner-Morse and Stokes having assumed symmetry and averaged diagonal terms. The present study found the linearity of diagonal terms to be quite varied. For example, for FSU specimens with a preload of 500 N (30 minutes) the mean R^2 value of stiffnesses $K_{1,5}$ and $K_{5,1}$ was 0.944 (s.d. 0.025) and 0.546 (s.d. 0.281) respectively. Averaging these values would not present the true nature of the stiffness matrices, which in addition to having non-symmetric stiffnesses, also demonstrate non-symmetric stiffness characteristics and linearity.

9.3.3 Axial Displacement during Testing

For the stiffness matrix tests, only one axis is moved at a time, with all others fixed. This includes the axial translation axis, TZ, through which the axial preload is applied. Between tests, the TZ axis was moved to correct the axial preload to the desired magnitude prior to commencing another test. The preload of 0 N generally required no axial adjustment but the preloads of 500 N, both after 30 and 60 minutes, did. The total axial displacement change due to the preload was recorded for each test. The majority of axial displacement occurred during the first 30 minutes of the application of the 500 N preload in all groups (a range of 58-87% of the total displacement), minor adjustments were made thereafter (Table 77). The data was found to be normally distributed for all four groups of data. ANOVA was completed with a Games-Howell post-hoc test to compare the total axial displacement due to the 500 N

preload. It was found that there was no difference between the two intact disc groups, or between the two In Motion disc groups, but there was a difference between the intact disc groups and the In Motion disc groups (Table 78).

Table 77: The Mean axial displacement due to the 500 N preload

	Mean Axial Displacement (mm)					
Specimen	0-30 min	Test 1	T1-60 min	Test2	Total	S.D.
FSU Intact	-1.67	-0.41	-0.28	-0.16	-2.51	0.37
FSU Device	-1.04	-0.28	-0.09	-0.08	-1.49	0.31
ISD Intact	-1.74	-0.24	-0.29	-0.11	-2.38	0.30
ISD Device	-0.95	-0.14	-0.03	-0.04	-1.16	0.20

Table 78: ANOVA comparing the axial displacement between specimen groups, black denoting a significant difference.

	FSU Intact	FSU Device	Isolated Intact	Isolated Device
FSU Intact		0.002	0.895	0.000
FSU Device	0.002		0.002	0.196
Isolated Intact	0.895	0.000		0.000
Isolated Device	0.000	0.196	0.000	

Such a result in the axial displacement was expected given the structure of the natural intervertebral disc compared to the In Motion disc. Over the time that the 500 N preload was applied, fluid would escape from the nucleus pulposus of the natural disc. Loads of over 1000 N in axial compression were common during testing and as a consequence the axial displacement would need adjusting to achieve a preload of 500 N for the subsequent test. The In Motion disc was not susceptible to fluid loss as it is a metal on polymer articulating assembly. The initial adjustment in axial displacement with the In Motion device may have been due to subsidence of the metal endplates into the vertebral bodies.

9.4 Discussion of Porcine Test Results

The stiffness matrix tests using both functional spinal units (FSU01-FSU06) and isolated discs (ISD01-06) showed considerable variation between specimens in many stiffness values. However, this is likely to reflect the in-vivo situation with a large range in the patient profile. The same total disc replacement device is used in this range of patients, and over a range of vertebral levels, which differ in stiffness.

Previous testing by Stokes and Gardner-Morse et al. [220, 221, 240, 241] used an equilibration time of 3 hours between applying a 500 N preload and completing a stiffness matrix test. This methodology was followed in the validation testing, albeit with a plastic wrapped, rather than saline submerged, specimen. The equilibration time of 3 hours would result in prohibitively long testing times because it would need to be applied twice; once with the intact disc and again after the disc replacement device had been implanted. Such extensive equilibration times would be likely to affect the mechanical properties of the specimen. This, combined with the preparation and testing time, meant that there was a danger of the specimens becoming degraded by the time the final tests were completed (Figure 118).

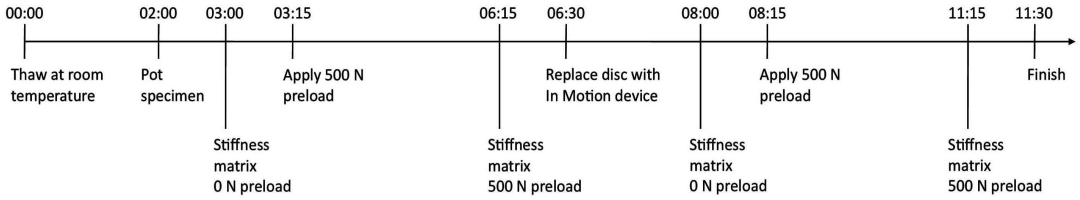

Figure 118: Estimated testing timeline if 3 hour equilibration of preload was used

In the previously described studies by Stokes and Gardner-Morse et al., a 3 hour equilibration time might have been necessary because the specimen was submerged in a 4°C saline bath during testing. It has been shown that the hydration level of specimens significantly affects the stiffness [267]. Pflaster et al. [260] demonstrated that a saline bath causes the intervertebral disc to swell by approximately 24 % after 7 hours, and even after the application of an axial preload of 445 N for 7 hours, the disc remained 10 % more hydrated than during specimen preparation. The same study showed that an unloaded specimen sprayed with saline and wrapped in plastic film showed little change in hydration

over a 3 hour period. Wilke et al. [261] found that the range of motion of air exposed and drip irrigated porcine or ovine specimens increased with the number of cycles completed to a greater extent than specimens wrapped and in saline moistened gauze and periodically sprayed with saline solution.

It is also possible that the low temperature of the saline bath used by Stokes and Gardner-Morse et al. would have significantly affected the mechanical properties of the specimens. In their studies, maintaining a low temperature was necessary because the quasistatic test method adopted required long testing times. In one study, the total testing time for a specimen was 76 hours [220]. In keeping the specimens at 4°C, it may be that the degradation of the tissue was avoided. However, Bass et al. [268] showed the material properties of the anterior longitudinal ligament in the porcine lumbar spine were temperature dependent. Tensile tests to 20 % strain at various load rates and at temperatures of 4.4, 12.8, 21.1, 29.4, and 37.8°C demonstrated an effect in both the viscoelasticity and the stiffness of the specimen. In particular, the stiffness increased over 100 % from the maximum temperature of 37.8°C to the lowest of 4.4°C. This difference was significant between all temperatures except 29.4 and 37.8°C.

It is generally the case that testing is completed at room temperature so as to reasonably reflect the in-vivo situation but without accelerating tissue degeneration with a temperature as high at 37° C [212]. Wilke et al. [212, 261] have recommended a maximum testing time of 20 hours at 20-30°C and demonstrated that the length of exposure time of a specimen is more critical than the moisture conditioning or deformation rate [261].

The work by Stokes and Gardner-Morse et al. were the only spinal studies found to have carried out tests at temperatures other than room temperature (20-30°C) or 37°C. It is possible that a temperature of 4°C would have caused the specimen to swell less in the saline bath than if it was at 20-30°C. However, no data was found in the literature to confirm this, and it was not a possibility that was mentioned by Stokes and Gardner-Morse et al. in any of the studies concerned.

The present study used specimens sprayed with 0.9 % saline and wrapped in food packaging plastic. This resulted in no significant difference between 30 or 60 minutes equilibration time after the application of a 500 N preload in any stiffness term, irrespective of specimen type

or condition. This is true in terms of the stiffness values, and the linearity of the stiffness data. This suggests that a preload equilibration period of 30 minutes is appropriate and a longer equilibration time is not necessary. However, this can only be said for the dynamic testing at room temperature on specimens sprayed with 0.9% saline and wrapped in food packaging plastic, and within a total thaw and test time of less than 7 hours (mean 6.28 hours).

The principal stiffnesses ($k_{1,1}$, $k_{2,2}$, $k_{3,3}$, $k_{4,4}$, $k_{5,5}$, $k_{6,6}$) should be regarded as the most important to consider when comparing the natural disc with a disc replacement device, as they relate to the direct opposition of a motion, rather than an associated force or moment. These stiffnesses terms tended to have the lowest data spread within groups and were more often significantly different as a result of changing the preload from 0 N to 500 N, or from an intact disc to the In Motion device. It is also more important to consider the results with the preload of 500 N, as this more closely resembles the in-vivo situation. Based on this, key non-principal stiffness terms were $k_{1,3}$, $k_{1,5}$, and $k_{6,2}$ in the functional spinal units and $k_{1,5}$, $k_{2,6}$, $k_{6,2}$, and $k_{6,4}$ in the isolated disc specimens (Table 79).

Table 79: Key non-principal stiffness terms

Stiffness Term	Description of force/moment and translation/rotation of the term
$K_{1,3}$	Axial compression/extension force due to anterior/posterior shear
$K_{1,5}$	Flexion/extension moment due to anterior/posterior shear
$k_{2,6}$	Axial moment due to lateral shear
$k_{6,2}$	Lateral shear force due to axial rotation
$k_{6,4}$	Lateral moment due to axial rotation

It was expected that the stiffnesses $k_{3,6}$, $k_{6,3}$, and $k_{6,5}$ would be negligible due to sagittal plane symmetry. Any asymmetry or misalignment of the specimens would be expected to cancel out over the sample size. It was therefore unexpected that in the isolated disc specimens there were significant differences between the intact disc and the In Motion device in these three stiffness terms.

The term $k_{3,6}$ was negative in all but one case with the intact disc, and positive in all but two cases with the In Motion disc (same specimen at with 500 N preload at 30 and 60 minutes). This change in direction of the moment produced under axial compression and extension

may be attributed to the elastomeric nature of the intact disc compared to the disc replacement, which is less stable due to the low-friction, ball and socket design. Though the reason why the stiffnesses did not cancel over the course of the study due to sagittal symmetry remains difficult to explain.

In comparing a prosthetic disc device to the intact disc it is important to consider clinical relevance in addition to the statistical analysis. If a term is significantly different, that does not necessarily mean that the prosthesis may not provide a suitable alternative. For this reason it was worthwhile to examine normalised data. The mean stiffness terms with the In Motion disc were expressed as a percentage of the mean stiffness terms with the intact disc.

The data with a 0 N and 500 N axial preload was used. As no significant difference was found between 30 and 60 minutes equilibrating time of the 500 N preload, only 30 minutes was used. Although the data with a 500 N preload more closely reflected the in-vivo situation, assessing the 0 N preload data would allow comparisons to be made with the normalised data of Cunningham et al. [217]. It is understood that the data reported by Cunningham et al. was normalised for each specimen, thus isolating the effect that instrumentation has on each specimen. This method can be used to minimise inter-specimen variability and potentially increase the statistical power of a study [212].

However, it was found during the analysis of data in this manner that if negative stiffnesses are present, normalising the data can be misleading. If a stiffness term is negative with the intact disc, and then decreases with the disc replacement to a negative stiffness of greater magnitude, the normalised data would suggest an increase in stiffness. In fact the stiffness would have decreased and the larger negative stiffness with the disc replacement would suggest an increase in instability.

For example, in flexion/extension with the isolated disc specimen and a 500 N (30 minutes) preload, the mean stiffness with the intact disc was 27,982 Nmm/rad but in one specimen the stiffness was negative. With the In Motion device, the mean stiffness was 12,404 Nmm/rad. In the specimen with stiffness of -4,400 Nmm/rad with the intact disc, the stiffness with the In Motion device was -12,834 Nmm/rad. If this is normalised it leads to the In Motion device having a stiffness of 292 % of the intact disc. This is clearly misleading as it suggests that the In Motion device dramatically increased the stiffness of the specimen,

which it did not. In all but one isolated disc specimen, the In Motion device reduced the stiffness of the specimen in flexion/extension compared to the intact disc, yet this is not reflected in the normalised data.

Therefore, rather than normalising the data of individual specimens and calculating the mean percentage change in stiffness due to the In Motion disc, the mean values of the stiffnesses were normalised. This allowed a comparison that could be more meaningfully interpreted.

Only stiffness terms that were significantly different to the intact disc were included in order to simplify the comparison. Both FSU specimens (Tables 80 and 81) and isolated disc specimens (Tables 82 and 83) were normalised, though the isolated disc matrix would provide the best comparison of how the prosthetic disc compared to the natural disc.

Table 80: Stiffness matrix of FSU specimens with an In Motion disc and 0 N preload, normalised to intact disc stiffness of 100 %

	TX	TY	TZ	RX	RY	RZ
FX	69 %					
FY		78 %				-20 %
FZ						
MX		66 %				
MY	51 %					-48 %
MZ		-46 %				22 %

Table 81: Stiffness matrix of FSU specimens with an In Motion disc and 500 N preload (30 minutes), normalised to intact disc stiffness of 100 %

	TX	TY	TZ	RX	RY	RZ
FX	86 %		665 %			
FY						-4 %
FZ	-25 %		89 %			
MX				16 %		
MY	25 %					
MZ						34 %

Table 82: Stiffness matrix of ISD specimens with an In Motion disc and 0 N preload, normalised to intact disc stiffness of 100 %

	TX	TY	TZ	RX	RY	RZ
FX	26 %	21 %				
FY		13 %				-1 %
FZ			72 %			-6 %
MX	5 %	11 %		**-3 %**		-2 %
MY		16 %			**12 %**	0 %
MZ		-1 %	-16 %			0 %

Table 83: Stiffness matrix of ISD specimens with an In Motion disc and 500 N preload (30 minutes), normalised to intact disc stiffness of 100 %

	TX	TY	TZ	RX	RY	RZ
FX	77 %					7 %
FY		104 %				0 %
FZ					-284 %	-9 %
MX				0 %		3 %
MY	63 %					17 %
MZ		-6 %	-32 %			2 %

It is important to consider the results in light of what the aim of the test methodology is; to assess the efficacy of disc prostheses. The preload of 0 N does not reflect the in-vivo situation for which the disc should have been designed. However, it may still be useful in assessing the suitability of a potential device. Under a 0 N preload, the loads due to misalignment are lower, and this may reduce potential inconsistencies relating to the transformation of moments MX and MY.

The study by Cunningham et al. [217] reported the normalised flexibility of multi-segment human lumbar specimens with intact discs and a Charité III disc implanted at one level, with data being normalised to the intact disc. Loads were applied as pure moments of ±8 Nm in the X, Y, and Z axes at a rate of 3°/sec and the motion of the vertebral levels measured using a non-contact method. The study reported the total range of motion at the operative level (L4-L5). The stiffness data measured using the spine simulator was inverted to allow an approximate comparison of the flexibility. The flexibility of the intact specimen and that with

the Charité disc implanted by Cunningham et al. were not significantly different in flexion/extension or lateral bending, but were significantly different in axial rotation; the mean axial rotation with the Charité disc was 144 % of the intact disc. The present study found that the mean flexibility of the In Motion disc implanted in FSU specimens with 0 N preload was 450 % of the intact disc.

Such a large disparity could be due to the difference between cadaveric and porcine specimens. From data published by Gardner-Morse and Stokes [220, 221] it can be observed that cadaveric FSU specimens are comparable to porcine FSU specimens in flexion/extension and lateral bending but stiffer in axial rotation. Further differences may be due to the insertion technique, as Cunningham et al. did not release the posterior longitudinal ligament (PLL). The operative technique for the In Motion device calls for the PLL to be released [263]. However, due to the small height of the porcine disc, combined with the necessity to fit the medium disc size in the correct position within the vertebral body of the small porcine disc space, the PLL was resected. The disc height has been shown to have more of an effect on the ROM than whether or not the PLL is resected [264]. However, the isolated disc stiffness results would have been affected by the entire resection of the PLL, though it is thought that the intact intervertebral disc would provide much more resistance to motion than the PLL.

The normalised data shows that with a 500 N preload, even though the stiffness terms were found to be significantly different, the In Motion device was comparable in shear stiffness to the intact isolated disc that it was designed to replace (77 % and 104 % in anterior/posterior and lateral shear stiffness respectively). This would suggest that the disc might reasonably replicate the shear and compressive characteristics of the natural disc. However, less emphasis should be put on shear motion compared to rotational motion, the principal movement that occurs in the natural disc in the form of flexion/extension, lateral bending, and axial rotation [258].

There were significant differences in axial compressive stiffness ($k_{3,3}$) between the intact disc and the In Motion device in tests of the FSU with 500 N preload, ISD with 0 N preload and 500 N preload (60 minutes). However, no significant difference was found with the FSU specimens with 0 N preload, and the ISD specimen with a 500 N (30 minutes) preload. In instances when there were significant differences, the In Motion device was similar in

stiffness to the intact disc (72-90 % of the intact disc), particularly when a preload of 500 N was applied.

Rotational stiffnesses, in contrast, were different with the In Motion disc, particularly with the ISD specimens. No significant difference in flexion/extension stiffness ($k_{5,5}$) was found with either 0 or 500 N preload using the FSU specimens (Figures 119 and 120), and no significant difference was found in the ISD specimens with a 500 N preload. The comparison of FSU and ISD specimens found the stiffness $k_{5,5}$ to be significantly different (p=0.000 with 0 N and 500 N preloads). This is because the facets and posterior ligaments contribute largely to the flexion/extension stiffness of a functional spinal unit.

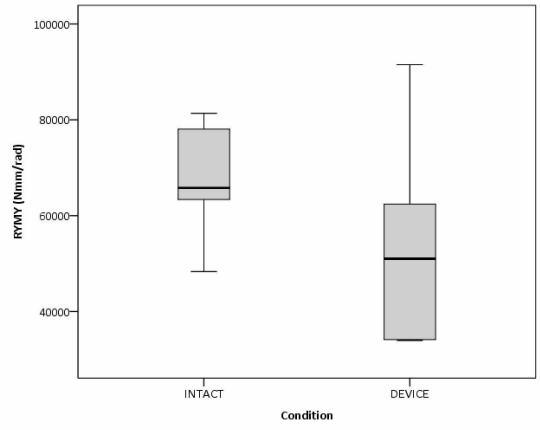

Figure 119: No significant difference of $k_{5,5}$ in FSU specimens with an intact disc and In Motion device, 0 N preload

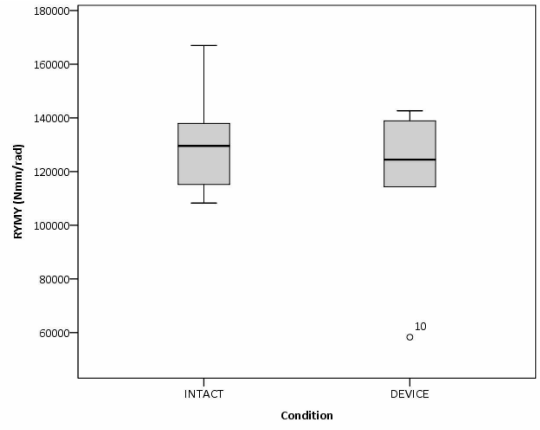

Figure 120: No significant difference of $k_{5,5}$ in FSU specimens with an intact disc and In Motion device, 500 N (30 min) preload

The principal stiffnesses due to lateral bending ($k_{4,4}$) and flexion/extension ($k_{5,5}$) of the ISD specimens with an In Motion disc were significantly lower than the intact disc with a preload of 0 N (Figures 121 and 122). Every ISD specimen with an In Motion device and 0 N preload exhibited a stiffness for both $k_{4,4}$ and $k_{5,5}$ that was within the zero error. This result is due to the low-friction design of the In Motion device, which offers very little resistance to motion when there is no preload present.

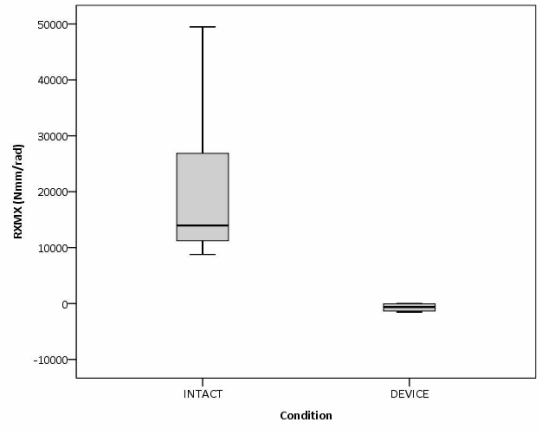

Figure 121: Significant difference of $k_{4,4}$ in ISD specimens with intact disc and In Motion device, 0 N preload

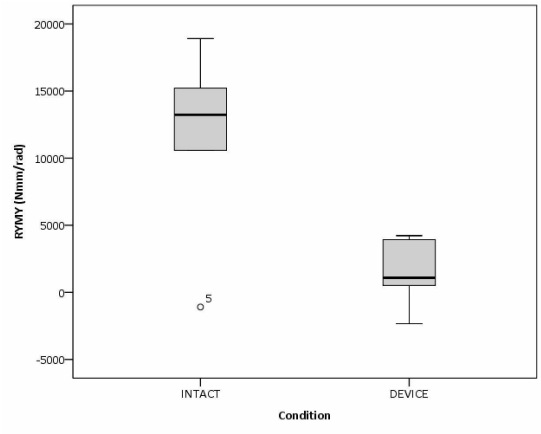

Figure 122: Significant difference of $k_{5,5}$ in ISD specimens with intact disc and In Motion device, 0 N preload

When an axial preload was applied to the ISD specimens, the lateral bending stiffness ($k_{4,4}$) remained significantly higher with the intact disc compared to the In Motion device (Figure 123), whilst the flexion/extension stiffness ($k_{5,5}$) did not (Figure 124).

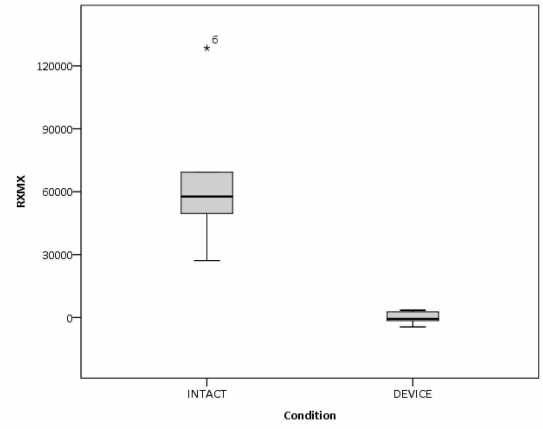

Figure 123: Significant difference of $k_{4,4}$ in ISD specimens with intact disc and In Motion device, 500 N (30 min) preload

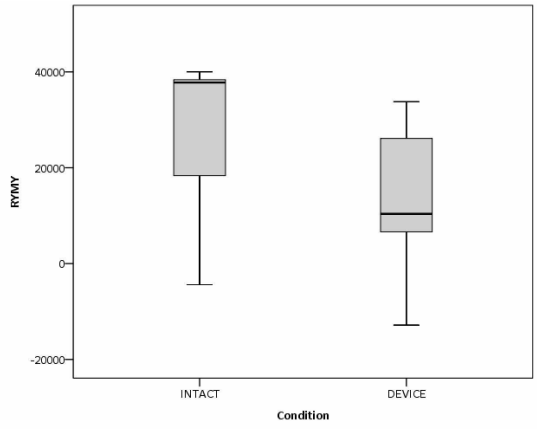

Figure 124: $k_{5,5}$ in ISD specimens, intact disc and In Motion device, 500 N preload

The stiffness $k_{5,5}$ demonstrated a large variability in magnitude, in both the intact disc, and the In Motion device. It is thought that this is due to the transformation of the moments from the six-axis load cell datum, to the centre of the superior vertebral body. As previously discussed, the transformation of the moment MY at the axis-axis loadcell requires the measured shear force FX to be multiplied by the distance from the six-axis load cell to the centre of the superior vertebral body. This means that the MY moment at the centre of the

superior vertebral body is a combination of two load signals. Such a situation can lead to increased noise on the signal, particularly when one, or both, of the loads are relatively low compared to the full-scale capacity of the load cell. When the specimens were tested in lateral bending and flexion/extension, the associated shear loads FX and FY were regularly below the zero error of ±127 N/rad (equivalent to 2.22 N/deg). This led to a relatively noisy signal, which was used to correct the appropriate moment. This could be improved with the use of a more accurate load cell, and the use of noise filters on the shear force signals.

Additionally, the shear forces varied in terms of being positive or negative between specimens, between disc condition (intact or In Motion device), and on occasion between tests on the same specimen at the same preload (the force was sometimes positive at a preload of 500 N after 30 minutes but negative after 60 minutes, or vice versa). These changes were more common in the ISD specimens, and this may be due to the structure being less stable without the facets and posterior ligaments. Although the shear forces measured were low in the ISD specimens, generally the minimum to maximum range was approximately 30 N, this is converted to a considerable moment for the transformation of the associated moment (30 N equates to almost 6 Nm). Often the measured moment range using both the on-axis load cell, and the six-axis loadcell for intact discs with a 500 N preload was in the region of 6 Nm. Clearly this would lead to large corrections due to the relatively small moments that were measured.

The lateral bending stiffness appeared to be less affected by the correction, and this is likely due to the larger moments combined with lower associated shear forces that were measured at the six-axis loadcell in the intact discs in lateral bending compared to flexion/extension. The variability of the shear forces may be due to the misalignment of the specimen, and it may be the case that this was less common in the coronal plane than in the sagittal plane, as it is easier to achieve medial-lateral alignment of the specimen, and of the In Motion device in the specimen.

It is noteworthy that, based on the mean stiffness values, the associated shear forces in lateral bending and flexion/extension ($k_{4,2}$ and $k_{5,1}$ respectively) were lower than 50 N/rad and therefore considered negligible in ISD specimens with intact discs for preloads of 0 N and 500 N. However, neither $k_{4,2}$ nor $k_{5,1}$ was below this value with the In Motion disc and preloads of 500 N. A similar result was observed in the FSU specimens, with $k_{5,1}$ considered

negligible in intact specimens with preloads of 0 and 500 N but non-negligible in specimens with In Motion devices at preloads of both 0 and 500 N. Such a phenomenon may be due to an alteration in the load transfer through the In Motion device compared to the intact disc. This may have led to an increased shear force, which affected the moment transformation as described above.

The on-axis load cell data and the uncorrected six-axis load cell data for flexion/extension stiffness in ISD specimens both demonstrate significant differences between the intact disc and the In Motion device with a 500 N (30 minutes) preload ($p=0.010$ and 0.005 respectively). However, the reduced difference in means of the corrected data (29055 and 11861 Nmm/rad for intact and In Motion discs respectively), combined with the large standard deviation (16565 and 16495 Nmm/rad for intact and In Motion discs respectively) led to no significant difference being measured ($p=0.117$). In flexion/extension stiffness after 60 minutes of 500 N preload application, the difference between the intact and In Motion disc approached significance ($p=0.054$).

The spread of flexion/extension stiffness data in the ISD specimens was increased further with one specimen exhibiting negative stiffness with both the intact disc and the In Motion device at preloads of 0 N and 500 N, and one specimen with the In Motion device produced a high stiffness due to core impingement.

The negative stiffness may have been caused by instability, whilst this was predicted to occur in some cases with the In Motion device due to the low-friction and mobile core design; it was surprising that it was measured in an intact disc.

It is thought the impingement was due to the misalignment of the disc during implantation. The data concerning this test showed that whilst the extension loosely resembled other tests (Figure 125), the flexion showed an increase in moment at approximately 2° (Figure 126). This was thought to have been caused by the superior endplate coming into contact with the outer ring of the core, and such a phenomenon was observed during the testing of this specimen. This created resistance to further rotation and caused the moment to increase, as seen in the measured moment.

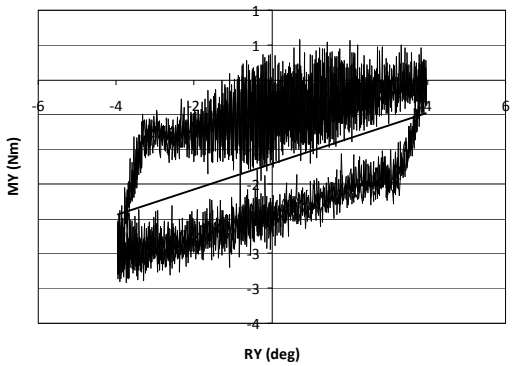

Figure 125: A typical graph of $k_{5,5}$ for an ISD In Motion device and 500 N preload

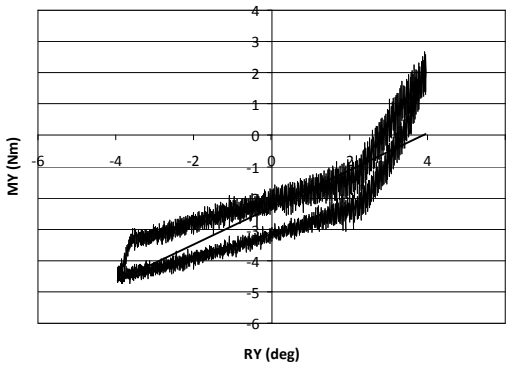

Figure 126: $k_{5,5}$ core impingement in flexion of ISD In Motion device, 500 N preload

Had these two specimens been discounted, the flexion/extension data would have been significantly different between the intact and In Motion discs (p=0.002 and 0.000 after 30 and 60 minutes respectively). However, it was felt that the data for these specimens should be kept and used for analysis along with all other results because there was no obvious reason that the negative stiffness values had occurred, and the misplacement of disc replacement devices has been reported to occur in-vivo [101, 117, 201], and was therefore regarded as clinically relevant.

Such a result emphasises the importance of attention to positioning of any implant device. The clinical results for total disc replacements emphasise this, with poorer ROM outcomes from patients with poorly positioned devices [101].

The stiffness in axial rotation was significantly different with the In Motion device irrespective of the preload. In the FSU specimens the stiffness was 22 % and 34 % of the natural disc with 0 N and 500 N preload respectively. This was reduced in the isolated disc specimens to 0 % and 2% with 0 N and 500 N preload respectively.

The structure of the natural disc is such that at least half of the collagen fibres of the annulus fibrosus are in tension under axial rotation. If a preload is applied, the incompressible gel-like nucleus pulposus will cause further tension in the annulus fibrosus. This resulted in the stiffness of intact isolated disc specimens significantly increasing when a preload of 500 N was applied. There is no resistance to axial rotation in the In Motion device other than friction, which is designed to be as low as possible. Any stiffness measured in the ISD

specimens with the In Motion device was due to articulating friction between the metal endplates and the polyethylene core. Whilst this friction would increase with the application of a preload, it remained almost negligible compared to the natural disc (approximately 1000 Nmm/rad compared to approximately 48,000 Nmm/rad).

9.5 Conclusions

The spine simulator and testing protocol that has been developed have been shown to be capable of measuring the dynamic stiffness of an intervertebral disc in six degrees of freedom. Furthermore, intervertebral disc replacement devices can be quantitatively compared to the natural disc in six degrees of freedom. Such comparisons are a worthwhile addition to the current pre-clinical testing requirements that provide a means to assess the suitability of a disc replacement for clinical use.

The spine simulator and stiffness matrix method provides valuable data of disc replacement devices and allows the suitability for clinical use to be assessed. It is also possible to use the spine simulator and stiffness matrix method as a practical step in the iterative design process of new disc prostheses.

The tests completed have shown that the In Motion device is has low resistance to rotation due to the double ball and socket design. The only resistance to rotational motion in any plane is articulating friction, which has been designed to be as low as possible so as to reduce wear. The stiffness in axial rotation was very low compared to the intact disc (2 %). However, the device does reasonably replicate the shear stiffness and axial compressive stiffness of the natural disc.

The stiffness in lateral bending with ISD specimens was found to be negative with the In Motion device, suggesting instability due to the low-friction, mobile core design. The same was not found in flexion/extension, though it is thought that this is due to the relatively low stiffness of the intact disc, combined with signal noise and the large effect that associated shear force measurements had on the moment transformation. These issues could be improved in future tests with the use of a noise filter, a more accurate lead cell, and the reduction of the distance between the six-axis load cell datum, and the centre of the superior vertebral body that the moments are transformed to.

The results for the different stiffness terms emphasise the difficulty in defining a suitable method of using the load and position data measured to calculate the stiffness. Using the linear least squares method has limitations in that it does not take into account the S-curve that a load/displacement plot may exhibit, and it does not take into account if there is a difference in stiffness in the positive and negative phase of a cycle. However, it was not always found to be the case that rotational motion exhibited such an S-curve, and under translations in the sagittal and coronal plane, the associated shear stiffness force was found to be highly linear. This was true of both FSU and ISD specimens. This showed that the method was a consistent way with which to measure the multitude of stiffness terms that the stiffness matrix is composed from, particularly when testing and completing comparisons of different specimen types, which may result in different stiffness characteristics. From the linear least squares method, a good understanding of how a disc replacement device compares to the natural can be acquired.

Following the completion of the stiffness matrix testing of porcine FSU and ISD specimens with both intact discs and the DePuy In Motion disc replacement, it has been shown that the spine simulator is a suitable apparatus for completing quantitative comparisons. The results have shown that it is more suitable to compare a disc replacement device with the natural structure that it will replace in-vivo. For disc replacement devices, this would be the isolated intact disc, and depending upon the individual surgical procedures, it may also include some ligaments.

In the case of the In Motion device, the anterior longitudinal ligament is removed from the operated level as part of the operative technique and the posterior longitudinal ligament is released, though it remains unclear exactly what role the PLL plays in terms of ROM and stability following a total disc replacement procedure [264]. It is therefore the case that the In Motion device should replicate not only the intervertebral disc but also the ALL and possibly the PLL, at least to some extent.

It has been shown that the most important factor affecting the mechanical properties of biological tissue for in-vitro testing is time [261]. With the protocol developed, all specimens were dissected on the day that they were acquired before being frozen. Then the total thaw and test time was less than seven hours. By spraying specimens with 0.9 % saline and

wrapping with food packaging plastic, the drying out of specimens during this time was also minimised [212, 260, 261].

The testing completed was the first dynamic stiffness matrix of porcine specimens, and a disc replacement device. It has shown that whilst the principal stiffnesses are generally more important in the comparison of disc prostheses with the intact disc, key non-principal stiffness terms may also provide insight into the behaviour of a disc replacement device compared to the natural disc.

9.6 Final Test Protocol Recommendation

It is recommended that the testing protocol is followed to compare the mechanical properties of disc replacement devices with the natural disc (Table 84). Further work may demonstrate whether better accuracy can be achieved by calculating stiffness terms using a method other than linear least squares, or if greater insight can be gained from calculating the stiffness separately for the positive and negative phases when different stiffnesses are exhibited in each phase, such as in flexion and extension.

Table 84: Summary of testing protocol

Step	Procedure
A	Dissect spine into isolated disc specimens with appropriate ligaments intact
B	Bag each specimen, labelling with spine number and the vertebral levels
C	Bag specimens of the same spine number
D	Bag all specimens
E	Freeze specimens (-24°C)
1	Take specimen out of freezer (-24°C) and allow to thaw at room temperature
2	During thawing, drive screws into cranial and caudal end of specimen
3	During thawing, pot cranial end of specimen in Wood's Metal, disc horizontal
4	During thawing, pot caudal end of specimen in Wood's Metal
5	During thawing, spray the specimen with 0.9 % saline solution
6	During thawing, wrap the specimen in food packaging plastic film
7	During thawing, mount specimen on 6-axis loadcell and spine simulator

Table 84 continued…

8	Thawing complete after three hours
9	Adjust position of specimen to zero loads on all axes
10	Fix base of specimen
11	Take 2 second reading
12	Use reading to calculate offsets for 6-axis loadcell
13	Adjust offsets of 6-axis loadcell
14	Complete randomised stiffness matrix test with 0 N preload
15	Change TZ axis to load control
16	Note axial displacement (mm)
17	Apply a preload of 500 N
18	After 30 minutes change TZ axis to position control
19	Note axial displacement (mm)
20	Complete randomised stiffness matrix test with 500 N preload
21	Adjust TZ as required during testing to maintain 500 N preload
22	Note axial displacement at end of stiffness matrix test (mm)
23	Adjust preload to zero
24	Remove specimen from the spine simulator and 6-axis loadcell
25	Remove food packaging plastic film from around specimen
26	Replace the intact disc with the disc replacement device
27	Spray the specimen with 0.9 % saline solution
28	Wrap the specimen in food packaging plastic film
29	Re-mount the specimen on the 6-axis loadcell and spine simulator
30	Take 2 second reading
31	Use reading to calculate offsets for 6-axis loadcell
32	Adjust offsets of 6-axis loadcell
40	Repeat steps 14-24
41	Unpot specimen and dispose of biological waste

10 OVERALL DISCUSSION AND CONCLUSIONS

Intervertebral disc replacements have been in clinical use for over fifty years, yet there has been limited improvement in the clinical results published in the literature of total disc arthroplasty. Generally the devices perform comparably to fusion surgery for the required two-year follow-up [100, 103, 128, 129, 269] but published data of long-term follow-up results are both small in numbers, and poor in terms of outcomes [21, 118, 126, 127]. The lack of development in disc arthroplasty outcomes, despite good improvements in hip and knee arthroplasty suggests a severe problem in the core philosophy of artificial disc replacement design and surgical procedure.

The natural disc comprises a soft tissue structure of gel-like nucleus pulposus and a collagen fibre based annulus fibrosus. It has six-degrees of freedom, and has resists motion in each of these degrees of freedom via the viscoelastic properties of the disc structure. The ball and socket based designs that are generally used clinically have no elasticity [270], and are in fact designed to have as little resistance to motion as possible.

The key to hip and knee replacement surgery is to replicate the natural joint closely as possible with the prosthesis, so that the procedure can restore the natural biomechanics, along with functionality of the joint. Such procedures are now commonplace and have good clinical results. The design of total disc arthroplasty prostheses used clinically has generally followed the technology of hips and knees, using low-friction articulating surfaces, rather than focusing on the replication of the natural biomechanics of the spine.

The Acroflex disc that was introduced in the late 1980s was an elastomeric device but due to potential carcinogenic properties of the vulcanisation process the device was implanted in only six patients [12]. A second generation was implanted in approximately 40 patients but because of debonding of the elastomer core with the metal endplates in clinical use, it was also discontinued [12]. It may be that these results caused a shift of manufacturers from elastomeric devices in fear of such problems. However, the majority of patents for new disc replacement devices remain elastomeric based and there has been resurgence in the potential of such devices in recent years, with a small number of elastomeric implants currently undergoing clinical trials.

The importance of new prosthetic devices in being able to withstand the in-vivo environment is crucial to their success. This includes the biological surroundings and the loading conditions. By using only materials that have a longstanding track record in clinical use, biological issues can be minimised early in the design stage. ASTM guidelines lay out testing regimes in order to measure the wear, fatigue, and yield properties of devices using both dynamic and static tests. Testing to assess the performance of new devices and allow comparison with the structure being replaced would be a useful addition to these requirements.

This is emphasised by the results of the patent review completed as part of the present study (Chapter 4.3, page 68), which not only found more elastomeric designs than any other, but also a recent increase in hybrid designs that integrate elastomeric or similar mechanisms into a ball and socket design. Yet there are only four elastomeric devices known to be in clinical use at present: The M6 disc (Spinal Kinetics), the Cadisc-L (Ranier Technology Limited, Cambridge, UK), the Physio-L (Nexgen Spine, Inc., Whippany, NJ, USA), and the Freedom lumbar disc (AxioMed Spine Corporation, Ohio, USA).

These devices are what one would describe as the latest generation of disc prostheses, which move away from the ball and socket devices that have failed to improve in clinical outcomes since being introduced in the 1980s.

With the history of total disc arthroplasty in mind, and the necessity for thorough pre-clinical testing methods to suitably evaluate the efficacy of prostheses, the current study was completed using a spine simulator and stiffness matrix testing protocol. Once the spine simulator had been built, it was tested and validated using both synthetic and porcine specimens in order to refine the performance and finalise the testing protocol for the full porcine stiffness tests that were completed.

Despite a multitude of studies investigating the multi-axis stiffness/flexibility properties of the spine [220, 221, 224, 233, 234, 237, 240, 241, 243, 244, 258, 271, 272], there have been few studies that have compared the multi-axis stiffness/flexibility properties of an intact intervertebral disc with a disc replacement device [217, 222, 253], and none that do so dynamically in six axes with axial preloads. The work completed is the first such study. This

has allowed the quantitative comparison of the intact porcine disc with a total disc replacement device dynamically in all six axes, and both without and with axial preload.

Through this protocol a leading intervertebral disc replacement device was compared to a porcine disc. The disc used was the DePuy In Motion lumbar disc, the most recent version of the well-established Charité disc, which was patented and first used clinically in 1984 [12, 94]. The In Motion device is a modification of the Charité III disc, with changes having been made to the endplates to facilitate improved implantation. The design of the double ball and socket of the In Motion device is unchanged from the Charité III device of 1987.

Tests were completed using porcine functional spinal units and porcine isolated disc specimens (L1-L2, L3-L4, and L5-L6). These were tested first with the intact disc and then with the In Motion device implanted. The stiffness of FSU specimens was significantly greater in all principal stiffness terms than the stiffness of ISD specimens, with the exception of axial stiffness. Such a result was previously reported by Gardner-Morse and Stokes, though without reporting if the difference between the specimen types was significant [220].

Analysis showed that there were significant differences between the intact disc and the In Motion disc in many of the principal stiffness terms, as well as some of the non-principal and coupled stiffness terms. This was more noticeable when isolated disc specimens were used, as the shielding effect of the facets and posterior ligaments was eliminated. Differences were also more evident when the axial preload of 500 N was applied. This was due to the associated increase in stiffness of the intact spine under an axial preload, which has been reported elsewhere [220, 221, 223, 240, 241, 249], combined with the instability of the In Motion device, and the low-friction nature of the disc design.

The behaviour measured in the In Motion device would be expected in other low-friction ball and socket based designs that do not feature any resistance to rotational motion. However, the instabilities measured may be more evident in other mobile core discs such as the Kineflex and Mobidisc lumbar prostheses, and the Kineflex-C, Mobi-C, and Discover cervical prostheses. Such designs are based primarily on the technology of hip and knee arthroplasty. This study has shown that they do not closely replicate the natural biomechanics of the intervertebral disc.

Based on the testing completed, it is possible that the performance of the In Motion device, or any similar device, through the introduction of some elastomeric material or assembly could be improved. Such a design change would of course require thorough analysis to optimise the stiffness characteristics, biocompatibility issues, and wear and fatigue properties, prior to any clinical use. Similar modifications have already been patented by DePuy [204] (Figure 48), suggesting that the manufacturers of the In Motion device are aware of the potential improvements that elastomeric structures would have. Further to this patent is another hybrid design patented by DePuy comprising a helical spring with a central core element to promote rotational motions about the disc centre [273].

The long-term results of the latest generation of elastomeric based prostheses will not be available for at least 10 years. It is possible that hybrid designs based on the In Motion disc will prove to have the long-term durability of the ball and socket, low-friction designs, combined with the stiffness of elastomeric designs.

Further testing using the spine simulator would provide useful comparisons of disc replacement devices with the natural spine. Future studies might compare cadaveric specimens rather than porcine, and integrate muscle forces, providing a means to even more closely compare disc replacement devices with the in-vivo environment, and assess efficacy of the devices prior to clinical use.

11 FURTHER WORK

This study has demonstrated clear differences in the stiffness characteristics of a leading invertebral disc prosthesis with a natural porcine disc. Further work would be useful in providing information about the natural disc, and how it may be possible to replicate the mechanical properties in a disc replacement device.

The stiffness characteristics of the spine simulator would be useful in determining if a correction factor needs applying to the stiffness results to take into account deflection of the simulator during stiffness testing. This could be completed on the current form of the spine simulator, and should be completed prior to any studies an upgraded version of the spine simulator that is described below.

11.1 Data Analysis

Research should be completed in regard to the analysis of the data acquired during this study. In particular the present study showed that the principal stiffnesses were generally the most consistent between specimens and were commonly significantly different when comparing a change in either preload (0 or 500 N), specimen type (FSU or ISD), or disc type (intact porcine or In Motion implant). Such is the overwhelming amount of data contained in a full stiffness matrix that it may be more suitable in future studies to analyse principal stiffness terms only, but do so based on the characteristics of the majority of specimens, rather than using a linear least squares method across all stiffness terms in the matrix. Such a method of data analysis could be completed using the raw data already acquired as part of this study, and may lead to a more accurate method of comparing intervertebral disc replacement devices with the natural disc.

Should a prosthetic disc closely resemble the natural disc in all six principal stiffnesses, it may then be appropriate to investigate key non-principal terms. However, the results obtained in this study have shown that the whilst the DePuy In Motion disc compares favourably in shear stiffnesses and axial compression, some instability of the design causes clear differences in rotational stiffnesses.

11.2 Spine simulator Upgrade

The spine simulator in its current form is limited to position control in four of the six axes. The two axes that can operate in load control, TZ and RZ, are operated by hydraulics via a separate controller and user interface. Ideally, all six axes should be able to operate simultaneously in either load or position control and should be controlled using the same control system and the same user interface.

Such modification could be achieved by removing the Zwick hydraulic machine and introducing of two axes driven by stepper motors. These stepper motors could be controlled using two more Maxon controllers that would link with the dSPACE system currently used. This would require a new outer frame system to apply the axial translations, and the gimbal head could be adapted to provide axial rotation.

In order for the spine simulator to work in load control, a new dSPACE timing board would be required to read the encoder signals. The DS3002 board is recommended for this alongside an upgrade of the dSPACE software. A control system has already been written that would allow position or load control, though this would need to be expanded to include all six axes, rather than the four it currently includes.

Based on the total cost of the current spine simulator, it is estimated that the upgrade to a standalone 6-axes apparatus would cost in the region of £8000. Doing this would not only provide more flexibility in how the spine simulator was used but it would also free up the 2-axis Zwick hydraulic testing machine for other research interests.

If the upgrades described above are to be undertaken, it should also be taken into account that muscle force simulation would be beneficial in gaining further understanding of spinal biomechanics and the behaviour of spinal instrumentation. Work was completed as part of this study to calculate suitable muscle forces and the application positions. Space for the application of muscle forces should be provided in any upgrade design of the spine simulator.

11.3 Future Studies

It would be useful to repeat the tests completed as part of the present study with other disc replacement devices in clinical use. This should include other low-friction ball and socket designs, and elastomeric designs.

Should the upgrades described above be completed, it would be useful to complete further stiffness matrix tests using porcine specimens and comparing them with a disc replacement device that is mounted without any biological tissue present. Should the direct stiffness matrix results compare with those of a disc replacement implanted into a porcine specimen, it would provide good evidence that this method could provide an initial insight into the efficacy of new devices. Such testing would eliminate tissue degradation, and specimen variability. It may therefore provide more consistent characterisation of new devices. Only once a design had been optimised would it then be necessary to undergo the more difficult and costly process of cadaveric testing.

Stiffness matrix testing could be completed using muscle force simulation. This could assess the effect that the muscles have on stabilising the spine in a specimen with an intact disc and after a disc arthroplasty procedure. It may be that the stability and resistance to motion that the muscles provide may offset the lack or resistance to rotational motion that low-friction disc replacements exhibit.

12 REFERENCES

1. Bridwell, K., 2007. Anatomical Planes of the Body. SpineUniverse: Montclair, NJ, USA. 06/12/2007 [Accessed 06/12/2007]. Available from: http://www.spineuniverse.com/displayarticle.php/article1023.html.
2. Gray, H., 1918. Gray's Anatomy. Twentieth Edition. Lea & Febiger: Philadelphia, PA, USA.
3. Nordin, M. and Frankel, V.H., 2001. Basic Biomechanics of the Musckuloskeletal System. Third Edition. Lippincott Williams & Wilkins: Philadelphia, PA, USA.
4. White III, A.A. and Panjabi, M.M., 1990. Clinical Biomechanics of the Spine. Second Edition. Lippincott Williams & Wilkins: Philadelphia, PA, USA.
5. Adams, M., Bogduk, N., Burton, K., and Dolan, P., 2006. The Biomechanics of Back Pain. Second Edition. Elsevier Ltd.: Philadelphia, PA, USA.
6. Bao, Q.B., McCullen, G.M., Higham, P.A., Dumbleton, J.H., and Yuan, H.A., 1996. The Artificial Disc: Theory, Design and Materials. Biomaterials, 17(12): p. 1157-1167.
7. Cassinelli, E.H. and Kang, J.D., 2000. Current Understanding of Lumbar Disc Degeneration. Operative Techniques in Orthopaedics, 10(4): p. 254-262.
8. Pollintine, P., Dolan, P., Tobias, J.H., and Adams, M.A., 2004. Intervertebral Disc Degeneration Can Lead to "Stress-Shielding" of the Anterior Vertebral Body: A Cause of Osteoporotic Vertebral Fracture? Spine, 29(7): p. 774-782.
9. Kulkarni, A.G. and Diwan, A.D., 2005. Prosthetic Lumbar Disc Replacement for Degenerative Disc Disease. Neurology India, 53(4): p. 499-505.
10. Carragee, E.J., 2007. (II) the Role of Surgery in Low Back Pain. Current Orthopaedics, 21(1): p. 9-16.
11. Boos, N., 2009. The Impact of Economic Evaluation on Quality Management in Spine Surgery. European Spine Journal, 18(0): p. 338-347.
12. Szpalski, M., Gunzburg, R., and Mayer, M., 2002. Spine Arthroplasty: A Historical Review. European Spine Journal, 11 Suppl 2: p. S65-S84.
13. Gamradt, S.C. and Wang, J.C., 2005. Lumbar Disc Arthroplasty. The Spine Journal, 5(1): p. 95-103.
14. Tropiano, P., Huang, R.C., Girardi, F.P., Cammisa, F.P., Jr., and Marnay, T., 2006. Lumbar Total Disc Replacement. Surgical Technique. Journal of Bone and Joint Surgery-American Volume, 88 Suppl 1 Pt 1: p. 50-64.

15. Huang, R.C., Girardi, F.P., Cammisa, F.P., and Wright, T.M., 2003. The Implications of Constraint in Lumbar Total Disc Replacement. Journal of Spinal Disorders & Techniques, 16(4): p. 412-417.
16. Mayer, M.H. and Andreas, K., 2002. Non-Fusion Technology in Degenerative Lumbar Spinal Disorders: Facts, Questions, Challenges. European Spine Journal, 11(0): p. S85-S91.
17. de Kleuver, M., Oner, F.C., and Jacobs, W.C.H., 2003. Total Disc Replacement for Chronic Low Back Pain: Background and a Systematic Review of the Literature. European Spine Journal, 12(2): p. 108-116.
18. Cakir, B., Richter, M., Kafer, W., Puhl, W., and Schmidt, R., 2005. The Impact of Total Lumbar Disc Replacement on Segmental and Total Lumbar Lordosis. Clinical Biomechanics, 20(4): p. 357-364.
19. Andrew J, H., 2002. Paraspinal Denervation and the Spinal Degenerative Cascade. The Spine Journal, 2(5): p. 372-380.
20. Anderson, P.A. and Rouleau, J.P., 2004. Intervertebral Disc Arthroplasty. Spine, 29(23): p. 2779-2786.
21. Huang, R.C., Tropiano, P., Marnay, T., Girardi, F.P., Lim, M.R., and Cammisa, Jr., 2006. Range of Motion and Adjacent Level Degeneration after Lumbar Total Disc Replacement. The Spine Journal, 6(3): p. 242-247.
22. Wai, E.K., Selmon, G.P.K., and Fraser, R.D., 2003. Disk Replacement Arthroplasties: Can the Success of Hip and Knee Replacements Be Repeated in the Spine? Seminars in Spine Surgery, 15(4): p. 473-482.
23. Kim, D.H., Cammisa Jr, F.P., and Fessler, R.G., 2006. Dynamic Reconstruction of the Spine. First Edition. Thieme Medical Publishers Inc.,: New York, NY, USA.
24. Randolph, G.B., Scioscia, T.N., and Wang, J.C., 2006. Lumbar Total Disc Arthroplasty: State of the Data. Seminars in Spine Surgery, 18(2): p. 61-71.
25. Bridwell, K., 2007. Vertebral Column. SpineUniverse: Montclair, NJ, USA. 12/06/12/2007 [Accessed 06/12/2007]. Available from: http://www.spineuniverse.com/displayarticle.php/article1286.html.
26. Bridwell, K., 2007. Ligaments. SpineUniverse: Montclair, NJ, USA. 06/12/2007 [Accessed 06/12/2007]. Available from: http://www.spineuniverse.com/displayarticle.php/article1268.html.

27. Bridwell, K., 2007. Muscles of the Spine. SpineUniverse: Montclair, NJ, USA. 06/12/2007 [Accessed 06/12/2007]. Available from: http://www.spineuniverse.com/displayarticle.php/article1272.html.

28. Stewart, T.D. and Hall, R.M., 2006. Basic Biomechanics of Human Joints: Hips, Knees and the Spine. Current Orthopaedics, 20(1): p. 23-31.

29. Dolan, P., Kingma, I., van, D.J., De Looze, M.P., Toussaint, H.M., Baten, C.T., and Adams, M.A., 1999. Dynamic Forces Acting on the Lumbar Spine During Manual Handling. Can They Be Estimated Using Electromyographic Techniques Alone? Spine, 24(7): p. 698-703.

30. Nachemson, A.L., 1981. Disc Pressure Measurements. Spine, 6(1): p. 93-97.

31. Mannion, A.F., Adams, M.A., and Dolan, P., 2000. Sudden and Unexpected Loading Generates High Forces on the Lumbar Spine. Spine, 25(7): p. 842-852.

32. Adams, M.A. and Dolan, P., 2005. Spine Biomechanics. Journal of Biomechanics, 38(10): p. 1972-1983.

33. Serhan, H.A., Dooris, A.P., Parsons, M.L., Ares, P.J., and Gabriel, S.M., 2006. In Vitro Wear Assessment of the Charite Artificial Disc According to Astm Recommendations. Spine, 31(17): p. 1900-1910.

34. Bogduk, N. and Mercer, S., 2000. Biomechanics of the Cervical Spine. I: Normal Kinematics. Clinical Biomechanics, 15(9): p. 633-648.

35. McGregor, A.H., McCarthy, I.D., Dore, C.J., and Hughes, S.P., 1997. Quantitative Assessment of the Motion of the Lumbar Spine in the Low Back Pain Population and the Effect of Different Spinal Pathologies of This Motion. Eur.Spine J., 6(5): p. 308-315.

36. Feipel, V., Rondelet, B., Le Pallec, J.P., and Rooze, M., 1999. Normal Global Motion of the Cervical Spine: An Electrogoniometric Study. Clinical Biomechanics, 14(7): p. 462-470.

37. Dolan, P. and Adams, M.A., 1993. The Relationship between Emg Activity and Extensor Moment Generation in the Erector Spinae Muscles During Bending and Lifting Activities. Journal of Biomechanics, 26(4-5): p. 513-522.

38. Wilke, H.J., Neef, P., Caimi, M., Hoogland, T., and Claes, L.E., 1999. New in Vivo Measurements of Pressures in the Intervertebral Disc in Daily Life. Spine, 24(8): p. 755-762.

39. Ledet, E.H., Tymeson, M.P., DiRisio, D.J., Cohen, B., and Uhl, R.L., 2005. Direct Real-Time Measurement of in Vivo Forces in the Lumbar Spine. The Spine Journal, 5(1): p. 85-94.

40. Rohlmann, A., Bergmann, G., and Graichen, F., 1999. Loads on Internal Spinal Fixators Measured in Different Body Positions. European Spine Journal, 8(5): p. 354-359.

41. Adams, M.A., May, S., Freeman, B.J.C., Morrison, H.P., and Dolan, P., 2000. Effects of Backward Bending on Lumbar Intervertebral Discs - Relevance to Physical Therapy Treatments for Low Back Pain. Spine, 25(4): p. 431-437.

42. Callaghan, J.P., Patla, A.E., and McGill, S.M., 1999. Low Back Three-Dimensional Joint Forces, Kinematics, and Kinetics During Walking. Clinical Biomechanics, 14(3): p. 203-216.

43. Ferguson, S.A., Gaudes-MacLaren, L.L., Marras, W.S., Waters, T.R., and Davis, K.G., 2002. Spinal Loading When Lifting from Industrial Storage Bins. Ergonomics, 45(6): p. 399-414.

44. Dennis, G.J. and Barrett, R.S., 2002. Spinal Loads During Individual and Team Lifting. Ergonomics, 45(10): p. 671-681.

45. Guo, H.R., Tanaka, S., Halperin, W.E., and Cameron, L.L., 1999. Back Pain Prevalence in Us Industry and Estimates of Lost Workdays. Am.J.Public Health, 89(7): p. 1029-1035.

46. Bertagnoli, R., Sabatino, C.T., Edwards, J.T., Gontarz, G.A., Prewett, A., and Parsons, J.R., 2005. Mechanical Testing of a Novel Hydrogel Nucleus Replacement Implant. The Spine Journal, 5(6): p. 672-681.

47. Health and Safety Executive, 2006. Hse Tackles Back Pain with Supermarket Workout. Health & Safety Executive: London, UK. 19/12/2007 [Accessed 19/12/2007]. Available from: http://www.hse.gov.uk/press/2006/e06107.htm.

48. Maniadakis, N. and Gray, A., 2000. The Economic Burden of Back Pain in the Uk. Pain, 84(1): p. 95-103.

49. Espicom Ltd., 2009. The Complete Guide to the Global Orthopaedic Market 2009. Espicom Ltd.: Chichester, West Sussex, UK. 12/05/2009 [Accessed 27/10/2011]. Available from: http://www.espicom.com/Prodcat2.nsf/Product_ID_Lookup/00001955?OpenDocument.

50. Lau, S. and Lam, K.S., 2007. (Iv) Lumbar Stabilisation Techniques. Current Orthopaedics, 21(1): p. 25-39.

51. Millar, L., 2011. United States Held 69% of Global Spine Device Market in 2010. ASC Communications. 25/10/2011 [Accessed 27/10/2011]. Available from: http://www.beckersorthopedicandspine.com/orthopedic-spine-device-implant-news/item/9652-united-states-held-69-of-global-spine-device-market-in-2010#startOfPage.

52. iData Research Inc., 2010. Rapid Growth of Nuvasive's Xlif for the Treatment of Back Pain Fuels Mis Spinal Fusion Procedures to Triple by 2016. iData Research Inc.: Vancouver, BC, Canada. [Accessed 27/10/2011]. Available from: http://www.idataresearch.net/idata/blog/?p=625#more-625.

53. Winkelstein, B.A. and Myers, B.S., 1997. The Biomechanics of Cervical Spine Injury and Implications for Injury Prevention. Medicine and Science in Sports and Exercise, 29(7): p. S246-S255.

54. Dolan, P., Greenfield, K., Nelson, R.J., and Nelson, I.W., 2000. Can Exercise Therapy Improve the Outcome of Microdiscectomy? Spine, 25(12): p. 1523-1532.

55. Ferguson, S.J. and Steffen, T., 2003. Biomechanics of the Aging Spine. European Spine Journal, 12: p. S97-S103.

56. Frost, H., Klaber Moffett, J.A., Moser, J.S., and Fairbank, J.C., 1995. Randomised Controlled Trial for Evaluation of Fitness Programme for Patients with Chronic Low Back Pain. BMJ, 310(6973): p. 151-154.

57. Frost, H., Lamb, S.E., Klaber Moffett, J.A., Fairbank, J.C.T., and Moser, J.S., 1998. A Fitness Programme for Patients with Chronic Low Back Pain: 2-Year Follow-up of a Randomised Controlled Trial. Pain, 75(2-3): p. 273-279.

58. gado-Lopez, P.D., Rodriguez-Salazar, A., Castilla-Diez, J.M., Martin-Velasco, V., and Fenandez-Arconada, O., 2005. Role of Surgery in Spinal Degenerative Disease. Analysis of Systematic Reviews on Surgical and Conservative Treatments from an Evidence-Based Approach. Neurocirugia, 16(2): p. 142-157.

59. Adams, M.A., McNally, D.S., and Dolan, P., 1996. 'Stress' Distributions inside Intervertebral Discs. The Effects of Age and Degeneration. J.Bone Joint Surg.Br., 78(6): p. 965-972.

60. Blumenthal, S.L., Ohnmeiss, D.D., Guyer, Hochschuler, S., McAfee, P., Garcia, R., Salib, R., Yuan, H., Lee, C., Bertagnoli, R., Bryan, V., and Winter, R., 2002. Artificial

Intervertebral Discs and Beyond, : A North American Spine Society Annual Meeting Symposium. The Spine Journal, 2(6): p. 460-463.

61. Swanson, K.E., Lindsey, D.P., Hsu, K.Y., Zucherman, J.F., and Yerby, S.A., 2003. The Effects of an Interspinous Implant on Intervertebral Disc Pressures. Spine, 28(1): p. 26-32.

62. Ruan, D., He, Q., Ding, Y., Hou, L., Li, J., and Luk, K.D.K. Intervertebral Disc Transplantation in the Treatment of Degenerative Spine Disease: A Preliminary Study. The Lancet, 369(9566): p. 993-999.

63. Hilibrand, A.S. and Robbins, M., 2004. Adjacent Segment Degeneration and Adjacent Segment Disease: The Consequences of Spinal Fusion? The Spine Journal, 4(6, Supplement 1): p. S190-S194.

64. Hannallah, D., White, A.P., Fassett, D., Kerr, S., Whang, P.G., and Hilibrand, A.S., 2007. Adjacent Level Degeneration in the Cervical Spine. Operative Techniques in Orthopaedics, 17(3): p. 178-182.

65. Panjabi, M.M., 2007. Hybrid Multidirectional Test Method to Evaluate Spinal Adjacent-Level Effects. Clinical Biomechanics, 22(3): p. 257-265.

66. Brantigan, J.W., Neidre, A., and Toohey, J.S., 2004. The Lumbar I/F Cage for Posterior Lumbar Interbody Fusion with the Variable Screw Placement System: 10-Year Results of a Food and Drug Administration Clinical Trial. The Spine Journal, 4(6): p. 681-688.

67. Food and Drug Administration, 1996. Premarket Approval of Spine-Tech, Inc.'S BAK™ Interbody Fusion System. Food and Drug Administration: Rockville, MD, USA.

68. Zindrick, M.R., Lorenz, M.A., and Bunch, W.H., 2005. Editorial Response to Parts 1 and 2 of the Fda Ide Study of Lumbar Total Disc Replacement with the Charite (Tm) Artificial Disc Vs. Lumbar Fusion. Spine, 30(14): p. E388-E390.

69. Sulzer Ltd, 2012. History. Sulzer Ltd: Winterthur, Switzerland. 19/01/2012 [Accessed 19/01/2012]. Available from: http://www.sulzer.com/desktopdefault.aspx/tabid-512/.

70. Orthopedic Network News, 2004. Backbreaking?: The Spine Industry and Juriprudence. Mendenhall Associates, Inc.: Ann Arbor, MI, USA.

71. Zimmer Inc., 2009. Our History. Zimmer Inc.: Warsaw, IN, USA. 11/03/2009 [Accessed 19/01/2012]. Available from:

http://www.zimmerspine.eu/z/ctl/op/global/action/1/id/9996/template/CP/navid
.

72. Zimmer Inc., 2003. Zimmer Announces Offer to Acquire Centerpulse Ag for Chf 120 Cash and 3.68 Zimmer Shares Per Centerpulse Share. Zimmer Inc.: Warsaw, IN, USA. 20/05/2003 [Accessed 19/01/2012]. Available from: http://investor.zimmer.com/releasedetail.cfm?releaseid=109497.
73. Food and Drug Administration, 1996. Summary of Safety and Effectiveness. Food and Drug Administration: Rockville, MD, USA.
74. Carl, A.L., Kostuik, J., Huckell, C.B., Abitbol, J.-J., Matsumoto, M., and Sieber, A., 2003. Surgeon Perceptions of the Complications and Value of Threaded Fusion Cages as a Spine Fusion Technique: Results of a Consensus Survey. The Spine Journal, 3(5): p. 356-359.
75. Kuslich, S.D., Danielson, G., Dowdle, J.D., Sherman, J., Fredrickson, B., Yuan, H., and Griffith, S.L., 2000. Four-Year Follow-up Results of Lumbar Spine Arthrodesis Using the Bagby and Kuslich Lumbar Fusion Cage. Spine (Phila Pa 1976), 25(20): p. 2656-62.
76. Button, G., Gupta, M., Barrett, C., Cammack, P., and Benson, D., 2005. Three- to Six-Year Follow-up of Stand-Alone BAK Cages Implanted by a Single Surgeon. The Spine Journal, 5(2): p. 155-160.
77. Mirza, S.K., 2005. Point of View: Commentary on the Research Reports That Led to Food and Drug Administration Approval of an Artificial Disc. Spine, 30(14): p. 1561-1564.
78. Bono, C. and Lee, C., 2002. 7:46 Critical Analysis of Trends in Fusion for Degenerative Disc Disease over the Last 20 Years: Influence of Technique on Fusion Rate and Clinical Outcome. The Spine Journal, 2(5, Supplement 1): p. 47-48.
79. Department of Orthopaedics, S.U.H., 2006. The Swedish Hip Arthroplasty Register - Annual Report 2005. Department of Orthopaedics, Sahlgrenska University Hospital: G”teborg, Sweden.
80. Department of Orthopedics, L.U.H., 2006. Annual Report 2006 - the Swedish Knee Arthroplasty Register. Wallin & Dalholm AB: Lund, Sweden.
81. Froning, E.C., 1975. Intervertebral Disc Prosthesis and Instruments for Locating Same. Froning, E.C. Patent: US3875595, 08/04/1975.
82. Jin, D.D., Qu, D.B., Zhao, L., Chen, J.T., and Jiang, J.M., 2003. Prosthetic Disc Nucleus (Pdn) Replacement for Lumbar Disc Herniation - Preliminary Report with

Six Months' Follow-Up. Journal of Spinal Disorders & Techniques, 16(4): p. 331-337.

83. Pfizer Hospital Prod., 1991. Hydrogel Intervertebral Disc Nucleus. Bao, Q.-B. and Higham, P.A. Patent: US5047055, 10/09/1991.

84. Raymedica Inc., 1998. Prosthetic Spinal Disc Nucleus. Ray, C.D., Dickhudt, E.A., and Assell, R.L. Patent: US5824093, 20/10/1998.

85. 2002. Intervertebral Disc Nucleus Implants and Methods. Trieu, H.H. Patent: US2002026244, 28/02/2002.

86. Impliant Ltd., Arnin, U.R.I., Sudin, Y., and Tauber, M., 2005. Elastomeric Spinal Disc Nucleus Replacement. Arnin, U.R.I., Sudin, Y., and Tauber, M. Patent: WO2005009299, 03/02/2005.

87. Bono, C.M. and Garfin, S.R., 2004. History and Evolution of Disc Replacement. The Spine Journal, 4(6, Supplement 1): p. S145-S150.

88. Bertagnoli, R., Yue, J.J., Pfeiffer, F., Fenk-Mayer, A., Lawrence, J.P., Kershaw, T., and Nanieva, R., 2005. Early Results after Prodisc-C Cervical Disc Replacement. Journal of Neurosurgery-Spine, 2(4): p. 403-410.

89. Fernstrom, U., 1966. Arthroplasty with Intercorporal Endoprothesis in Herniated Disc and in Painful Disc. Acta Chirurgica Scandinavica Supplementum, 357: p. 154-159.

90. McKenzie, A.H., 1972. Steel Ball Arthroplasty of Lumbar Intervertebral Discs - a Preliminary Report. Journal of Bone and Joint Surgery-British Volume, B 54(1): p. 766-766.

91. Reitz, H. and Joubert, M.J., 1964. Intractable Headache and Cervico-Brachialgia Treated by Complete Replacement of Cervical Intervertebral Discs with a Metal Prosthesis. South African Medical Journal, 38: p. 881-884.

92. Fassio, B., 1978. Prothese Pour Disques Intervertebraux. Patent: FR2372622, 30/06/1978.

93. Link, H.D., 2002. History, Design and Biomechanics of the Link Sb Charite© Artificial Disc. European Spine Journal, 11(0): p. S98-S105.

94. Univ Berlin Humboldt, 1986. Intervertebral-Disc Prosthesis. Buttner-Janz, K., Derr, B., Erkel, K.-P., Helisch, H.-J., Schellnack, K.D., and Schumann, R. Patent: EP0176728, 09/04/1986.

95. Link Waldemar Gmbh, C.O., 1989. Surgical Instrument Set. Keller, A. Patent: DE3809793, 05/10/1989.

96. DePuy Spine, I., 2003. Acquisition to Expand Spine Product Portfolio. DePuy Spine, Inc.: Raynham, MA, USA. 23/08/2007 [Accessed 23/08/2011]. Available from: http://www.depuyspine.com/about/about.press.050703.asp.

97. Pimenta, L., McAfee, P.C., Cappuccino, A., Bellera, F.P., and Link, H.D., 2004. Clinical Experience with the New Artificial Cervical PCM (Cervitech) Disc. The Spine Journal, 4(6, Supplement 1): p. S315-S321.

98. Food and Drug Adminstration, 2004. FDA Approves Artificial Disc; Another Alternative to Treat Low Back Pain. Food and Drug Administration: Rockville, MD, USA. 12/12/2007 [Accessed 12/12/2007]. Available from: http://www.fda.gov/bbs/topics/ANSWERS/2004/ANS01320.html.

99. O'Leary, P., Nicolakis, M., Lorenz, M.A., Voronov, L.I., Zindrick, M.R., Ghanayem, A., Havey, R.M., Carandang, G., Sartori, M., and Gaitanis, I.N., 2005. Response of Charite Total Disc Replacement under Physiologic Loads: Prosthesis Component Motion Patterns. The Spine Journal, 5(6): p. 590-599.

100. Zeegers, W.S., Bohnen, L.M.L.J., Laaper, M., and Verhaegen, M.J.A., 1999. Artificial Disc Replacement with the Modular Type Sb Charite III: 2-Year Results in 50 Prospectively Studied Patients. European Spine Journal, 8(3): p. 210-217.

101. McAfee, P.C., Cunningham, B., Holsapple, G., Adams, K., Blumenthal, S., Guyer, R.D., Dmietriev, A., Maxwell, J.H., Regan, J.J., and Isaza, J., 2005. A Prospective, Randomized, Multicenter Food and Drug Administration Investigational Device Exemption Study of Lumbar Total Disc Replacement with the Charite (TM) Artificial Disc Versus Lumbar Fusion Part Ii: Evaluation of Radiographic Outcomes and Correlation of Surgical Technique Accuracy with Clinical Outcomes. Spine, 30(14): p. 1576-1583.

102. Blumenthal, S.L., Ohnmeiss, D.D., Guyer, R.D., and Hochschuler, S.H., 2003. Prospective Study Evaluating Total Disc Replacement: Preliminary Results. Journal of Spinal Disorders & Techniques, 16(5): p. 450-454.

103. Blumenthal, S., McAfee, P.C., Guyer, R.D., Hochschuler, S.H., Geisler, F.H., Holt, R.T., Garcia, R., Regan, J.J., and Ohnmeiss, D.D., 2005. A Prospective, Randomized, Multicenter Food and Drug Administration Investigational Device Exemptions Study of Lumbar Total Disc Replacement with the Charite (TM) Artificial Disc Versus Lumbar Fusion Part I: Evaluation of Clinical Outcomes. Spine, 30(14): p. 1565-1575.

104. Regan, J.J., McAfee, P.C., Blumenthal, S.L., Guyer, R.D., Geisler, F.H., Garcia, R., and Maxwell, J.H., 2006. Evaluation of Surgical Volume and the Early Experience with Lumbar Total Disc Replacement as Part of the Investigational Device Exemption Study of the Charite Artificial Disc. Spine, 31(19): p. 2270-2276.

105. Ogon, M., Krismer, M., Söllner, W., Kantner-Rumplmair, W., and Lampe, A., 1996. Chronic Low Back Pain Measurement with Visual Analogue Scales in Different Settings. Pain, 64(3): p. 425-428.

106. Fairbank, J.C., Couper, J., Davies, J.B., and O'Brien, J.P., 1980. The Oswestry Low Back Pain Disability Questionnaire. Physiotherapy, 66(8): p. 271-273.

107. Fairbank, J.C. and Pynsent, P.B., 2000. The Oswestry Disability Index. Spine, 25(22): p. 2940-52; discussion 2952.

108. Ware Jr., J.E., 2011. SF-36® Health Survey Update. Medical Outcomes Trust: Hanover, NH, USA. [Accessed 30/11/2011]. Available from: http://www.sf-36.org/tools/sf36.shtml.

109. Food and Drug Administration, 2004. Orthopedic and Rehabilitation Devices Panel of the Medical Devices Advisory Committee - Wednesday, June 2, 2004. Food and Drug Administration: Rockville, MD, USA.

110. Carragee, E.J. and Weiner, B.K., 2010. Re: The Charité Five-Year Follow-up Study: The Editors' Response to Dr. Guyer. The Spine Journal, 10(4): p. 361-363.

111. Food and Drug Administration, 2004. In-Depth Statistical Review for Expedited PMA (P040006) Charité Artifical Disc, Depuy Spine, Inc. Food and Drug Administration: Rockville, MD, USA.

112. Food and Drug Administration, 2004. Summary of Safety and Effectiveness - Charité Artificial Disc. Food and Drug Administration: Rockville, MD, USA.

113. Guyer, R.D., McAfee, P.C., Banco, R.J., Bitan, F.D., Cappuccino, A., Geisler, F.H., Hochschuler, S.H., Holt, R.T., Jenis, L.G., Majd, M.E., Regan, J.J., Tromanhauser, S.G., Wong, D.C., and Blumenthal, S.L., 2009. Prospective, Randomized, Multicenter Food and Drug Administration Investigational Device Exemption Study of Lumbar Total Disc Replacement with the Charite Artificial Disc Versus Lumbar Fusion: Five-Year Follow-Up. The Spine Journal, 9(5): p. 374-386.

114. Food and Drug Administration, 2006. Summary of Safety and Effectiveness - Prodisc-L Total Disc Replacement. Food and Drug Administration: Rockville, MD, USA.

115. Food and Drug Administration, 2004. Depuy Spine Charité Artificial Disc - Clinical Review. Food and Drug Administration: Rockville, MD, USA.

116. Link Waldemar Gmbh Co., 1993. Intervertebral Disc Endoprosthesis. Buettner-Janz, K., Keller, A., and Lemaire, J.-P. Patent: EP0560141, 15/09/1993.

117. Lemaire, J.P., H., C., el-H., S., W., S., and F., L., 2005. Clinical and Radiological Outcomes with the Charite Artificial Disc: A 10-Year Minimum Follow-Up. Journal of Spinal Disorders & Techniques, 18(4): p. 353-359.

118. Putzier, M., Funk, J.F., Schneider, S.V., Gross, C., Tohtz, S.W., Khodadadyan-Klostermann, C., Perka, C., and Kandziora, F., 2006. Charite Total Disc Replacement - Clinical and Radiographical Results after an Average Follow-up of 17 Years. European Spine Journal, 15(2): p. 183-195.

119. Acromed, C., 1990. Artificial Spinal Disc. Steffee Arthur, D. Patent: EP0392076, 17/10/1990.

120. Acromed, C., 1998. Spinal Disc. Serhan, H., Kuras, J., McMillin, C., and Persenaire, M. Patent: US5824094, 20/10/1998.

121. Aesculap AG. & Co. KG., 1999. Intervertebral Implant. Patent: DE29911422U, 12/08/1999.

122. Fehlmann, P., 2003. Synthes-Stratec Agrees to Acquire Spine Solutions, Inc., a Leading Developer of Total Spine Disc Replacement. Synthes-Stratec, Inc.: Oberdorf, Switzerland. 12/12/2007 [Accessed 12/12/2007]. Available from: http://www.synthes.com/html/Feb-06-2003-Synthes-Stratec.4509.0.html.

123. Food and Drug Adminstration, 2012. Prodisc®-L Total Disc Replacement - P050010. Food and Drug Administration: Rockville, MD, USA. 10/01/2012 [Accessed 10/01/2012]. Available from: http://www.fda.gov/MedicalDevices/ProductsandMedicalProcedures/DeviceApprovalsandClearances/Recently-ApprovedDevices/ucm077620.htm.

124. Tripiano, P., Huang, R.C., Girardi, F.P., Cammisa, F.P., and Marnay, T., 2005. Lumbar Total Disc Replacement - Seven to Eleven-Year Follow-Up. Journal of Bone and Joint Surgery-American Volume, 87A(3): p. 490-496.

125. Zigler, J.E., 2004. Lumbar Spine Arthroplasty Using the Prodisc II. The Spine Journal, 4(6, Supplement 1): p. S260-S267.

126. Huang, R.C., Girardi, F.P., Cammisa Jr, F.P., Tropiano, P., and Marnay, T., 2003. Long-Term Flexion-Extension Range of Motion of the Prodisc Total Disc Replacement. Journal of Spinal Disorders & Techniques, 16(5): p. 435-440.

127. Huang, R.C., Girardi, F.P., Cammisa, F.P., Lim, M.R., Tropiano, P., and Marnay, T., 2005. Correlation between Range of Motion and Outcome after Lumbar Total Disc Replacement: 8.6-Year Follow-Up. Spine, 30(12): p. 1407-1411.

128. Chung, S.S., Lee, C.S., and Kang, C.S., 2006. Lumbar Total Disc Replacement Using Prodisc II: A Prospective Study with a 2-Year Minimum Follow-Up. Journal of Spinal Disorders & Techniques, 19(6): p. 411-415.

129. Delamarter, R.B., Fribourg, D.M., Kanim, L.F.A., and Bae, H., 2003. Prodisc Artificial Total Lumbar Disc Replacement: Introduction and Early Results from the United States Clinical Trial. Spine, 28(20): p. S167-S175.

130. Milgram, A., 2009. A Letter to the Acting Commissioner of the U.S. Food and Drug Administration. Office of the Attorney General, Department of the Law and Public Safety: State of New Jersey, USA.

131. Office of the Attorney General, 2011. State Board of Medical Examiners, with Division of Consumer Affairs, Reprimands Prominent Orthopedic Surgeons. Office of the Attorney General: The State of New Jersey, USA. 03/05/2009 [Accessed 24/08/2011]. Available from: http://www.nj.gov/oag/newsreleases11/pr20110503a.html.

132. 2004. Intervertebral Implant, Insertion Tool and Method of Inserting Same. Marnay, T., Bertagnoli, R., Magee, F., and Eckhof, S. Patent: US2004117022, 17/06/2004.

133. Eisner, G., 2007. Synthes Receives Approvable Letter from Fda for Prodisc™-C (Cervical) Total Disc Replacement. Synthes GmbH: Solothurn, Switzerland. 14/12/2007 [Accessed 14/12/2007]. Available from: http://www.synthes.com/html/October-25-2007-Synthes-rec.7298.0.html.

134. Nabhan, A., Ahlhelm, F., Shariat, K., Pitzen, T., Steimer, O., Steudel, W.I., and Pape, D., 2007. The Prodisc-C Prothesis - Clinical and Radiological Experience 1 Year after Surgery. Spine, 32(18): p. 1935-1941.

135. Medtronic Inc., 2007. About the Prestige® Cervical Disc. Medtronic Inc.: Minneapolis, MN, USA. 20/03/2008 [Accessed 20/03/2008]. Available from: http://www.prestigedisc.com/pages/about_the_prestige_disc.html.

136. Sofamor Danek Holdings Inc., 2000. Artificial Intervertebral Joint Permitting Translational and Rotational Motion. Gill, S.S., Walker, C., Van Hoeck, J., and Gause, L. Patent: US6113637, 05/09/2000.

137. Mehren, C. and Mayer, H.M., 2005. Artificial Cervical Disc Replacement - an Update. Neurology India, 53(4): p. 440-444.

138. Food and Drug Adminstration, 2007. Fda Approves First of a Kind Medical Device to Treat Cervical Degenerative Disc Disease. Food and Drug Administration: Rockville, MD, USA. 18/12/2007 [Accessed 18/12/2007]. Available from: http://www.fda.gov/bbs/topics/NEWS/2007/NEW01668.html.

139. Traynelis, V.C., 2004. The Prestige Cervical Disc Replacement. The Spine Journal, 4(6, Supplement 1): p. S310-S314.

140. Sawin, P., Ceola, W., Stachniak, J., and Mummaneni, P., 2005. P86. Cervical Disc Arthroplasty with the Prestige Cervical Disc: Preliminary Results from a Multicenter Randomized Controlled Trial. The Spine Journal, 5(4, Supplement 1): p. S151.

141. Burkus, J.K., 2004. 85. A Prospective Randomized Controlled Investigation of the Prestige Artificial Cervical Disc in the Treatment of Cervical Disc Disease. The Spine Journal, 4(5, Supplement 1): p. S44.

142. Ceola, W.M. and Mace, C., 2004. A Prospective, Randomized, Controlled Investigation of the Prestige Cervical Disc: Early Experience at a Participating Investigational Site. Neurosurgery, 55(2): p. 454-454.

143. Anderson, P.A., Sasso, R.C., Rouleau, J.P., Carlson, C.S., and Goffin, J., 2004. The Bryan Cervical Disc: Wear Properties and Early Clinical Results. The Spine Journal, 4(6, Supplement 1): p. S303-S309.

144. Medtronic Sofamor Danek, 2007. About the Bryan® Cervical Disc. Medtronic Sofamor Danek: Memphis, TN, USA. 19/12/2007 [Accessed 19/12/2007]. Available from: http://www.bryandisc.com/about-bryan-disc.html.

145. Spinal Dynamics Corp., Bryan, V., Kunzler, A., Conta, B.O.B., and Rouleau, J., 2002. Implantable Joint Prosthesis. Bryan, V., Kunzler, A., Conta, B.O.B., and Rouleau, J. Patent: WO0211650, 14/02/2002.

146. Food and Drug Adminstration, 2006. Bryan Cervical Disc - P060023. Food and Drug Administration: Rockville, MD, USA. 29/06/2009 [Accessed 23/08/2011]. Available from: http://www.fda.gov/MedicalDevices/ProductsandMedicalProcedures/DeviceApprovalsandClearances/Recently-ApprovedDevices/ucm162968.htm.

147. Sasso, R., Hacker, R., and Heller, J., 2006. 5:5639. Artificial Disc Versus Fusion for the Treatment of Cervical Radiculopathy: A Prospective, Randomized Study with 2-Year Follow-Up. The Spine Journal, 6(5, Supplement 1): p. 19S.

148. Goffin, J., Van Loon, J., and Van Calenbergh, F., 2006. 3:57124. Cervical Arthroplasty with the Bryan Disc: 4-Year Results. The Spine Journal, 6(5, Supplement 1): p. 62S-63S.

149. Serhan, H., Mhatre, D., Defossez, H., and Bono, C.M., 2011. Motion-Preserving Technologies for Degenerative Lumbar Spine: The Past, Present, and Future Horizons. SAS Journal, 5(3): p. 75-89.

150. Mathews, H.H., LeHuec, J.C., Friesem, T., Zdeblick, T., and Eisermann, L., 2004. Design Rationale and Biomechanics of Maverick Total Disc Arthroplasty with Early Clinical Results. The Spine Journal, 4(6, Supplement 1): p. S268-S275.

151. Medtronic Sofamor Danek., 2007. About the Maverick™ Artificial Disc. Medtronic Sofamor Danek: Memphis, TN, USA. 20/12/2007 [Accessed 20/12/2007]. Available from: http://www.maverickdisc.com/about-maverick-disc.html.

152. ClinicalTrials.gov, 2011. Maverick™ Total Disc Replacement - Pivotal Study. ClinicalTrials.gov: Bethesda, MD, USA. 28/10/2011 [Accessed 10/01/2012]. Available from: http://clinicaltrials.gov/ct2/show/NCT00635843?term=maverick+total+disc&rank=2.

153. Gornet, M.F., Mathews, H.H., Burkus, J.K., Johnson Ii, D.R., Rahn, K.A., Peloza, J.H., and Dryer, R.F., 2006. 4:57131. Maverick Total Disc Replacement: Initial Report of 24-Month Clinical Outcomes from Six Investigational Centers. The Spine Journal, 6(5, Supplement 1): p. 66S.

154. LDR Medical, 2002. Intervertebral Disc Prosthesis and Fitting Tools. Beaurain, J., Delecrin, J., Onimus, M., Chataigner, H., Allain, J., and Steib Jean, P. Patent: FR2824261, 08/11/2002.

155. P. R. Newswire, 2007. Ldr Medical Reaches 350 Human Implantations of Cervical and Lumbar Artificial Discs. PR Newswire Europe Ltd.: Troyes, France. 19/12/2007 [Accessed 19/12/2007]. Available from: http://www.prnewswire.co.uk/cgi/news/release?id=146855.

156. Mayer, H.M. and Siepe, C., 2007. (Iii) Total Lumbar Disc Arthroplasty. Current Orthopaedics, 21(1): p. 17-24.

157. LDR Medical, 2012. Mobidisc®. LDR Medical: Troyes, France. 10/01/2012 [Accessed 10/01/2012]. Available from: http://www.ldrmedical.com/mobidisc.php?

158. LDR Medical, 2012. Mobi-C®. LDR Medical: Troyes, France. 10/01/2012 [Accessed 10/01/2012]. Available from: http://www.ldrmedical.com/mobi-c.php?

159. LDR Medical, 2004. Intervertebral Disc Prosthesis Has Core and Lower Plate Connected to Prevent Relative Movements between Them. Dufour, T., Huppert, J., Beaurain, J., Fuentes Jean, M., and Vital Jean, M. Patent: FR2846550, 07/05/2004.

160. ClinicalTrials.gov, 2007. Ldr Spine USA Mobi-C® Cervical Disc Prosthesis IDE. ClinicalTrials.gov: Bethesda, MD, USA. 19/12/2007 [Accessed 19/12/2007]. Available from: http://clinicaltrials.gov/ct2/show/NCT00389597?term=mobi-c&rank=1.

161. 2003. Instrumentation and Methods for Use in Implanting an Artificial Intervertebral Disc. Errico, J.P., Dudasik, M.W., and Zubok, R. Patent: US2003069586, 10/04/2003.

162. Stryker Corporation, 2004. Stryker Announces Acquisition of Spinecore, Inc. Stryker Corporation: Kalamazoo, MI, USA. 19/12/2007 [Accessed 19/12/2007]. Available from: http://phx.corporate-ir.net/phoenix.zhtml?c=118965&p=irol-newsArticle&ID=594599&highlight=.

163. Spine-health.com, 2008. Cervical Artificial Disc Replacement Technologies. Spine-health.com: Chicago, IL, USA. 20/03/2008 [Accessed 20/03/2008]. Available from: http://www.spine-health.com/Treatment/Artificial-Discs/Cervical-Artificial-Disc-Update/Cervical-Artificial-Disc-Replacement-Technologies.html.

164. Spinecore Inc. and Zubok, R., 2006. Intervertebral Disc and Insertion Methods Therefor. Zubok, R. Patent: WO2006130460, 07/12/2006.

165. Phillips, F.M. and Garfin, S.R., 2005. Cervical Disc Replacement. Spine, 30(17): p. S27-S33.

166. Link Waldemar Gmbh Co., 2003. Intervertebral Prosthesis for the Cervical Spine. Keller, A. and McAfee, P. Patent: EP1344507, 17/09/2003.

167. Link Waldemar Gmbh Co., 2003. Cervical Intervertebral Prosthesis. Patent: WO03075804, 18/09/2003.

168. Cervitech Inc., 2005. Cervical Intervertebral Prosthesis. Arnold, K. and McAfee Paul, C. Patent: CN1649552, 03/08/2005.

169. NuVasive Inc., 2009. PCM Acquisition. NuVasive, Inc.: San Diego, CA, USA. 2009 [Accessed 27/08/2011]. Available from: http://www.nuvasive.com/external/Cervitech-PCM-Information.pdf.

170. Ramadan, A., Mitulescu, A., and Schmitt, P., 2007. Total Cervical Disc Replacement with the Discocerv-® (Cervidisc Evolution) Cervical Prosthesis: Early Results of a Second Generation. European Journal of Orthopaedic Surgery & Traumatology, 17(6): p. 513-520.

171. Scient'X, Ramadan, A., and Buhler, M., 2001. Disc Prosthesis for Cervical Vertebra. Ramadan, A. and Buhler, M. Patent: WO0164140, 07/09/2001.

172. Scient'X, Carli, O., and Ben-Mokhtar, M., 2005. Intervertebral Discal Prosthesis. Carli, O. and Ben-Mokhtar, M. Patent: WO2005067823, 28/07/2005.

173. Medical News Today, 2007. Scient'x Reaches Milestone of 1.000 Second-Generation Cervical Disc Prosthesis Implanted Worldwide. Medilexicon International: Bexhill-on-Sea, UK. 20/12/2007 [Accessed 20/12/2007]. Available from: http://www.medicalnewstoday.com/articles/77557.php.

174. De Villiers, M. and Ulrich Reinhard, H., 2004. Intervertebral Prosthesis. De Villiers, M. and Ulrich Reinhard, H. Patent: WO2004026187, 01/04/2004.

175. Spinal Motion Inc., 2011. Kineflex Technology. Spinal Motion, Inc.: Mountain View, CA, USA. 2011 [Accessed 10/01/2012]. Available from: http://www.spinal-motion.com/index.php/kineflex-technology.

176. SpinalMotion Inc., 2011. Kineflex Disc Fixation. SpincalMotion Inc.: Mountain View, CA, USA. 2011 [Accessed 10/01/2012]. Available from: http://www.spinal-motion.com/index.php/fixation.

177. Hahnle, U., Weinberg, I.R., and De Villiers, M., 2006. P53. Kineflex (Centurion) Lumbar Disc Prosthesis: Two-Year Results. The Spine Journal, 6(5, Supplement 1): p. 109S-110S.

178. 2005. Prosthetic Intervertebral Disc and Methods for Using the Same. Kim, D.H., Lee, K., Frank, C.W., and Ha Sung, K.Y.U. Patent: US2005027364, 03/02/2005.

179. Spinal Kinetics Inc., 2011. M6-C Overview. Spinal Kinetics Inc.: Sunnyvale, CA, USA. 2011 [Accessed 10/01/2012]. Available from: http://www.spinalkinetics.com/m6-c/m6-c-overview/.

180. Kim, D., Lim, J., Lee, M., and Park, J., 2005. P87. Range of Motion of Cervical Spine Arthroplasty with Spinal Kinetics (Elastomer), Prodisc-C (Metal to Uhmwpe),

Prestige (Metal Only) Artificial Discs and Anterior Cervical Discectomy and Fusion. The Spine Journal, 5(4, Supplement 1): p. S151-S152.

181. Kim, D., Limm, J., Lee, M., and Park, J., 2005. P92. Adjacent Disc Pressure and Facet Force Comparison for Cervical Spine Arthroplasty with Spinal Kinetics, Prodisc-C, Prestige Artificial Discs, and Anterior Cervical Discectomy and Fusion. The Spine Journal, 5(4, Supplement 1): p. S154-S156.

182. Spinal Kinetics Inc., 2011. Spinal Kinetics Completes 10,000th Implant of M6® Artificial Spinal Disc. Spinal Kinetics Inc.: Sunnyvale, CA, USA. 22/03/2011 [Accessed 10/01/2012]. Available from: http://www.spinalkinetics.com/wp-content/uploads/2011/04/Spinal-Kinetics-PR-032211.pdf.

183. Spinal Kinetics Inc., 2009. Spinal Kinetics Implants First M6®-L Artificial Lumbar Disc. Spinal Kinetics Inc.: Sunnyvale, CA, USA. 18/02/2009 [Accessed 10/01/2012]. Available from: http://www.spinalkinetics.com/wp-content/uploads/2011/04/Spinal-Kinetics-PR-021809.pdf.

184. Petka, J., 2005. Globus Begins Cervical Disc Ide Clinical Trial. Globus Medical, Inc.: Audubon, PA, USA. 04/02/2008 [accessed 04/02/2008]. Available from: http://www.globusmedical.com/corporate_profile/press_releases/2005_07_08.php.

185. Du, J., Li, M., Liu, H., Meng, H., He, Q., and Luo, Z., 2011. Early Follow-up Outcomes after Treatment of Degenerative Disc Disease with the Discover Cervical Disc Prosthesis. The Spine Journal, 11(4): p. 281-289.

186. ClinicalTrials.gov, 2007. Comparison of Discover™ Artificial Cervical Disc and Acdf for Treatment of Cervical Ddd (IDE Study). ClinicalTrials.gov: Bethesda, MD, USA. 20/12/2007 [Accessed 20/12/2007]. Available from: http://clinicaltrials.gov/ct2/show/NCT00432159?cond=%22Polyradiculoneuropathy%22&rank=23.

187. Pearsalls Ltd., McLeod, A.R., and Reah, C., 2005. Prosthetic Spinal Disc. McLeod, A.R. and Reah, C. Patent: WO2005092247, 06/10/2005.

188. Medical News Today, 2006. Nuvasive Treats First Patient with Neodisc(TM). MediLexicon International Ltd.: Bexhill-on-Sea, UK. 04/02/2008 [Accessed 04/02/2008]. Available from: http://www.medicalnewstoday.com/articles/52177.php.

189. ClinicalTrials.gov, 2012. Evaluating the Safety and Effectiveness of the Neodisc Versus ACDF in Subjects with Single-Level Cervical Disc Disease. ClinicalTrials.gov:

Bethesda, MD, USA. 04/01/2012 [Accessed 23/01/2012]. Available from: http://www.clinicaltrials.gov/ct2/show/NCT00478088?term=neodisc&rank=1.

190. Ranier Technology Ltd., 2007. High Precision Manufacture of Polyurethane Products Such as Spinal Disc Implants Having Gradual Modulus Variation Snell, R., Andrews, G., Cable, M., and Johnson, S. Patent: US2007043443 22/02/2007.

191. ClinicalTrials.gov, 2010. Safety and Performance Study of the Cadisc-L Lumbar Spinal Disc Replacement Device for CE Marking (Discern). ClinicalTrials.gov: Bethesda, MD, USA. 14/10/2010 [Accessed 10/01/2012]. Available from: http://clinicaltrials.gov/ct2/show/NCT00949936.

192. Ranier Technology Limited, 2012. Ranier Announces Completion of Its Discern European Clinical Study Enrolment for Cadisc™-C, Its Revolutionary Cervical Spinal Disc Ranier Technology Limited: Cambridge, UK. 2012 [Accessed 10/01/2012]. Available from: http://www.ranier.co.uk/index.php?public/news-and-events/news/view/ranier-announces-completion-of-its-discern-european-clinical-study-enrolment-for-cadisc-c-its-revolutionary-cervical-spinal-disc-.

193. Nexgen Spine Inc., Lee, C., Markris, G., and Clemow, A., 2006. Elastomeric Intervertebral Disc Prosthesis. Lee, C., Markris, G., and Clemow, A. Patent: WO2006078663 27/07/2006.

194. Nexgen Spine Inc., Lee, C., Markris, G., and Clemow, A., 2006. Fixation of Elastomer to Rigid Structures Lee, C., Markris, G., and Clemow, A. Patent: WO2006078662 27/07/2006.

195. Nexgen Spine Inc., Ogilvie, W.F., and Markris, G., 2009. Device Assembly with Elements Coupled by a Retaining Structure Ogilvie, W.F. and Markris, G. Patent: WO2009042935, 02/04/2009.

196. Pimenta, L., Springmuller, R., Lee, C.K., Oliveira, L., Roth, S.E., and Ogilvie, W.F., 2010. Clinical Performance of an Elastomeric Lumbar Disc Replacement: Minimum 12 Months Follow-Up. SAS Journal, 4(1): p. 16-25.

197. AxioMed Spine Corporation, 2008. Method and Apparatus for Replacing a Damaged Spinal Disc Benzel, E.C., Lieberman, I.H., Strnad, L., Kuras, J.M., Ross, R.S., Birchall, C.F.J., Duke, K., and Zimmers, K. Patent: WO2005058194, 30/06/2005.

198. ClinicalTrials.gov, 2011. Freedom Lumbar Disc in the Treatment of Lumbar Degenerative Disc Disease (FLD). ClinicalTrials.gov: Bethesda, MD, USA.

04/04/2011 [Accessed 11/01/2012]. Available from: http://clinicaltrials.gov/ct2/show/NCT00775801?term=freedom+disc&rank=1.

199. ClinicalTrials.gov, 2011. Xl TDR® Extreme Lateral Total Disc Replacement for the Treatment of Lumbar Degenerative Disc Disease (Ddd). ClinicalTrials.gov: Bethesda, MD, USA. 23/11/2011 [Accessed 11/01/2012]. Available from: http://clinicaltrials.gov/ct2/show/NCT00927238?term=xl+tdr&rank=1.

200. ClinicalTrials.gov, 2011. Triumph Lumbar Artificial Disc IDE: A Pilot Study. ClinicalTrials.gov: Bethesda, MD, USA. 10/06/2011 [Accessed 11/01/2012]. Available from: http://clinicaltrials.gov/ct2/show/NCT01198470?term=triumph+AND+disc&rank=1.

201. Truumees, E., 2008. Lumbar Disc Replacement: Where Are We in 2007? Seminars in Spine Surgery, 20(2): p. 132-145.

202. LDR Medical, 2005. Intervertebral Disc Prosthesis. Hovorka, I. and Bernard, P. Patent: FR2865629, 05/08/2005.

203. U. K. Intellectual Property Office, 2007. Advanced Search. UK Interllectual Property Office: Newport, UK. 01/03/2007 [Accessed 01/03/2007]. Available from: http://gb.espacenet.com/search97cgi/s97_cgi.exe?Action=FormGen&Template=gb/en/advanced.hts.

204. Depuy Spine Inc., Moumene, M., and Masson, M., 2007. Intervertebral Disc Prosthesis and Associated Methods. Moumene, M. and Masson, M. Patent: WO2007002602, 04/01/2007.

205. 2005. Spinal Implant. Diaz, R.L. and Doubler, R.L. Patent: US2005197703, 08/09/2005.

206. Kinetic Spine Technologies Inc., Duplessis, S.J., Sekhon, L., and Hurlbert, R.J., 2006. Intervertebral Disc Prosthesis. Duplessis, S.J., Sekhon, L., and Hurlbert, R.J. Patent: WO2006116851, 09/11/2006.

207. Sulzer Medizinaltechnik AG., 1993. Atrificial Spinal Disc. Baumgartner, W. Patent: EP0566810, 27/10/1993.

208. Fournitures Hospitalieres Ind., 2005. Intervertebral Disc Prosthesis Comprises a Cushion Enclosed within Two Rigid Half-Covers, One of Which Has a Central Stud That Fits into a Sleeve on the Other. Aaron, A. Patent: FR2863868, 24/06/2005.

209. 2005. Artificial Intervertebral Disc. Rivin, E.I. Patent: US2005154468, 14/07/2005.

210. 2006. Artificial Disc and Joint Replacements with Modular Cushioning Components. Ferree, B.A. and Tompkins, D. Patent: US2006235535, 19/10/2006.

211. Goel, V.K., Panjabi, M.M., Patwardhan, A.G., Dooris, A.P., and Serhan, H., 2006. Test Protocols for Evaluation of Spinal Implants. Journal of Bone and Joint Surgery-American Volume, 88 Suppl 2: p. 103-109.

212. Wilke, H.J., Wenger, K., and Claes, L., 1998. Testing Criteria for Spinal Implants: Recommendations for the Standardization of in Vitro Stability Testing of Spinal Implants. European Spine Journal, 7(2): p. 148-154.

213. ASTM International, 2006. F 2423-05 - Standard Guide for Functional, Kinematic, and Wear Assessment of Total Disc Prostheses. ASTM International: West Conshohocken, PA, USA.

214. ASTM International, 2005. F 2346-05 - Standard Test Methods for Static and Dynamic Characterization of Spinal Artificial Discs. ASTM International: West Conshohocken, PA, USA.

215. British Standards Institution, 2011. Bs Iso 18192-1:2011 - Implants for Surgery - Wear of Total Intervertebral Spinal Disc Prostheses - Part 1. British Standards Institution: London, UK.

216. Chung, S.M., Teoh, S.H., Tsai, K.T., and Sin, K.K., 2002. Multi-Axial Spine Biomechanical Testing System with Speckle Displacement Instrumentation. Journal of Biomechanical Engineering, 124(4): p. 471-477.

217. Cunningham, B.W., Gordon, J.D., Dmitriev, A.E., Hu, N.B., and McAfee, P.C., 2003. Biomechanical Evaluation of Total Disc Replacement Arthroplasty: An in Vitro Human Cadaveric Model. Spine, 28(20): p. S110-S117.

218. Dickey, J.P., Dumas, G.A., and Bednar, D.A., 2003. Comparison of Porcine and Human Lumbar Spine Flexion Mechanics. Veterinary and Comparative Orthopaedics and Traumatology, 16(1): p. 44-49.

219. Dickey, J.P. and Kerr, D.J., 2003. Effect of Specimen Length: Are the Mechanics of Individual Motion Segments Comparable in Functional Spinal Units and Multisegment Specimens? Medical Engineering & Physics, 25(3): p. 221-227.

220. Gardner-Morse, M.G. and Stokes, I.A., 2003. Physiological Axial Compressive Preloads Increase Motion Segment Stiffness, Linearity and Hysteresis in All Six Degrees of Freedom for Small Displacements About the Neutral Posture. Journal of Orthopaedic Research, 21(3): p. 547-552.

221. Gardner-Morse, M.G. and Stokes, I.A.F., 2004. Structural Behavior of Human Lumbar Spinal Motion Segments. Journal of Biomechanics, 37(2): p. 205-212.

222. Kotani, Y., Cunningham, B.W., Abumi, K., Dmitriev, A.E., Hu, N.B., Ito, M., Shikinami, Y., McAfee, P.C., and Minami, A., 2006. Multidirectional Flexibility Analysis of Anterior and Posterior Lumbar Artificial Disc Reconstruction: In Vitro Human Cadaveric Spine Model. European Spine Journal, 15(10): p. 1511-1520.

223. Wilke, H.J., Claes, L., Schmitt, H., and Wolf, S., 1994. A Universal Spine Tester for in Vitro Experiments with Muscle Force Simulation. European Spine Journal, 3(2): p. 91-97.

224. Lysack, J.T., Dickey, J.P., Dumas, G.A., and Yen, D., 2000. A Continuous Pure Moment Loading Apparatus for Biomechanical Testing of Multi-Segment Spine Specimens. Journal of Biomechanics, 33(6): p. 765-770.

225. Calisse, J., Rohlmann, A., and Bergmann, G., 1999. Estimation of Trunk Muscle Forces Using the Finite Element Method and in Vivo Loads Measured by Telemeterized Internal Spinal Fixation Devices. Journal of Biomechanics, 32(7): p. 727-731.

226. Martinez, J.B., Oloyede, V.O.A., and Broom, N.D., 1997. Biomechanics of Load-Bearing of the Intervertebral Disc: An Experimental and Finite Element Model. Medical Engineering & Physics, 19(2): p. 145-156.

227. Rohlmann, A., Bauer, L., Zander, T., Bergmann, G., and Wilke, H.J., 2006. Determination of Trunk Muscle Forces for Flexion and Extension by Using a Validated Finite Element Model of the Lumbar Spine and Measured in Vivo Data. Journal of Biomechanics, 39(6): p. 981-989.

228. Renner, S.M., Natarajan, R.N., Patwardhan, A.G., Havey, R.M., Voronov, L.I., Guo, B.Y., Andersson, G.B., and An, H.S., 2006. Novel Model to Analyze the Effect of a Large Compressive Follower Pre-Load on Range of Motions in a Lumbar Spine. Journal of Biomechanics, 40(6): p. 1326-1332.

229. Shirazi-Adl, A., Sadouk, S., Parnianpour, M., Pop, D., and El-Rich, M., 2002. Muscle Force Evaluation and the Role of Posture in Human Lumbar Spine under Compression. European Spine Journal, 11(6): p. 519-526.

230. Noailly, J., Wilke, H.J., Planell, J.A., and Lacroix, D., 2007. How Does the Geometry Affect the Internal Biomechanics of a Lumbar Spine Bi-Segment Finite Element Model? Consequences on the Validation Process. Journal of Biomechanics, 40(11): p. 2414-2425.

231. Teo, E.C. and Ng, H.W., 2001. Evaluation of the Role of Ligaments, Facets and Disc Nucleus in Lower Cervical Spine under Compression and Sagittal Moments Using Finite Element Method. Medical Engineering & Physics, 23(3): p. 155-164.

232. Schmidt, H., Heuer, F., Drumm, J., Klezl, Z., Claes, L., and Wilke, H.J., 2007. Application of a Calibration Method Provides More Realistic Results for a Finite Element Model of a Lumbar Spinal Segment. Clinical Biomechanics, 22(4): p. 377-384.

233. Wilke, H.J., Wolf, S., Claes, L.E., Arand, M., and Wiesend, A., 1996. Influence of Varying Muscle Forces on Lumbar Intradiscal Pressure: An in Vitro Study. Journal of Biomechanics, 29(4): p. 549-555.

234. Rohlmann, A., Neller, S., Claes, L., Bergmann, G., and Wilke, H.J., 2001. Influence of a Follower Load on Intradiscal Pressure and Intersegmental Rotation of the Lumbar Spine. Spine, 26(24): p. E557-E561.

235. Wilke, H.J., Rohlmann, A., Neller, S., Graichen, F., Claes, L., and Bergmann, G., 2003. Issls Prize Winner: A Novel Approach to Determine Trunk Muscle Forces During Flexion and Extension: A Comparison of Data from an in Vitro Experiment and in Vivo Measurements. Spine, 28(23): p. 2585-2593.

236. Lebwohl, N.H., Cunningham, B.W., Dmitriev, A., Shimamoto, N., Gooch, L., Devlin, V., Boachie-Adjei, O., and Wagner, T.A., 2002. Biomechanical Comparison of Lumbosacral Fixation Techniques in a Calf Spine Model. Spine, 27(21): p. 2312-2320.

237. Gedet, P., Thistlethwaite, P.A., and Ferguson, S.J., 2007. Minimizing Errors During in Vitro Testing of Multisegmental Spine Specimens: Considerations for Component Selection and Kinematic Measurement. Journal of Biomechanics, 40(8): p. 1881-1885.

238. Gay, R.E., Ilharreborde, B., Zhao, K., Boumediene, E., and An, K.N., 2008. The Effect of Loading Rate and Degeneration on Neutral Region Motion in Human Cadaveric Lumbar Motion Segments. Clinical Biomechanics, 23(1): p. 1-7.

239. Ilharreborde, B., Zhao, K., Boumediene, E., Gay, R., Berglund, L., and An, K.N., 2010. A Dynamic Method for in Vitro Multisegment Spine Testing. Orthopaedics & Traumatology: Surgery & Research, 96(4): p. 456-461.

240. Stokes, I.A., Gardner-Morse, M., Churchill, D., and Laible, J.P., 2002. Measurement of a Spinal Motion Segment Stiffness Matrix. Journal of Biomechanics, 35(4): p. 517-521.

241. Stokes, I.A.F. and Gardner-Morse, M., 2003. Spinal Stiffness Increases with Axial Load: Another Stabilizing Consequence of Muscle Action. Journal of Electromyography and Kinesiology, 13(4): p. 397-402.

242. Gilbertson, L.G., Doehring, T.C., and Kang, J.D., 2000. New Methods to Study Lumbar Spine Biomechanics: Delineation of in Vitro Load-Displacement Characteristics by Using a Robotic/Ufs Testing System with Hybrid Control. Operative Techniques in Orthopaedics, 10(4): p. 246-253.

243. Cripton, P.A., Bruehlmann, S.B., Orr, T.E., Oxland, T.R., and Nolte, L.P., 2000. In Vitro Axial Preload Application During Spine Flexibility Testing: Towards Reduced Apparatus-Related Artefacts. Journal of Biomechanics, 33(12): p. 1559-1568.

244. Miura, T., Panjabi, M.M., and Cripton, P.A., 2002. A Method to Simulate in Vivo Cervical Spine Kinematics Using in Vitro Compressive Preload. Spine, 27(1): p. 43-48.

245. Freudiger, S., Dubois, G., and Lorrain, M., 1999. Dynamic Neutralisation of the Lumbar Spine Confirmed on a New Lumbar Spine Simulator in Vitro. Archives of Orthopaedic and Trauma Surgery, 119(3-4): p. 127-132.

246. Miller, J.A.A., Schultz, A.B., Warwick, D.N., and Spencer, D.L., 1986. Mechanical Properties of Lumbar Spine Motion Segments under Large Loads. Journal of Biomechanics, 19(1): p. 79-84.

247. Andersson, G.B., An, H.S., Oegema, T.R., Jr., and Setton, L.A., 2006. Directions for Future Research. Journal of Bone and Joint Surgery-American Volume, 88 (Suppl 2): p. 110-114.

248. Moorhouse, K.M. and Granata, K.P., 2005. Trunk Stiffness and Dynamics During Active Extension Exertions. Journal of Biomechanics, 38(10): p. 2000-2007.

249. Tawackoli, W., Marco, R., and Liebschner, M.A., 2004. The Effect of Compressive Axial Preload on the Flexibility of the Thoracolumbar Spine. Spine, 29(9): p. 988-993.

250. Patwardhan, A.G., Havey, R.M., Meade, K.P., Lee, B., and Dunlap, B., 1999. A Follower Load Increases the Load-Carrying Capacity of the Lumbar Spine in Compression. Spine, 24(10): p. 1003-1009.

251. Busscher, I., Ploegmakers, J., Verkerke, G., and Veldhuizen, A., 2010. Comparative Anatomical Dimensions of the Complete Human and Porcine Spine. European Spine Journal, 19(7): p. 1104-1114.

252. Dath, R., Ebinesan, A.D., Porter, K.M., and Miles, A.W., 2007. Anatomical Measurements of Porcine Lumbar Vertebrae. Clinical Biomechanics, 22(5): p. 607-613.

253. O'Reilly, O.M., Metzger, M.F., Buckley, J.M., Moody, D.A., and Lotz, J.C., 2009. On the Stiffness Matrix of the Intervertebral Joint: Application to Total Disk Replacement. Journal of Biomechanical Engineering, 131(8): p. 081007.

254. Dolan, P., Earley, M., and Adams, M.A., 1994. Bending and Compressive Stresses Acting on the Lumbar Spine During Lifting Activities. Journal of Biomechanics, 27(10): p. 1237-1248.

255. El-Rich, M., Shirazi-Adl, A., and Arjmand, N., 2004. Muscle Activity, Internal Loads, and Stability of the Human Spine in Standing Postures: Combined Model and in Vivo Studies. Spine, 29(23): p. 2633-2642.

256. Bazrgari, B., 2007. Biodynamic of the Human Spine. University of Montreal: Montreal, Canada.

257. Bogduk, N., Johnson, G., and Spalding, D., 1998. The Morphology and Biomechanics of Latissimus Dorsi. Clinical Biomechanics, 13(6): p. 377-385.

258. Spenciner, D., Greene, D., Paiva, J., Palumbo, M., and Crisco, J., 2005. The Multidirectional Bending Properties of the Human Lumbar Intervertebral Disc. The Spine Journal, 6(3): p. 248-257.

259. Edwards, W.T., Hayes, W.C., Posner, I., White, A.A., 3rd, and Mann, R.W., 1987. Variation of Lumbar Spine Stiffness with Load. Journal of Biomechanical Engineering, 109(1): p. 35-42.

260. Pflaster, D.S., Krag, M.H., Johnson, C.C., Haugh, L.D., and Pope, M.H., 1997. Effect of Test Environment on Intervertebral Disc Hydration. Spine, 22(2): p. 133-139.

261. Wilke, H.-J., Jungkunz, B., Wenger, K., and Claes, L.E., 1998. Spinal Segment Range of Motion as a Function of in Vitro Test Conditions: Effects of Exposure Period, Accumulated Cycles, Angular-Deformation Rate, and Moisture Condition. The Anatomical Record, 251(1): p. 15-19.

262. PCB Piezotronics Inc., 2011. Load Cell Technical Information. PCB Piezotronics Inc.: Depew, NY, USA. [Accessed 17/12/2011]. Available from: http://www.pcb.com/Linked_Documents/Force-Torque/Catalog/Sections/FTQ200G_0107_9.pdf.

263. DePuy International Ltd., 2008. In Motion Lumbar Artificial Disc Surgical Technique & Product Catalogue. DePuy International Ltd.: Leeds, UK.

264. Cakir, B., Richter, M., Schmoelz, W., Schmidt, R., Reichel, H., and Wilke, H., 2009. Resect or Not to Resect: The Role of Posterior Longitudinal Ligament in Lumbar Total Disc Replacement. European Spine Journal: p. 1-7.

265. Maxwell, S.E. and Delaney, H.D., 1990. Designing Experiments and Analyzing Data. Wadsworth Publishing Company: Belmont, California, USA. 109-110.

266. Rasch, D., Teuscher, F., and Guiard, V., 2007. How Robust Are Tests for Two Independent Samples? Journal of Statistical Planning and Inference, 137(8): p. 2706-2720.

267. Costi, J.J., Hearn, T.C., and Fazzalari, N.L., 2002. The Effect of Hydration on the Stiffness of Intervertebral Discs in an Ovine Model. Clinical Biomechanics, 17(6): p. 446-455.

268. Bass, C.R., Planchak, C.J., Salzar, R.S., Lucas, S.R., Rafaels, K.A., Shender, B.S., and Paskoff, G., 2007. The Temperature-Dependent Viscoelasticity of Porcine Lumbar Spine Ligaments. Spine, 32(16): p. E436-E442.

269. Hochschuler, S.H., Ohnmeiss, D.D., Guyer, R.D., and Blumenthal, S.L., 2002. Artificial Disc: Preliminary Results of a Prospective Study in the United States. European Spine Journal, 11: p. S106-S110.

270. Sears, W.R., McCombe, P.F., and Sasso, R.C., 2006. Kinematics of Cervical and Lumbar Total Disc Replacement. Seminars in Spine Surgery, 18(2): p. 117-129.

271. Wilke, H.J., Rohlmann, A., Neller, S., Schultheiss, M., Bergmann, G., Graichen, F., and Claes, L.E., 2001. Is It Possible to Simulate Physiologic Loading Conditions by Applying Pure Moments? A Comparison of in Vivo and in Vitro Load Components in an Internal Fixator. Spine, 26(6): p. 636-642.

272. Cunningham, B.W., 2004. Basic Scientific Considerations in Total Disc Arthroplasty. The Spine Journal, 4(6, Supplement 1): p. S219-S230.

273. DePuy Spine Inc., Moumene, M., Toselli, R., Masson, M., and Afshari, P., 2008. Intervertebral Motion Disc with Helical Shock Absorber. Moumene, M., Toselli, R., Masson, M., and Afshari, P. Patent: WO2009002976, 31/12/2008.

13 APPENDIX

This appendix documents more comprehensive data regarding the twelve stiffness matrices of the full porcine study, with six corresponding to the FSU specimens (Tables 85-90), and six corresponding to the ISD specimens (Tables 91-96). The matrices listed below comprise the mean stiffness values as reported in the main body of this document (Chapter 9.3.1., page 185), with the addition of the standard deviation for each stiffness term. All stiffnesses are reported in N, mm, and rad.

Table 85: Matrix FSU01, mean stiffness with 0 N preload and an intact disc, standard deviation in parentheses

	TX		TY		TZ		RX		RY		RZ	
FX	**32**	**(1.5)**	2	(0.3)	2	(2.4)	-16	(17)	-7	(84)	-41	(55)
FY	-1	(1.2)	**36**	**(4.6)**	1	(2.2)	-77	(47)	-8	(21)	369	(174)
FZ	15	(9.6)	-3	(2.5)	**326**	**(130)**	-168	(767)	-2,910	(1,045)	19	(142)
MX	-107	(100)	766	(92)	568	(681)	**41,245**	**(25,269)**	639	(6,047)	7,048	(8,954)
MY	-1,025	(93)	-228	(48)	-3,088	(1,769)	5,317	(6,153)	**67,118**	**(11,850)**	-3,552	(1,243)
MZ	-88	(129)	210	(175)	32	(283)	-4,200	(11,485)	-425	(1,759)	**108,056**	**(18,152)**

Table 86: Matrix FSU02, mean stiffness with 500 N (30 min) preload and an intact disc, standard deviation in parentheses

	TX		TY		TZ		RX		RY		RZ	
FX	**37**	**(1.4)**	2	(0.4)	-3	(8.3)	-8	(26)	-39	(136)	13	(30)
FY	-1	(0.4)	**40**	**(0.7)**	4	(6.4)	-91	(77)	-26	(49)	365	(176)
FZ	31	(13)	-4	(6.0)	**1,195**	**(67)**	-700	(1,365)	-6,918	(1,667)	-137	(235)
MX	239	(883)	708	(158)	1,612	(2,082)	**119,600**	**(57,065)**	-2,367	(11,426)	2,022	(10,707)
MY	-1,280	(117)	-260	(81)	-13,486	(2,529)	15,978	(15,335)	**131,253**	**(20,616)**	-3,191	(3,206)
MZ	-68	(38)	351	(157)	-354	(353)	-294	(11,659)	990	(2,192)	**124,931**	**(27,991)**

Table 87: Matrix FSU03, mean stiffness with 500 N (60 min) preload and an intact disc, standard deviation in parentheses

	TX		TY		TZ		RX		RY		RZ	
FX	**37**	**(1.3)**	2	(0.5)	-3	(11)	0	(45)	-18	(150)	9	(28)
FY	-1	(0.5)	**40**	**(0.8)**	4	(6.4)	-78	(90)	-37	(47)	341	(180)
FZ	33	(8.8)	-4	(4.9)	**1,278**	**(53)**	-375	(1,471)	-7,532	(2,332)	-139	(229)
MX	-102	(87)	669	(159)	2,101	(1,889)	**152,472**	**(51,477)**	-1,317	(13,454)	2,908	(13,042)
MY	-1,337	(213)	-280	(86)	-13,876	(2,717)	12,915	(15,054)	**145,169**	**(28,070)**	-3,700	(3,431)
MZ	-64	(50)	321	(182)	-301	(421)	2,347	(11,092)	1,431	(1,950)	**122,627**	**(27,972)**

Table 88: Matrix FSU04, mean stiffness with 0 N preload and an In Motion disc, standard deviation in parentheses

	TX		TY		TZ		RX		RY		RZ	
FX	**22**	**(4.4)**	1	(1.2)	-10	(13)	13	(33)	123	(230)	0	(20)
FY	-1	(0.8)	**28**	**(3.3)**	-2	(4.0)	-180	(142)	7	(42)	-74	(183)
FZ	-3	(24)	-8	(7.3)	**405**	**(98)**	-765	(474)	-2,416	(1,408)	-179	(370)
MX	-122	(34)	503	(102)	487	(1,011)	**20,993**	**(9,807)**	902	(3,910)	-1,818	(4,354)
MY	-524	(332)	-104	(162)	-3,569	(1,273)	9,939	(8,172)	**54,004**	**(21,464)**	1,718	(3,889)
MZ	-7	(62)	-97	(278)	-59	(291)	2,267	(3,221)	318	(2,916)	**23,429**	**(5,303)**

Table 89: Matrix FSU05, mean stiffness with 500 N (30 min) preload and an In Motion disc, standard deviation in parentheses

	TX		TY		TZ		RX		RY		RZ	
FX	**32**	**(2.9)**	2	(0.4)	-17	(21)	19	(45)	74	(370)	10	(27)
FY	-1	(0.7)	**40**	**(1.2)**	4	(7.0)	-176	(143)	-3	(85)	-16	(244)
FZ	-8	(28)	-1	(4.9)	**1,062**	**(38)**	-1,969	(1,435)	-7,165	(2,210)	-174	(765)
MX	-159	(80)	662	(130)	564	(1,970)	**19,573**	**(17,277)**	2,104	(12,636)	-5,907	(7,796)
MY	-318	(785)	-276	(68)	-12,700	(3,732)	23,729	(17,544)	**117,174**	**(31,132)**	573	(7,501)
MZ	-37	(64)	515	(174)	-68	(686)	3,433	(5,485)	152	(6,550)	**41,900**	**(9,005)**

Table 90: Matrix FSU06, mean stiffness with 500 N (60 min) preload and an In Motion disc, standard deviation in parentheses

	TX		TY		TZ		RX		RY		RZ	
FX	**32**	**(3.3)**	2	(0.3)	-17	(21)	26	(60)	95	(390)	2	(25)
FY	-1	(0.7)	**41**	**(1.4)**	5	(6.4)	-183	(140)	-11	(83)	-35	(249)
FZ	-6	(28)	0	(5.4)	**1,109**	**(62)**	-2,053	(1,540)	-7,907	(2,781)	-164	(814)
MX	-181	(80)	652	(131)	519	(1,866)	**17,638**	**(18,697)**	3,252	(14,876)	-6,608	(8,563)
MY	-708	(497)	-289	(71)	-13,083	(4,432)	25,803	(18,712)	**114,325**	**(35,077)**	667	(7,375)
MZ	-27	(48)	514	(160)	-5	(597)	4,403	(6,468)	59	(7,186)	**43,358**	**(10,598)**

Table 91: Matrix ISD01, mean stiffness with 0 N preload and an intact disc, standard deviation in parentheses

	TX		TY		TZ		RX		RY		RZ	
FX	**29**	**(2.1)**	1	(0.9)	3	(12)	1	(44)	-8	(122)	26	(60)
FY	-1	(0.8)	**28**	**(4.7)**	1	(3.7)	20	(163)	7	(14)	326	(61)
FZ	15	(17)	-5	(3.2)	**392**	**(48)**	-699	(444)	-58	(1,047)	-110	(76)
MX	-109	(66)	700	(158)	640	(408)	**20,704**	**(15,472)**	-39	(2,047)	6,306	(2,600)
MY	-634	(791)	-180	(48)	-364	(1,391)	1,246	(5,706)	**11,682**	**(6,872)**	-2,509	(2,104)
MZ	-46	(39)	291	(111)	-139	(122)	-1,048	(3,707)	812	(915)	**39,619**	**(2,105)**

Table 92: Matrix ISD02, mean stiffness with 500 N (30 min) preload and an intact disc, standard deviation in parentheses

	TX		TY		TZ		RX		RY		RZ	
FX	**33**	**(2.4)**	2	(0.3)	-6	(25)	23	(51)	2	(158)	44	(32,)
FY	-1	(0.3)	**38**	**(1.1)**	9	(7.3)	15	(136)	4	(26)	374	(65)
FZ	17	(13)	6	(7.6)	**1,245**	**(91)**	-1,741	(1,039)	-882	(2,675)	-202	(171)
MX	-78	(71)	856	(242)	2,314	(1,238)	**65,000**	**(34,259)**	-969	(6,224)	8,651	(1,162)
MY	-989	(291)	-213	(48)	-1,304	(4,191)	1,584	(7,425)	**27,982**	**(17,811)**	-3,466	(1,982)
MZ	-46	(28)	396	(105)	-147	(171)	-3,298	(3,459)	644	(529)	**48,220**	**(3,889)**

Table 93: Matrix ISD03, mean stiffness with 500 N (60 min) preload and an intact disc, standard deviation in parentheses

	TX		TY		TZ		RX		RY		RZ	
FX	**32**	**(2.1)**	1	(0.3)	-6	(27)	26	(53)	-37	(153)	37	(37)
FY	-1	(0.6)	**37**	**(0.8)**	10	(7.6)	34	(108)	3	(25)	366	(69)
FZ	28	(24)	7	(7.8)	**1,323**	**(60)**	-1,532	(1,055)	-924	(2,665)	-211	(137)
MX	-65	(73)	825	(284)	2,497	(1,350)	**95,604**	**(33,375)**	429	(5,604)	9,103	(1,903)
MY	-971	(322)	-197	(46)	-1,423	(4,551)	2,369	(7,730)	**39,941**	**(23,341)**	-3,187	(2,100)
MZ	-52	(32)	395	(105)	395	(120)	-2,840	(3,082)	324	(586)	**46,438**	**(4,115)**

Table 94: Matrix ISD04, mean stiffness with 0 N preload and an In Motion disc, standard deviation in parentheses

	TX		TY		TZ		RX		RY		RZ	
FX	**8**	**(3.2)**	0	(0.7)	0	(7.1)	-6	(33)	-22	(33)	-2	(10)
FY	0	(0.9)	**4**	**(2.4)**	3	(2.1)	4	(29)	9	(11)	-3	(25)
FZ	6	(13)	3	(16)	**283**	**(55)**	-601	(284)	585	(620)	7	(35)
MX	-5	(35)	74	(78)	543	(380)	**-692**	**(631)**	1,344	(1,545)	-155	(615)
MY	-71	(346)	-28	(24)	307	(771)	-824	(1,968)	**1,419**	**(2,423)**	8	(414)
MZ	-14	(7.0)	-2	(7)	22	(12)	-14	(72)	36	(40)	**59**	**(26)**

Table 95: Matrix ISD05, mean stiffness with 500 N (30 min) preload and an In Motion disc, standard deviation in parentheses

	TX		TY		TZ		RX		RY		RZ	
FX	**25**	**(3.7)**	2	(0.4)	-5	(21)	14	(29)	-129	(167)	3	(27)
FY	-1	(0.4)	**40**	**(1.0)**	10	(7.2)	112	(65)	24	(17)	-1	(75)
FZ	18	(30)	7	(6.4)	**1,135**	**(82)**	-2,200	(812)	2,504	(1,982)	19	(38)
MX	-51	(63)	946	(153)	2,035	(1,704)	**-184**	**(2,901)**	5,373	(6,035)	265	(1,968)
MY	-619	(183)	-204	(38)	1,909	(3,673)	-5,846	(6,010)	**12,404**	**(16,434)**	-581	(860)
MZ	-53	(29)	-23	(82)	47	(62)	-302	(300)	302	(329)	**969**	**(144)**

Table 96: Matrix ISD06, mean stiffness with 500 N (60 min) preload and an In Motion disc, standard deviation in parentheses

	TX		TY		TZ		RX		RY		RZ	
FX	**25**	**(3.6)**	2	(0.2)	-5	(21)	17	(24)	-150	(160)	2	(24)
FY	-1	(0.4)	**38**	**(3.1)**	11	(6.5)	111	(70)	24	(14)	-7	(79)
FZ	27	(24)	8	(6.3)	**1,195**	**(71)**	-2,238	(861)	2,628	(2,108)	45	(26)
MX	-42	(77)	873	(50)	2,140	(1,791)	**-397**	**(2,829)**	5,508	(6,470)	150	(2,456)
MY	-636	(182)	-192	(50)	2,364	(3,640)	-4,756	(3,788)	**13,380**	**(18,261)**	-692	(715)
MZ	-54	(29)	-22	(153)	52	(49)	-329	(300)	308	(335)	**1,078**	**(171)**